Author:
Bose, Sam

Title:
Exploiting Species Differences to Understand the Function and Pharmacology of the Cystic Fibrosis Transmembrane Conductance Regulator

Exploiting Species Differences to Understand the Function and Pharmacology of the Cystic Fibrosis Transmembrane Conductance Regulator

Samuel Jitu Bose

A dissertation submitted to the University of Bristol in accordance with the requirements for award of the degree of Doctor of Philosophy in the Faculty of Life Sciences

School of Physiology, Pharmacology and Neuroscience

September 2018

49,688 words

Abstract

Cystic fibrosis (CF) is caused by mutations in the cystic fibrosis transmembrane conductance regulator (CFTR) Cl^- channel. The licensing of the CFTR potentiator ivacaftor (VX-770, Vertex Pharmaceuticals Inc.), provided proof of concept for the use of small molecules to treat CF. However, the mechanism of action of ivacaftor is not well understood. Studies exploiting species differences in CFTR pharmacology have previously been used to identify binding sites of CFTR modulators. We hypothesised that differences in the response of CFTR orthologues to ivacaftor may be used to determine regions of the protein involved in its mechanism of action.

CFTR orthologues from human, pig, sheep, ferret, mouse and zebrafish were studied using single-channel patch-clamp recordings. These studies identified differences in the single-channel current amplitude (i) and open probability (P_o) of CFTR orthologues. Single-channel recordings also demonstrated that the P_o of mouse F508del-CFTR after rescue of its plasma membrane expression was not reduced compared to mouse wild-type (WT)-CFTR and channel activity remained stable at 37 °C in contrast to human F508del-CFTR. Furthermore, neither mouse WT-CFTR nor rescued mouse F508del-CFTR were potentiated by ivacaftor. We therefore developed a high-throughput assay utilising automated whole-cell patch-clamp recording to test a selection of human-mouse CFTR chimeras for their response to ivacaftor. From these studies, we identified five sequence alterations from the human to the mouse sequence, A326T, L327V, K329N, I332V and A349S, located in the third extracellular loop (ECL3) and on transmembrane helix 6 (TM6), that when expressed in human CFTR prevented potentiation by ivacaftor. These experiments were further supported by single-channel recordings of human-mouse CFTR chimeras.

In conclusion, this study has identified structural regions within the transmembrane helices of CFTR that may be targeted for the development of novel CFTR potentiators to be used in conjunction with CFTR correctors for the treatment of CF.

Acknowledgements

The completion of this work would not have been possible without funding from the Medical Research Council and the support and encouragement that I have received from family, friends and colleagues throughout. First and foremost, I would like to thank my wife Hannah. Without her unending support, patience and love through both the highs and the lows of the past four years, this work would not have been possible.

I would also like to express my gratitude to my supervisor, Professor David Sheppard. This work is a testament to the kindness, dedication and generosity that David has shown towards me throughout. David's professionalism and commitment to his research will remain an inspiration to me for the rest of my professional career. I will always be indebted to him for the guidance, support, and encouragement that he has provided during the course of this project.

I would also like to acknowledge the support that I have received from my mother, father and brother. They have always stood by me and without their belief in my ability, I would not have had the strength to complete this work.

The most valuable thing to have been gained from the time I have spent working on this project has been the friendships I have made. In particular I would like to thank Joe Wrennall and Bartholomew Harvey, who have provided encouragement, humour and support, both in the lab and in the Robin Hood on a Friday evening! Secondly, I would like to thank Majid Al Salmani, Bethan Hawley and Caroline Wang for their continued guidance and encouragement. I would also like to express my gratitude to the students that have passed through the lab during my time here and made this time particularly special. In particular I would like to thank Beatrice Cornu-Hewitt, Rachel Haigh, Kimi Worsdell, Shenelle Samodee, Kamonshanok Kraidith, Walailak Jantarajit, Nookkanik Khuituan, and Ming Yang Valentine.

I owe particular gratitude to the talented scientists who have trained me and aided my research. I would like to thank Zhiwei Cai, who trained me in the single-channel patch-clamp technique and provided a huge amount of support to me during the early stages

of my project. Secondly, I would like to thank Hongyu Li for the guidance that she has provided to me throughout. I would like to thank my friends and colleagues at the Novartis Institutes for Biomedical Research, especially my supervisor Kevin Coote who made my visit to Novartis both possible, and immensely enjoyable. I would also like to thank Kelly McKiernan, for her assistance with transfection protocols and for training me in the use of the QPatch automated patch-clamp system.

Finally, I would like to thank our collaborators at the University of Edinburgh, Chris Boyd, Ann Doherty and Laura Hyndman, who developed and amplified most of the cDNA constructs used in this project.

Author’s declaration

I declare that the work in this dissertation was carried out in accordance with the requirements of the *University's Regulations and Code of Practice for Research Degree Programmes* and that it has not been submitted for any other academic award. Except where indicated by specific reference in the text, the work is the candidate's own work. Work done in collaboration with, or with the assistance of, others, is indicated as such. Any views expressed in the dissertation are those of the author.

Samuel Jitu Bose

SIGNED: ..... DATE:.....

Abbreviations

a.a. = amino acid

AAV = adeno-associated virus

AMPK = 5' adenosine monophosphate-activated protein kinase

Apo = unbound

ATP = adenosine triphosphate

ADP = adenosine diphosphate

AQP = aquaporin

ASL = airway surface liquid

BHK = baby hamster kidney

bp = base pair

cAMP = cyclic adenosine monophosphate

CF = cystic fibrosis

CFTR = cystic fibrosis transmembrane conductance regulator

CHO = Chinese hamster ovary

DMEM = Dulbecco's modified Eagle's medium

DMSO = Dimethyl sulphoxide

DPBS = Dulbecco's phosphate-buffered saline

$\mathbf{E_{Cl}}$ = equilibrium constant for chloride

EGTA = ethylene glycol-bis(β-aminoethyl ether)-N,N,N',N'-tetra acetic acid

EM = electron microscopy

EMA = European Medicines Agency

ENaC = epithelial sodium channel

ER = endoplasmic reticulum

ERAD = endoplasmic reticulum associated degradation

ERQC = endoplasmic reticulum quality control

F = the Faradays constant (9.648533×10^4 $C \cdot mol^{-1}$)

FABP = fatty acid binding protein

FACS = fluorescence activated cell sorting

FBS = foetal bovine serum

fCFTR = ferret CFTR

FDA = U.S. Food and Drug Administration

FSK = forskolin

GTA = gene transfer agent

hCFTR = human CFTR

HDX = hydrogen/deuterium exchange mass spectrometry

HEPES = 4-(2-hydroxyethyl)-1-piperazineethanesulfonic acid

KCN = potassium channel

MCC = mucociliary clearance

mCFTR = mouse CFTR

NHE1 = Na^+/H^+ antiporter 1

NKCC1 = Na^+, K^+, Cl^-cotransporter

NMDG = *N*-Methyl-D-glucamine

NPPB = 5-nitro-2-(3-phenylpropylamino) benzoate

pCFTR = pig CFTR

pEGFP-N1 = Enhanced green fluorescent protein N1 plasmid

PKA = protein kinase A

PKC = protein kinase C

PM = plasma membrane

PP_i = Pyrophosphate

PTC = premature termination codon

R = universal gas constant (8.314472 $J \cdot K^{-1} \cdot mol^{-1}$)

RD = regulatory domain

RI = regulatory insertion

sCFTR = sheep CFTR

SD = Standard deviation

SEM = Standard error of the mean

T = temperature

TES = *N*-tris[hydroxymethyl]methyl-2-aminoethanesulphonic acid

TM = transmembrane helix

TMD = transmembrane domain

TMEM16A = Ca^{2+}-activated Cl^- channel

WA = Walker A site

WB = Walker B site

z = valency

zCFTR = zebrafish CFTR

Contents

Abstract ii

Acknowledgements iii

Author's declaration v

Abbreviations vi

Contents viii

List of figures xii

List of tables xvi

1. Introduction 1

1.1 Aetiology and epidemiology of cystic fibrosis 1

1.2 Role of CFTR in epithelial fluid transport 4

1.3 CFTR structure and function 8

1.3.1 Structure of CFTR 8

1.3.2 Control of CFTR gating 11

1.4 Classification of CF causing mutations 15

1.5 Current landscape in the treatment of CF 19

1.5.1 Symptomatic treatments for cystic fibrosis 22

1.5.2 Small molecule modulators of CFTR: Correctors and potentiators 22

1.5.3 Genetic medicine strategies for cystic fibrosis 25

1.6 Evolution and Diversity of CFTR orthologues 27

1.7 Use of functional differences between CFTR orthologues in CF research 31

1.7.1 Current understanding of species differences in CFTR structure, function and pharmacology 32

1.7.2 Animal models of CF 38

1.7.3 Use of CFTR orthologues to study CFTR structure and function 39

1.7.4 Use of CFTR orthologues to study the mechanism of action of small molecule CFTR modulators 40

1.8 Current understanding of the mechanism of action of ivacaftor 43
1.8.1 Potentiation of CFTR by ivacaftor: Comparison with other CFTR potentiators 43
1.8.2 Potential binding sites for ivacaftor 46
1.9 Hypothesis and aims of the present study 48
2. Materials and methods 50
2.1 Single-channel patch-clamp recordings 50
2.1.1 Cell Culture 50
2.1.2 Plasmid design 52
2.1.3 Reagents 53
2.1.4 Electrophysiological recordings 54
2.1.5 Analysis and statistics 57
2.2 Automated whole-cell patch-clamp 61
2.2.1 Cell culture and transfection 61
2.1.3 Reagents 64
2.1.4 QPatch automated electrophysiological recordings 64
2.1.5 Analysis of QPatch recordings 68
2.1.6 Statistics 69
3. Species differences in WT and F508del-CFTR function as demonstrated using single-channel patch-clamp recording 70
3.1 Introduction 70
3.2 Comparison of WT-CFTR gating behaviour between diverse species 72
3.2.1 Single-channel gating behaviour of diverse CFTR orthologues 72
3.3 Different effects of the F508del mutation in diverse CFTR orthologues 78
3.3.1 The impact of F508del on human CFTR 78
3.3.2 The impact of F508del on sheep CFTR 82
3.3.3 The impact of F508del on mouse CFTR 84
3.3.4 Thermal stability of F508del-CFTR orthologues at 37 °C 87

3.4: Discussion 90
3.4.1 Variations in the gating behaviour of CFTR orthologues 90
3.4.2 Variation in the impact of the F508del mutation on CFTR orthologues 92
3.4.3 Thermal stability of mouse F508del-CFTR 94

4. The effects of small molecule CFTR modulators on the single-channel activity of WT and F508del-CFTR orthologues 97

4.1 Introduction 97

4.2 Effects of ivacaftor on the activity of CFTR orthologues 98
4.2.1 Potentiation of WT-CFTR from diverse species by ivacaftor 98
4.2.2 Effect of ivacaftor on the single-channel behaviour of F508del-CFTR from diverse species 112
4.3.3 Effect of genistein on the single-channel behaviour of CFTR orthologues 116

4.4 Discussion 117

5. Investigating the mechanism of action of ivacaftor using CFTR chimeras 123

5.1 Introduction 123
5.1.1 Overview of the use of chimeras to determine drug-binding sites 123
5.1.2 Selection and design of chimeras 124
5.1.3. Experimental approach for studying the effect of ivacaftor on human-mouse CFTR chimeras 125

5.2 Response of human and mouse WT-CFTR to ivacaftor using the whole-cell automated patch-clamp technique 127
5.2.1 Response of Human WT-CFTR to ivacaftor 127
5.2.2 Response of mouse WT-CFTR to ivacaftor 129

5.3 Determining compound-interacting domains using automated whole-cell patch-clamp technique to study human-mouse CFTR chimeras 131
5.3.1 Effect of ivacaftor on whole-domain CFTR chimeras 131
5.3.2 Effect of ivacaftor on TM-helix CFTR chimeras 135

5.4 The gating behaviour of human-mouse CFTR chimeras as determined using single-channel patch-clamp recordings 141

5.5 Determining the binding domain of ivacaftor using human-mouse CFTR chimeras 144

5.5.1 Effect of ivacaftor on whole-domain CFTR chimeras 144

5.5.2 Effect of ivacaftor on TM-helix CFTR chimeras 146

5.6 Determining regions of the CFTR protein involved in the mechanism of action of ivacaftor 149

5.6.1 Sequence alterations that affect the response of human CFTR to ivacaftor 149

5.7 Discussion 150

5.7.1. Interpretation of the data collected from automated whole-cell patch-clamp of human-mouse CFTR chimeras 150

5.7.2. Interpretation of the data collected from single-channel patch-clamp of human-mouse CFTR chimeras 158

6. General discussion 161

6.1 Species differences in CFTR structure and function 161

6.1.1 Variations in the structure and gating behaviour of CFTR orthologues from diverse species 161

6.1.2 Differences in the effect of CF causing mutations on diverse species orthologues of CFTR 164

6.2 Relevance and implications of species differences in function and pharmacology of CFTR orthologues for the use of CF animal models 165

6.3 Differences in pharmacology between CFTR orthologues 166

6.4 Identification of residues involved in the mechanism of action of ivacaftor 167

6.5 Implications for future research and development of CF therapies .. 169

7. Conclusion 171

References 173

Appendices 213

Appendix 1: Sequence alignment of studied CFTR orthologues..... 214

Appendix 2: Sequence alignment of human-mouse CFTR chimeras..... 218

List of figures

Figure 1.1: Schematic cartoon indicating the domain arrangement of CFTR **3**

Figure 1.2: Schematic of the pathways involved in epithelial fluid transport **6**

Figure 1.3: Structure of the human CFTR ion channel **9**

Figure 1.4: ATP-binding and hydrolysis at the CFTR nucleotide-binding domains .. **12**

Figure 1.5: The proposed gating cycle for CFTR **15**

Figure 1.6: Classification of CF-causing mutations **16**

Figure 1.7: Cladogram showing the evolutionary diversity of CFTR orthologues **29**

Figure 1.8: Sequence alignment of CFTR RD from diverse species **31**

Figure 1.9: Recording the single-channel activity of CFTR using excised inside-out membrane patches **33**

Figure 1.10: Single-channel behaviour of diverse CFTR orthologues **35**

Figure 1.11: Ivacaftor modifies the gating cycle of CFTR **45**

Figure 1.12: Potential binding sites of ivacaftor based upon HDX exchange **47**

Figure 2.1. Current amplitude histogram generated from 30 s single-channel recording of human WT-CFTR at -50 mV **58**

Figure 2.2. Example dwell-time histograms for open- and closed-time events generated from single-channel recordings of human WT-CFTR **59**

Figure 2.3: Experimental well from the QPlates used for QPatch experiments **66**

Figure 2.4. Voltage protocol used for whole-cell patch-clamp experiments using QPatch screening station **67**

Figure 2.5: Example QPatch recording of human WT-CFTR activity in response to 10 μM forskolin followed by 10 μM ivacaftor and 30 μM $CFTR_{inh}$-172 ..... **68**

Figure 3.1: Cladogram of CFTR orthologues studied **71**

Figure 3.2. The single-channel activity of CFTR from diverse species **73**

Figure 3.3: Single-channel properties of CFTR orthologues **74**

Figure 3.4: Comparison of i and P_o for human WT- and F508del-CFTR **79**

Figure 3.5. Representative dwell-time histograms for open- and closed-time events of human WT- and F508del-CFTR **81**

Figure 3.6: Comparison of i and P_o for sheep WT- and F508del-CFTR **83**

Figure 3.7: Comparison of i and P_o for mouse WT- and F508del-CFTR **85**

Figure 3.8. Representative dwell-time histograms for open- and closed-time events of mouse WT- and F508del-CFTR **86**

Figure 3.9: Thermal stability of mouse F508del-CFTR **89**

Figure 4.1: Effect of ivacaftor on human WT-CFTR in the presence of 1 mM ATP and 75 nM PKA **99**

Figure 4.2: Effect of ivacaftor on human WT-CFTR in the presence of 0.3 mM ATP **101**

Figure 4.3: Effect of ivacaftor on sheep WT-CFTR in the presence of 0.3 mM ATP **103**

Figure 4.4: Effect of ivacaftor on pig WT-CFTR in the presence of 1 mM ATP **105**

Figure 4.5: Effect of ivacaftor on ferret WT-CFTR in the presence of 1 mM ATP **107**

Figure 4.6: Effect of ivacaftor on mouse WT-CFTR in the presence of 1 mM ATP **109**

Figure 4.7: Effect of ivacaftor on zebrafish WT-CFTR in the presence of 1 mM ATP **111**

Figure 4.8: Effect of ivacaftor on human and mouse F508del-CFTR following low temperature correction **113**

Figure 4.9: Effect of ivacaftor on human and mouse F508del-CFTR following correction with 3 μM lumacaftor **115**

Figure 4.10: Effect of 50 μM genistein on human and mouse F508del-CFTR following low temperature correction **117**

Figure 4.11: Summary of the response of CFTR orthologues from diverse species to 1 and 10 μM ivacaftor as studied using single-channel patch-clamp **118**

Figure 4.12. Temperature-dependence of mouse F508del-CFTR treated with ivacaftor **121**

Figure 5.1: Structural models of human-mouse CFTR chimeras **126**

Figure 5.2: Representative QPatch whole-cell recording showing the response of human WT-CFTR to ivacaftor **128**

Figure 5.3: Response of human WT-CFTR to ivacaftor as recorded using automated whole-cell patch-clamp technique **129**

Figure 5.4: Representative QPatch whole-cell recording showing the response of mouse WT-CFTR to ivacaftor **130**

Figure 5.5: Response of mouse WT-CFTR to ivacaftor as recorded using automated whole-cell patch-clamp technique **131**

Figure 5.6: Representative QPatch whole-cell recordings showing the response of human-mouse CFTR whole-domain chimeras to ivacaftor **133**

Figure 5.7: Effects of ivacaftor on human-mouse CFTR whole-domain chimeras **134**

Figure 5.8: Representative QPatch whole-cell recordings showing the response of human-mouse CFTR TM-helix chimeras to ivacaftor **137**

Figure 5.9: Effects of ivacaftor on human-mouse CFTR TM-helix chimeras **138**

Figure 5.10: Representative QPatch whole-cell recordings showing the effects of 10 μM ivacaftor on human-mouse CFTR RD and RI chimeras **140**

Figure 5.11: Effects of ivacaftor on the human-mouse CFTR chimeras hmRD and hmRI **140**

Figure 5.12: Summary of gating properties of human-mouse CFTR chimeras **143**

Figure 5.13: Effects of ivacaftor on the single-channel activity of the human-mouse NBD1/2 chimera **145**

Figure 5.14: Effects of ivacaftor on the single-channel activity of the human-mouse TM5+6 chimera **147**

Figure 5.15: Effects of ivacaftor on the single-channel activity of the human-mouse TM5+6:9+10 chimera **148**

Figure 5.16. Sequence alignment of human WT CFTR and hmTM5+6 chimera between residues 307 and 355 ..... **149**

Figure 5.17: Identities and locations of human-mouse sequence alterations involved in determining the potentiation of CFTR by ivacaftor..... **150**

Figure 5.18: Effect of 10 μM ivacaftor on human-mouse CFTR chimeras following activation by FSK **154**

Figure 5.19: Sequence alignment for human and mouse NBD1..... **155**

Figure 5.20: Human-Mouse sequence alignment of residues within ICL4 identified as a potential ivacaftor-binding site by HDX **156**

Figure 6.1: Relationship between CFTR single channel conductance (γ) and mean body temperature in endothermic vertebrates **164**

List of tables

Table 1.1: *Example CF-causing mutations according to classification and potential therapeutic aims/strategies*..... **19**

Table 1.2: *Key non-symptomatic treatments for cystic fibrosis* **21**

Table 2.1: *Human and mouse WT and chimeric cDNA constructs* **53**

Table 3.1: *Sequence homologies of CFTR orthologues used in this study*..... **72**

Table 3.2: *Open- and closed-time constants of human WT- and F508del-CFTR* **82**

Table 3.3: *Open- and closed-time constants of mouse WT- and F508del-CFTR* **87**

Table 5.1: *Human and mouse WT and chimeric cDNA constructs used in this study*..... **125**

1. Introduction

1.1 Aetiology and epidemiology of cystic fibrosis

Cystic fibrosis (CF) is one of the most common life-shortening autosomal recessive disorders among Caucasians with an estimated incidence of 1 in 2,000-3,000 births in European-derived populations, corresponding to a carrier frequency of up to 1 in every 26 individuals (Romeo *et al.*, 1989; Farrell, 2000; Bobadilla *et al.*, 2002). Whilst incidence of CF within European countries is variable (ranging from 1 in 1,400 in Ireland and 1 in 2,400 in the UK to 1 in 25,000 in Finland), it is much lower in non-European populations (e.g. 1 in 15,000 in African Americans and 1 in >100,000 in Asians) (O'Sullivan & Freedman, 2009; Bell *et al.*, 2015). Once considered to be primarily a paediatric disease due to low life expectancy, in recent decades advances in evidence-based care and, more recently, the development of small molecule CFTR modulators that target the underlying defect in CF have extended average life expectancy beyond ~40 years (Elborn *et al.*, 1991; Burgel *et al.*, 2015; Elborn, 2016; Ramsey & Welsh, 2017). However, there is still no cure for the disease.

CF disrupts fluid movement across epithelial membranes throughout the body, including the respiratory, gastro-intestinal and reproductive systems, and can lead to diverse organ pathologies that may include respiratory disease, pancreatic insufficiency, intestinal obstruction and male infertility (Frizzell & Hanrahan, 2012; Wang *et al.*, 2014b). However, airway disease resulting from defective transport of fluid across the respiratory epithelia and the build-up of thick, dehydrated mucus, represents the major cause of mortality in patients with CF (Ratjen *et al.*, 2015). Effective fluid secretion across the airway epithelium is necessary to ensure that mucus lining the airways is sufficiently fluid to enable clearance via ciliary beating (Quinton, 1999). This process of mucociliary clearance (MCC) is required for the effective removal of potentially harmful bacteria such as *Staphylococcus aureus* and *Pseudomonas aeruginosa* as well as other pathogens including viruses and fungi (e.g. *Aspergillus spp.*) from the respiratory system (Gilligan, 1991). In patients with CF however, disruption of fluid movement across this epithelium results in a build-up of viscous mucus that cannot be cleared, increasing the risk of infection. Repeated and

chronic pulmonary infections in the CF lung can therefore lead to scarring and progressive deterioration in lung function, reducing the capacity of the CF lung for normal gaseous exchange and eventually leading to pulmonary failure (Gilligan, 1991; Rowe *et al.*, 2005).

In the early 1980s, Quinton (1983) determined that reduced Cl^- permeability in the sweat ducts of CF patients was the cause of poor NaCl reabsorption. Riordan *et al.* (1989) identified the gene involved in CF, a region spanning over 250 kb on chromosome 7 and consisting of 27 exons that encode a protein with 1480 amino acids (a.a.) with a molecular mass of 168,138 Daltons. The protein in question was found to share structural similarities with the mammalian multi-drug resistance protein P-glycoprotein, a member of the ATP-binding cassette (ABC) transporter family of membrane transporters (Juliano & Ling, 1976; Riordan *et al.*, 1989; Senior & Gadsby, 1997). These similarities included 2 repeated motifs, each with a transmembrane-spanning domain (TMD) and a nucleotide-binding domain (NBD), although CFTR also includes an additional regulatory domain (RD) between these two motifs that is unique to CFTR (Figure 1.1) (Riordan *et al.*, 1989). For this reason, Riordan *et al*. (1989) hypothesised that the protein in question was likely to be involved in membrane transport, and so named it the Cystic Fibrosis Transmembrane Conductance Regulator (CFTR), although it's role as an ion channel at that time was not known. CFTR is now known to belong to the C subfamily of the ABC transporter superfamily of membrane proteins and as such has been given the designation ABCC7 (Holland, 2003; Jordan *et al.*, 2008). However unlike other ABC transporters, which utilise the energy derived from ATP hydrolysis to actively transport substrates across the plasma membrane, CFTR is unique, functioning as a low conductance (6 - 10 pS), ATP-regulated anion-selective channel with channel gating regulated by binding of ATP at the NBDs and phosphorylation of consensus phosphorylation sites located within the RD (Sheppard & Welsh, 1999; Vergani *et al.*, 2005b).

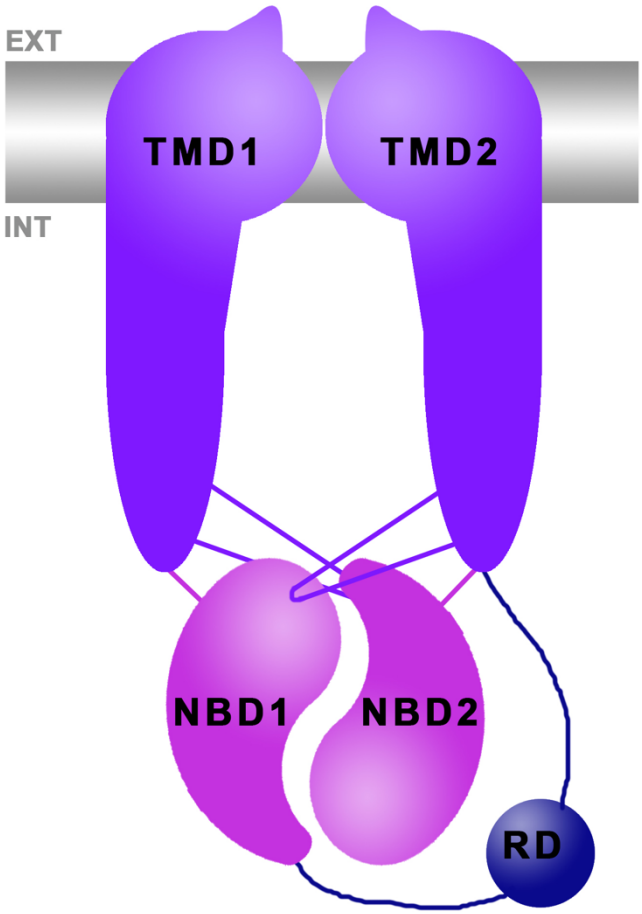

Figure 1.1: Schematic cartoon indicating the domain arrangement of CFTR. The CFTR protein shares many structural similarities with other members of the ABC-transporter family of membrane proteins and consists of two repeated motifs, each comprising a membrane bound transmembrane domain (TMD) and a nucleotide-binding domain (NBD). These two repeated domains are connected via a fifth, regulatory domain (RD), phosphorylation of which is involved in regulating the gating behaviour of CFTR (Riordan *et al.*, 1989). EXT = extracellular, INT = intracellular.

CFTR plays an important role in controlling fluid flux across epithelial membranes, principally via regulation of Cl^- secretion, which establishes both the electrochemical and osmotic driving forces for Na^+ and H_2O movement (Frizzell & Hanrahan, 2012). In addition, CFTR facilitates HCO_3^- secretion, which has an antibacterial role, is important for neutralising mucosal pH and contributes to the physiochemical properties of the mucosal layer (Frizzell & Hanrahan, 2012; Shamsuddin & Quinton, 2014; Stoltz *et al.*, 2015). The key role of CFTR in epithelial fluid flux underlies the diverse pattern of organ dysfunction observed in CF (Wang *et al.*, 2014b). Historically, treatment of CF has primarily been targeted at the symptoms of the disease, including physiotherapy

to aid clearance of lung mucus, combined with antibiotics to target infection, anti-inflammatories and where possible surgery and lung transplant (Fajac & De Boeck, 2017). However, since identification of the gene involved in CF, the CF research community has focussed on the development of targeted therapies for CF that treat the root cause of the disease. Such approaches have included the use of small molecule pharmacological compounds that restore function to mutant CFTR (Becq *et al.*, 2011), gene therapy (Griesenbach *et al.*, 2015; Alton *et al.*, 2016), or bypassing the need for CFTR altogether by targeting alternative Cl^- transporters (Li *et al.*, 2016; Li *et al.*, 2017). However, in addition to the need to overcome a multitude of organ pathologies, the task of developing successful treatments for CF is further complicated by the diversity of mutations that lead to the disease. Since its discovery, over 2,000 mutations have now been identified in CFTR that can cause cystic fibrosis and a continually updated database of these mutations is maintained by the Cystic Fibrosis Mutation Database at http://genet.sickkids.on.ca/app. The vast majority of these mutations are rare, with many being identified in only one individual, however the major exception to this is the deletion of phenylalanine at position 508, commonly referred to as F508del (Kerem *et al.*, 1989). As many as 90% of CF patients are thought to carry at least one copy of the F508del allele, with ~70% patients homozygous for the mutation worldwide (Bobadilla *et al.*, 2002; Bell *et al.*, 2015).

1.2 Role of CFTR in epithelial fluid transport

Effective epithelial fluid secretion is essential for the healthy function of multiple organ systems and CFTR plays a pivotal role in this process in conjunction with other ion channels and transporters (Frizzell & Hanrahan, 2012; Saint-Criq & Gray, 2017). This involvement of CFTR is demonstrated by the multiple organ pathology observed in CF patients, with defective CFTR function contributing to impaired epithelial transport in the lungs, exocrine pancreatic insufficiency, impaired intestinal secretion (resulting in blockage of ducts and demonstrated by meconium ileus, obstruction of the small intestine in some newborn babies with CF), male infertility and ‘salty sweat’ (Rowe *et al.*, 2005; Wang *et al.*, 2014b). In the airways, the movement of H_2O and formation of the airway surface liquid (ASL) layer at the apical surface of airway epithelia is regulated via the coordination of a network of ion transport pathways, principally

involving Na^+, Cl^-, HCO_3^-, Ca^{2+}, and K^+. Figure 1.2 provides an overview of the ion channels, transporters and pathways that are known to be involved in mediating fluid secretion and maintaining the ASL. The extent to which these pathways contribute to epithelial fluid transport may vary between organ systems, as well as between different species (Ostedgaard *et al.*, 2007; Frizzell & Hanrahan, 2012; Stahl *et al.*, 2012). As progressive deterioration in lung function as a result of defective fluid secretion is the main cause of death in patients with CF, ion channels and transporters involved in this process have the potential as therapeutic targets for CF (Li *et al.*, 2017).

As shown in Figure 1.2, movement of water across epithelia may occur by either the paracellular pathway or the transcellular route through aquaporins. This movement is dependent upon an osmotic gradient from the basolateral to the apical side of the epithelial cell layer. The net movement of Na^+ and Cl^- is a major factor involved in establishing this gradient (Frizzell & Hanrahan, 2012). Na^+ ions pass via the paracellular pathway in response to the electrochemical driving force established by the transport of other ions, key to which is the transcellular transport of Cl^- (Frizzell & Hanrahan, 2012). Whilst a number of pathways are available for the apical transport of Cl^-, for example via the SLC26A9 Cl^- channel and the Ca^{2+}-activated chloride channel TMEM16A, CFTR is the predominant pathway for apical Cl^- movement in human airway epithelia (Frizzell & Hanrahan, 2012) (Figure 1.2). Furthermore, as CFTR gating is dependent upon both binding of ATP at the NBDs and phosphorylation of the RD, the role of CFTR in apical movement of Cl^- facilitates regulation of fluid movement via the cAMP/PKA signalling pathway (Riordan *et al.*, 1989; Vergani *et al.*, 2005a). Absorption of Na^+ occurs via the amiloride-sensitive epithelial sodium channel (ENaC), and it has been proposed that specific regions of airway epithelia are specialised for either absorption or secretion (Shamsuddin & Quinton, 2012). The apical absorption of Na^+ via ENaC is enhanced in patients with CF and there appears to be a reciprocal relationship between CFTR-mediated Cl^- efflux and ENaC activity, suggesting a mechanism of interaction between CFTR and ENaC, either directly or via intermediary proteins (Stutts *et al.*, 1995; Letz & Korbmacher, 1997; Berdiev *et al.*, 2009).

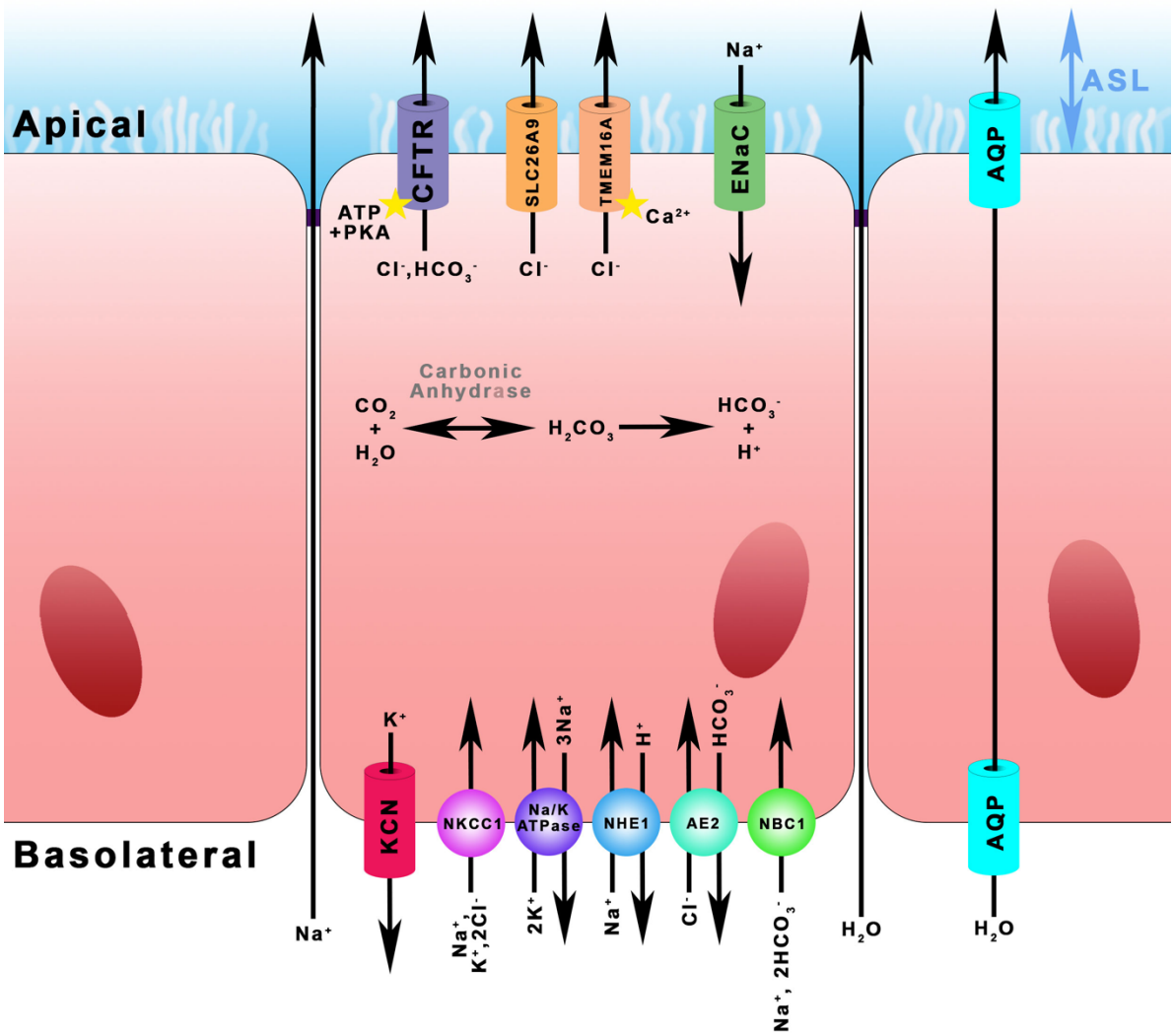

Figure 1.2: Schematic of the pathways involved in epithelial fluid transport. Net secretion of Cl^- establishes a gradient for the transepithelial movement of Na^+ via paracellular pathways and this in turn establishes an osmotic gradient favouring the secretion of H_2O via the paracellular pathway or transcellular pathway through aquaporins (AQP) such as AQP3 (Frizzell & Hanrahan, 2012; Saint-Criq & Gray, 2017). At the basolateral membrane, Cl^- transport occurs primarily via cotransport with Na^+ and K^+ by the NKCC1 cotransporter. This is driven by the electrochemical gradient established by the Na^+/K^+ATPase, which exchanges Na^+ for K^+, and subsequent K^+ efflux via KCN channels (e.g. KCNQ1, KCNE2, KCNE3 and KCNN4). Basolateral Cl^- transport is supplemented by the Na^+-independent anion exchanger AE2 (SLC4A2) in exchange for HCO_3^-. Cellular pH is regulated by basolateral transport of HCO_3^- via the electrogenic sodium bicarbonate cotransporter 1 (NBC1/SLC4A4) in conjunction with Na^+ and via the conversion of CO_2 and H_2O to HCO_3^- and H^+ as catalysed by carbonic anhydrase. H^+ efflux at the basolateral membrane occurs via the sodium-hydrogen antiporter 1 (NHE1/SLC9A1). At the apical membrane, Cl^- efflux into the airway surface liquid (ASL) layer occurs principally via CFTR. Apical Cl^- efflux is also supplemented via the Ca^{2+}-activated Cl^--channel TMEM16A and SLC26A9. Absorption of Na^+ at the apical membrane occurs via the epithelial sodium channel (ENaC) and is enhanced in patients with CF, contributing to ASL dehydration. Figure adapted from Frizzell and Hanrahan (2012) and Saint-Criq and Gray (2017).

The primary route for Cl^- entry to epithelial cells at the basolateral membrane is via the Na^+, K^+, Cl^--cotransporter (NKCC1), the driving force for which, the inward electrochemical gradient of Na^+, is established by the active transport of Na^+ and K^+ via the Na^+/K^+-ATPase. The Na^+/K^+-ATPase transports three Na^+ ions out of the cell in exchange for two K^+ ions, the energy for which is derived from the conversion of one molecule of ATP to ADP (Skou, 1957, 1965, 1998). K^+ ions that have entered the cell are then able to exit via KCN channels in the basolateral membrane, the identity of which varies between cell type, but in airway epithelia includes the cAMP-activated KCNE1,2 and KCNQ1 channels, as well as Ca^{2+}-activated KCNN4 (Liao *et al.*, 2005; Frizzell & Hanrahan, 2012; Saint-Criq & Gray, 2017). This efflux of K^+ is a major determinant of the negative-inside basolateral membrane potential. Splice variants of KCNN4 have also been identified at the apical membrane where they are able to enhance the driving force for Cl^- secretion following activation by elevated Ca^{2+} (Joiner *et al.*, 2003; Nanda Kumar *et al.*, 2010; Frizzell & Hanrahan, 2012; Saint-Criq & Gray, 2017). Additional basolateral Cl^- transport may occur in exchange for HCO_3^- via the Na^+-independent anion exchanger AE2 (SLC4A2), which is highly expressed in gut epithelial cells and has also been identified in cultured human airway epithelial cells (Calu-3) (Loffing *et al.*, 2000; Gawenis *et al.*,2004; Garnett *et al.* 2011; Shan *et al.*, 2011; Frizzell & Hanrahan, 2012; Huang *et al.*, 2012; Haq *et al.*, 2016).

Intracellular pH is a further determinant of epithelial anion secretion. Intracellular pH is primarily controlled by the co-ordination of the basolateral Cl^-/HCO_3^- and Na^+/H^+ exchangers AE2 and NHE1 (Novak & Young, 1986; Pirani *et al.*, 1987; Haq *et al.*, 2016), basolateral HCO_3^- entry via the Na^+/HCO_3^- cotransporter 1 (NBC1) and the conversion of intracellular CO_2 and H_2O to HCO_3^- and H^+ as catalysed by carbonic anhydrase (Frizzell & Hanrahan, 2012; Saint-Criq & Gray, 2017). CFTR also plays an important role in the secretion of HCO_3^- which is important for maintaining the pH of the ASL and secretions in other organs including the pancreas (Poulsen *et al.*, 1994; Shamsuddin & Quinton, 2014). Maintenance of correct pH is important for the action of antibacterial defence mechanisms and maintaining the correct mucosal structure (Shamsuddin & Quinton, 2014).

1.3 CFTR structure and function

1.3.1 Structure of CFTR

CFTR shares many structural similarities with other members of the ABC transporter family. As shown in Figure 1.3, CFTR forms a largely symmetrical protein, with two transmembrane domains (TMD1 and 2), each consisting of six transmembrane helices (TM1-12) that together form the transmembrane pore of the protein, and two cytoplasmic nucleotide-binding domains (NBDs) (Liu *et al.*, 2017). As their name suggests, the NBDs contain two ATP-binding sites, each formed by the Walker A (WA) and Walker B (WB) sites on the 'head' of one NBD and the ABC-specific signature sequence (LSGGQ) located on the 'tail' of the opposing NBD (Figures 1.3 and 1.4) (Vergani *et al.*, 2005b). An additional domain, the regulatory domain (RD) is unique to CFTR among the ABC transporter family and consists of a ~200 a.a. region linking the C-terminus of NBD1 with the N-terminus of TMD2. The RD contains consensus protein kinase A (PKA) phosphorylation sites as well as sites for phosphorylation by protein kinase C (PKC) and 5' adenosine monophosphate-activated protein kinase (AMPK) (Riordan *et al.*, 1989; Dahan *et al.*, 2001; Moran, 2017). More recently, the use of electron cryo-microscopy (cryo-EM) has revealed an additional structure formed by the N-terminal region of TMD1, termed the lasso motif (LM) due to its resemblance to a lasso, that appears to lie perpendicular to the TM helices of TMD1 (Zhang & Chen, 2016; Liu *et al.*, 2017) (Figure 1.3). The functional importance of this motif is as yet unclear, although there is evidence that interaction between the LM and NBD1 is involved in regulating ATPase activity (Ehrhardt *et al.*, 2016). The transmembrane helices of the TMDs are linked by four intra- and six extracellular loops (ICLs and ECLs, respectively) as shown in the cartoon in Figure 1.3B. Of these, the ICLs are much larger, extending well below the plasma membrane into the cytoplasm where they form coupling helices with the NBDs. The ECLs are considerably smaller than the ICLs. However, ECL4 is larger than the others and undergoes co-translational *N*-glycosylation at two sites, N894 and N900 (McClure *et al.*, 2016).

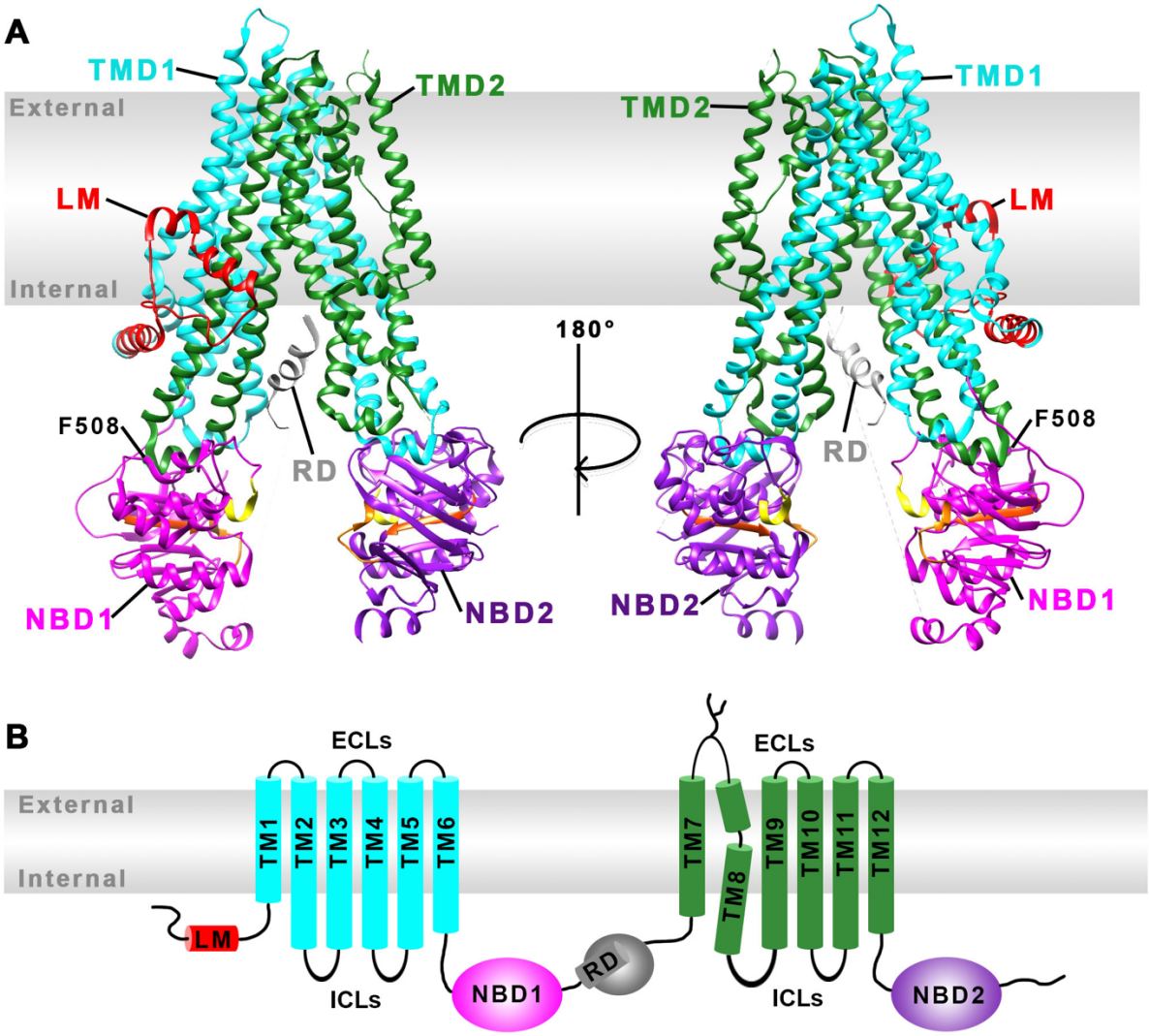

Figure 1.3: Structure of the human CFTR ion channel. A Structure of human CFTR based upon cryo-EM data, PDB: 5UAK (Liu *et al.*, 2017). Structures include lasso motif (LM, red), transmembrane domains (TMD1, cyan; TMD2, green) and nucleotide-binding domains (NBD1, magenta; NBD2, purple). The structure of the regulatory domain (RD, grey) has not yet been observed distinctly from cryo-EM studies. However, a helical structure thought to correspond to part of the RD has been observed located within the intracellular vestibule between the TMDs and is shown here. The NBD sequences corresponding to the LSGGQ, Walker A and Walker B consensus sequences, which are involved in binding and hydrolysis of ATP are highlighted here in yellow, orange and dark orange, respectively. The grey shaded area represents the predicted location of the plasma membrane. The location of F508 has been highlighted. **B** Cartoon indicating the domain structure of CFTR. Branched structures in ECL4 represent sites of N-glycosylation.

For many years, the lack of a high-resolution structure of CFTR, confounded by the challenges associated with expressing and purifying sufficient quantities of the protein, provided a major barrier to CF research (Pollock *et al.*, 2015). Whilst x-ray crystallography enabled determination of the structure of the NBDs at an atomic level

(Lewis *et al.*, 2004; Atwell *et al.*, 2010; Lewis *et al.*, 2010), a high-resolution structure of the TMDs and RD remained elusive until advances were made in cryo-EM. Prior to this, high-resolution structures obtained for related ABC transporters including the multidrug resistance transporter P-glycoprotein (Pgp) (Aller *et al.*, 2009), the bacterial transporter Sav1866 (Dawson & Locher, 2006, 2007) and bacterial lipid flippase MsbA (Ward *et al.*, 2007) provided the best approximation of CFTR structure. These homologues provided the basis for a number of CFTR models that could be used to make inferences about CFTR structure-function relationships (Mornon *et al.*, 2008; Serohijos *et al.*, 2008; Dalton *et al.*, 2012; Corradi *et al.*, 2015).

The first high-resolution structure of the entire CFTR protein itself was obtained using the zebrafish CFTR orthologue in the inactive (closed) ATP-free, unphosphorylated state (Zhang & Chen, 2016), closely followed by the human CFTR structure as shown in Figure 1.3A (Liu *et al.*, 2017). Despite only sharing 55% amino acid identity, the resulting structures of these two CFTR orthologues were remarkably similar (Liu *et al.*, 2017; Zhang *et al.*, 2017). These structures identified a number of unique features that had not been predicted using homology models. One such feature was the presence of a novel interfacial motif termed the ‘lasso-motif’ due to its morphological resemblance to a rope lasso and possible involvement in mediating protein-protein interactions (Ford, 2017). In addition, a break in the secondary structure of TM8 was observed, possibly enabling interaction of main-chain residues with ions and water within the channel pore (Zhang *et al.*, 2017). To date however, cryo-EM models have not succeeded in showing a consistent structural feature that can be attributed to the RD, likely due to a largely disordered organisation of this domain, which would fail to be resolved in cryo-EM images (Zhang & Chen, 2016). However, as shown in Figure 1.3A, an α-helical region was identified that occupies the intracellular vestibule of the channel pore between the ICLs, and this structure has been proposed to correspond to a section of the RD (Zhang & Chen, 2016). As the structure solved by Zhang and Chen (2016) was obtained using the non-phosphorylated closed configuration of the channel, it was suggested that the RD appears to occupy the space between the ICLs and NBDs in this state, preventing tight dimerisation of the NBDs. This observation suggests the possibility that phosphorylation of the RD may be required in order to expose the ATP-binding sites for interaction with ATP and allow NBD dimerisation (Baker *et al.*, 2007), in line with experimental data for human CFTR that show

decreased CFTR ATPase activity in the absence of phosphorylation (Li *et al.*, 1996; Eckford *et al.*, 2012).

1.3.2 Control of CFTR gating

Gating of CFTR is strongly linked to ATP binding and hydrolysis at the NBDs (Vergani *et al.*, 2003; Vergani *et al.*, 2005b; Jih & Hwang, 2012, 2013), which as with many other ABC transporters form a head-to-tail dimer with two ATP-binding sites located in-between them (Lewis *et al.*, 2004) (Figure 1.4). As mentioned above, these ATP-binding sites are each formed by the WA and WB sites on the head of one NBD and the corresponding ABC-specific "LSGGQ" signature sequence on the tail of the other (Smith *et al.*, 2002; Higgins & Linton, 2004). Channel closing is linked to the dissociation of the NBD dimer, and is therefore dependent upon hydrolysis of ATP at the site formed by the WA and WB of NBD2 (Carson *et al.*, 1995a; Gunderson & Kopito, 1995; Vergani *et al.*, 2005b) (Figure 1.4). At the time of writing, a high resolution cryo-EM structure of the fully open CFTR channel has not yet been obtained, however the Chen group have published a structure of the zebrafish CFTR channel in the phosphorylated, ATP-bound, NBD dimerised conformation (Zhang *et al.*, 2017). In order to achieve this, a mutated version of the zebrafish CFTR channel was used (E1372Q, equivalent to E1371Q in the human sequence) where a glutamic acid residue located within the WB consensus site of NBD2 was switched to a glutamine residue, abolishing ATP hydrolysis at this site and prolonging pore closure (Vergani *et al.*, 2005b; Zhang *et al.*, 2017). In this case, the pore itself remains occluded at the apical, extracellular opening due to the configuration of the extracellular loops, however the structure does show some important structural changes that occur as result of NBD dimerisation.

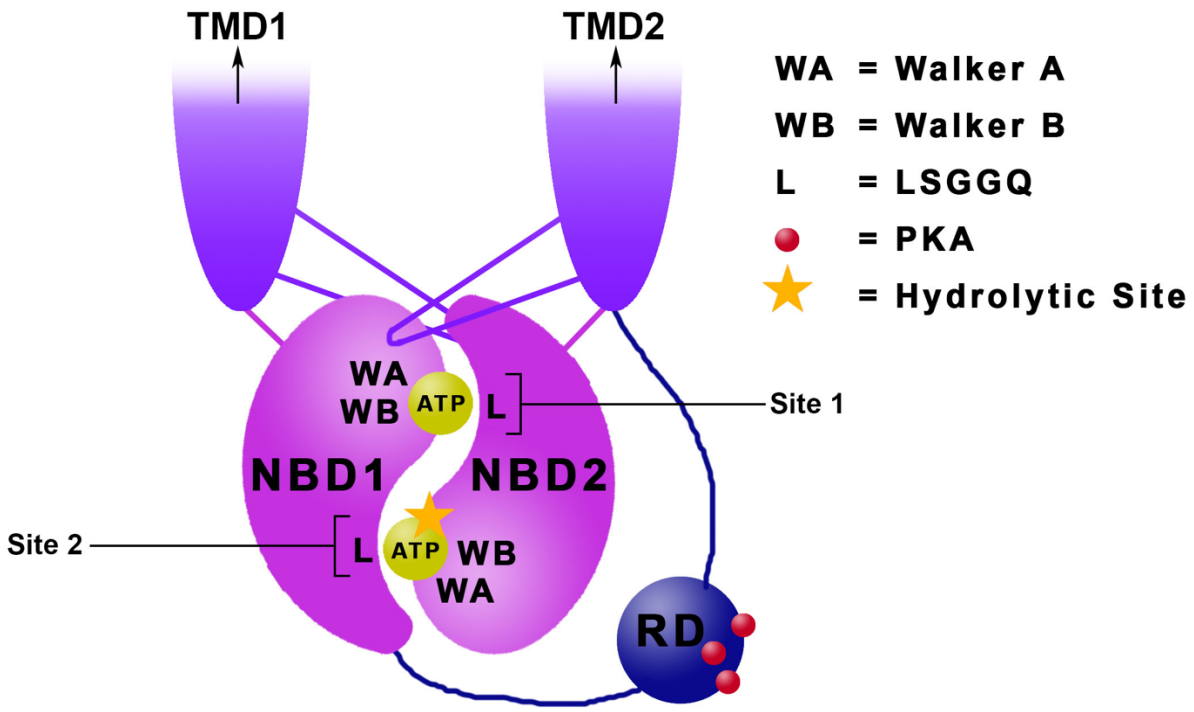

Figure 1.4: ATP-binding and hydrolysis at the CFTR nucleotide-binding domains. CFTR gating is linked to binding of ATP in binding pockets located at the interface between NBD1 and NBD2. In common with other members of the ABC transporter superfamily of membrane proteins, each binding pocket is formed by the association of the Walker A and B (WA and WB) sites located within the 'head' region of one NBD and the ABC-specific signature sequence LSGGQ located within the tail of the opposite NBD. Whilst ATP may remain bound for several minutes at the so-called 'degenerate' site at the head of NBD1, channel closing is linked to the hydrolysis of ATP at the hydrolytic site formed by the head of NBD2 (Vergani *et al.*, 2005a; Vergani *et al.*, 2005b). CFTR gating is further dependent upon phosphorylation of consensus sequences located within the regulatory domain by both PKA and PKC (Riordan *et al.*, 1989; Chappe *et al.*, 2003; Seavilleklein *et al.*, 2008).

In contrast to the structures obtained for the ATP-free CFTR channels from human and zebrafish, the structure of the phosphorylated, ATP-bound zebrafish channel does not show any density that could correspond to the RD, suggesting that on phosphorylation the RD becomes completely disordered and no longer occupies the region between the ICLs and NBDs (Zhang *et al.*, 2017). It is proposed that this disengagement of the RD facilitates NBD dimerisation by the binding of ATP at the two ATP-binding sites, leading to changes in the structural conformation that follow the longitudinal axis of the protein via the ICLs to the TMDs and subsequent opening of an ion conductance pathway (Sorum *et al.*, 2015; Zhang *et al.*, 2017). In the past this conformational change has been described as a "flip" between an inwardly facing,

closed configuration of the channel with a larger, inward facing intracellular vestibule formed between the ICLs, and an outward facing configuration, much like that observed for other homologous members of the ABC transporter family (Corradi *et al.*, 2015; Sorum *et al.*, 2017). However, the Chen model suggests a more subtle, rotational movement of two halves of the CFTR channel towards the molecular core. These two halves consist of TMs 1-3, 6, 10 and 11 plus NBD1 on the one side, and TMs 4-5, 7-9 and 12, plus NBD2 on the other (Zhang *et al.*, 2017). The rotational movement of these TM helices facilitates the opening of an ion conductance pathway lined with positively charged amino acid residues through the channel (Li *et al.*, 2018). However as tight dimerisation of the NBDs itself occludes the direct central ion conductance pathway at the intracellular end, the cytoplasmic entry point to the pathway is likely to involve at least one 'lateral portal' between the ICLs that is surrounded by positively charged residues that facilitate anion entry (Li *et al.*, 2018). Using patch-clamp recordings in conjunction with mutagenesis of several amino acids within the ICLs with positively charged side chains, Li et al (2018) have proposed a potential location for this lateral pore adjacent to residues R248 (ICL2) and K370 (located within the C-helix between TM6 and the regulatory insertion RI).

Due to the dependence upon ATP-binding at the NBDs, it has been proposed that gating of the CFTR channel can be considered to act in accordance with the del Castillo-Katz mechanism for agonist-activated gated ion channels, where intracellular ATP acts as the agonist for CFTR activity (del Castillo & Katz, 1957; Colquhoun, 1998; Scott-Ward *et al.*, 2007):

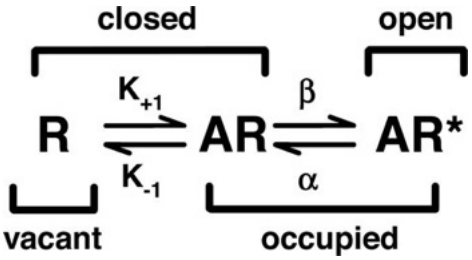

In the above mechanism, CFTR can be considered to fulfil the role of the ligand-activated receptor 'R,' with 'R*' representing the open channel following activation by binding of the ligand 'A,' in this case ATP. From this equation, the agonist equilibrium constant K_{-1}/K_{+1} represents the affinity of ATP binding to CFTR whilst β/α represents

the equilibrium constant between open and closed states of CFTR (i.e. ATP efficacy) (Colquhoun, 1998; Scott-Ward *et al.*, 2007). However, gating of CFTR relies upon further processes, i.e. binding of two molecules of ATP, phosphorylation of the RD and hydrolysis of ATP at the second ATP-binding site. Due to this asymmetry, CFTR gating is not reversible as described by the del Castillo-Katz mechanism for most ion channels, and so the equation must be modified to apply to CFTR. The scheme shown in Figure 1.5 below is an extension of the gating cycle of CFTR that has been proposed by Jih and Hwang (2013). In this representation, O1 and O2 represent stable and unstable open channel configurations, respectively, whilst C1 and C2 represent stable and unstable closed states (Jih & Hwang, 2013). According to this model, each stage in the cycle is reversible and equilibrium constants may be calculated by the rate constants indicated by the Greek letters. The stable closed, non-ATP-bound, non-phosphorylated channel is represented in this scheme by C1. The rate of transition from C2 to C1 is slow for CFTR and rare in the presence of ATP (Jih & Hwang, 2013). Binding of one molecule of ATP and phosphorylation of the RD ($C2_{ATP}$) is normally required to result in channel opening. Binding of a second ATP molecule ($C2_{ATP2}$) and NBD dimerisation ($C2_{ATP2*}$) leads to CFTR opening and the more stable open state ($O1_{2ATP*}$). Following ATP hydrolysis at the hydrolytic ATP binding site formed by WA and WB on the head of NBD2 it is proposed that CFTR may enter a brief less stable open state (O2) which will either proceed rapidly back to the closed state C2 or revert back to the stable O1 state via re-entry of ATP at the hydrolytic ATP binding site. This re-entry pathway is represented by the dashed box.

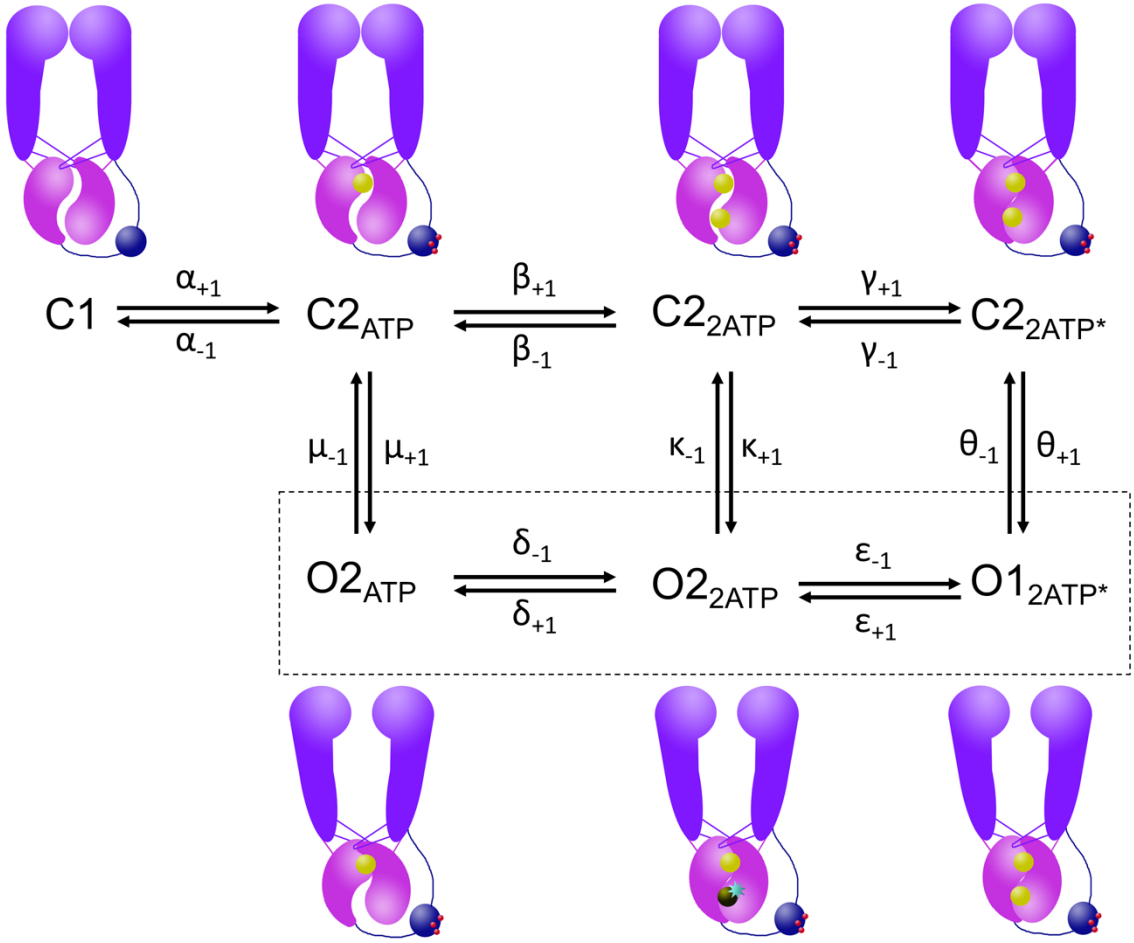

Figure 1.5: The proposed gating cycle for CFTR, adapted from Jih and Hwang (2013). In this model, CFTR may proceed from a stable closed state (C1) to a less stable closed state (C2) by binding of ATP at the non-hydrolytic site formed by WA and WB sites on the head of NBD1. Binding of ATP at the second, hydrolytic ATP binding site results in channel opening and the more stable O1 open state. Following hydrolysis of ATP at the second ATP binding site the channel enters the less stable O2 open state which will either revert back to the less stable C2 state or may return to O1 following re-entry of ATP at the hydrolytic site. This re-entry process is represented by the dashed box. Rate constants for each transition are represented by Greek letters (see text for further information).

1.4 Classification of CF causing mutations

CF-causing mutations have traditionally been classified into six groups according to their effects on channel production, processing, function, and membrane stability (Welsh & Smith, 1993; Zielenski & Tsui, 1995; Rowe *et al.*, 2005). The purpose of this classification system was to group CF-causing mutations according to potential

therapeutic strategies with the aim of developing mutation-specific personalised medicines (Amaral, 2015). This scheme for classification is summarised in Figure 1.6 with common example mutations from each class summarised in Table 1.1. Some mutations, such as the gating mutation G551D can be neatly categorised into just one of these classes, however other mutations may result in multiple defects and belong to more than one group. For this reason, it may be more appropriate to consider mutations according to their phenotype when developing therapeutic strategies (Veit *et al.*, 2016), although the traditional classification scheme remains useful for descriptive purposes. One such mutation is F508del, which results in defective CFTR processing, gating and stability at the plasma membrane (PM) and therefore can be described as a class II, III and VI mutation (Veit *et al.*, 2016). Such mutations pose a problem for the development of treatments for cystic fibrosis as multiple defects must be addressed for clinical benefit (Wang *et al.*, 2014b).

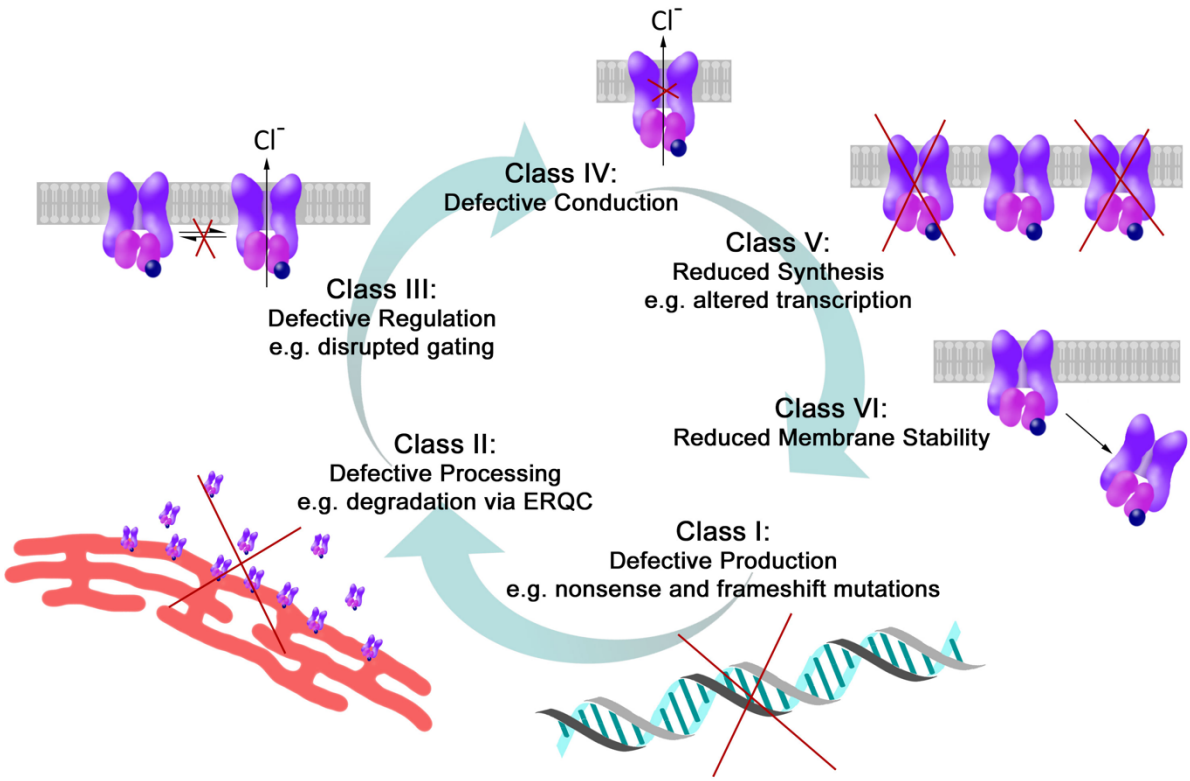

Figure 1.6: Classification of CF-causing mutations. Over 2,000 CFTR mutations have been identified that may result in a CF phenotype (http://www.genet.sickkids.on.ca/cftr/app). These mutations may be classified according to their effects on channel production (Class I), processing (Class II), regulation (Class III), conduction (Class IV), synthesis (Class V) and membrane stability (Class VI) (Welsh & Smith, 1993; Zielenski & Tsui, 1995; Rowe *et al.*, 2005). Figure previously published in (Bose *et al.*, 2015).

- **Class I mutations** result in defective channel production leading to either complete absence or a severe reduction in the amount of CFTR protein produced. Class I mutations may include premature termination codons (PTCs), splicing, frameshift or nonsense mutations (Welsh & Smith, 1993; Zielenski & Tsui, 1995; Veit *et al.*, 2016).

- **Class II mutations** include changes that result in defective channel processing and biogenesis. A classic example of a class II mutation is F508del, which results in protein misfolding and premature degradation via the endoplasmic reticulum quality control system (ERQC). Class II mutations result in a reduction in the availability of mature CFTR, leading to a deficit in the amount of active CFTR expressed at the cell membrane (Welsh & Smith, 1993; Zielenski & Tsui, 1995; Veit *et al.*, 2016).

- **Class III mutations** lead to defective channel regulation, primarily impacting channel gating and typically resulting in a reduction in channel activity by prolonging channel closures and decreasing the proportion of time that channels occupy the stable open configuration (O1 in Figure 1.5) (Welsh & Smith, 1993; Zielenski & Tsui, 1995; Veit *et al.*, 2016).

- **Class IV mutations** impact the ion permeability pathway through the CFTR protein, resulting in a decrease in channel conductance and a reduction in the overall rate of cellular anion efflux (Sheppard *et al.*, 1993; Welsh & Smith, 1993; Zielenski & Tsui, 1995; Hämmerle *et al.*, 2001; Veit *et al.*, 2016).

- **Class V mutations** reduce CFTR expression levels, for example by affecting promoter sequences or via splice mutations. Class V mutations, e.g. A455E (Sheppard *et al.*, 1995) and P574H (Ostedgaard *et al.*, 1999) differ from Class I mutations as they do not affect CFTR structure itself, but regulate CFTR expression (Highsmith *et al.*, 1994; Zielenski & Tsui, 1995; Highsmith *et al.*,

1997; Veit *et al.*, 2016). Silent single nucleotide polymorphisms (sSNPs) that affect translation rate such as T2562G may also belong to class V (Kirchner *et al.*, 2017).

- **Class VI mutations** lead to a destabilisation of CFTR in post ER-compartments or at the PM, either by decreasing conformational stability (Haardt *et al.*, 1999) or by promoting internalisation (Silvis *et al.*, 2003; Veit *et al.*, 2016). This is well demonstrated by the thermal instability exhibited by corrected F508del-CFTR at the plasma membrane at 37 °C (Wang *et al.*, 2011b).

The classification system discussed above has become well established over past decades. However, these classifications do have some limitations, particularly as many of the most common and severe CF-causing mutations, including F508del, may result in defects that apply to multiple classes. As such the system is frequently under review and a more combined approach may need to be taken when determining the potential therapeutic targets for treating such mutations (Veit *et al.*, 2016).

	Mutation Classification					
	Class I	**Class II**	**Class III**	**Class IV**	**Class V**	**Class VI**
Defect	Defective production	Defective processing	Defective regulation	Defective conduction	Reduced synthesis	Reduced membrane stability
Example Mutations	G542X W1282X 1717-1G	F508del N1303K A561E	G551D S549N G1349D F508del	R117H R334W R347P	A455E 3272-26A>G 3849+10 kb C>T	c.120del23 F508del
Therapeutic aim	Restore synthesis	Rescue CFTR trafficking	Restore channel activity	Restore channel activity	Correct splicing /processing	Promote stability
Potential therapeutic strategies	Read-through compounds, AONs, Gene therapy	CFTR correctors (e.g. VX-809)	CFTR potentiators (e.g. VX-770)	CFTR potentiators (e.g. VX-770)	AONs potentiators Correctors	CFTR stabilisers

Table 1.1: Example CF-causing mutations according to classification and potential therapeutic strategies. Abbreviations: AON, antisense oligonucleotides; VX-770, ivacaftor and VX-809, lumacaftor. This table is adapted from Amaral (2015).

1.5 Current landscape in the treatment of CF

In 2015 an important milestone was reached that highlights advances in the development of CF therapy in recent decades. For the first time in the US, the number of adult patients (aged over 18) outnumbered the number of children with the disease (Burgel *et al.*, 2015). This remarkable statistic highlights both the dramatic leap in life expectancy that has resulted from decades of CF research, improved understanding of the disease and development of novel therapies for the disease and evidence-based care. However, it also highlights how much further there is to go in searching for a cure for the disease. Despite the work that is still to be done, there is great encouragement to be had from the fact that CF patients in 2018 can now expect to live long enough to have careers and families. This success is due to the development of therapeutic strategies that target both the symptoms of the disease (i.e.

physiotherapy and antibiotics) and the underlying cause of the disease, including pharmacological modulators of CFTR (Quon & Rowe, 2016). Since the discovery of the gene involved in the disease, there has been a shift in the direction of research into treatments for CF with a focus on targeting the root cause of the disease. Part of this effort has been to produce treatments that aim to target each of the classes of defect highlighted in Section 1.4 with the aim of developing either mutation-specific treatments or mutation-independent treatments that will be suitable for a wider range of patients regardless of the mutation involved. Recent years have seen the licensing of such compounds, including small molecule CFTR modulators such as ivacaftor and Orkambi (Vertex), and promising clinical trials of other strategies including antisense oligonucleotides (AONs) and gene therapy are currently in progress (Fajac & De Boeck, 2017). Table 1.2 summarises CF therapies that are currently either approved or undergoing clinical trials. Although a complete cure for CF is still the goal, the progress that has been made, including the licensing of ivacaftor and Orkambi, provides a proof of concept that CF may be treated using small molecule therapies. Furthermore, as CF is the most common autosomal recessive disorder among Caucasian populations, the research and treatment strategies that have been, or are being developed for CF provide hope for the treatment of other, less common monogenetic disorders (Amaral, 2015).

Table 1.2 (opposite page): Key non-symptomatic treatments for cystic fibrosis. Key treatments either approved or in development aiming at correcting the underlying defects in CFTR resulting in CF. Treatments are grouped according to their type as discussed in Section 1.5. Information in this Table is derived in part from Fajac and De Boeck (2017) with updated information on the development phase accessed at https://clinicaltrials.gov (accessed June 2018). FDA = U.S. Food and Drug Administration, EMA = European Medicines Agency.

Type	Name	Company	Development/Trial Stage
Correctors	**Lumacaftor (VX-809)**	Vertex Pharmaceuticals	FDA and EMA Approved
	Tezacaftor (VX-661)	Vertex Pharmaceuticals	FDA approved
	VX-152	Vertex Pharmaceuticals	Phase IIb (In combination)
	VX-440	Vertex Pharmaceuticals	Phase IIb (In combination)
	Riociguat (Adempas)	Bayer	Phase II
	GLPG2222	Galapagos/AbbVie	Phase II
	FDL169	Flatley Discovery Lab	Phase I (Complete)
Potentiators	**Ivacaftor (VX-770; Kalydeco)**	Vertex Pharmaceuticals	FDA and EMA Approved
	QBW251	Novartis	Phase II
	GLPG1837	Galapagos/AbbVie	Phase II (Complete)
	CTP-656	Concert Pharmaceuticals/ Vertex	Phase II
Combination Therapies	**Orkambi (Ivacaftor + Lumacaftor)**	Vertex Pharmaceuticals	FDA and EMA Approved
	Symdeko (Tezacaftor + Ivacaftor)	Vertex Pharmaceuticals	FDA Approved
	VX-659 + Tezacaftor + Ivacaftor	Vertex Pharmaceuticals	Phase III
	VX-445 + Tezacaftor + Ivacaftor	Vertex Pharmaceuticals	Phase III
AONs	**Eluforsen (QR-010)**	Pro-QR Therapeutics	Phase I (Complete)
Gene Therapy	**cDNA-liposome complex (pGM169/GL67A)**	UK Cystic Fibrosis Gene Therapy Consortium	Phase IIb (Complete)
Read-through agents	**Ataluren (PTC 124)**	PTC Therapeutics	Phase III (Failed)

1.5.1 Symptomatic treatments for cystic fibrosis

Since the 1960s, treatments that targeted the organ-specific symptomatic defects of CF rather than specific defects caused by CFTR mutations formed the major strategy for patients with CF (Cohen-Cymberknoh *et al.*, 2011; Quon & Rowe, 2016; Fajac & De Boeck, 2017). The general approach for the symptomatic treatment of CF involves a combination of antibiotics to guard against and treat existing bacterial infections, treatment of inflammation, and the use of physiotherapy and other treatments to aid mucociliary clearance (Fajac & De Boeck, 2017). Mucociliary clearance in the airways may be facilitated through the use of inhaled treatments including dornase alfa (Fuchs *et al.*, 1994), hypertonic saline (Elkins *et al.*, 2006) and mannitol (Bilton *et al.*, 2013; Quon & Rowe, 2016). Whilst focus since the identification of the CFTR gene has been on treating the underlying defects of CF, it is important to note that symptomatic treatments must continue to be developed alongside targeted medicines. Not only is this important until a cure for CF has been developed, but also for patients for whom these targeted treatments have come too late to prevent existing conditions from taking hold. Furthermore, as life expectancy for CF patients is extended through the development of novel therapies, it may be necessary to develop therapies for alternative organ defects and diseases that may result from CFTR dysfunction and have hitherto been under reported due to the limited life expectancy of the disease.

1.5.2 Small molecule modulators of CFTR: Correctors and potentiators

CFTR potentiators enhance the activity of CFTR present in the PM by favouring the stable open state of the channel and are targeted for the treatment of class III and class IV mutations (Figure 1.6 and Table 1.1) (Amaral, 2015; De Boeck & Amaral, 2016). The CFTR potentiator ivacaftor (VX-770; Kalydeco®, Vertex Pharmaceuticals) was the first small molecule modulator of CFTR to be approved by the FDA (Van Goor *et al.*, 2009; Ramsey *et al.*, 2011). Ivacaftor was initially licensed for the treatment of patients carrying the third most common CF-causing class III mutation worldwide G551D, which results in a severe gating defect (Cai *et al.*, 2006; Bompadre *et al.*, 2007). However, its use has since been extended to cover a range of 38 other mutations including S549R and G1349D, as well as the class IV mutation R117H (Moss *et al.*, 2015; Sheppard *et al.*, 2017). However, CFTR potentiators rely on an existing pool of CFTR protein that is already present at the PM and as such are

unsuitable for use in patients carrying mutations that affect CFTR expression, including F508del, unless used in combination with other compounds. To date, despite benefits to many patients, combination therapies such as Orkambi and Symdeko (discussed below) have not succeeded in demonstrating the degree of efficacy demonstrated by ivacaftor for patients with pure class III mutations like G551D. For this reason, there remains a requirement for the development of CFTR potentiators that have a greater efficacy. As shown in Table 1.2, a number of candidates are currently in clinical trials including QBW251 (Novartis), CTP-656 (Concert Pharmaceuticals) and GLPG1837 (AbbVie/Galapagos), (Quon & Rowe, 2016; Fajac & De Boeck, 2017). One hurdle to the development of such compounds is that the mechanism of action of existing potentiators, including ivacaftor, is currently poorly understood. A better understanding of the mechanism by which existing CFTR potentiators work could benefit the development of novel potentiator compounds with greater efficacy for a wider range of mutations; they may also be more effective when used in combination with other compounds such as correctors. Identification of potentiators that act via different regions of the CFTR protein to correctors, for example via the TMDs rather than the NBDs, may increase efficacy. In addition, identification of multiple CFTR potentiators with different sites of action may aid the development of potentiator combinations that could be used in conjunction with correctors for mutations such as F508del.

CFTR correctors work to correct abnormal folding and processing of class II (and potentially class V) CFTR mutant channels such as F508del, increasing the number of channels that are successfully processed and therefore expressed at the PM (Quon & Rowe, 2016). CFTR mRNA is translated at the ER and the majority of tertiary folding occurs at this stage co-translationally (Kleizen *et al.*, 2005). Wild-type (WT) CFTR undergoes additional post-translational folding and is trafficked to the PM via the Golgi apparatus where glycans that have been added to the CFTR channel undergo further modification before the mature channel is expressed (Cheng *et al.*, 1990; Mijnders *et al.*, 2017). Class II mutations such as F508del however result in protein misfolding at the point of co-translational folding (Hoelen *et al.*, 2010). In this case, misfolded protein is recognised by ERQC factors and targeted to proteasomes for endoplasmic reticulum associated degradation (ERAD) (Lukacs *et al.*, 1994; Ward *et al.*, 1995). CFTR corrector compounds may therefore work by a number of mechanisms. Firstly,

they may act as a pharmacological chaperone by binding to the developing CFTR protein itself as it is translated at the ER and facilitating correct folding, preventing targeting to ERAD. Secondly, they may interact with misfolded CFTR post-translationally to correct the folded structure. Alternatively, they may function as proteostasis modulators, interacting with non-CFTR proteins that are part of the CFTR interactome and are involved in determining correct protein folding and trafficking of CFTR to either the Golgi or the proteasome (Balch *et al.*, 2008; Balch *et al.*, 2011). Lumacaftor (VX-809, Vertex Pharmaceuticals) is a corrector that is thought to interact with residues in TMD1 to stabilise mutant CFTR and correct folding early in biogenesis (Loo *et al.*, 2013; Ren *et al.*, 2013; Fajac & De Boeck, 2017).

F508del is by far the most common CF mutation with ~70% patients homozygous for this variant of the disease, (Bobadilla *et al.*, 2002) and as such the development of small molecule therapies for CF that demonstrate efficacy for patients with F508del is a key priority. In WT-CFTR, residue F508 is located in NBD1 at the interface between NBD1 and ICL4 of TMD2 (Figure 1.3) (Serohijos *et al.*, 2008; Hoelen *et al.*, 2010). Whilst F508del affects structural folding of NBD1, the correct folding of NBD2 is also reliant upon integrity of NBD1 and as a result, the mutation appears to indirectly affect the correct folding of NBD2, leading to recognition of misfolded CFTR by ERQC and subsequent degradation (Hoelen *et al.*, 2010). WT-CFTR is a relatively inefficiently folded protein, with only around 30-50% successfully reaching the PM depending upon cell type (Lukacs *et al.*, 1994; Ward & Kopito, 1994; Kleizen *et al.*, 2005). As CF is an autosomal recessive disorder and heterozygous carriers of the F508del mutation are asymptomatic, it is considered that 50% rescue of CFTR expression would be sufficient to provide enough CFTR protein at the PM for normal function. However, patients expressing just 5 – 14% of normal levels of CFTR exhibit a relatively mild CF phenotype and as such the actual amount of corrected CFTR protein required may be less than this (Ramalho *et al.*, 2002; Van Goor *et al.*, 2011). The requirement for a relatively low level of correctly processed CFTR provides strong rationale for the use of correctors in combination with potentiators to treat F508del patients. Orkambi, approved by the FDA in 2015 is one such combination therapy, combining ivacaftor and lumacaftor with the aim of achieving this goal (Okiyoneda *et al.*, 2013; Wainwright *et al.*, 2015). Lumacaftor alone has demonstrated correction of F508del-CFTR processing to levels 14% of WT (Van Goor *et al.*, 2011), a level that should

theoretically be sufficient to restore near normal levels of CFTR function to patients when used in combination with a potentiator (Ramalho *et al.*, 2002). However, by itself lumacaftor was without clinical benefit for CF patients homozygous for F508del (Clancy *et al.* 2012). Moreover, whilst the benefits of Orkambi proved sufficient to warrant FDA approval, they were relatively limited for F508del homozygous CF patients, equating to a 4.3 – 6.7% increase in the forced expiratory volume in 1 s (FEV_1) with a high percentage of patients discontinuing use of the drug due to side effects (Wainwright *et al.*, 2015). This compared to a 10.6% increase in FEV_1 and an incidence of adverse events that was lower than placebo for patients carrying the G551D mutation treated with ivacaftor alone (Ramsey *et al.*, 2011). In 2018, the FDA have approved a second combination therapy from Vertex Pharmaceuticals, Symdeko, which combines ivacaftor with the corrector tezacaftor (VX-661) taken in combination with additional doses of ivacaftor alone (Taylor-Cousar *et al.*, 2017). Combination of ivacaftor with tezacaftor rather than lumacaftor resulted in similar levels of restoration in FEV_1 compared to Orkambi, but improved levels of tolerance (Taylor-Cousar *et al.*, 2017). The relatively low level of improvements in FEV_1 resulting from these double-therapy strategies may be improved however by the use of multiple corrector compounds with different mechanism of action or binding sites, as has been shown recently for the triple combination of MCG1516A, RDR1 and VX-809, three corrector compounds that interact with different sites on NBD1 (Carlile *et al.*, 2018). Furthermore, the results from two recent phase II trials for such therapies, involving the use of either VX-659 or VX-445 in combination with ivacaftor and tezacaftor, have shown increases in FEV_1 of 13.3% (VX-659) and 13.8% (VX-445), respectively (Davies *et al.*, 2018; Keating *et al.*, 2018). This level of response exceeds that of ivacaftor for patients with G551D (Ramsey *et al.*, 2011) and it is hoped that levels of tolerance for these therapies will be comparable to those shown by Symdeko (Davies *et al.*, 2018; Keating *et al.*, 2018).

1.5.3 Genetic medicine strategies for cystic fibrosis

Due to the variety of defects that can lead to CF, targeted medicines such as small molecule modulators that can correct specific classes of CF mutation may be limited to identified populations with certain mutations. Furthermore, as the vast majority of CF mutations are rare, often only reported in one individual, this presents challenges

for both the FDA and clinicians in terms of determining the potential efficacy and tolerance of treatments for such rare mutations. Whilst great advances are being made in developing assays that can test the likely efficacy in individuals (Oliver *et al.*, 2017; Cholon & Gentzsch, 2018), it is hoped that gene therapy may hold the key to a mutation-independent approach for treating CF.

As the most common autosomal recessive disease in Western populations, discovery of the gene involved in CF led to the hope that successful correction of the disease through gene therapy would pave the way for similar success with other rare genetic disorders and since 1989 there have been a total of 27 clinical trials in CF gene therapy (Alton *et al.*, 2016). The primary aim has been to restore the production of functional CFTR in the epithelial tissue of the CF lung. Several approaches have been attempted, including the introduction of the corrected CFTR DNA sequence into the cell nucleus, mRNA therapy, which bypasses the need to introduce the whole CFTR gene into the nucleus, gene editing (e.g. via CRISPR/Cas9) and mRNA repair using antisense oligonucleotides (AONs) (Alton *et al.*, 2016).

Perhaps the largest barrier to successful genetic medicines for CF is the efficacious delivery of genetic material to lung tissue. The favoured route of administration for specific treatment of lung epithelia is via inhalation of aerosolised vectors (Alton *et al.*, 2016). In addition to penetrating the cell membrane (and nuclear membrane for gene editing and gene therapy strategies), such vectors must be able to penetrate airway mucus, mucociliary clearance and the sputum barrier as well as bypassing immune responses (Alton *et al.*, 2016). Moreover, the choice of vector must be capable of accommodating the large size of the CFTR gene (250 kb). A number of trials have been carried out utilising adenovirus or adenoassociated viruses (AAVs), however these approaches have suffered from a fall in efficacy over time as a result of immune responses following repeated doses (Griesenbach *et al.*, 2015; Alton *et al.*, 2016). For this reason, non-viral gene transfer agents (GTAs) may provide a better solution due to the reduced risk of induced immune response. Currently, the UK CF Gene Therapy Consortium has demonstrated the most promising results using a combination of the liposome-based GTA GL67A in conjunction with the pGM169 plasmid containing codon optimised CFTR cDNA (Alton *et al.*, 2015). Monthly administration of nebulised pGM169/GL67A over a period of 12 months was sufficient to improve FEV_1 in patients

by 6.4%, showing a benefit without a detectable improvement in quality of life (Alton *et al.*, 2015). Whilst the results of this trial were modest compared to trials using small molecule CFTR modulators, this is to date the first demonstration of a benefit over an extended period of administration for CF gene therapy and provides proof of concept that gene therapy is able to alter the progression of CF-related lung disease (Alton *et al.*, 2015; Alton *et al.*, 2016).

Gene editing techniques including the use of zinc finger nucleases (ZFNs), CRISPR/Cas9, and TAL-Effector Nucleases (TALENs) have all been or are currently being investigated for the treatment of CF (Urnov *et al.*, 2005; Li *et al.*, 2011; Lee *et al.*, 2012; Schwank *et al.*, 2013). However again, the biggest hurdle faced by these approaches is deliverability (Alton *et al.*, 2016).

RNA editing with the use of AONs is another genetic strategy under current investigation and has the benefits of both requiring a smaller vector for delivery and having a cytosolic activity, thereby removing the requirement to cross the nuclear membrane (Zamecnik *et al.*, 2004; Igreja *et al.*, 2016). QR-010 (eluforsen) from ProQR Therapeutics is an AON that is designed to bind to F508del-CFTR mRNA in the region of the missing F508 codon and facilitate generation of the full CFTR sequence (Zamecnik *et al.*, 2004; Beumer *et al.*, 2015). Recent results from a phase 1b study of QR-010 were promising (Elborn *et al.*, 2017).

1.6 Evolution and Diversity of CFTR orthologues

Given the similarity in structure with other members of the ABC transporter family, such as ABCC4, which utilise the energy released from ATP hydrolysis at the NBDs for active transport, is likely that CFTR evolved from an active membrane transporter, with loss of an internal gate and inclusion of the RD between NBD1 and TMD2 (Chen & Hwang, 2008; Jordan *et al.*, 2008; Sebastian *et al.*, 2013). As shown in the cladogram in Figure 1.7, the CFTR gene is present in Gnathostomata (jawed vertebrates), but absent from the non-vertebrate chordate subphyla tunicates and cephalochordates (Bose *et al.*, 2015). A report of an apparent CFTR gene expressed in the cephalochordate amphioxus *Branchiostoma floridae* (accession no.

XP002597646.1) (Pederzoli *et al.*, 2014) actually appears to be an orthologue of SLC9A2, a member of the Na^+/H^+ exchanger family and CFTR does not appear to be present within the *B. floridae* genome (Putnam *et al.*, 2008) (BLAST search of XP002597646.1 using Ensembl Genome Browser v.92 confirmed 66% shared amino acid identity with SLC9A2 (Zerbino *et al.*, 2018)). Cephalochordates are considered an extant equivalent to an early common chordate ancestor (Blair & Hedges, 2005). The identification of a CFTR orthologue that does not include the RD in lampreys (Sebastian *et al.*, 2013; Cui *et al.*, 2017), suggests that CFTR is likely to have arisen in early aquatic chordates between 652 and 891 million years ago (Blair & Hedges, 2005).

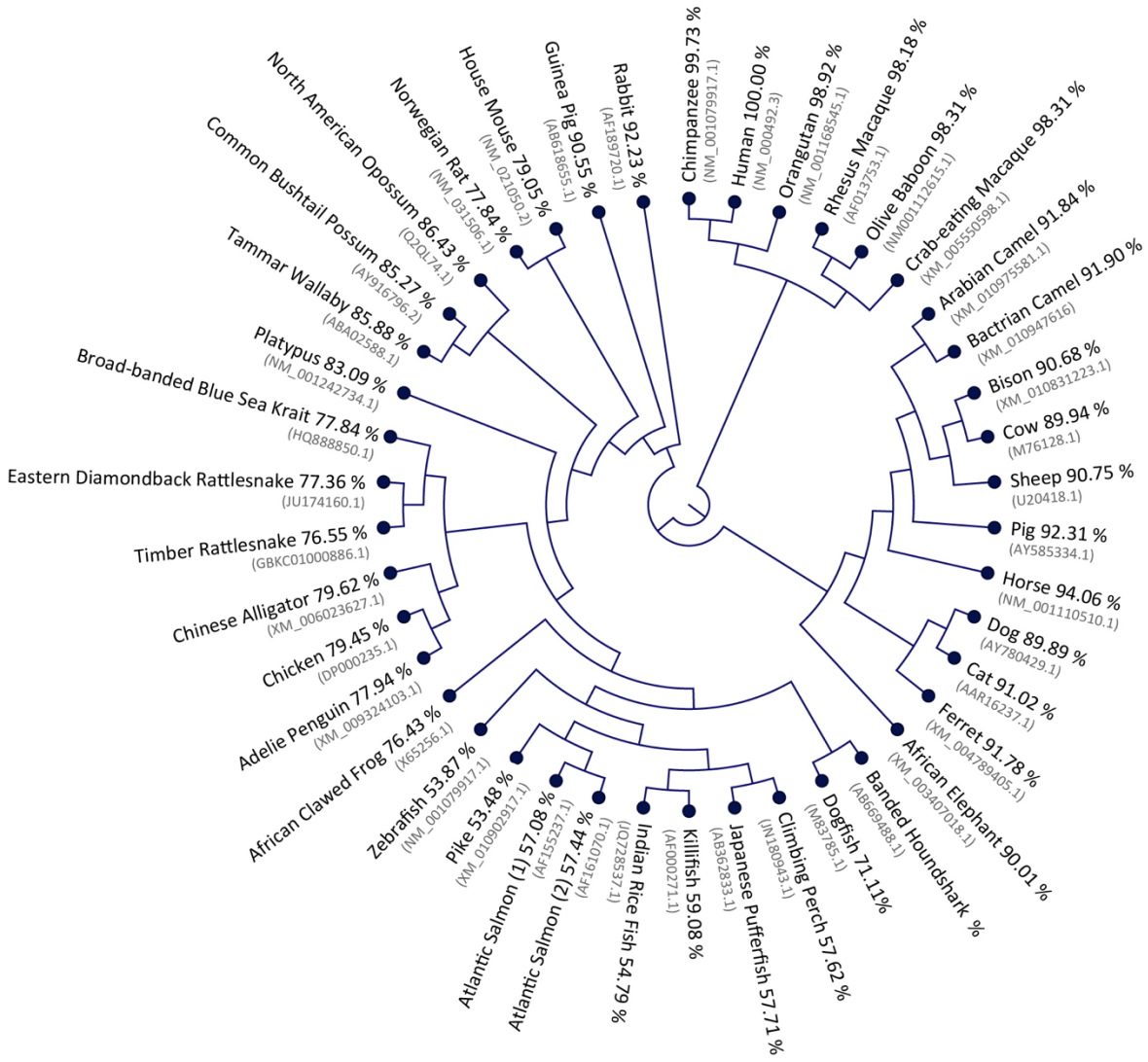

Figure 1.7: Cladogram showing the evolutionary diversity of CFTR orthologues. Cladogram was constructed by ClustalO alignment of experimentally-derived and predicted sequences using CLC sequence viewer software v.7 (Qiagen Bioinformatics). Percentages shown represent shared amino acid identity. Accession numbers for the sequences used are indicated in grey. Figure modified from Bose *et al.* (2015)

CFTR orthologues have been studied in a number of species of teleost fish, including *Takifugu rubripes* (Japanese pufferfish) (Davidson *et al.*, 2000), *Fundulus heteroclitus* (killifish) (Singer *et al.*, 1998), *Salmo salar* (Atlantic Salmon) (Chen *et al.*, 2001) and as mentioned in Section 1.3, *Danio rerio* (Zebrafish) (Navis & Bagnat, 2015; Zhang & Chen, 2016; Zhang *et al.*, 2017). In both *S. salar* and *Anguilla japonica* (Japanese eel), both euryhaline species that can move between salt and freshwater, two separate forms of CFTR are expressed in the gills (Figure 1.7) (Chen *et al.*, 2001; Nilsen *et al.*, 2007; Wong *et al.*, 2016). Regulation of the relative expression of these CFTR variants

alters according to both season and prolonged exposure to freshwater, supporting the possibility that CFTR may have evolved for the purpose of osmoregulation (Nilsen *et al.*, 2007; Bose *et al.*, 2015).

The RD, encoded by exon 15, is a unique feature of CFTR that is absent from all other members of the ABC-transporter family (Sebastian *et al.*, 2013), although Pgp does possess a linker region containing regulatory phosphorylation sites (Hardy *et al.*, 1995). Comparing the CFTR sequence with that of ABCC4, the most closely related ABC transporter homologue, Sebastian *et al.* (2013) hypothesize that the RD originates from an originally intronic sequence following the loss of a splice donor site in exon 14. Given the absence of the RD from lamprey CFTR, this inclusion is thought to have happened between 650 and 550 million years ago (Sebastian *et al.*, 2013). Sequence alignments of CFTR orthologues demonstrate that the RD is the least well conserved domain, although phosphorylation sites within the RD are highly conserved (Figure 1.8 and Appendix 1). Interestingly, sequence evolution within the RD appears to have followed a different pattern compared to other regions of CFTR and has not followed the same pattern as species evolution, accounting for the differences observed between the cladogram in Figure 1.7 and the phylogenetic tree for the same species (Sebastian *et al.*, 2013). The RD is the main region involved in this evolutionary divergence, suggesting a variation in the selection pressures for evolution of this domain, particularly in species such as mouse and rat where the evolution of CFTR appears to diverge considerably from the pattern of the phylogenetic tree (Figure 1.7) (Sebastian *et al.*, 2013).

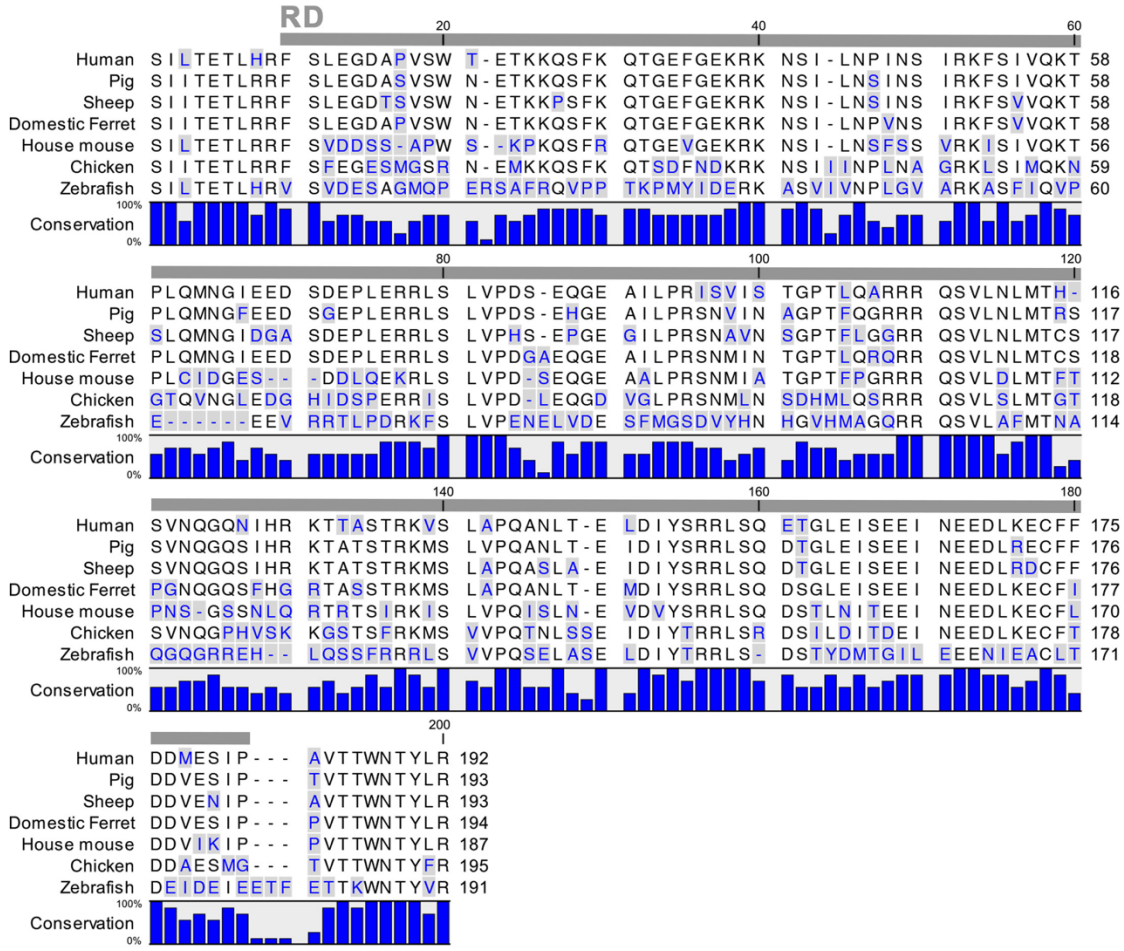

Figure 1.8: Sequence alignment of CFTR RD from diverse species. Sequences for the RD + 10 residues 5' and 3' to the human RD boundaries (F669 – P841) were aligned by ClustalO using CLC sequence viewer v.7.5 (Qiagen Bioinformatics). RD residues are indicated by the horizontal grey bar. Blue bars indicate percentage conservation.

1.7 Use of functional differences between CFTR orthologues in CF research

The large diversity of available species orthologues of CFTR has implications for CF research beyond simply gaining an understanding of how CFTR may have evolved. Species orthologues provide a repository of functional and structural variations of a protein that may demonstrate differences in both function and pharmacology that can be studied experimentally (Ostedgaard *et al.*, 2007; Stahl *et al.*, 2012; Bose *et al.*, 2015). For example, such studies may provide valuable insight into the suitability of certain species for use as animal models. These studies may also provide important insight into links between structural regions of the protein and function, or indeed

pharmacology, where specific differences are observed between orthologues with structural differences (Bose *et al.*, 2015).

1.7.1 Current understanding of species differences in CFTR structure, function and pharmacology

1.7.1.1 Species differences in CFTR conductance and gating

High-resolution, single-channel recording with the patch-clamp technique provides the best tool for characterising the gating behaviour and conductance of CFTR orthologues (Neher & Sakmann, 1976; Cai *et al.*, 2011). Utilising the excised, inside-out configuration of this technique, it is possible to activate CFTR by adding ATP and PKA to the intracellular side of the channel in the presence of an electrochemical Cl^- gradient to maximise the driving force for Cl^- movement from the intracellular (bath) solution to the extracellular (pipette) solution (Cai *et al.*, 2011). This configuration facilitates accurate control of the compositions of intra- and extracellular solutions and precise manipulation of the conditions affecting CFTR gating (Sheppard *et al.*, 2004). By holding the voltage across the cell membrane fixed (i.e. voltage-clamped) it is possible to record the change in current that occurs during channel openings, producing recordings such as those shown in Figure 1.9B. From these recordings it is possible to calculate the proportion of time that the channel occupies the open configuration (open probability, P_o), single-channel current amplitude (i), single-channel conductance ($\gamma = i/V$), mean burst duration (MBD) and interburst interval (IBI) (Figure 1.9) (Cai *et al.*, 2011). Through the generation of dwell-time histograms, it is also possible to differentiate between interburst closures and the short-lived, intraburst closures which account for the flickery closures that are present within open bursts of the channel (Figure 1.9B) (Cai *et al.*, 2011).

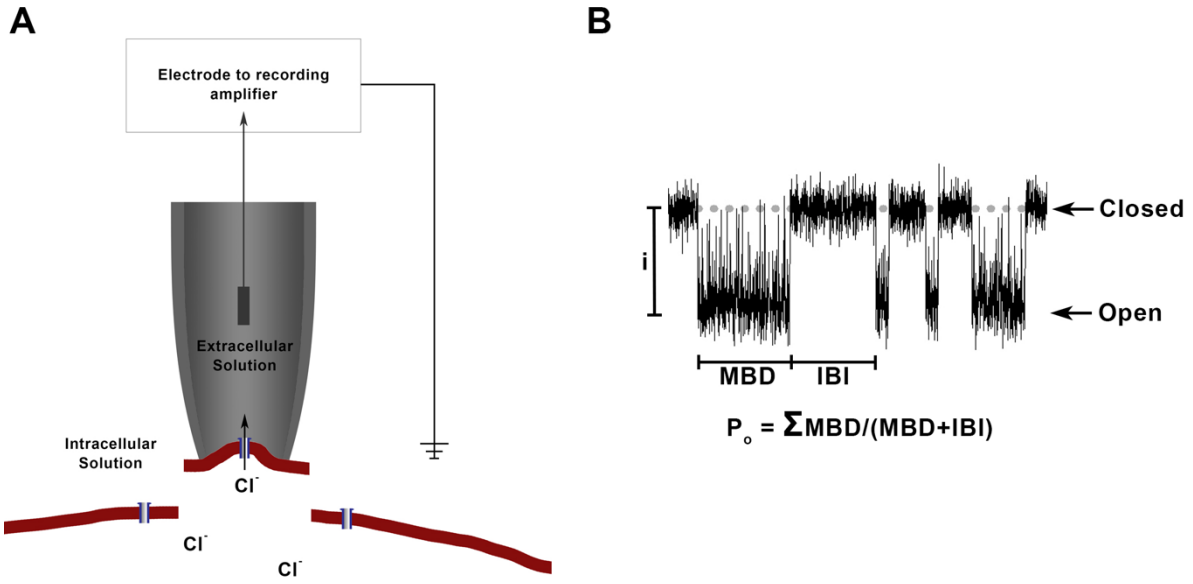

Figure 1.9: Recording the single-channel activity of CFTR using excised inside-out membrane patches. A Schematic diagram showing excised inside-out configuration of the patch-clamp technique. After the patch-pipette lightly touches the cell membrane, negative pressure is applied to the pipette to form a high resistance seal with the cell membrane (giga seal). The pipette is then withdrawn to excise a region of the membrane that contains a single CFTR channel. Following activation of CFTR by ATP and PKA added to the intracellular (bath) solution, Cl^- ions move into the low Cl^- extracellular (pipette) solution when a CFTR channel opens. Currents are recorded via a patch-clamp amplifier. **B** Example single-channel recording showing calculation of P_o. Downward deflections in the trace from the closed level (dotted line) represent channel openings. The open probability (P_o) represents the proportion of time that the channel spends in the open configuration.

Single-channel data have previously been characterised for CFTR orthologues from spiny dogfish (*Squalus acanthus*), African clawed frog (*Xenopus laevis*), house mouse (*Mus musculus*), domestic chicken (*Gallus gallus domesticus*), Australian common bushtail possum (*Trichosurus vulpecula*), European rabbit (*Oryctolagus cuniculus*), domestic sheep (*Ovis aries*) and domestic pig (*Sus scrofa domestica*) (Hanrahan *et al.*, 1993; Price *et al.*, 1996; Lansdell *et al.*, 1998a; Al-Nakkash & Reinach, 2001; Ostedgaard *et al.*, 2007; Demmers *et al.*, 2010; Aleksandrov *et al.*, 2012; Cai *et al.*, 2015). In these studies, all CFTR orthologues demonstrated cAMP-dependent and PKA-regulated Cl^- currents (Bose *et al.*, 2015). However, whilst allowing for experimental differences between separate studies, all orthologues studied have shown species-dependent variations in gating behaviour (Lansdell *et al.*, 1998b),

conductance (Cai *et al.*, 2015), ion permeability (Price *et al.*, 1996) and in some cases pharmacology (Lansdell *et al.*, 1998a).

One of the first CFTR orthologues to be studied in detail after human was mouse CFTR (Lansdell *et al.*, 1998a). Mouse CFTR was of particular interest due to the generation of mouse models of CF disease, which were quickly developed following the identification of the CFTR gene (Wilke *et al.*, 2011). Mouse WT-CFTR stably expressed in Chinese hamster ovary (CHO) cells exhibited a distinct gating behaviour that differed considerably from that of human CFTR (Lansdell *et al.*, 1998a; Lansdell *et al.*, 1998b). As shown in Figure 1.10A, additional filtering of single-channel recordings of mouse CFTR reveal two distinct conductance states, a highly active sub-conductance state (O_1) with a high P_o exceeding that of the full open state of human CFTR, and a second, fully open state that is very short lived, with brief openings and a low P_o (Figure 1.10C) (Lansdell *et al.*, 1998a; Lansdell *et al.*, 1998b). Furthermore, single-channel conductance for this O_2 state is reduced compared to human CFTR, resulting in a lower single-channel current when compared to human CFTR at the same membrane potential (Figure 1.10B) (Lansdell *et al.*, 1998a).

The reduced activity of mouse CFTR may in part account for some of the phenotypic differences between mouse models of CF and the human CF phenotype. Mouse models of CF do not exhibit the lung pathology of the human disease (Wilke *et al.*, 2011). CFTR plays a less prominent role in epithelial fluid secretion in mouse airways, with other ion channels such as TMEM16A taking over the role of the main pathway for Cl^- efflux (Wilke *et al.*, 2011). Whilst the reduced involvement of CFTR in Cl^- secretion may be the result of lower conductance, it may also be possible that the unique gating behaviour of mouse CFTR has evolved subsequent to divergence of the mouse genotype as a result of differences in the role of the channel in epithelial transport.

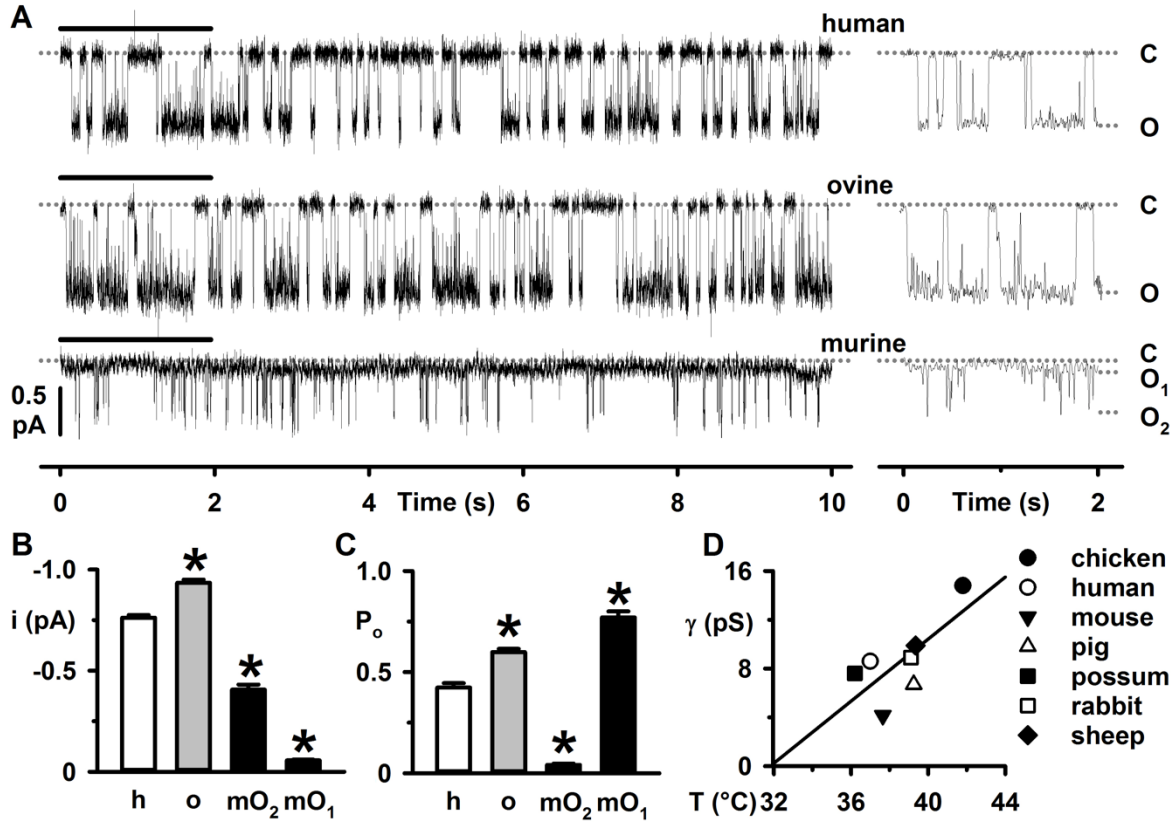

Figure 1.10: Single-channel behaviour of diverse CFTR orthologues. A Representative single-channel recordings of human, sheep (ovine) and mouse (murine) recombinant CFTR expressed in CHO cells and studied using excised inside-out membrane patches. Recordings were made in the presence of a Cl^- gradient (intracellular [Cl^-] = 147 mM, extracellular [Cl^-] = 10 mM) and following activation of CFTR using 0.3 mM ATP and 75 nM PKA. Single-channel traces were filtered at 500 Hz, digitised at 5 kHz and a 5-fold data reduction has been applied for the purpose of illustration. Expanded traces shown on the right were further filtered at 50 Hz. The closed channel state (C), sub-conductance state of mouse CFTR (O_1) and the full-open state (human and sheep = O, mouse = O_2) are indicated by dotted lines. **B** and **C** Single-channel current amplitude (i) and open probability (P_o) of human (h), sheep (o) and mouse (m) CFTR. Experimental conditions are the same as for **A**. Data are means ± SEM (human n = 10, sheep n = 24, mouse n = 5), * = $P < 0.05$ compared to human CFTR. **D** Relationship between body temperature and single-channel conductance (γ) of CFTR orthologues from endothermic vertebrates. Values of mean body temperature were accessed from Dawson & Hulbert, (1970), Hudson & Scott, (1979) and Aiello & Moses, (2010), values for single-channel conductance have been sourced from Hanrahan *et al.* (1993), Price *et al.* (1996), Lansdell *et al.* (1998a), Al-Nakkash & Reinach, (2001), Ostedgaard *et al.* (2007), Demmers *et al.* (2010), Aleksandrov *et al.* (2012) and Cai *et al.* (2015). The continuous line represents line of best fit as a result of first-order regression of the data (r^2 = 0.51). Figure 1.10 was originally published in Bose *et al.* (2015) and has been reproduced by permission of the authors.

In contrast to the reduced activity of mouse CFTR, other CFTR orthologues have been demonstrated to exhibit higher levels of activity compared to human CFTR. Sheep CFTR was characterised using single-channel patch-clamp recording by Cai *et al.* (2015), in part to assess the suitability of sheep as a potential animal model for CF. Sheep CFTR shares close homology with human CFTR, with 91% shared amino acid identity (Figure 1.7) (Cai *et al.*, 2015). Yet despite this high degree of sequence conservation, sheep CFTR demonstrated increased activity compared to human CFTR, with an increased single-channel current amplitude and higher P_o (Cai *et al.*, 2015) (Figure 1.10, A-C). Like sheep CFTR, chicken CFTR has also been shown to have an increased single-channel current amplitude and conductance compared to human CFTR, albeit with a lower P_o (Aleksandrov *et al.*, 2012). One hypothesis for the variation in CFTR conductance between species is a relationship with metabolic rate and internal body temperature (Figure 1.10D) (Bose *et al.*, 2015). However, such a relationship is highly speculative and differences in experimental conditions used across different studies must be taken into account when comparing channel conductance recordings. It must also be noted that the linear relationship shown in Figure 1.10D (r^2 = 0.51) is not maintained when poikilothermic species (e.g. X*. laevis* and *S. acanthus*) are included in the analysis.

1.7.1.2 Species variation in the effect of CF-related mutations

The two-stage pattern of CFTR glycosylation that takes place during channel maturation facilitates assessment of CFTR biosynthesis via protein assays such as Western blot and immunoprecipitation (Ostedgaard *et al.*, 2007). Immature CFTR that has undergone ER core-glycosylation and the mature forms that have undergone further glycosylation at the Golgi apparatus produce distinct bands following gel electrophoresis corresponding to ~150 kDa (band B) and ~170-190 kDa (band C) respectively (nascent, unglycosylated protein forms band A) (Ostedgaard *et al.*, 2007). Furthermore, the stability of CFTR expressed at the PM may be quantified by metabolic ^{35}[*S*]-methionine pulse-chase (Aleksandrov *et al.*, 2012; Fisher *et al.*, 2012) or by monitoring run-down of channel activity during electrophysiological recording (Wang *et al.*, 2014a). Studies utilising such techniques have highlighted cross-species variation in both WT and mutant CFTR maturation and membrane stability.

WT-CFTR homologues from a number of species, including both domestic ferret (*Mustela putorius furo*) (Fisher *et al.*, 2012) and chicken (Aleksandrov *et al.*, 2012) demonstrate enhanced maturation efficiency and stability at the PM compared to human CFTR. In addition, increased levels of F508del-CFTR maturation have been described for murine and porcine F508del-CFTR homologues when compared to human (Ostedgaard *et al.*, 2007), and the mutation appears to have a limited impact on function and maturation of chicken (Aleksandrov *et al.*, 2012) and ovine CFTR (Cai *et al.*, 2015). Increased maturation and functionality of murine and porcine F508del-CFTR is not specific to the cell line in which homologues are expressed, suggesting that structural differences between CFTR homologues are responsible for the differences in processing (Ostedgaard *et al.*, 2007). This hypothesis is further supported by the observation that substitution of key F508-interacting residues in human CFTR by their avian equivalents restores CFTR processing despite the presence of the F508del mutation (Aleksandrov *et al.*, 2012). The enhanced maturation of mouse F508del-CFTR may also be linked to the inclusion of a threonine residue at position 539 in the mouse CFTR sequence (Ostedgaard *et al.*, 2007; Hoelen *et al.*, 2010). In the case of human F508del-CFTR, the mutation I539T acts as a revertant mutant, reversing the processing defect resulting from F508del, and indeed the T539 residue is found in a number of CFTR orthologues that demonstrate enhanced maturation and membrane stability (deCarvalho *et al.*, 2002; Aleksandrov *et al.*, 2012).

Improving CFTR stability at the PM lies at the heart of therapeutic approaches for correction of class VI CF-causing mutations, including F508del. Indeed, the combined use of correctors and potentiators for the treatment of F508del is likely to be insufficient unless the issue of thermodynamic instability is also addressed (Aleksandrov *et al.,* 2012; Wang *et al.*, 2014a). In addition to the limited detrimental effects of F508del on chicken CFTR gating and maturation, chicken F508del-CFTR also appears to have little change in thermostability compared to WT (Aleksandrov *et al.*, 2012). Again, understanding how such thermostability is mediated will be a key step towards improving the efficacy of treatments for such mutations.

1.7.2 Animal models of CF

The development of animal models that accurately replicate the diverse organ pathologies of CF is essential for increasing our understanding of the disease and for testing potential new CF therapies. The first mouse model of CF was developed shortly after identification of the CFTR gene (Snouwaert *et al.*, 1992). Subsequently, a range of CF mouse models were developed by either the introduction of null mutations that result in CFTR knock-out, or introduction of CF mutations such as F508del, G551D and R117H into the mouse CFTR gene (Wilke *et al.*, 2011; McCarron *et al.*, 2018). Unfortunately, whilst these mouse models have proven useful for studying certain aspects of the disease, particularly intestinal disease, they do not accurately replicate many features of human pathology, including the airway disease phenotype (Wilke *et al.*, 2011). Furthermore, the initial mouse models of CF experienced high rates of early mortality due to intestinal obstruction (Kent *et al.*, 1996; Wilke *et al.*, 2011). The reasons for these differences in phenotype may be varied. For example, in addition to the differences in gating behaviour between human and mouse orthologues discussed earlier, CFTR plays a less dominant role in Cl^- transport in mouse airway epithelia and it has been suggested that the calcium-activated chloride channel TMEM16A takes over this role in mice (Clarke *et al.*, 1994; Grubb *et al.*, 1994; Grubb & Boucher, 1999; Wilke *et al.*, 2011; McCarron *et al.*, 2018). In addition, there are considerable differences in the anatomy and physiology of the mouse lung compared to the human (Wilke *et al.*, 2011), and as discussed earlier, mutations such as F508del do not have the same effect on mouse CFTR processing and function as they do when expressed in the human gene (Ostedgaard *et al.*, 2007).

As a result of the differences observed between the mouse and human CF phenotype, a number of advances have been made in the generation of mouse CF models. One such advance was the development of ‘gut-corrected’ mouse models, where the human CFTR gene is expressed in the mouse intestine with local expression controlled by linking the gene to the fatty acid-binding protein (FABP) (Zhou *et al.*, 1994; McCarron *et al.*, 2018). These gut corrected CF mice are less susceptible to early mortality caused by intestinal obstruction (Zhou *et al.*, 1994). The development of so-called ‘humanised’ mouse models that express human CFTR exclusively may also prove to more accurately replicate the human disease (Hodges *et al.*, 2016; McCarron *et al.*, 2018). In addition, a mouse model has been developed in which the

β-subunit of ENaC is overexpressed in the airways, resulting in a lung phenotype that more closely resembles that of human CF patients (Mall *et al.*, 2004; Zhou *et al.*, 2011). Despite these advances, the requirement for animal models that accurately replicate the human airway disease phenotype has led to the development of models using species that share closer lung physiology to humans, with models developed in rat (Tuggle *et al.*, 2014), rabbit (Xu *et al.*, 2016), ferret (Sun *et al.*, 2010) and pig (Rogers *et al.*, 2008b). A sheep CF model has also recently been developed that demonstrates many similarities to the human CF phenotype, including pancreatic fibrosis, intestinal obstruction and absence of the vas deferens (Fan *et al.* 2018). As was the case with the CF pig (Rogers *et al.*, 2008b) and CF ferret (Sun *et.al.* 2010) models, 100% of the sheep CF animals developed severe meconium ileus leading to early mortality (Fan *et al.* 2018). As such, it is not clear whether sheep CF models replicate the lung pathology observed in human patients, however the close similarities in lung physiology between sheep and humans provides rationale for the use of gut corrected sheep CF models for this purpose. (Harris, 1997; Cai *et al.*, 2015, Fan *et al.* 2018). Whilst not replicating CF airway disease, CF models have also been generated in zebrafish for the purpose of studying gastrointestinal and pancreatic insufficiency (Navis & Bagnat, 2015), and a model has been developed in Drosophila which, although not a species that expresses CFTR, replicates a CF-like phenotype as a result of enhanced ENaC activity (Kim *et al.*, 2017).

1.7.3 Use of CFTR orthologues to study CFTR structure and function

Observed differences in function between diverse CFTR orthologues provide a basis for studying structure-function relationships. One technique that has been well exploited for such studies is the use of chimeric channels, where structural regions from one orthologue are exchanged with sequences from another and used in functional studies to determine the role of specific domains in channel function (Price *et al.*, 1996; Scott-Ward *et al.*, 2007; Dong *et al.*, 2012). Whilst site-directed mutagenesis is an important tool for carrying out structure-function relationships, the use of chimeras carries certain advantages. As demonstrated by the large number of CF-related mutations identified, a single change in CFTR sequence can have dramatic effects on the processing and function of CFTR, and as such small changes in CFTR structure can lead to the generation of proteins that are not amenable to study using

single-channel patch-clamp recording. Species orthologues however, provide a library of structural variations in CFTR that can be expressed using recombinant cDNA and should produce functional versions of the protein that can be more easily studied. In addition, the CFTR channel has the propensity for multiple potentiator binding sites, and the possibility of multiple binding sites for a given potentiator may result in potential binding sites being missed by the use of site-directed mutagenesis studies (Cui *et al.*, 2016). A study by Stahl *et al.* (2012) demonstrates the potential value of using chimeras over the approach of site-directed mutagenesis. In this study, the effect of the CFTR inhibitors $CFTR_{inh}$-172 (Ma *et al.*, 2002; Caci *et al.*, 2008), glibenclamide (Sheppard & Robinson, 1997) and GlyH-101 (Muanprasat *et al.*, 2004) were studied on human, killifish, pig and shark CFTR orthologues. Stahl *et al.* (2012) reported species specific responses to CFTR inhibitors despite conservation of residues identified in previous studies using site-directed mutagenesis that were thought to correspond to the binding sites for these compounds.

As reviewed in Bose *et al.* (2015), the first example of the use of CFTR chimeras to identify structure-function relationships of the channel was the use of human-*Xenopus* chimeras to determine the involvement of ECL1 in CFTR gating (Price *et al.*, 1996). Price *et al.* (1996) generated a human-*Xenopus* chimera containing the complete *Xenopus* TMD1 sequence (hX1-6) with the remaining protein maintaining the human sequence. The hX1-6 chimera demonstrated a gating pattern that was distinct from both human and *Xenopus* WT-CFTR and shared similarities with that of the ECL1 CF mutation R117H (Sheppard *et al.*, 1993). Introduction of the ECL1 human sequence alone into the hX1-6 chimera was sufficient to restore gating behaviour to a pattern resembling that of human WT-CFTR, demonstrating the involvement of specific ECL1 residues in determining CFTR gating (Price *et al.*, 1996). In a subsequent study by Cui *et al.* (2014), three highly conserved charged residues in ECL1, D110, E116 and R117, were found to stabilise the CFTR pore by forming salt bridges with other proximal charged residues located within the outer vestibule of the CFTR pore.

1.7.4 Use of CFTR orthologues to study the mechanism of action of small molecule CFTR modulators

In addition to functional differences, species orthologues of CFTR have also been shown to exhibit notable differences in pharmacology. Lansdell *et al.* (1998a) studied the effects of the non-hydrolysable ATP analogue 5'-adenylyl-imidodiphosphate (AMP-PNP) and the inorganic phosphate analogue PP_i on mouse CFTR, two compounds that were originally used to determine the role of ATP hydrolysis in CFTR gating (Anderson *et al.*, 1991; Gunderson & Kopito, 1994; Hwang *et al.*, 1994; Carson *et al.*, 1995b). In the presence of ATP, AMP-PNP normally acts on human CFTR by prolonging the duration of open bursts (Gunderson & Kopito, 1994; Hwang *et al.*, 1994; Carson *et al.*, 1995a). In the case of mouse CFTR, AMP-PNP causes an increase in P_o but without locking the channel in the open configuration as observed for human CFTR. PP_i, which causes a robust potentiation of human CFTR and prolongs burst duration to a greater extent than AMP-PNP (Gunderson & Kopito, 1994; Carson *et al.*, 1995a; Carson *et al.*, 1995b), also had no effect on the P_o of mouse CFTR (Lansdell *et al.*, 1998a).

Further studies (de Jonge *et al.*, 2007) have also reported similar findings for other CFTR potentiators, including the Vertex potentiator VRT-532 and the benzamide derivative 5-nitro-2-(3-phenylpropylamino) benzoate (NPPB), a dual acting compound that potentiates CFTR gating at low concentrations by promoting NBD dimerization, whilst also acting as a CFTR pore blocker (Wang *et al.*, 2005; Lin *et al.*, 2016). However, there is some discrepancy in the literature regarding the response of mouse CFTR to ivacaftor. Reports from both Van Goor *et al.* (2009) and de Jonge *et al.* (2007) have suggested that mouse CFTR is not potentiated by ivacaftor. Conversely, Cui and McCarty have shown that mouse CFTR does respond to ivacaftor (Cui & McCarty, 2015; Cui *et al.*, 2016). Experimental differences do not seem to wholly account for these discrepancies, with all groups studying the effect of ivacaftor on either macroscopic membrane patches or intact epithelia at room temperature. However, the experiments performed by Cui and McCarty (2015) were carried out using mouse CFTR expressed in *Xenopus* oocytes rather than mammalian cell lines and it is therefore possible that the nature of the lipid bilayer in which the channel is expressed may have an effect on the behaviour of the channel. Indeed, it is notable that Cui and McCarty (2015) did not observe the distinct O_1 and O_2 sub-conductance and full-open

levels of mouse CFTR recorded by other groups, but reported a much higher level of sub-conductance and a full-open state of the mouse channel with a higher P_o than previously reported (Cui & McCarty, 2015). Again, it is possible that these differences are related to the environment in which the channel has been expressed, however it should be noted that other studies have shown that CFTR orthologues exhibit consistent gating behaviour regardless of expression cell type (Lansdell *et al.*, 1998a; Ostedgaard *et al.*, 2007).

Building on the observation that PP_i has no effect on P_o of mouse CFTR, Scott-Ward et al. (2007) carried out further studies using CFTR chimeras to investigate the gating properties of this orthologue and to determine the binding domain of PP_i. Human-mouse CFTR chimeras were constructed using homologous recombination where the RD, NBD1, NBD2 or both NBD1 and 2 in human CFTR were replaced by the equivalent regions from mouse CFTR. Cells expressing these chimeras produced single-channel recordings that demonstrated a current amplitude that was close to that of human CFTR and gating characteristics that were intermediate between mouse and human CFTR depending upon the domains included in the chimera (Scott-Ward *et al.*, 2007). More specifically, it was observed that inclusion of both NBD1 and NBD2 of mouse CFTR, but not the RD, was sufficient to endow the human-mouse chimeras with the gating pattern associated with the O_1 state of mouse CFTR and that inclusion of mouse NBD2, but not NBD1 augmented channel activity. These studies highlight the involvement of structural differences between human and mouse CFTR that determine channel function. By studying the effects of PP_i on human-mouse CFTR chimeras, Scott-Ward et al. (2007) demonstrated that PP_i potentiated channels containing human NBD2, but not mouse NBD2. The data suggest that, given that PP_i potentiates human, but not mouse CFTR (Lansdell *et al.*, 1998a), the mechanism of action of PP_i involves interaction of the compound with NBD2 and highlight the potential for chimeric CFTR channels to study the mechanism of action of CFTR modulators.

1.8 Current understanding of the mechanism of action of ivacaftor

1.8.1 Potentiation of CFTR by ivacaftor: Comparison with other CFTR potentiators

Potentiators act to increase the P_o of CFTR and can do so by prolonging pore openings (increased MBD) or by shortening pore closures (decreased IBI). As discussed in Section 1.3.2 and Figure 1.5, opening of the CFTR pore is dependent upon the following steps: (1) Phosphorylation of the RD, (2) ATP binding at the NBDs, (3) Tight dimerisation of the NBDs, (4) Transmission of movement along the longitudinal axis of CFTR from the NBDs to the TMDs. Pore closure is then dependent upon ATP hydrolysis (Vergani *et al.*, 2005b). CFTR activators such as UC_{CF}-152 (Pyle *et al.*, 2011) may enhance RD phosphorylation. CFTR potentiators however act by enhancing the favourability of post-phosphorylation events leading to channel opening (Yeh *et al.*, 2017), or by inhibiting ATP hydrolysis and thereby prolonging pore opening (Eckford *et al.*, 2012).

Hydrolysable ATP analogues such as N^6-(2-phenylethyl)-ATP (P-ATP) (Zhou *et al.*, 2005), 2'- and 3'- deoxy-ATP (dATP) (Aleksandrov *et al.*, 2002; Cai *et al.*, 2006) and N^6-(2-phenylethyl)-2'-deoxy-ATP (P-dATP) (Miki *et al.*, 2010) act as potentiators for CFTR by both binding more efficiently at the ATP-binding sites, and by enhancing NBD dimerisation (Yeh *et al.*, 2017). Ivacaftor however appears to potentiate CFTR independently of ATP as well as in the presence of ATP, as shown both by potentiation of the channel in the absence of Mg-ATP when purified recombinant CFTR is expressed in planar lipid bilayers (Eckford *et al.*, 2012), and after washout of ATP in excised inside-out membrane patches (Jih & Hwang, 2013). This may in part explain the efficacy of ivacaftor for patients carrying the G551D mutation, which affects the hydrolytic site formed by the WA and WB motifs on NBD2, and demonstrates only ATP-independent gating, failing to respond to dATP or AMP-PNP (Li *et al.*, 1996; Bompadre *et al.*, 2007). One proposed mechanism for ivacaftor-mediated potentiation of CFTR is therefore that the compound enhances ATP-independent gating (Eckford *et al.*, 2012).

CFTR activators promote phosphorylation of the RD. The isoxazole UC_{CF}-152 for example has been shown to act as a CFTR activator, inducing PKA-dependent phosphorylation of the RD (Pyle *et al.*, 2011). In the same study however, it was shown that neither VRT-532 nor ivacaftor enhanced phosphorylation of the RD (Pyle *et al.*, 2011). Furthermore, it has been demonstrated that ivacaftor potentiates CFTR channels that lack the RD (ΔR-CFTR) (Csanády *et al.*, 2000; Bompadre *et al.*, 2005; Jih & Hwang, 2013).

The CFTR permeant anion NO_3^- has similarly been shown to increase the P_o of ΔR-CFTR (Yeh *et al.*, 2015). However, in addition to testing NO_3^- on ΔR-CFTR, Yeh *et al.* (2015) tested both NO_3^- and ivacaftor using CFTR that had been truncated to remove NBD2 (ΔNBD2-CFTR). Both NO_3^- and ivacaftor increased the P_o of ΔNBD2-CFTR, indicating that the mechanism by which potentiation was being facilitated was independent of NBD dimerisation and ATP hydrolysis at the hydrolytic site (Yeh *et al.*, 2015). This finding is further supported by the observation that ivacaftor is effective for the potentiation of the CF mutation W1282X, which results in a truncated CFTR protein missing the C-terminal half of NBD2 (Haggie *et al.*, 2017). Interestingly, the effect of NO_3^- and ivacaftor when used in conjunction was additive, indicating independent mechanisms for potentiation (Yeh *et al.*, 2015).

Given these observations, it is therefore likely that ivacaftor favours CFTR pore opening by affecting the movement of the TMDs and acting independently of ATP binding and RD phosphorylation. According to the schematic gating model shown in Figure 1.11, we can therefore infer that ivacaftor is likely to affect the transition rates μ_{+1} κ_{+1} and θ_{+1}. Furthermore, Jih and Hwang (2013) have proposed a 're-entry' mechanism in which there is a short window of opportunity for ATP to re-occupy the hydrolytic binding site that is vacated post-hydrolysis, shifting CFTR from the unstable $O2_{ATP}$ open state back to the more stable $O1_{2ATP}$ open state (a shift from left to right in the dashed box as indicated by the red arrow in Figure 1.11) (Jih & Hwang, 2013). Jih and Hwang (2013) used multiple assays to demonstrate this idea. Firstly, using macroscopic currents recorded from inside-out membrane patches, CFTR was activated in the presence of 2.75 mM ATP which was then switched to the non-hydrolysable ATP analogue PP_i for 1 second before washout (Jih & Hwang, 2013). In the absence of ivacaftor, a current ~50 % of that in the presence of ATP was observed

following the switch to PP_i, which decayed exponentially as channels closed. This current, which was enhanced in the presence of ivacaftor, likely represents the current flowing through channels that have been locked in the O2 open state. In addition, Jih and Hwang (2013) tested the effect of ivacaftor on R352C-CFTR, a mutated channel that shows two distinct open levels of single-channel current thought to correspond to O1 and O2, respectively. In this case, ivacaftor was observed to result in a greater increase in the time the channel spent in the O2 state rather than the O1 state, suggesting that ivacaftor is prolonging the O2 state and increasing the time available for ATP re-entry at the hydrolytic binding site (Jih & Hwang, 2013).

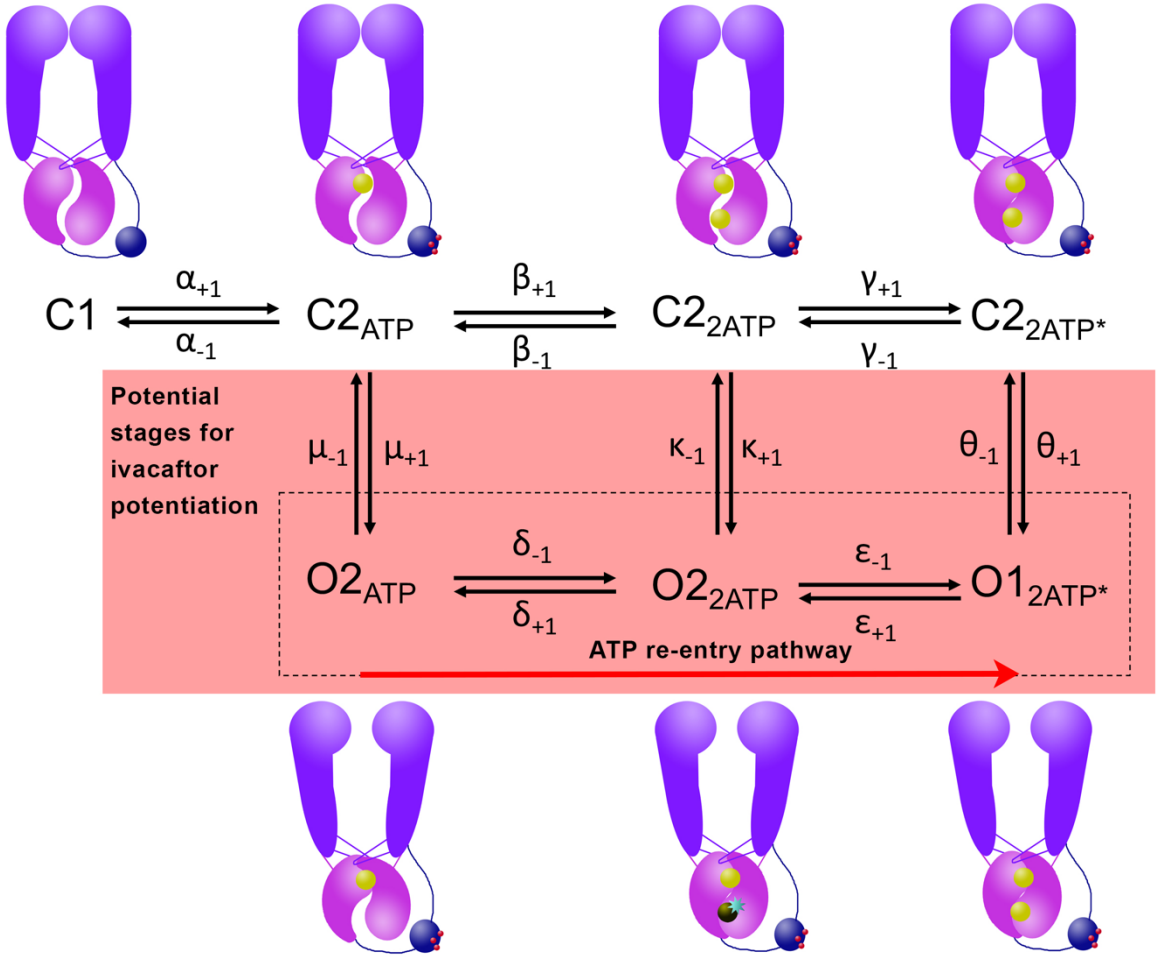

Figure 1.11: Ivacaftor modifies the gating cycle of CFTR. Potential stages in the gating cycle of CFTR that may be affected by ivacaftor are indicated by the red shading. Other details as in Figure 1.5. Adapted from Jih and Hwang (2013).

These studies indicate that ivacaftor may potentiate CFTR via two routes, increasing the likelihood of ATP-independent gating and by promoting the re-entry of ATP at the hydrolytic binding site (Eckford *et al.*, 2012; Jih & Hwang, 2013).

1.8.2 Potential binding sites for ivacaftor

Identifying the binding site for ivacaftor would represent a major step forward in determining mechanism of action and would greatly assist the design and development of novel CFTR potentiators. Ivacaftor is a highly hydrophobic compound and is therefore likely to occupy the lipid bilayer when applied to cells (Jih & Hwang, 2013). Indeed, ivacaftor has been shown to accumulate within the inner leaflet of the plasma membrane (Baroni *et al.*, 2014) and a recent study has also demonstrated that the destabilising effect of ivacaftor on CFTR membrane stability is likely to be the result of increased membrane fluidity and disruption of lipid rafts (Chin *et al.*, 2018). The accumulation of ivacaftor in the plasma membrane, coupled with the data discussed in Section 1.8.1, suggest that the binding site of ivacaftor is most likely to be located on the TMDs where they interact with the lipid bilayer, or at the interface between the TMDs and NBDs, reducing the energy barrier for pore opening independent of ATP binding at the NBDs (Jih & Hwang, 2013; Sorum *et al.*, 2015). Furthermore, this idea is supported by the observation that in excised membrane patches, ivacaftor demonstrates similar efficacy when applied either from the intra- or extracellular side of the membrane (Jih & Hwang, 2013). This result would not be expected if ivacaftor was binding at the NBDs.

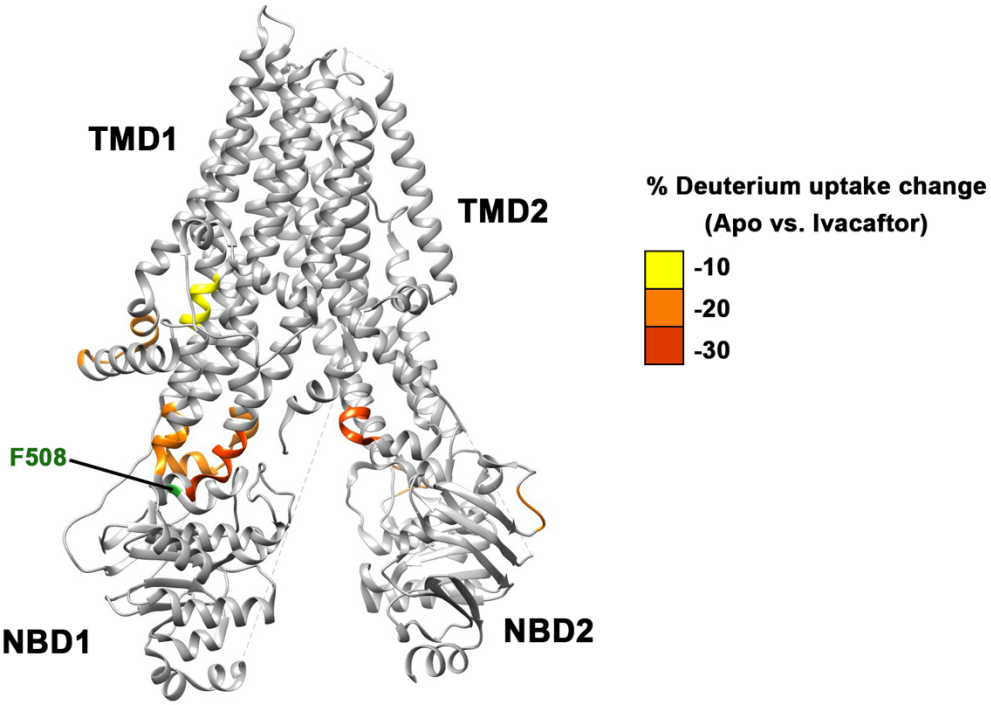

Figure 1.12: Potential binding sites of ivacaftor based upon HDX exchange. Regions where HDX exchange was reduced by -10% of that of the apo CFTR profile following addition of ivacaftor are highlighted. Regions where HDX reduction were greatest are highlighted in red. The F508 residue is highlighted in green. Based on data published by Byrnes *et al.* (2018).

A recent study by Byrnes *et al.* (2018) utilised hydrogen/deuterium exchange (HDX) mass spectrometry to identify potential binding sites for ivacaftor. In HDX, hydrogen atoms covalently bonded to amides in the backbone residues of a protein are exchanged for deuterium, with the rate of deuterium uptake indicating the solvent accessibility of these residues. Byrnes *et al.* (2018) compared deuterium uptake for both the unbound (apo) and ivacaftor bound CFTR protein to identify regions in the N-terminus, ICLs, TMD1 and NBD2 that showed protection to deuterium uptake after addition of ivacaftor (Figure 1.12) (Byrnes *et al.*, 2018). The regions that showed the highest level of protection to HDX were located within the vicinity of F508, corresponding to the interfaces between TMD2 and both NBD1 and NBD2 (Figure 1.12) (Byrnes *et al.*, 2018). These data strongly support the hypothesis that ivacaftor binds to the TMDs, facilitating movement of the protein along the longitudinal axis and subsequent opening of the channel pore. However, as average uptake of deuterium by the apo CFTR protein is only 60%, with low coverage at the TMDs due to decreased solvent accessibility in this region, it is not possible to rule out the potential for

alternative or more preferential binding sites in the regions not covered by HDX (Byrnes *et al.*, 2018). The use of functional studies, including for example the use of CFTR chimeras, could therefore yield more powerful support to these hypotheses.

1.9 Hypothesis and aims of the present study

Based on the data collected to date for the mechanism of CFTR potentiation by ivacaftor, this study aims to address the following hypothesis:

"The mechanism of action of ivacaftor involves interactions with the transmembrane helices of CFTR."

In order to test this hypothesis, we will employ the use of CFTR chimeras in a similar manner to Scott-Ward *et al.* (2007), and will be addressing the following aims:

1) **Characterise species differences in the function of diverse CFTR orthologues** - We will investigate the gating properties and single-channel behaviour of a diverse range of CFTR orthologues covering a wide spectrum of the phylogenetic tree. In order to do this, recombinant CFTR cDNAs will be expressed in mammalian cell lines and studied using high-resolution single-channel recordings.

2) **Characterise the effect of CF-causing mutations on diverse CFTR orthologues** - The impact of CF-causing mutations will be assessed on diverse CFTR orthologues. Focus will be placed on determining the effect of mutations on the gating behaviour and membrane thermal stability of CFTR.

3) **Assess pharmacological differences between different CFTR orthologues** - CFTR orthologues will be tested for their response to small molecule modulators with particular focus on ivacaftor.

4) **Identify structural regions of the CFTR protein that are involved in the mechanism of action of ivacaftor using CFTR chimeras** - Where species-specific variation in the response of CFTR orthologues are identified, we will generate CFTR chimeras and identify structural regions involved in the mechanism of action of ivacaftor by studying the effect of ivacaftor on these chimeras. These experiments will be carried out in conjunction with our industrial partner (Novartis Institutes for Biomedical Research) where the use of high-throughput, automated electrophysiology will enable testing of a large number of CFTR constructs.

2. Materials and methods

2.1 Single-channel patch-clamp recordings

2.1.1 Cell Culture

2.1.1.1 Cell lines stably expressing CFTR constructs

For single-channel patch-clamp studies of human CFTR, we used baby hamster kidney (BHK-21), Chinese hamster ovary (CHO), or NIH 3T3 cells stably transfected with WT or F508del-CFTR homologues. Cell line choice depended upon the experiment being carried out as indicated in the Results chapters and mean data represents a single choice of stable cell line throughout. BHK cells were cultured in a 1:1 mixture of Dulbecco's modified Eagle's Medium (DMEM) and Ham's F-12 nutrient medium (DMEM/F-12) that had been supplemented with 5% foetal bovine serum (FBS), 100 $U \cdot ml^{-1}$ penicillin, 100 $\mu g \cdot ml^{-1}$ streptomycin (all purchased from Invitrogen Ltd., Paisley, UK) and 200 $\mu g \cdot ml^{-1}$ methotrexate (Merck Chemicals Ltd., Nottingham, UK or AAH Pharmaceuticals Ltd., Coventry, UK). CHO cells were cultured in Ham's F-12 nutrient mixture that had been supplemented with 10% FBS, 100 $U \cdot ml^{-1}$ penicillin and 100 $\mu g \cdot ml^{-1}$ streptomycin (Invitrogen Ltd.) and 0.6 $mg \cdot ml^{-1}$ neomycin (Merck, previously Sigma-Aldrich Company Ltd., Gillingham, UK). NIH 3T3 cells were cultured in DMEM supplemented with 1% GlutaMAX supplement (Invitrogen Ltd.), 10% FBS, 100 $U \cdot ml^{-1}$ penicillin, 100 $\mu g \cdot ml^{-1}$ streptomycin and 0.25 $mg \cdot ml^{-1}$ G-418. All cells were maintained in 25 ml rectangular canted neck cell culture flasks (Corning, New York, USA) at 37 °C in a humidified atmosphere containing 5% CO_2 except where otherwise stated. Media was changed every 24-48 hours and cells were passaged when > 95% confluence was achieved by first washing with Versene solution before dissociation with 0.05% Trypsin (both from Invitrogen Ltd.). For storage, cryovials containing > 5 million cells suspended in a freezing media containing 10% dimethyl sulfoxide (DMSO) and 90% FBS were preserved in liquid nitrogen. Following defrosting, cells were used for a maximum of 10 weeks.

CHO cells stably expressing mouse WT- and F508del-CFTR were also cultured using Ham's F-12 nutrient mixture supplemented with 10% FBS, 100 $U \cdot ml^{-1}$ penicillin and

100 μg·ml^{-1} streptomycin with either 0.2 mg·ml^{-1} neomycin (mouse WT-CFTR) or 200 μg·ml^{-1} methotrexate (mouse F508del-CFTR).

For patch-clamp experiments, cells expressing WT-CFTR orthologues were seeded at low density and grown on glass coverslips in 35 x 10 mm Petri dishes (Corning) with 2.5 ml DMEM/F-12 media, incubated at 37 °C in a humidified atmosphere containing 5% CO_2 for 24-48 hours prior to each experiment. Cells expressing F508del-CFTR homologues were seeded following the same protocol as WT homologues but incubated at 27 °C in a humidified atmosphere with 5% CO_2 for at least 24 hours prior to experiments. This protocol was followed to correct the processing defect caused by the F508del mutation and restore CFTR expression at the cell membrane (Denning *et al.*, 1992). Coverslips were cut into smaller sections and media was renewed up to 24 hours prior to experiments.

2.1.1.2 Cell lines transiently expressing CFTR constructs

For generation of transiently transfected cell lines, CHO-K1 cells that did not express endogenous CFTR were used. Cells were cultured in Ham's F-12 nutrient medium supplemented with 10% FBS, 100 U·ml^{-1} penicillin and 100 μg·ml^{-1} streptomycin (all purchased from Invitrogen Ltd.). All cells were maintained in 25 ml rectangular canted neck cell culture flasks (Corning) at 37 °C in a humidified atmosphere with 5% CO_2 except where otherwise stated. Media was changed every 24-48 hours and cells were passaged as described above when > 95% confluence was achieved.

For patch-clamp experiments, cells were seeded at low density and grown on glass coverslips in 35 x 10 mm Petri dishes (Corning) with 2.5 ml Ham's F-12 media, incubated at 37 °C in a humidified atmosphere comprising 5% CO_2 for 24 - 48 hours prior to transfection. Cells were co-transfected with plasmids containing the desired CFTR orthologue together with the enhanced green fluorescent protein N1 plasmid (pEGFP-N1) transfection marker at least 24 hours before experiments using the Lipofectamine transfection system (Invitrogen Ltd.). Cells expressing F508del-CFTR orthologues were seeded following the same protocol as WT homologues, but incubated at 27 °C in a humidified atmosphere with 5% CO_2 for at least 24 - 48 hours

prior to experiments. Coverslips were cut into smaller sections and media was renewed up to 24 hours prior to experiments.

2.1.2 Plasmid design

Table 2.1 lists the human CFTR chimeras that were used in this study. Human-mouse CFTR chimeras were designed by Dr. Christopher Boyd (University of Edinburgh, UK), with the exception of constructs 5, and 16 (Table 2.1), which were generated by the laboratory of Prof. Michael J. Welsh (University of Iowa, USA). Whole-domain chimeras (constructs 3, 4 and 15) were generated via homologous recombination. Constructs 6-14 were generated following the insertion of restriction sites placed at regular intervals within the modified backbone of human WT-CFTR. Regions to be inserted were constructed by GeneArt® Gene Synthesis (ThermoFisher Scientific, Regensberg, Germany). The protocol for generation of chimeras as outlined in Scott-Ward *et al.* (2007) and Dong *et al*. (2012) was as follows:

i) Target domains from mouse-CFTR cDNA expressed in pFLM-CFTR plasmids were amplified via polymerase chain reaction (PCR) using primers containing human-CFTR sequences corresponding to the 5' ends.

ii) pCMV/pcDNA.3.1-CFTR plasmids expressing the human-CFTR sequence were linearised in the domain of interest.

iii) Products of step i) and ii) were co-electroporated into the recombinogenic *E. coli* strain DH10B-U/pSpRecGam.

iv) Intact chimeric plasmids were recovered where intermolecular recombination had been successful between homologous sequences of linear pCMV/pcDNA3.1-CFTR and PCR products.

v) Sequences were confirmed by sequencing.

vi) For automated electrophysiology, constructs were amplified to a concentration of 5 mg/ml in sterile water by LakePharma Inc., Belmont, USA

Construct No.	Construct	Residue boundaries	Plasmid	Source
1	human WT	N/A	pCMV	Edinburgh
2	mouse WT	N/A	pCMV	Edinburgh
3	hmNBD1/2	432-611:1226-1419	pCMV	Edinburgh
4	hmNBD1	432-611	pCMV	Edinburgh
5	hmNBD2	1178-1480	pcDNA3.1	Iowa
6	hmTM1-12	79-355:858-1152	pCMV	Edinburgh
7	hmTM1-6	79-355	pCMV	Edinburgh
8	hmTM7-12	858-1152	pCMV	Edinburgh
9	hmTM5+6	307-355	pCMV	Edinburgh
10	hmTM5+6:TM1+2	307-355:78-153	pCMV	Edinburgh
11	hmTM5+6:TM3+4	307-355:154-306	pCMV	Edinburgh
12	hmTM5+6:TM7+8	307-355:858-935	pCMV	Edinburgh
13	hmTM5+6:TM9+10	307-355:987-1034	pCMV	Edinburgh
14	hmTM5+6:TM11+12	307-355:1095-1152	pCMV	Edinburgh
15	hmRD	653-837	pCMV	Edinburgh
16	hmRI	404-436	pcDNA3.1	Iowa

Table 2.1: Human and mouse WT and chimeric cDNA constructs created by the Boyd (Edinburgh) and Welsh (Iowa) labs and used in this study. Construct names indicate the regions of the protein that have been exchanged from the human to the mouse sequence, for example hmNBD1 indicates a human CFTR background with a mouse sequence for NBD1, whilst hmTM5+6 indicates a human sequence for CFTR with mouse sequence for TM5 and TM6. Residue boundaries refer to the mouse residues that are present in the chimera.

2.1.3 Reagents

Protein kinase A (PKA) purified from bovine heart was obtained from Calbiochem (Merck Chemicals Ltd., Nottingham, UK). Unless otherwise stated, all other chemicals were supplied by the Sigma-Aldrich Company Ltd. (now Merck). The low-Cl^- pipette (extracellular) solution contained 140 mM *N*-methyl-D-glucamine (NMDG), 140 mM aspartic acid, 5 mM $CaCl_2$, 2 mM $MgSO_4$ and 10 mM *N*-tris[hydroxymethyl]methyl-2-aminoethanesulphonic acid (TES). Pipette solution pH was adjusted to 7.3 using Tris ($[Cl^-]$ = 10 mM, mean osmolarity = 281 ± 0.5 mosM, *n* = 3). Bath (intracellular) solution

contained 140 mM NMDG, 3 mM $MgCl_2$, 1 mM CsEGTA and 10 mM TES. Bath solution pH was adjusted to 7.3 using HCl ($[Cl^-]$ = 147 mM, $[Ca^{2+}]_{free}$ = $<10^{-8}$ M, mean osmolarity = 279 ± 0.5 mosM, *n* = 3). Fresh 0.2 M ATP stock solutions were made on each day of experiments and stored in ice before use. Ivacaftor and lumacaftor were sourced from Selleckchem (Munich, Germany) and added to DMSO to create a 10 mM stock. Genistein was purchased from LC laboratories (Woburn, MA, USA) and added to DMSO to give a 50 mM stock. $CFTR_{inh}$-172 was sourced from Sigma and added to DMSO to create a 30 mM stock. Stock solutions of all drugs were stored at -20°C in aliquots of 20 µl and used immediately after defrosting.

2.1.4 Electrophysiological recordings

Three patch-clamp setups were used for single-channel patch-clamp recordings. However, the configuration of equipment used for data acquisition and analysis of recordings remained the same regardless of the setup used. After cutting to size, coverslips with transfected cells were transferred to the 0.5 ml experimental chamber of a temperature-controlled microscope stage (Brook Industries, Lake Villa, IL, USA) mounted to an inverted microscope (patch-clamp setup 1: Nikon Diaphot 200 inverted microscope, Nikon, Tokyo, Japan; patch-clamp setups 2 and 3: Leica DMiRB or DMi8, Leica Microsystems, Wetzlar, Germany). All experiments were carried out at 37 C unless otherwise stated.

Single-channel patch-clamp experiments to measure CFTR activity were carried out using excised inside-out membrane patches. Glass patch pipettes were pulled from filamented thin-walled borosilicate glass capillary tubing (for higher resistance pipettes, length = 75.0 mm, outer diameter = 1.50 mm, inner diameter = 1.17 mm; for lower resistance pipettes, length = 75.0 mm, outer diameter = 1.50 mm, inner diameter = 0.86 mm, Harvard Apparatus UK, Biochrom Ltd., Cambridge, UK) using either a two stage vertical pipette puller (David Kopf Instruments, model 750; Clark Electromedical Instruments, Reading, UK) or a P-97 Flaming/Brown Micropipette Puller (Sutter Instruments, Novato, CA, USA) programmed for a two stage pull. Fresh pipettes were fabricated for each day of experiments and stored in a closed container to prevent dust contamination. Pipette resistance for pipettes pulled using the Sutter P-97 puller were within the range 10-90 MΩ when filled with low Cl^- pipette solution with resistance

tailored to the expression level of CFTR. Pipette capacitance was controlled by coating pipettes with Sylgard to within 1 mm of the pipette tip (Merck Ltd., Lutterworth, UK). Pipette resistances for pipettes pulled using the Kopf 750 puller were higher to adjust for the high expression of CFTR in BHK cells, in the range 80-150 MΩ.

Voltage-clamp and current amplification were achieved using an Axopatch 200A (setup 1) or 200B (setups 2 and 3) patch-clamp amplifier (Axon Instruments Inc., now Molecular Devices Corp., San Jose, CA, USA) and data acquired using pCLAMP software (v 6.02, 9.2 or 10.3; Molecular Devices Corp.). Where traces from single-channel patch-clamp experiments are shown, the conventional standard has been used throughout; where positive current represents movement of positive charge passing from intra- to extracellular solutions. For most single-channel recordings, holding voltage (V_H) was clamped at either -50 mV or -80 mV. For generation of single-channel current/voltage (i/V) relationships, voltage was stepped at 20 mV intervals from -100 mV to +20 mV for periods of at least 30 s at each voltage.

For initial experiments, data obtained from single-channel recordings were filtered at a bandwidth of 10 kHz using the amplifiers built-in 80 dB/decade Bessel filter and recorded to digital audio tape (DAT) at a sampling rate of 48 kHz using a digital tape recorder (Biologic Scientific Instruments, model DTR-1204; Intracel Ltd., Royston, UK). For analysis, records were filtered using an eight-pole Bessel Filter (Frequency Devices, model 902LPF2; supplied by SCENSYS Ltd., Aylesbury, UK) on playback at a corner frequency of 500 Hz and digitised using a DigiData 1200 or 1320A AD-converter interface and pCLAMP software (v 6.02 or 9.2, Axon Instruments Inc.) at a sampling rate of 5 kHz. Due to the difficulty of sourcing DAT recording tapes, data acquisition and storage was switched to external hard drives for the latter stages of the project. For subsequent recordings, data were filtered at a bandwidth of 10 kHz using the amplifiers built-in Bessel filter and recorded to external hard drive (Toshiba) using pCLAMP software v 9.2 (setup 2) or v 10.3 (setup 3) at a sampling frequency of 50 kHz. For analysis, data were filtered as previously described at a corner frequency of 500 Hz using an eight-pole Bessel Filter (Frequency Devices, model 902LPF2) and a sampling frequency of 5 kHz. For the purpose of illustration, example patch-clamp recordings used in figures have undergone an additional 5-fold data reduction.

Patch-clamp experiments were performed as follows: Cover-slips seeded with cells were added to the experimental chamber. The tips of filamented glass patch pipettes were dipped in extracellular solution with positive pressure applied to the rear of pipettes as contact was made at the air-liquid interface to prevent accumulation of debris. Negative pressure was then applied to the rear of the pipette to aid filling of the narrow tip section. Pipettes were back-filled with extracellular solution to around 10 mm from the end of the pipette using MicroFil micropipette (MF28G67-5, World Precision Instruments, Sarasota, FL, USA) and checked to ensure that solution was continuous with the tip section of the patch pipette. Patch pipettes were attached to the headstage of the patch-clamp amplifier with current recorded to the patch-clamp amplifier via an AgCl coated silver wire and the ground input of the amplifier headstage was connected to the experimental chamber via an agar bridge comprising 10 cm polythene tubing filled with 5% agar and 1M KCl. A fresh agar bridge was used for each day of experiments and agar bridges were stored in 1 M KCl at 5 °C before use. Positive pressure was applied to the rear of the pipette to reduce the risk of tip blockage with debris before the pipette was lowered into the experimental chamber which contained 0.5 ml intracellular solution. Short voltage pulses were applied across the tip of the pipette to measure the electrical resistance of the pipette at the junction between the intracellular and extracellular solutions. The pipette offset resulting from this liquid junction was corrected to zero immediately after pipettes had been lowered into the intracellular solution, and immediately before contact was made with the cell membrane. Cells were selected for experiments by visual inspection based on morphology of the cells and intensity of fluorescence if using transiently transfected cells expressing pEGFP. After identification of target cells, the pipette was lowered until contact was made with the cell membrane, as confirmed visually and by a change in the resistance recorded across the pipette tip. Negative pressure was then applied to the rear of the pipette to aid formation of a giga ohm seal (> 10 MΩ). The resulting membrane patch was excised by lifting the pipette to form an inside-out membrane patch. To reduce the risk of electrical noise in recordings, pipettes containing excised patches were raised to the level of the surface film of the intracellular solution.

CFTR was activated by adding ATP and PKA to the bath (internal) solution at a final bath concentration of 1 mM ATP and 75 nM PKA. Maintenance of pH at 7.3 was obtained by adding NaOH in conjunction with the ATP. For experiments where 0.3 mM

ATP was used, CFTR was first activated with 1 mM ATP before complete exchange of bath solution via perfusion with 10 ml bath solution containing 0.3 mM ATP. PKA was added to all internal solutions and maintained throughout experiments to avoid channel rundown. All experiments were initially voltage clamped at -50 mV. Because of the difficulty of washing ivacaftor from the experimental chamber, ivacaftor had to be added cumulatively to the experimental chamber for dose response experiments via direct addition. Prior to experiments, ivacaftor was stored in aliquots of 10 mM stock maintained at -20 °C. Before use, aliquots were defrosted and diluted to 0.5 mM in DMSO, before serial dilution to 0.05 mM and 0.005 mM stocks in bath solution before addition to the experimental chamber at the desired final concentration. All stock solutions added were pre-mixed in 30 µl bath solution prior to addition to the chamber to ensure sufficient dispersal. After experiments, chambers were washed in 40% DMSO for 24 hours to prevent ivacaftor contamination of subsequent experiments. For dose response experiments, control recordings were made for a minimum of 5 minutes following stable activation of CFTR channels. Subsequent recordings were made for a minimum of 5 minutes at each concentration of the test compound. For experiments using genistein, after obtaining control data, 10 ml intracellular solution containing 50 µM genistein and 1 mM ATP was continuously perfused through the experimental chamber at a rate of 160 $\mu l \cdot s^{-1}$ to ensure complete exchange of solution. 75 nM PKA was added to the experimental chamber via direct addition before recordings were made in the presence of the drug.

2.1.5 Analysis and statistics

2.1.5.1 Analysis of single-channel recordings

Recordings were analysed using pClamp software v9.2 or v10.3 (Molecular Devices Corp.). Single-channel current amplitude (i) was measured by fitting Gaussian distributions to current amplitude histograms as shown in Figure 2.1, and calculated from the difference between the closed (mu-1) and open (mu-2) levels (Cai *et al.*, 2004; Sheppard *et al.*, 2004). Current amplitude histograms were generated from recordings containing $\leq$ 5 simultaneous channel openings and fitted using a 2-component Gaussian equation. The total number of channels present in a membrane patch (*N*) was determined from the maximum number of simultaneous channel openings present within a recording of a minimum duration of 5 minutes for active

channels, or 10 minutes for inactive channels (e.g. mouse WT-CFTR or human F508del-CFTR). To facilitate correct determination of *N*, experimental conditions were designed to strongly enhance CFTR activity by using 1.0 mM ATP or by using a CFTR potentiator (ivacaftor). However, it is possible that for inactive channels, the value calculated for *N* is an underestimate despite these criteria.

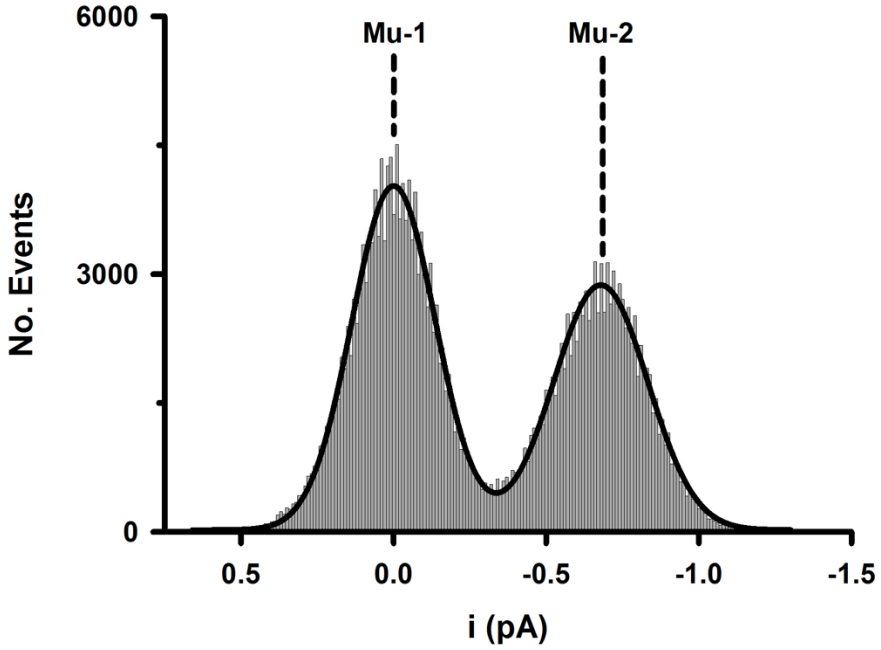

Figure 2.1: Current amplitude histogram generated from 30 s single-channel recording of human WT-CFTR at -50 mV. Histograms were fitted using a 2-component Gaussian fit (continuous black line) and single-channel current amplitude (i) was calculated as the differences between Mu-1 (closed) and Mu-2 (open) levels.

The open probability (P_o) for single-channel recordings containing ≤ 5 channels was calculated from event lists generated from open- and closed-times using a half-amplitude crossing criterion for event detection. Events were determined where a change in current was detected that was > 50% that of the current recorded for the previous event (Cai *et al.*, 2004). Events of a duration < 1 ms were excluded from analysis, corresponding to the rise time predicted by the corner frequency (f_c) of the eight-pole Bessel filter used for recordings (f_c at 500 Hz = ~ 0.73 ms). P_o was calculated using equation 1:

Eq. 1:

$$P_o = \frac{T_1+T_2+...+T_N}{N\,T_{tot}}$$

Where N indicates the maximum number of simultaneous channel openings recorded, T_N = the duration of time spent at a given level for the number of channels N, and T_{tot} = the total time period for the analysed recording.

Where only one channel was observed for the duration of an experiment, mean burst duration (MBD) and interburst interval (IBI) were calculated by burst analysis using pCLAMP software v6.0. Dwell time histograms were generated from event lists for open- and closed-events using logarithmic *x*-axes and 10 bins·decade^{-1} (Figure 2.2). Histograms were fitted using one or more component exponential functions using the maximum likelihood method and used to calculate mean open- (τ_o) and closed- (τ_c) times.

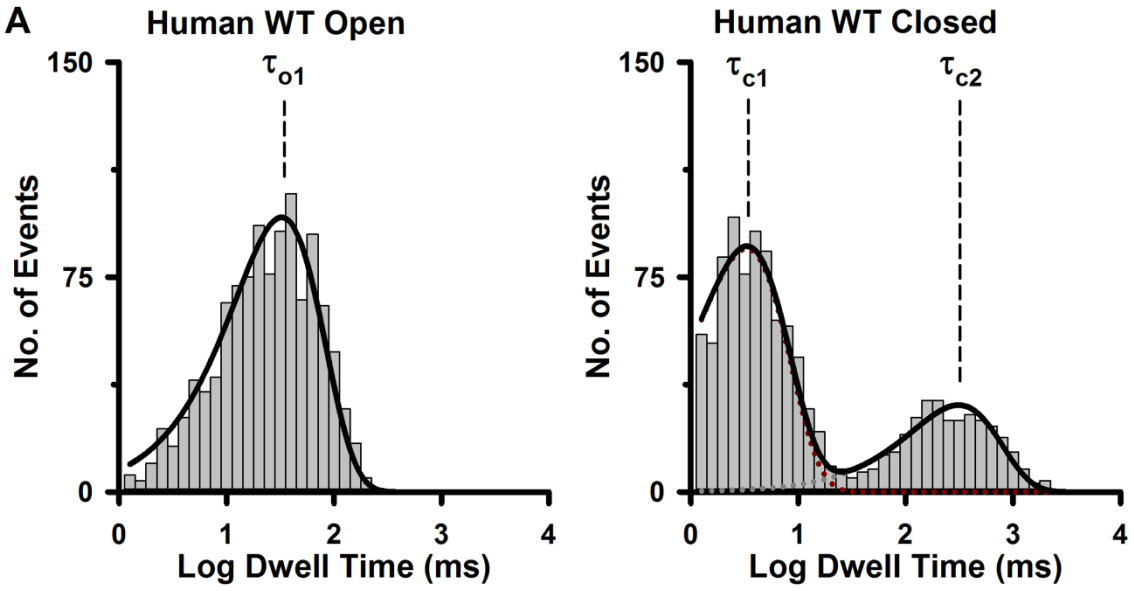

Figure 2.2: Example dwell-time histograms for open- and closed-time events generated from single-channel recordings of human WT-CFTR. Histograms have been fitted with one- (open) or two-component (closed) exponential functions (continuous black line). Logarithmic x-axes are used for both open and closed time histograms plotted with 10 bins·decade^{-1}. Dashed lines indicate mean open (τ_o) and mean closed (τ_{c1} and τ_{c2}) durations. Individual components for the τ_{c1} and τ_{c2} of the closed-time histogram are indicated by red and grey dotted lines, respectively.

To further investigate the duration of channel openings, the burst delimiter t_c, representing the time that differentiates intraburst closures from interburst closures, was calculated after fitting closed-time dwell-time histograms using the maximum likelihood method (Carson *et al.*, 1995a). Events lists generated from recordings were used to calculate MBD and the open probability within bursts using pClamp software v6.02. Mean IBI was calculated using the following equation;

Eq. 2:

$$P_o = \frac{T_b}{MBD + IBI}$$

where T_b = MBD x the open probability within a burst.

Where i/V relationships were plotted using data collected from single-channel recordings, the reversal potentials were compared to equilibrium potentials calculated using the Nernst equation:

Eq. 3.

$$E_{Cl} = \frac{RT}{zF} ln \frac{[Cl^-]_o}{[Cl^-]_i}$$

In this equation, R = the universal gas constant (8.314472 $J \cdot K^{-1} \cdot mol^{-1}$), T = temperature (310 K), z = valency (i.e. -1 for Cl^-), F = Faraday constant (9.648533 $x10^4$ $C \cdot mol^{-1}$), $[Cl^-]_o$ = concentration of extracellular Cl^- (147 mM) and $[Cl^-]_i$ = concentration of intracellular Cl^- (10 mM).

2.1.5.2 Statistics

Unless indicated otherwise, results have been expressed as means ± standard error of the mean (SEM) of *n* observations. Where *n* = 2, results have been expressed as means ± standard deviation (SD). Differences were considered statistically significant when $P < 0.05$ and power analysis was performed for all statistics with significance requiring a power of 0.8 where $\alpha = 0.05$. All tests were performed using SigmaStat™ (SigmaPlot™ version 13.0, Systat Software Inc., San Jose, CA, USA).

To test for differences between two groups of data a two-tailed Student's *t*-test was used and where two sets of data were obtained from the same cell or membrane patch, a paired, two-tailed Student's *t*-test was used.

Where multiple concentrations of a drug compound were used in the same experiment, data were analysed using one-way repeated measures ANOVA and where a statistically significant difference was observed interventions were compared with control using Dunnett's multiple comparison test.

Dose response curves for drugs were fitted using a 3-parameter sigmoidal equation:

Eq. 4:

$$f(x) = \frac{y_{max}}{(1 + exp\,(-\frac{x - x0}{K_D}))}$$

Where K_D is the apparent dissociation constant and y_{max} = the maximum predicted value for y.

2.2 Automated whole-cell patch-clamp recordings

2.2.1 Cell culture and transfection

Untransfected CHO-K1 cells were cultured in F-12K medium (Kaighn's Modification of Ham's F-12 Medium, American Type Culture Collection, Manassas, USA) supplemented with 10% FBS, 1% L-glutamine, 100 $U \cdot ml^{-1}$ penicillin and 100 $\mu g \cdot ml^{-1}$ streptomycin. All cells were maintained in either 150 cm^2 rectangular canted neck cell culture flasks (Corning) or in HYPERflasks (Corning) at 37 °C in a humidified atmosphere with 5% CO_2 except where otherwise stated. Media was changed every 24-48 hours and cells were passaged when > 95% confluent by washing with Dulbecco's phosphate buffered saline (DPBS) before dissociating using Detachin™ (Genlantis, San Diego, USA).

Transient cell lines were generated by electroporation of cells with CFTR cDNA plasmids. To ensure maximum transfection efficiency for automated patch-clamp

recording, CHO-K1 cells were transfected using a MaxCyte STX Scalable Transfection System (MaxCyte Inc., Gaithersburg, USA). Initial optimisation protocols were run for cDNA plasmids as follows:

- CHO-K1 cells were cultured as described above and harvested for optimisation by first washing with 14 ml DPBS followed by 4 ml Detachin™ (Genlantis). Cells were centrifuged at 1500 rpm for 5 minutes and rinsed with MaxCyte electroporation buffer, before being centrifuged again at 1500 rpm for 5 minutes and re-suspended in electroporation buffer at high density (2 $x10^8$ cells·ml^{-1}).

- Re-suspended cells were mixed with cDNA plasmids at concentrations of 100, 200 and 300 µg·ml^{-1} and transferred to MaxCyte OC-100 processing assemblies and transfected using the recommended MaxCyte electroporation protocol for CHO cells.

- Following transfection, cells were transferred to a multiwell dish and allowed to recover for 20 minutes at 37 ˚C before being transferred to 75 ml cell culture flasks (Corning) with F-12K culture medium.

- Cells were incubated at 37 °C in a humidified atmosphere with 5% CO_2 for 24 hours before being transferred to 27 °C to prevent further cell growth.

- Expression levels were tested at 24, 48 and 72 hour time points by comparing the success rate for observing $CFTR_{inh}$-172-sensitive forskolin-induced whole-cell currents when cells were tested using either QPatch HTX (Sophion Bioscience A/S, Ballerup, Denmark) or a SyncroPatch 384PE (Nanion Technologies GmbH, Munich, Germany), automated patch-clamp systems as described below. (MaxCyte optimisation protocols carried out using the SyncroPatch 384PE platform were kindly performed by Kelly McKiernan (NIBR)).

- Optimum protocols were selected for plasmids based on cell viability, percentage of cells exhibiting CFTR-mediated current, and the maximum

current amplitude generated. The optimum protocol for all plasmids was transfection at 300 μg·ml^{-1} and incubation for 72 hours prior to cryopreservation.

Following optimisation of the transfection protocol, cell lines were generated and scaled up for cryopreservation using MaxCyte electroporation for each of the constructs listed in Table 2.1. Prior to transfection, CHO-K1 cells were cultured as described above in 150 cm^2 rectangular canted neck cell culture flasks (Corning) before being transferred to HYPERflask M cell culture flasks (Corning) which enabled generation of up to 1.72 x10^8 cells per flask. For each cell line, cells were harvested from HYPERflasks by washing with 100 ml DPBS and adding 50 ml Detachin™. Cells were incubated at 37 °C with Detachin for 10 minutes and once all cells were fully dissociated, 50 ml culture medium was added to deactivate the Detachin™. Cell viability and density were measured using a Vi-CELL XR cell counter (Beckman-Coulter Life Sciences, Indiana, USA), resuspended in MaxCyte electroporation buffer at a concentration of 2.0 x10^8 cells ml^{-1} and added to plasmid cDNA to give a final cDNA concentration of 300 μg·ml^{-1}. 400 μl of each cDNA-cell suspension was then added to a MaxCyte OC-400 processing assembly and transfection was carried out via electroporation using the appropriate transfection protocol designated for CHO-K1 cells. Following transfection, cell suspensions were transferred from the OC-400 processing assemblies to multi-well plates and incubated for 20 minutes at 37 °C to allow recovery from the electroporation process. Cells were transferred to HYPERflasks in 500 ml culture medium and incubated at 37 °C for 24 hours, before being transferred to 27 °C and incubated for a further 48 hours before cryopreservation. Cells were harvested as described above, divided into aliquots of 5 x10^6 cells and frozen at -80 °C in freezing media (90% FBS, 10% DMSO) using CoolCell freezing containers (Corning). For long term use, aliquots were transferred to liquid nitrogen after initial freezing at -80 °C for a minimum of 24 hours. For experiments, cells were rapidly thawed, re-suspended in serum-free suspension media (CHO-S-SFM II, Invitrogen) at a minimum cell density of 2 x10^6 cells·ml^{-1} and transferred to the QPatch cell storage tank. Cells were used for experiments within 4 hours after thawing and maintained in solution by stirring at room temperature before use.

2.1.3 Reagents

All chemicals were supplied by Sigma-Aldrich (now Merck) unless stated otherwise. For QPatch assays, extracellular solution contained 160 mM NaCl, 4.5 mM KCl, 2 mM $CaCl_2$, 1 mM $MgCl_2$, 5 mM Glucose, 10 mM 4-(2-hydroxyethyl)-1-piperazineethanesulfonic acid (HEPES, Invitrogen) and 2 mM Mg-ATP ($[Cl^-]$ = 171 mM, osmolarity = 295 mOsm). Extracellular solution pH was adjusted to 7.3 with NaOH. Intracellular solution contained 145 mM KCl, 10 mM NaCl, 2 mM $MgCl_2$, 10 mM ethylene glycol-bis(β-aminoethyl ether)-N,N,N',N'-tetraacetic acid (EGTA), 10 mM HEPES and 5 mM Na-ATP ($[Cl^-]$ = 159 mM, osmolarity = 290 mOsm). Intracellular solution pH was adjusted to pH 7.2 with CsOH. Responses to the vehicle control were tested using DMSO diluted to 3% in extracellular solution. CFTR was activated using 10 μM forskolin (FSK) and CFTR-specific responses were recorded by inhibiting activity with 30 μM $CFTR_{inh}$-172 at the end of each protocol. All reagents were diluted to the required concentration in extracellular solution, stored in QPatch MTP-96 plates at room temperature and added to the extracellular side of each QPlate well for experiments. 10 mM forskolin stock was stored in aliquots at -20 °C when not in use. Ivacaftor was sourced in powdered from Selleckchem. and added to DMSO to create a 10 mM stock that was stored at -20 °C. $CFTR_{inh}$-172 was purchased from Sigma in powdered form and stored in 30 mM solution (DMSO) at -20 °C until required.

2.1.4 QPatch automated electrophysiological recordings

For experiments using the QPatch HTX screening station, harvested cells were counted, centrifuged, and resuspended in suspension media at a concentration of 2.5 $x10^6$ cells·ml^{-1}. Cells were allowed to rest for at least 1 hour at room temperature and maintained in solution by stirring before being added to individual wells of a 48 well QPlate. Figure 2.3 shows a schematic diagram of an individual well from a QPlate used for experiments on the QPatch HTX screening station. Before experiments, QPatch pipettes were washed using 50 ml H_2O. The experimental process for running experiments on the QPatch HTX screening station ran as follows (details adapted from protocol as described in the Sophion QPatch HTX Screening Station Handbook, ©2004-2012 Sophion Bioscience A/S):

I. Intracellular solution was added to the intracellular well by the application pipettes.

II. The intracellular well was primed by application of pressurised air for duration of 3 minutes to press liquid into the channel of the QPlate.

III. The protective manifold was moved into position to cover the QPlate and provide electrical isolation of the experiment.

IV. Extracellular solution was added to the cell and compound well and a vacuum applied to the waste reservoir in order to ensure sufficient uptake of liquid to the extracellular chamber.

V. Integrated Ag/AgCl electrodes were allowed to stabilise for a period of 120 s.

VI. Resistance and offset potential were measured between the working and reference electrodes and offset potential was compensated for by the QPatch built in amplifier.

VII. Cells that had been washed and resuspended in extracellular solution were added to the cell and compound wells of the QPlate.

VIII. Negative pressure applied to the intracellular solution wells of the QPlate to position cells onto the patch-clamp orifice (Figure 2.3).

IX. Following successful positioning of cells, gigaohm seals were obtained using the parameters set in the whole-cell protocol of the QPatch Assay software (see below).

X. System capacitance (C-Fast) was recorded throughout the process of gigaseal establishment and values for C-Fast used to compensate for the capacitive component of measured current.

XI. Following gigaseal formation, whole-cell configuration was obtained using the sequence defined in the whole-cell protocol and whole-cell configuration was detected by an increase in cell capacitance (C-Slow).

XII. C-Slow (typically between 4 and 15 pF), series resistance (R-Series) and membrane resistance (R-Membrane) were monitored and recorded throughout the duration of experiments.

XIII. Experiments proceeded according to the sequence specified in the application protocol specified in the QPatch Assay software.

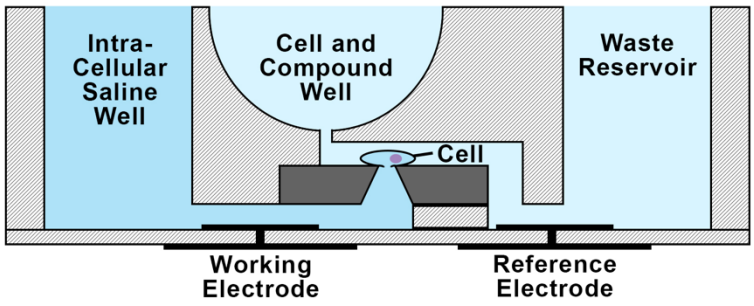

Figure 2.3: Experimental well from the QPlates used for QPatch experiments. Qplates are primed with intra- and extracellular solutions prior to cell addition. After cells are applied to the QPlate wells, suction at the intracellular side of the plate aids positioning of cells at the patch-clamp orifice and gigaohm seals and whole-cell patch-clamp configuration were obtained using the whole-cell protocol. Compounds were tested by addition to the extracellular solution.

Assays for use with the QPatch HTX screening station were designed using QPatch Assay v5.6 (Sophion). All experiments were carried out at room temperature (21 °C) Assays consisted of a whole-cell protocol for establishing the whole-cell patch-clamp configuration, an application protocol for applying test compounds and a voltage protocol. For testing the response of cells expressing either WT-CFTR constructs or CFTR chimeras to CFTR potentiators, these protocols were set up as follows:

- **Whole-cell protocol:** For positioning of cells, a wait time of 5 s was set and a positioning pressure of -100 mbar. The resistance increase for success was set to 750% with a positioning timeout of 30 s. For formation of gigaseals, minimum seal resistance was set to 0.1 GΩ, holding potential -30 mV and holding pressure -20 mbar. Time set for improving gigaseal resistance was 180 s. For whole-cell configuration minimum seal resistance was set to 0.05 GΩ (typical seal resistance = ~ 1GΩ), holding potential -30 mV and holding pressure -20

mbar. For gigaseal formation, start pressure was set to -70 mbar, wait time before holding voltage change was 8 s. QPatch software abandoned experiments where the criteria for gigaseal was no longer met.

- **Application protocol:** For testing CFTR potentiatiors, solutions were added using the following application protocol; break in > saline (extracellular solution), 5 min > DMSO (3%), 5 min > forskolin (10 μM), 15 min > ivacaftor (10 μM), 5 min > $CFTR_{inh}$-172 (30 μM), 5 min. For each liquid period, complete exchange of solution was achieved via perfusion. 10 μM Forskolin was present in solutions throughout the ivacaftor and $CFTR_{inh}$-172 phases. During each experiment, compounds were stored at room temperature for use in an MTP-96 plate.

- **Voltage protocol:** Figure 2.4 shows the voltage protocol used for each sweep during QPatch experiments. Sweeps were repeated every 10 seconds for the duration of each experiment. Whole-cell patches were maintained at a holding potential (V_H) of -30 mV. Voltage was stepped to -80 mV for 50 ms after the start of each sweep and maintained for 20 ms before being ramped from -80 mV to +80 mV over a period of 200 ms before returning to V_H. Leak current was calculated from the current observed at -30 mV.

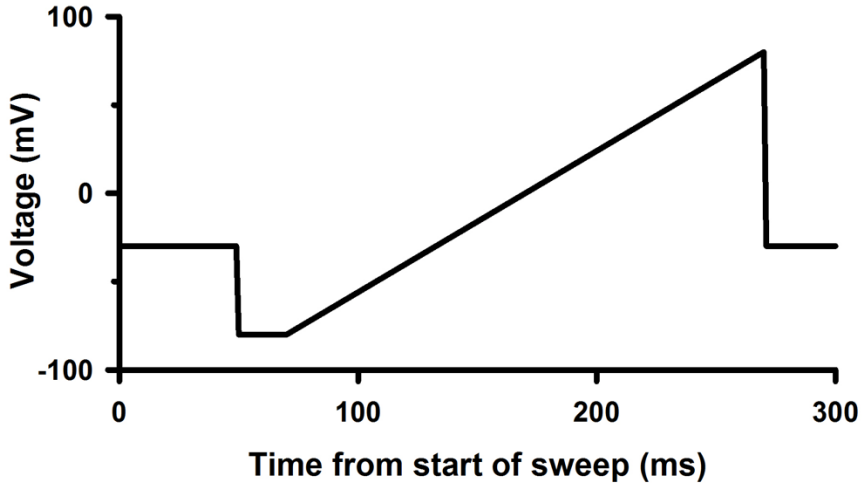

Figure 2.4: Voltage protocol used for whole-cell patch-clamp experiments using QPatch screening station. Holding voltage (V_H) was -30 mV. After 50 ms, voltage was stepped to -80 mV for 20 ms before being ramped to 80 mV over a period of 200 ms.

2.1.5 Analysis of QPatch recordings

Analysis of data obtained from the QPatch screening station was performed using QPatch Assay v5.6 software. Figure 2.5 shows an example recording of human WT-CFTR from a QPatch experiment detailing the protocol used. QPatch software discounted experiments where the criteria for the whole-cell configuration were no longer met (i.e. minimum seal resistance was lost due to unstable patch). Data were then manually inspected for CFTR expression as indicated by a response to 10 µM forskolin following washout of the 3% DMSO vehicle control period. Whole-cell recordings were not analysed where no response to forskolin and subsequent inhibition by $CFTR_{inh}$-172 was observed. For each experiment, mean values were taken for the maximum outward (+80 mV) and inward (-80 mV) current for each intervention from the final 10 voltage sweeps in each liquid handling phase (indicated by the green areas of shading in Figure 2.5). The lower traces shown in example figures from QPatch recordings represent the current recorded at -30 mV for each sweep (Figure 2.5). This value was subtracted from the current recorded at +80 mV for each sweep.

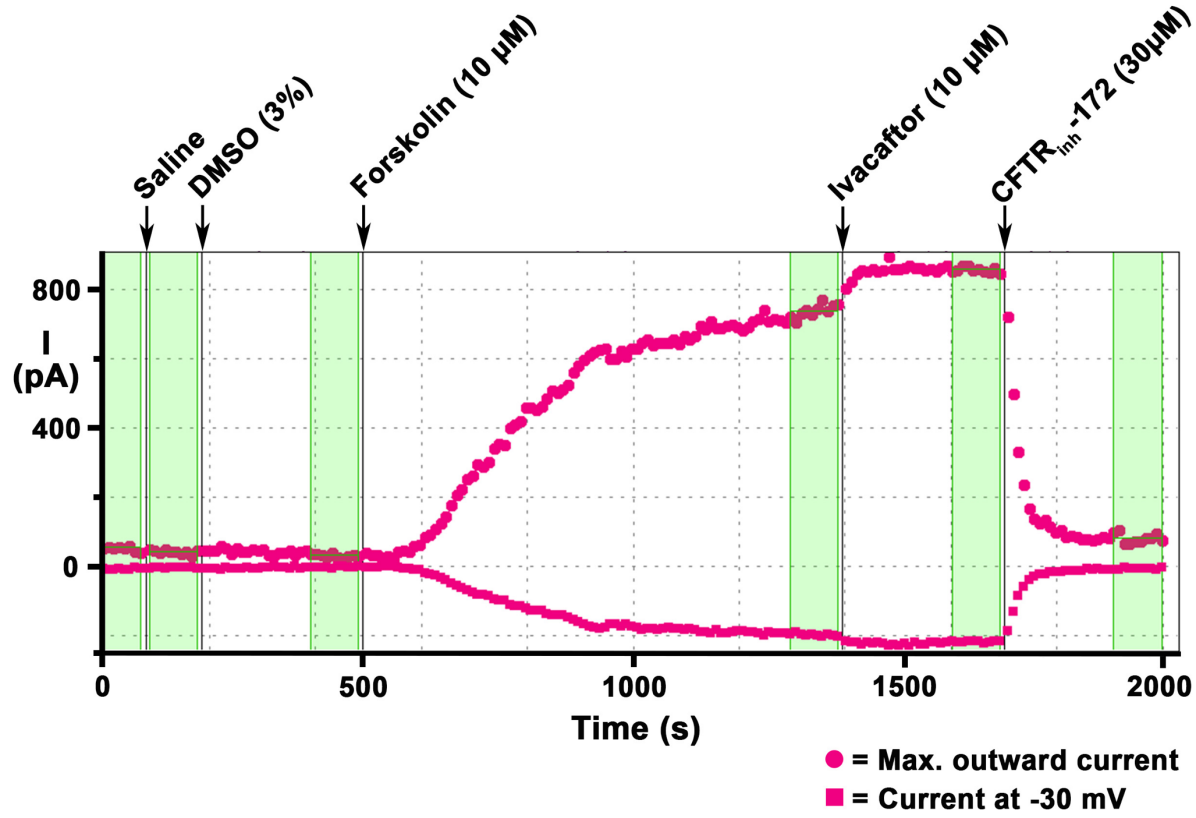

Figure 2.5: Example QPatch recording of human WT-CFTR activity in response to 10 µM forskolin followed by 10 µM ivacaftor and 30 µM $CFTR_{inh}$-172.

All data were normalised for cell size by dividing by the values recorded for C-Slow in each liquid handling phase. Specific CFTR responses to forskolin and ivacaftor were calculated by subtraction of the remaining current following addition of 30 μM $CFTR_{inh}$-172.

2.1.6 Statistics

For testing the response of constructs to 10 μM ivacaftor, the response current of individual cells to ivacaftor was compared to that of forskolin from the same cell using paired, two-way Students t-test ($P < 0.05$ = significant). As all cell stock for each construct was sourced from a single MaxCyte transfection protocol, experiments performed on individual cells were considered as individual repeats (i.e. $n = 5$ represents 5 cells). All tests were performed using SigmaStat™ (SigmaPlot™ version 13.0).

3. Species differences in WT and F508del-CFTR function as demonstrated using single-channel patch-clamp recording

3.1 Introduction

CFTR orthologues from a number of species have been studied at the single-channel level, including spiny dogfish (Hanrahan *et al.*, 1993), *Xenopus* (Price *et al.*, 1996), mouse (Lansdell *et al.*, 1998a), domestic chicken (Aleksandrov *et al.*, 2012), Australian common bushtail possum (Demmers *et al.*, 2010), European rabbit (Al-Nakkash & Reinach, 2001), sheep (Cai *et al.*, 2015), and pig (Ostedgaard *et al.*, 2007). The gating behaviour of these diverse orthologues shows variance that does not appear to follow the pattern of homology (see Figure 1.7). For example, mouse CFTR has been shown to possess a unique gating behaviour characterised by a highly active sub-conductance state and brief openings to a fully open state, despite sharing 79% amino acid (a.a.) sequence identity with human CFTR (Figure 1.10) (Lansdell *et al.*, 1998b). In contrast, *Xenopus* CFTR demonstrates gating behaviour that more closely resembles human CFTR, despite sharing only 76% a.a. identity with human CFTR (Price *et al.*, 1996). Closely related orthologues such as sheep (91% a.a. identity) and pig (92% a.a. identity) still show differences in gating and conductance compared to human CFTR (Ostedgaard *et al.*, 2007; Cai *et al.*, 2015). Before investigating the pharmacology of CFTR orthologues from diverse species, we therefore considered it important to determine the single-channel gating behaviour and conductance properties of CFTR orthologues from diverse species. In addition, previous studies have highlighted differences in the effects of CF-causing mutations when expressed in different CFTR orthologues (Ostedgaard *et al.*, 2007; Aleksandrov *et al.*, 2012; Cai *et al.*, 2015). We therefore aimed to investigate the effect of the F508del mutation on divergent orthologues.

Given the wide range of CFTR orthologues available to study, it was decided to focus on six different CFTR orthologues (including human CFTR) that would represent a broad range of species from across the evolutionary tree. In deciding upon which species to investigate, we also opted for species that are currently being developed,

or being considered for the development of CF animal models, i.e. sheep, pig, ferret, mouse, rat, rabbit and zebrafish (McCarron *et al.*, 2018). It was considered that an understanding of the gating behaviour of these species as well as their pharmacology, was essential for assessing the suitability of these models as investigational tools for CF research. The chosen species encompassed a broad spectra of mammalian species as well as an example of teleost fish (zebrafish). CFTR orthologues from other phyla, including birds, amphibians and marsupials but not reptiles have been previously characterised (Price *et al.*, 1996; Demmers *et al.*, 2010; Aleksandrov *et al.*, 2012). Figure 3.1 shows the cladogram of the species we chose to study based upon ClustalO alignment of the full CFTR sequences (Appendix 1), whilst Table 3.1 shows the comparison of homologies for these orthologues.

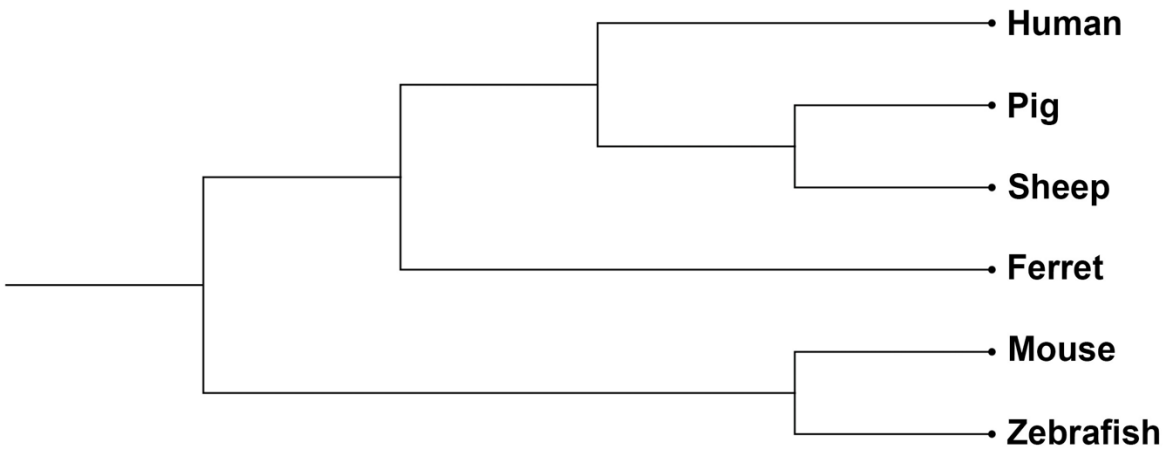

Figure 3.1: Cladogram of CFTR orthologues studied. Cladogram illustrates the degree to which the investigated CFTR orthologues are likely to be related based on amino acid sequence identity. Constructed by ClustalO sequence alignment using CLC Sequence Viewer software (v7.5).

Common Name	Latin name	GenBank Accession No.	Shared amino acid identity with human CFTR (%)
Human	*Homo sapiens*	NM_000492.3	100
Pig	*Sus scrofa*	AY585334.1	92
Sheep	*Ovis aries*	U20418.1	91
Domestic Ferret	*Mustela putorius furo*	XM_004789405.1	92
House Mouse	*Mus musculus*	NM_021050.2	79
Zebrafish	*Danio rerio*	NM_001044883.1	54

Table 3.1: Sequence homologies of CFTR orthologues used in this study. Shared amino acid identity was calculated following ClustalO sequence alignment using CLC Sequence Viewer software (v7.5). GenBank accession numbers for the sequences used are shown.

3.2 Comparison of WT-CFTR gating behaviour between diverse species

3.2.1 Single-channel gating behaviour of diverse CFTR orthologues

Figure 3.2 shows representative examples of single-channel recordings from all six of the species that were used for this study. The recordings highlight the diversity exhibited in the gating behaviour of these different species. Figure 3.3 summarises the quantification of single-channel recordings from these CFTR orthologues. Due to the low conductance that was observed for ferret, mouse and zebrafish CFTR, traces from these species have been displayed at -80 mV (ferret and mouse) and -100 mV (zebrafish) respectively in Figure 3.2. Specific details for each species are discussed in the following sections:

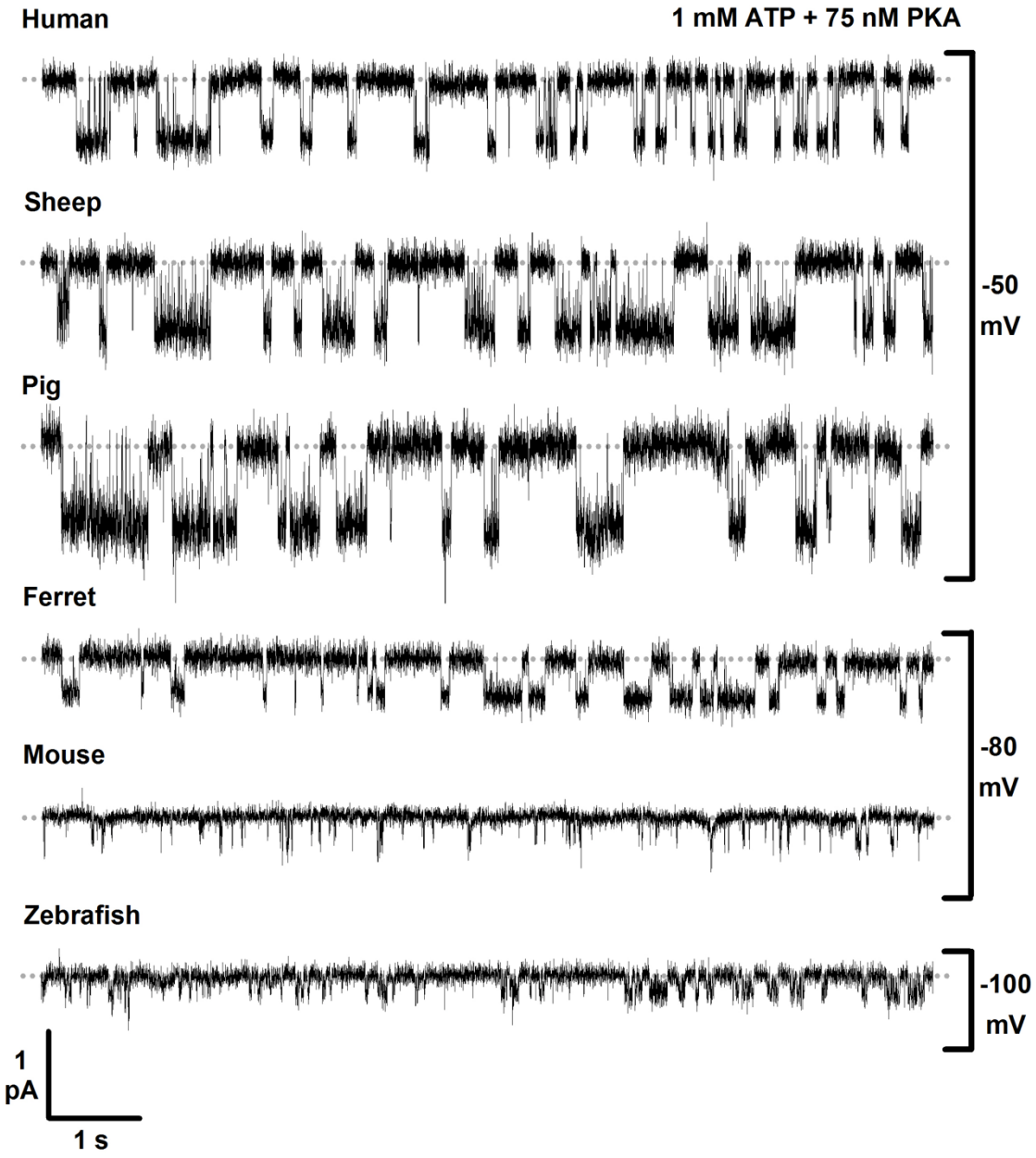

Figure 3.2: The single-channel activity of CFTR from diverse species. Representative single-channel recordings of WT-CFTR orthologues from diverse species recorded using excised inside-out membrane patches. ATP (1 mM) and PKA (75 nM) were continuously present in the intracellular solution. For the purpose of illustration, recordings have been filtered at 500 Hz and digitised at 5 kHz before file size was compressed by 5-fold data reduction. Dotted grey lines represent the closed level for each channel. For human, sheep and pig, holding potential was -50 mV. Due to the low conductance of ferret, mouse and zebrafish CFTR, example traces for ferret and mouse were made at -80 mV, whilst the trace for zebrafish CFTR was recorded at -100 mV. For all recordings, temperature was maintained at 37 °C in the presence of a Cl^- concentration gradient across the membrane patch ($[Cl^-]_{internal}$ = 147 mM; $[Cl^-]_{external}$ = 10 mM).

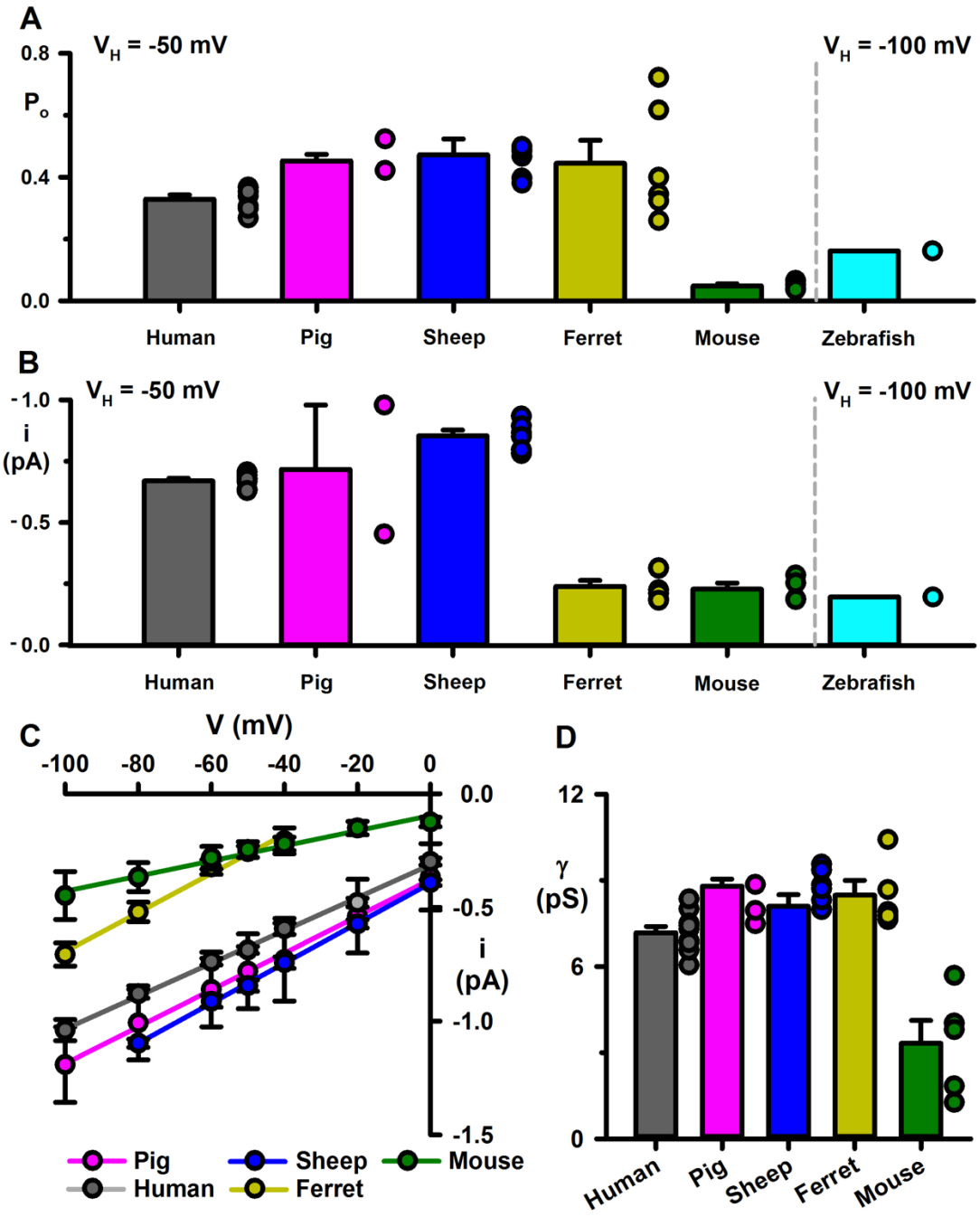

Figure 3.3: Single-channel properties of CFTR orthologues. A Comparison of the P_o recorded for CFTR orthologues. P_o for all species was recorded from single-channel patch-clamp recordings following activation of CFTR by 1 mM ATP and 75 nM PKA in the presence of a Cl^- concentration gradient. For mouse CFTR, data are for the full open (O_2) state. Holding potential (V_H) was -50 mV for all species except zebrafish. For zebrafish, measurement of P_o was only possible at -100 mV. **B** Comparison of i values for CFTR orthologues at V_H of -50 or -100 mV. Experimental conditions were the same as described for **A**. **C** i/V relationships for CFTR orthologues. V_H was stepped from -100 to 0 mV for periods of at least 30 s. Continuous lines indicate best fit by linear regression. **D** slope conductance measurements calculated from the i/V relationships reported in **C**. For all graphs, error bars represent SEM or SD when *n* = 2 and individual data points are indicated by the circles adjacent to bars (human, *n* = 5-10; pig, *n* = 2-3; sheep *n* = 6; ferret *n* = 6; mouse, *n* = 4; zebrafish *n* = 1).

3.2.1.1 Human CFTR

As shown in Figure 3.2, following activation by PKA-dependent phosphorylation human CFTR stably expressed in BHK cells produced single-channel currents in the presence of an asymmetric Cl^- gradient ($[Cl^-]_{internal}$ = 147 mM; $[Cl^-]_{external}$ = 10 mM) with the same characteristics at -50 mV as previously reported for human CFTR single-channel recordings (Sheppard & Welsh, 1999). Human CFTR produced single-channel activity characterised by open channel bursts as represented by downward deflections in the example trace with a P_o of 0.33 ± 0.01 and single-channel current of -0.68 ± 0.01 pA at -50 mV (n = 7) (Figure 3.2 and Figure 3.3A and B). In order to quantify the slope conductance for human CFTR, i/V relationships were constructed by measuring single-channel current following step changes in voltage from -100 mV to 0 mV with each voltage clamped for a minimum of 30 seconds (Figure 3.3C). Under asymmetric Cl^- concentrations, CFTR demonstrates inward rectification with minimal current at positive voltages (Sheppard et al., 1993). However, at negative voltages Human WT-CFTR produced a linear i/V relationship with a slope conductance (γ) of 7.18 ± 0.22 pS (n = 10) (Figure 3.3D).

3.2.1.3 Pig CFTR

Unfortunately, only limited data were collected for pig CFTR with only two successful single-channel patches obtained from transiently expressed pig CFTR in CHO cells. However, currents were observed following channel activation by PKA-dependent phosphorylation and where single-channel currents were observed gating behaviour appeared to be similar to that of human WT-CFTR. A number of macroscopic currents were observed suggesting that there was not a processing deficit present for pig CFTR. However due to the large variance in single-channel current between the patches that were obtained for this orthologue it is not possible to infer details regarding the single-channel current and conductance of this channel without further experiments. From the data that were obtained, single-channel current was calculated as -0.72 ± 0.26 pA at -50 mV, whereas P_o was 0.47 ± 0.05 (n = 2) (Figure 3.3A and B). The data for P_o does correlate with data that have been published for pig CFTR which showed activity to be similar to human (Ostedgaard et al., 2007). However, this previously study reported a decreased conductance of pig CFTR compared to human CFTR, in contrast to the increase observed from our data (8.10 ± 0.4 pS, n = 3, Figure

3.3C and D). It is likely that this variance results from the low power of our recordings and more data would be required to confirm the conductance of pig WT-CFTR.

3.2.1.2 Sheep CFTR

Sheep CFTR, transiently expressed in CHO cells produced Cl^- currents after activation by PKA-dependent phosphorylation at -50 mV with a similar gating behaviour to that of human CFTR (Figure 3.2). However, sheep WT-CFTR had a higher P_o (0.45 ± 0.05) and single-channel current (-0.85 ± 0.06 pA) (*n* = 6) at -50 mV, indicating increased activity when compared to human CFTR (Figure 3.3A and B). Slope conductance calculated from the i/V curve from -80 mV to 0 mV was 8.79 ± 0.25 pS, confirming an increased conductance compared to human CFTR (Figure 3.3C and D). These data for sheep CFTR are consistent with previous recordings for sheep CFTR that have been published by our group (Cai *et al.*, 2015), and confirm that sheep CFTR is more active than human CFTR at the single-channel level.

3.2.1.4 Ferret CFTR

Ferret CFTR transiently expressed in CHO cells produced a Cl^- current after activation by PKA-dependent phosphorylation that demonstrated similar gating properties to those observed for human, sheep and pig CFTR, albeit with a decreased single-channel current, which was -0.24 ± 0.02 pA at -50 mV (n = 6, Figures 3.2 and 3.3B). P_o for ferret CFTR was recorded as 0.44 ± 0.07 (n = 6, Figure 3.3A). Despite the low single-channel current observed for ferret CFTR, slope conductance calculated from the i/V slope from -100 mV to -40 mV was high (8.48 ± 0.52 pS, Figure 3.3C and D). Due to the low signal to noise ratio and small single-channel current at voltages more positive to -40 mV, it was not possible to calculate the single-channel current at more positive voltages. According to the Nernst equation (Equation 3, section 2.1.5), the equilibrium potential for Cl^- (E_{Cl}) under the experimental conditions used was calculated as 71.8 mV. Linear extrapolation of the i/V relationships for the majority of CFTR orthologues tested, as shown in Figure 3.3C, suggests a reversal potential of around +20 mV to +30 mV, although CFTR does demonstrate inward rectification at positive voltages in the presence of a Cl^- concentration gradient (Sheppard & Welsh, 1999). It is therefore possible that the high slope conductance calculated for ferret CFTR at voltages below -40 mV is indicative of rectification at voltages more positive

to -40 mV. Indeed, previous studies have identified inward rectification for some CFTR orthologues (e.g. mouse) (Cai *et al.* 2003; Cui & McCarty, 2015). Further testing, either using macroscopic Cl^- currents or alternatively under symmetrical Cl^- conditions, would be required to confirm this rectification property for ferret CFTR.

3.2.1.5 Mouse CFTR

As shown by the example traces in both Figure 3.2 and Figure 3.7, mouse CFTR demonstrates a unique gating behaviour following activation by PKA-dependent phosphorylation compared to the other CFTR orthologues tested. As reported by Lansdell et al. (1998b), mouse CFTR expressed in CHO cells demonstrated two levels of opening, with a highly active sub-conductance state (O_1) that was visible when traces underwent additional filtering at 50 Hz, and brief openings to a fully open state (O_2) with a reduced single-channel current of -0.21 ± 0.02 pA (n = 5) at -50 mV, representing 37% of human CFTR (Figure 3.3B). The P_o of the O_2 state of mouse WT-CFTR was 0.05 ± 0.01 (n = 5), representing an 88% reduction compared to human WT-CFTR. In addition, mouse CFTR demonstrated a low slope conductance calculated from the i/V relationship from -100 mV to 0 mV, with γ = 3.32 ± 0.80 pS (n = 5).

3.2.1.6 Zebrafish CFTR

Only one single-channel patch was obtained for zebrafish CFTR and caution must therefore be used in the interpretation of these data. However, the data showed that transient expression of zebrafish CFTR in CHO cells resulted in the activation of single-channels by 1 mM ATP and 75 nM PKA at negative voltages. From visual comparison of the recording obtained for zebrafish CFTR with other CFTR orthologues (Figure 3.2), zebrafish CFTR appeared to demonstrate a gating behaviour intermediate between that of mouse CFTR and human CFTR. Zebrafish CFTR demonstrated brief openings that were more active than those of mouse CFTR, but not as active as human CFTR, with a P_o of 0.16 and a single-channel current of -0.20 pA at -50 mV (*n* = 1). It was not possible to generate an i/V relationship from these data as analysis was only possible at a holding potential of -100 mV due to the small amplitude of single-channel current and low signal to noise ratio of this recording. The

small single-channel current amplitude at -100 mV suggests that conductance of zebrafish CFTR is lower than that of the other orthologues tested at negative membrane potentials.

3.3 Different effects of the F508del mutation in diverse CFTR orthologues

Previous studies have highlighted that CFTR orthologues from different species are affected differently by CF-related mutations (Ostedgaard *et al.*, 2007; Aleksandrov *et al.*, 2012; Cai *et al.*, 2015). We therefore chose to investigate the effect of the common CF mutation F508del on sheep and mouse CFTR to determine if the effects of this mutation were different for these orthologues when compared to human F508del-CFTR.

3.3.1 The impact of F508del on human CFTR

Figure 3.4 shows the effects of the F508del mutation on the gating behaviour of human CFTR as observed following activation by PKA-dependent phosphorylation. 1 s sections of traces in Figure 3.4 A and B (indicated by black bars) have been expanded for comparison. For these experiments, both human F508del- and WT-CFTR were stably expressed in NIH 3T3 cells. Cells expressing F508del-CFTR were incubated at 27 °C for at least 24 hours prior to experiments to correct for the processing defect caused by the F508del mutation. For cells expressing human F508del-CFTR, addition of 1 mM ATP and 75 nM PKA resulted in the observation of single-channel currents at a holding potential of -50 mV with a P_o of 0.08 ± 0.03 and single-channel current of -0.61 ± 0.05 pA (n = 7). These data demonstrate that F508del results in a severe gating defect of human CFTR with an 81% reduction in P_o (P < 0.05) compared to WT and no change in single-channel current amplitude (Figure 3.4B, C and D).

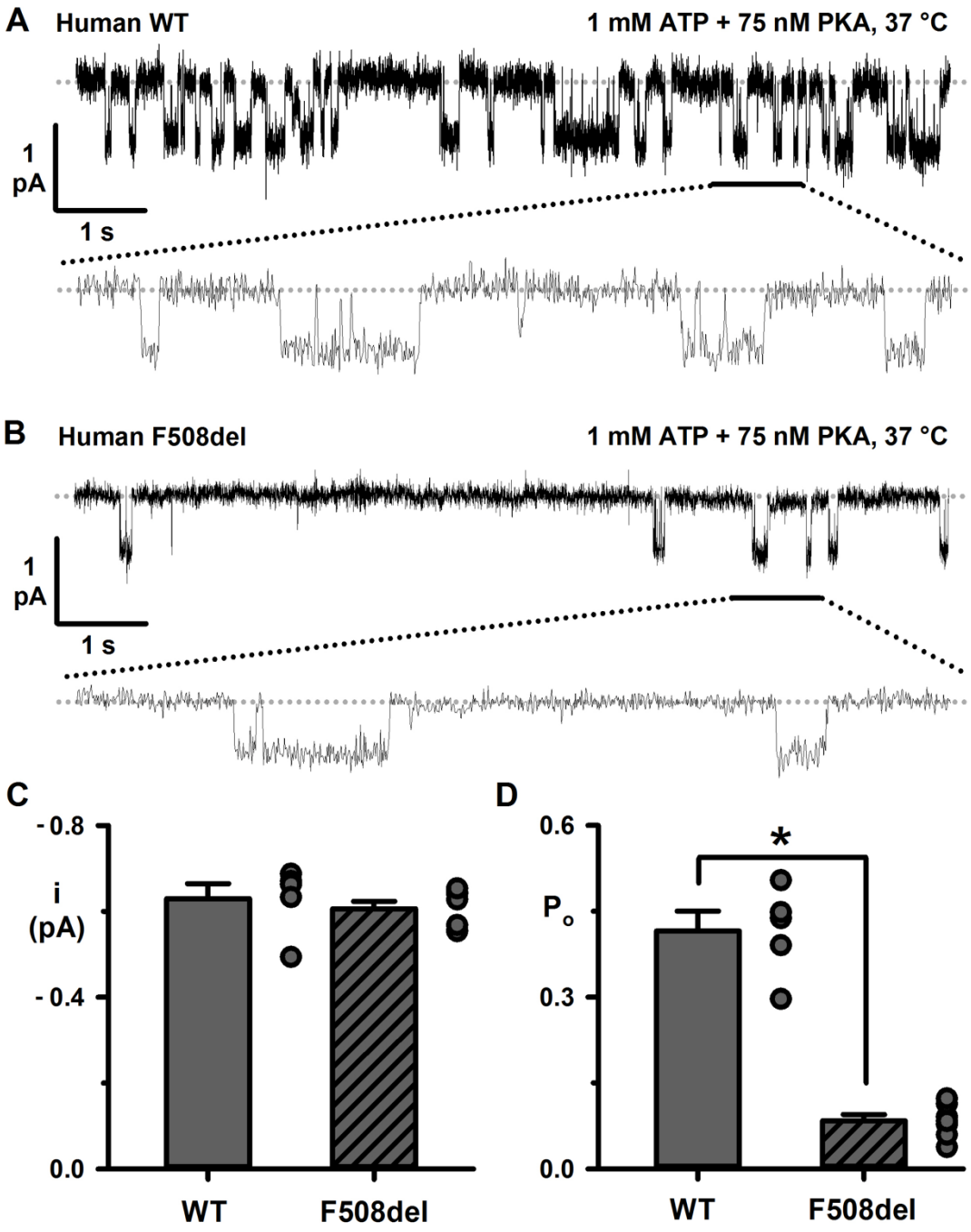

Figure 3.4: Comparison of i and P_o for human WT- and F508del-CFTR. A Representative trace recorded following activation of human WT-CFTR by 1 mM ATP and 75 nM PKA at -50 mV and 37 °C. For the purpose of illustration, recordings have been filtered at 500 Hz and digitised at 5 kHz before file size was compressed by 5-fold data reduction. Dotted grey lines represent the closed level for each channel. Lower trace shows expanded 1 s region as indicated by black horizontal bar. **B** Representative trace recorded following activation of human F508del-CFTR. Conditions were the same as described for **A**. **C** and **D** i and P_o for human WT- and F508del-CFTR. Error bars represent SEM and individual data points are indicated by circles adjacent to each bar (human WT-CFTR, n = 5; human F508del-CFTR, n = 7; * = $P < 0.05$, unpaired, two-way Student's t-test).

From visual inspection of the traces shown in Figure 3.4A and B, the gating defect of F508del appears to result in an increase in IBI and potentially a decrease in MBD. Only one excised-membrane patch was obtained for cells expressing human F508del-CFTR where only one level of opening was observed for the duration of the experiment. From this recording, dwell-time histograms were generated using pClamp software (v6.02) and used to measure mean open- (τ_o) and closed- (τ_c) times (Figure 3.5 and Table 3.2). As shown in Figure 3.5B and Table 3.2, human F508del-CFTR demonstrated two populations of open-times (τ_{o1} and τ_{o2}) representing brief openings (τ_{o1}) and longer openings (τ_{o2}) with a reduced frequency compared to the single population of human WT-CFTR openings (τ_{o1}) as indicated by the area under the curve (Table 3.2). Both human WT-CFTR and F508del-CFTR showed two populations of closed-times representing intraburst (τ_{c1}) and interburst (τ_{c2}) closures respectively. These data show that the reduced P_o of human F508del-CFTR compared WT-CFTR results primarily from an increase in τ_{c2} (Table 3.2).

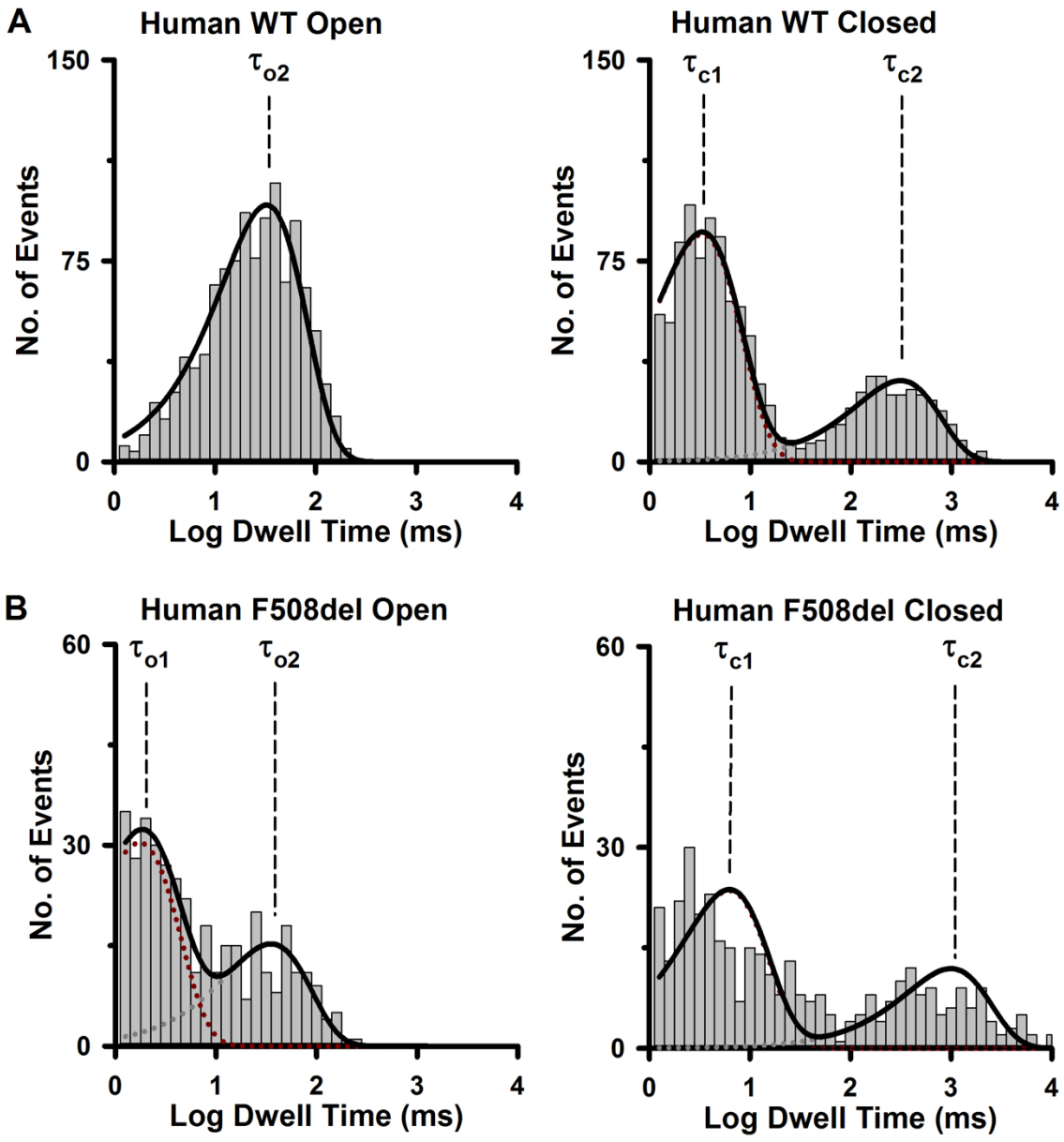

Figure 3.5: Representative dwell-time histograms for open- and closed-time events of human WT- (A) and F508del-CFTR (B). Histograms have been fitted with one- or two-component exponential functions (solid black lines). Logarithmic x-axes are used for both open and closed time histograms plotted with 10 bins·decade^{-1}. Dashed lines indicate mean open (τ_{o1} and τ_{o2}) and mean closed (τ_{c1} and τ_{c2}) durations. Individual components for the τ_{c1} and τ_{c2} of the closed-time histogram are indicated by red and grey dotted lines respectively. Measurements were made using the conditions described in Figure 3.4.

	Human WT-CFTR	Human F508del-CFTR
τ_{O1} (ms)	-	1.74
τ_{O2} (ms)	32.4 ± 10.9	35.1
τ_{C1} (ms)	4.16 ± 2.15	6.21
τ_{C2} (ms)	117 ± 14.1	995
Area under curve τ_{O1}	-	0.67
Area under curve τ_{O2}	1	0.33
Area under curve τ_{C1}	0.69 ± 0.03	0.66
Area under curve τ_{C2}	0.31 ± 0.03	0.34
n	3	1

Table 3.2: Open- and closed-time constants of human WT- and F508del-CFTR. Open- (τ_{o1} and τ_{o2}) and closed-time (τ_{c1} and τ_{c2}) constants were derived from dwell time histograms as shown in Figure 3.5. Areas under curve indicate the proportion of the total area under the fitted exponential curve.

3.3.2 The impact of F508del on sheep CFTR

Figure 3.6 shows the impact of the F508del mutation on sheep CFTR when recombinant cDNA was transiently expressed in CHO cells. Figure 3.6A shows a representative recording demonstrating the gating behaviour of sheep WT-CFTR. As mentioned earlier, sheep WT-CFTR shows increased activity compared to human WT-CFTR with a 7% increase in P_o and a 35% increase in single-channel current (Figure 3.3). Compared to sheep WT-CFTR, sheep F508del-CFTR demonstrated a P_o of 0.19 ± 0.08 and single-channel current of -0.81 ± 0.07 pA (*n* = 5) at -50 mV, representing a 58% reduction in P_o ($P < 0.05$) and no change in single-channel current (Figure 3.6C and D). These results suggest that the F508del mutation results in a gating defect in sheep-CFTR that is less severe than that caused by F508del when present in human CFTR. Unfortunately, insufficient data were collected from cells expressing sheep F508del-CFTR to enable the generation of dwell-time histograms and calculation of τ_o and τ_c for this orthologue.

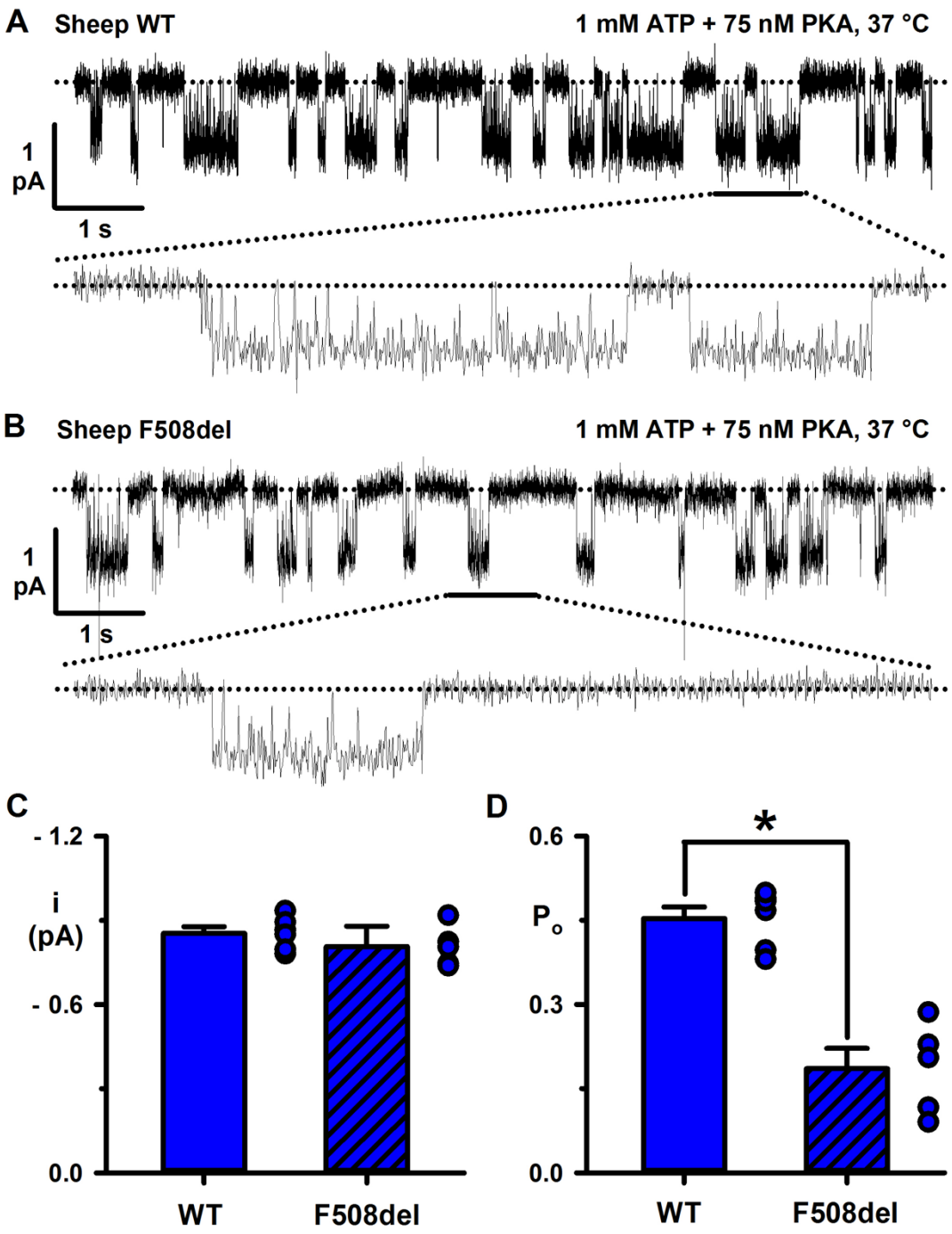

Figure 3.6: Comparison of i and P_o for sheep WT- and F508del-CFTR A Representative trace recorded following activation of sheep WT-CFTR by 1 mM ATP and 75 nM PKA at -50 mV and 37 °C. For the purpose of illustration, recordings have been filtered at 500 Hz and digitised at 5 kHz before file size was compressed by 5-fold data reduction. Dotted grey lines represent the closed level for each channel. Lower trace shows expanded 1 s region as indicated by black horizontal bar. **B** Representative trace recorded following activation of sheep F508del-CFTR. Conditions were the same as described for **A**. **C** and **D** i and P_o for sheep WT- and F508del-CFTR. Data for sheep WT-CFTR are the same as that shown in Figure 3.3. Error bars represent SEM and individual data points are indicated by circles adjacent to each bar (sheep WT-CFTR, $n = 6$; sheep F508del-CFTR, $n = 5$; * = $P < 0.05$, unpaired, two-way Student's *t*-test).

3.3.3 The impact of F508del on mouse CFTR

Figure 3.7 shows the effect of the F508del mutation on mouse CFTR cDNA transiently expressed in CHO cells. Following addition of 1 mM ATP and 75 nM PKA, at -50 mV, mouse WT-CFTR produced single-channel currents as indicated by downward deflections in the recorded trace (Figure 3.7A). Following introduction of the F508del mutation in mouse CFTR, single-channel currents were observed that showed close resemblance to those of mouse WT-CFTR (Figure 3.7B). The gating behaviour of mouse WT-CFTR was characterised by brief openings to the fully open (O_2) state and a highly active sub-conductance (O_1) state as discussed earlier in Section 3.2. Due to the small amplitude of the sub-conductance state (O_1) and low signal to noise ratio of recordings, it was not possible to quantify this level. However, quantification of the second, fully open level (O_2) is shown in Figures 3.7C and D. Data from human WT- and F508del-CFTR expressed in NIH 3T3 cells are also shown in Figures 3.7C and D for the purpose of comparison (human data are the same as that shown in Figure 3.4). P_o of mouse F508del-CFTR was 0.06 ± 0.02, whereas single-channel current was -0.35 ±0.04 pA at -50 mV (*n* = 3) suggesting that the F508del mutation did not have an effect on the activity of the O_2 state of mouse F508del-CFTR when compared to mouse WT-CFTR.

Figure 3.8 and Table 3.3 show dwell-time histograms and values for τ_o and τ_c generated from single-channel recordings for mouse WT- and F508del- CFTR. Only one membrane patch showing a single level of channel-opening was obtained for either mouse WT- or F508del-CFTR and caution must therefore be used in the interpretation of these data. However, as shown in Figure 3.8, both mouse WT- and F508del- showed three populations of closed-times as reported previously (Lansdell *et al.*, 1998a). These data suggest that τ_o and τ_c were similar for both mouse WT- and F508del-CFTR.

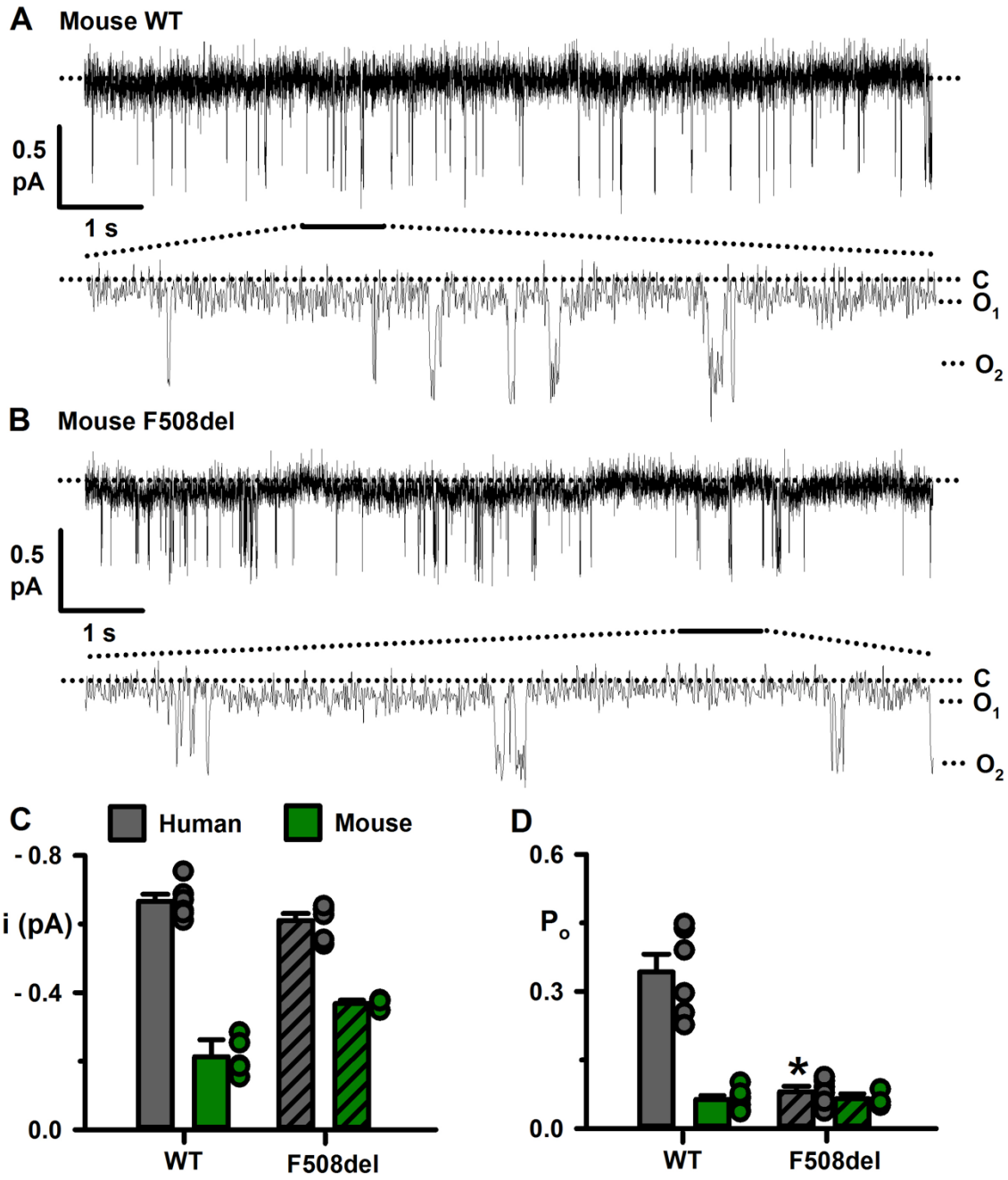

Figure 3.7: Comparison of i and P_o for mouse WT- and F508del-CFTR A Representative trace recorded following activation of mouse WT-CFTR by 1 mM ATP and 75 nM PKA at -50 mV and 37 °C. For the purpose of illustration, recordings have been filtered at 500 Hz and digitised at 5 kHz before file size was compressed by 5-fold data reduction. Dotted grey lines represent the closed level for each channel. Lower trace shows expanded 1 s region as indicated by black horizontal bar. Sub-conductance and full open levels of mouse CFTR are indicated by O_1 and O_2, respectively. **B** Representative trace recorded following activation of mouse F508del-CFTR. Conditions were the same as described for **A**. **C** and **D** i and P_o for human and mouse WT- and F508del-CFTR. Data for human WT-CFTR and human F508del-CFTR are from Figure 3.3. Data are means ± SEM, individual data points are indicated by circles adjacent to each bar (mouse WT-CFTR, n = 5; mouse F508del-CFTR, n = 3; * = $P < 0.05$, two-way unpaired Student's t-test).

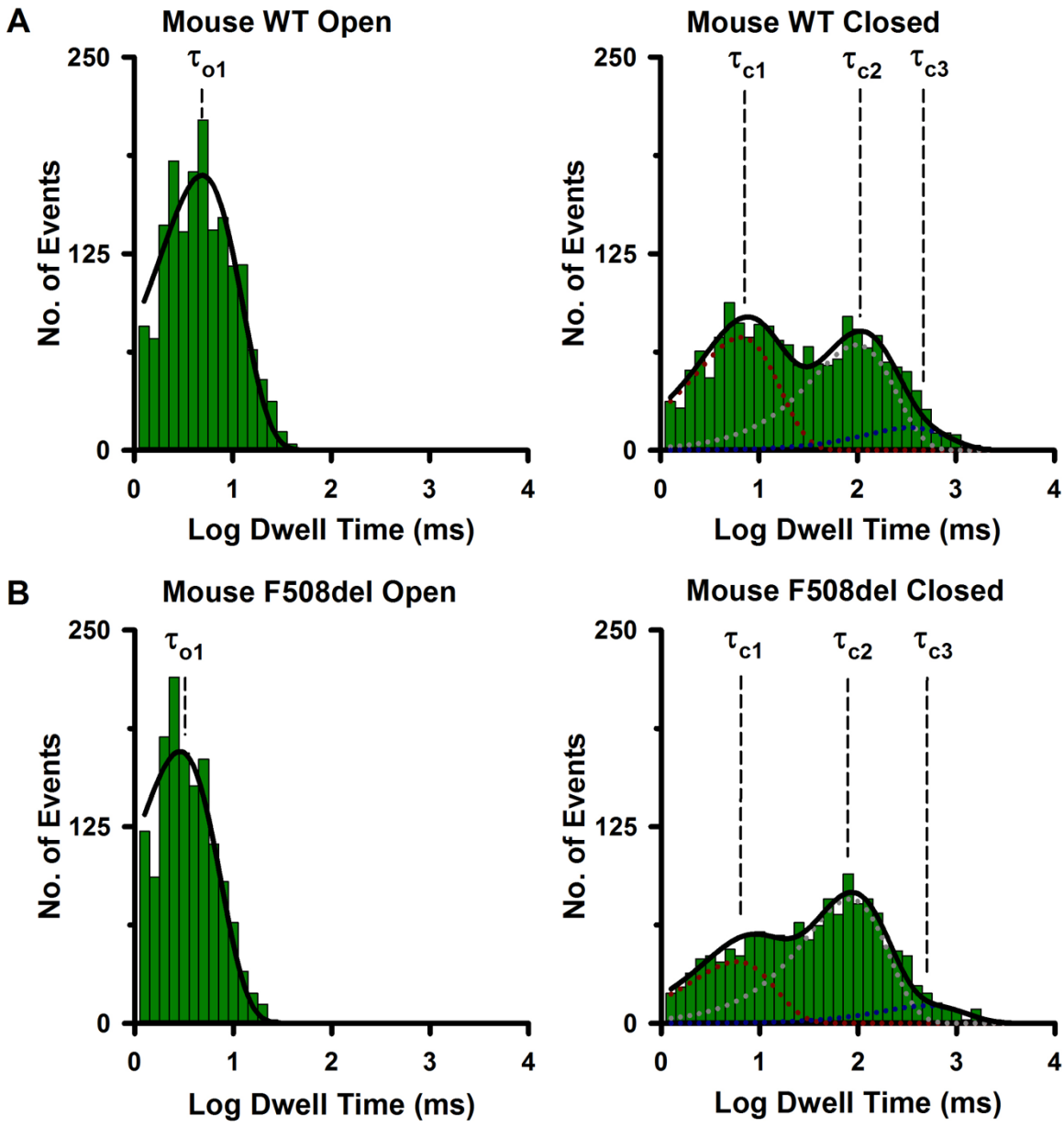

Figure 3.8: Representative dwell-time histograms for open- and closed-time events of mouse WT- (A) and F508del-CFTR (B). Histograms have been fitted with one- or three-component exponential functions (solid black lines). Logarithmic x-axes are used for both open and closed time histograms plotted with 10 bins·decade^{-1}. Dashed lines indicate mean open (τ_{o1}) and mean closed (τ_{c1}, τ_{c2} and τ_{c3}) durations. Individual components for the τ_{c1}, τ_{c2} and τ_{c3} of the closed-time histogram are indicated by red, grey and blue dotted lines respectively. Measurements were made using the conditions described in Figure 3.4.

	Mouse WT-CFTR	Mouse F508del-CFTR
τ_{O1} (ms)	4.88	2.88
τ_{C1} (ms)	6.5	5.84
τ_{C2} (ms)	98.4	82.4
τ_{C3} (ms)	342	501
Area under curve τ_{O1}	1	1
Area under curve τ_{C1}	0.47	0.3
Area under curve τ_{C2}	0.44	0.61
Area under curve τ_{C3}	0.09	0.09
n	1	1

Table 3.3: Open- and closed-time constants of mouse WT- and F508del-CFTR. Open- (τ_{o1}) and closed-time (τ_{c1}, τ_{c2} and τ_{c3}) constants were derived from dwell time histograms as shown in Figure 3.8. Areas under curve indicate the proportion of the total area under the fitted exponential curve.

3.3.4 Thermal stability of F508del-CFTR orthologues at 37 °C

In addition to effects on gating behaviour, the F508del mutation also results in a reduction in the thermal stability of human CFTR at the PM (Lukacs *et al.*, 1993; Schultz *et al.*, 1999; Wang *et al.*, 2014a). Using single-channel patch-clamp experiments, this thermal instability can be observed as a rundown in CFTR activity from patches maintained at 37 °C (Schultz *et al.*, 1999; Wang *et al.*, 2014a). As our results shown in Figure 3.9 demonstrate that the F508del mutation does not affect the gating behaviour of mouse CFTR, we aimed to determine if the resistance of the mouse CFTR orthologue to the effects of F508del extended to the thermal instability (Class V) defect of this mutation (Wang *et al.*, 2011b). In order to test this idea, mouse F508del-CFTR stably expressed in CHO cells was first activated at 27 °C using 1 mM ATP and 75 nM PKA. Following full activation of the channels, the temperature of the experimental chamber was then rapidly increased to 37 °C (temperature increased from 27 °C to 37 °C in less than 2 minutes). The activity of single-channels was then recorded for an extended period (10 to 30 minutes) and P_o was quantified for 30 s intervals for the first 10 minutes. The example trace shown in Figure 3.9A shows the continuous recording made from a membrane patch containing two mouse F508del-CFTR channels for a period of 10 minutes. As shown by the expanded regions in

Figure 3.9B, taken from early, mid-point and late sections of the trace, the activity of mouse F508del-CFTR was sustained for the 10-minute duration of this recording. The P_o recorded for 30 s intervals from multiple patches was quantified and shown in Figure 3.9C (green bars). For the first 10 minutes after temperature had been increased to 37 °C, the P_o of the O_2 state of mouse F508del-CFTR was maintained between 0.05 ± 0.01 and 0.07 ± 0.01 indicating that P_o remained steady for the duration of the experiment. The grey line plotted in Figure 3.9C shows the results from the same experimental protocol using human F508del-CFTR. These data were collected by our group prior to this project and have been used here with permission from the original authors (Wang *et al.*, 2014a). These data demonstrate a rapid reduction in the P_o of human F508del-CFTR during the first 5 minutes after temperature was increased to 37 °C, with complete loss of channel activity after ~7 mins (Figure 3.9C). The data collected for mouse-CFTR therefore demonstrates that mouse F508del-CFTR shows increased thermal stability at the PM at 37 °C compared to human F508del-CFTR under the same experimental conditions.

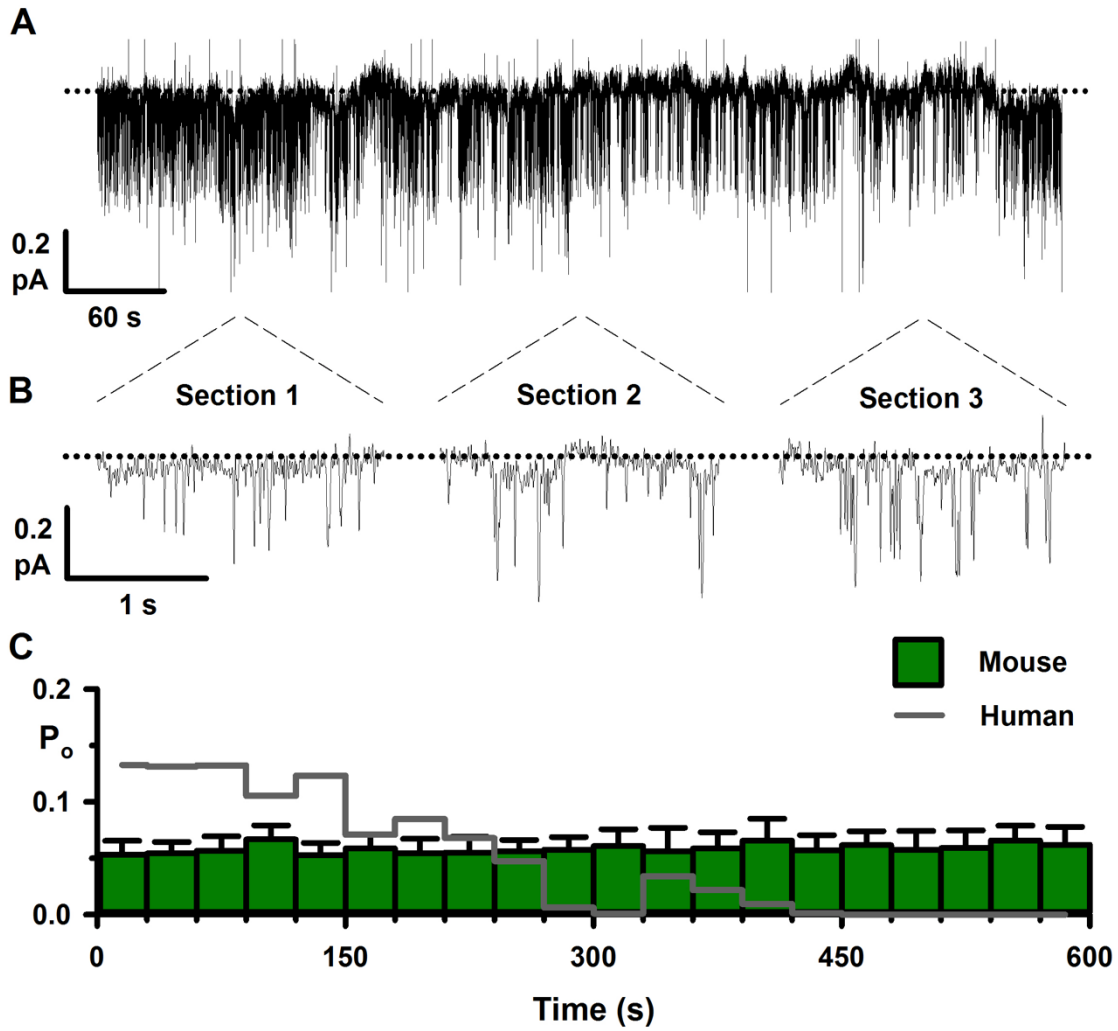

Figure 3.9: Thermal stability of mouse F508del-CFTR A Representative 10-minute recording from an excised inside-out membrane patch from a CHO cell expressing mouse F508del-CFTR at -50 mV. CFTR was activated at 27 °C with 1 mM ATP and 75 nM PKA. Following full activation of CFTR, temperature was rapidly increased (< 2 minutes) to 37 °C. **B** 2-s long recordings labelled sections 1-3 taken from beginning, middle and end of the recording shown in **A** as indicated by the dashed lines. For the purpose of illustration, recordings in **A** and **B** have been filtered at 500 Hz and digitised at 5 kHz before file size was reduced by 5-fold data reduction. Dotted lines in A and B represent the closed state of channels. **C** P_o time-course of mouse F508del-CFTR for the initial 10 minutes following increase in temperature to 37 °C. Data are means ± SEM (n = 3). Values for P_o were calculated for each 30-s time interval as shown by vertical green bars. Grey line represents data for human F508del-CFTR as previously published (Wang *et al.*, 2014a).

3.4: Discussion

3.4.1 Variations in the gating behaviour of CFTR orthologues

Figures 3.2 and 3.3 highlight the diversity observed in the gating behaviour of CFTR orthologues from different species. The first three species studied, human, pig and sheep, are more closely related as indicated by the cladogram in Figure 3.1 and have shared amino acid identities of > 90%. It may therefore be expected that these CFTR orthologues would demonstrate similarities in gating. Despite this, within this group variations were observed indicating that relatively minor changes in sequence can lead to changes in gating behaviour. For example, sheep CFTR shares 91% shared a.a. identity with human CFTR, with most of the sequence variation occurring in the RD (Appendix 1). However, sheep CFTR showed a 7% increase in P_o and a 35% increase in single-channel current amplitude compared to human CFTR. Comparison of the architecture of the channel pore of human and sheep CFTR has shown that the structure of these regions is similar between the different orthologues, suggesting that sequence variations in other, non-regulatory regions of the channel may have an influence on gating properties (Cai *et al.*, 2015). Our data are at variance with data published by Aleksandrov *et al.* (2012) where sheep CFTR was expressed in planar lipid bilayers. However as discussed in Cai *et al.* (2015) these variations may result from differences in the orthologues used, for example the CFTR construct used in our study includes the F229L polymorphism and lacks the C-terminus attached green fluorescent protein tag used by Aleksandrov *et al.* (2012). Of the orthologues tested, pig CFTR is the most closely related to human, with 92% shared a.a. identity. Unfortunately, only two successful single-channel patches were obtained for this orthologue and as such caution must be used in interpreting these data. However, keeping this in mind, pig and sheep CFTR do appear to share more similarities in gating behaviour with human CFTR than the other CFTR orthologues that were tested. These similarities provide support for the use of both pig and sheep animal models of CF although further clarification of the gating behaviour of pig CFTR is required.

Although only one excised inside-out membrane patch was successfully obtained for zebrafish CFTR, the data that were obtained for zebrafish CFTR does suggest that this orthologue shows a very different gating pattern to human CFTR and may be more

closely related to mouse CFTR. Zebrafish CFTR demonstrated a reduced single-channel current amplitude and P_o compared to human CFTR. The activity of zebrafish CFTR was higher than that of mouse CFTR. However, visual comparison of the mouse and zebrafish traces in Figure 3.2 show similarities, principally the presence of brief channel openings. It may also be possible that zebrafish CFTR demonstrates mouse-like sub-conductance, although it was not possible to accurately determine this possibility from the data collected. Zebrafish shares 54% a.a. identity with human CFTR and is one of the most divergent CFTR orthologues to have been studied at the single-channel level. Despite this variance, comparison of the high resolution cryo-EM structures of human CFTR and zebrafish CFTR showed that these two orthologues share remarkably similar structure despite this difference (Zhang & Chen, 2016; Liu *et al.*, 2017). This observation suggests that the percentage of shared amino acid identity is not a good predictor of structural similarity.

The cladogram shown in Figure 3.1 suggests two evolutionary clades of the orthologues that were tested in this investigation based on sequence alignments. The first clade includes human, pig and sheep CFTR, whilst the second includes mouse and zebrafish. Of the sequences tested however, ferret CFTR occupies a clade of its own. Indeed, whilst ferret CFTR demonstrated a pattern of channel gating that was closer to human, pig and sheep CFTR, the single-channel current amplitude of ferret CFTR was notably smaller than these species, but higher than mouse and zebrafish. It therefore appears that there may be correlation between the evolutionary divergence of CFTR sequence as highlighted in the construction of the cladogram in Figure 3.1 and channel function as shown in Figures 3.2 and 3.3. CFTR function has most likely evolved in a way that is optimised for its role in different species (Bose *et al.*, 2015). The cladogram shown in Figure 1.7 in Section 1.6 suggests that ferret CFTR shares a similar structure with that of dog and cat CFTR. It would therefore be interesting to compare the gating behaviour of these species to determine if they are more closely related to ferret in terms of CFTR function than to human. Indeed, both dog and cat models of CF may be considered in addition to the existing ferret models. However, the differences in function between human and ferret CFTR identified in this study may have relevance for the use of existing ferret CF models.

In an early study of the mouse CFTR orthologue, Lansdell *et al*. (1998b) showed that

heavy filtering of single-channel current traces recorded from cells expressing mouse CFTR revealed a sub-conductance state (O_1) with a small amplitude corresponding to around 10% of the amplitude of the full conductance state (O_2). This sub-conductance state has subsequently been observed in other studies both at 37 °C (Scott-Ward *et al.*, 2007) and at 25 °C (Ostedgaard *et al.*, 2007). Due to the small amplitude of this sub-conductance state at a holding potential of -50 mV and the signal to noise ratio present in recordings, it has not been possible to provide a detailed analysis of this sub-conductance state beyond observing that the P_o of O_1 appears to be considerably higher than that of O_2 (Figure 3.7). Interestingly, a second sub-conductance state with a current amplitude lying between those of O_1 and O_2 has been observed by Cui & McCarty (2015) in excised inside-out membrane patches studied at room temperature and with a holding potential of -100 mV. However, this sub-conductance state has not been observed either in our experiments or in previous studies by other groups (Lansdell *et al.*, 1998a; Lansdell *et al.*, 1998b; Ostedgaard *et al.*, 2007; Scott-Ward *et al.*, 2007).

3.4.2 Variation in the impact of the F508del mutation on CFTR orthologues

A number of previous studies have examined the impact of F508del in different CFTR orthologues and have shown that this mutation may have species-specific effects on channel processing and gating activity (Ostedgaard *et al.*, 2007; Fisher *et al.*, 2011; Aleksandrov *et al.*, 2012; Cai *et al.*, 2015). For example, whereas human F508del-CFTR is characterised by a severe processing defect that results in targeting by the endoplasmic-reticulum-associated degradation (ERAD) pathway (Lukacs *et al.*, 1994; Ward *et al.*, 1995), both mouse and pig F508del-CFTR have been shown to retain levels of expression at the plasma membrane (Ostedgaard *et al.*, 2007). Aleksandrov *et al.* (2012) have also demonstrated variation in the maturation of F508del-CFTR in a wide range of both mammalian and non-mammalian species. Understanding the impact of mutations on different species is important, for example in determining the suitability of CF animal models based on gene mutations rather than knock-out and it should be kept in mind that mutations will not affect all orthologues for a given gene in the same way. Additionally, understanding the structural variations between diverse CFTR orthologues that relate to differences in the susceptibilities of these orthologues

to CF-related mutations may provide insights for the development of potential therapeutic strategies for CF.

Human F508del-CFTR shows severely reduced activity compared to WT-CFTR when the processing defect of this mutation is corrected, characterised by a reduction in the duration of channel openings and a prolongation of channel closures (Figures 3.4 and 3.5) (Dalemans *et al.*, 1991). In contrast, our data showed that in the case of both mouse and sheep CFTR, the F508del mutation does not cause a severe reduction in activity (Figures 3.6 and 3.7). In the case of sheep F508del-CFTR, our data showed that P_o was reduced compared to WT, however this corresponded to a 58% reduction compared to the 81% reduction observed for human F508del-CFTR (Figure 3.4).

Whilst previous studies have demonstrated that the F508del mutation has a minimal impact on the processing of mouse CFTR (Ostedgaard *et al.*, 2007), our data suggest that the disruption to channel gating normally associated with F508del is absent in the case of mouse CFTR (Figure 3.7). In previous studies of the F508del mutation in human, pig, mouse and sheep the reduction in P_o caused by F508del has been shown to result mainly from an increase in the inter-burst interval (IBI) corresponding to channel closures, rather than a severe reduction in the mean burst duration (MBD) (Ostedgaard *et al.*, 2007; Cai *et al.*, 2015). As discussed in Section 1.3.2, channel opening is dependent upon tight dimerization of NBD1 and NBD2 on binding of ATP (Vergani *et al.*, 2005b; Hwang & Sheppard, 2009). The increase in IBI observed in the case of F508del therefore likely results from an increase in the energy barrier for channel opening, suggesting that the gating defect caused by F508del may be linked to disruption of the formation of the NBD1-NBD2 dimer (Cai *et al.*, 2015). Jih *et al*. (2011) have further examined the effect of F508del on CFTR gating using PP_i, which locks the channel in the fully bound NBD1-NBD2 dimer configuration, and by testing the ligand exchange time for ATP/P-dATP, a measure of the stability of the dimer following ATP hydrolysis at site 2. This study demonstrated that the F508del mutation destabilises both the full and partial NBD dimer configurations during the CFTR gating cycle (Jih *et al.*, 2011). These data are further supported by evidence from studies using nuclear magnetic resonance that also appear to show that the F508del mutation results in impaired NBD dimerization (Chong *et al.*, 2015).

Taking these points into consideration, our data appear to show that the disruption observed in NBD dimer formation by the F508del mutation does not appear to affect the gating properties of mouse CFTR. It is therefore possible that in the case of mouse CFTR, structural differences compared to the human CFTR channel may provide stabilisation to this dimer interface. In addition, many structural models of CFTR suggest a close interaction between ICL4 and the region of NBD1 that includes F508, which includes the helical regions H3 and H4, known as the H loop (Callebaut *et al.*, 2004; Mornon *et al.*, 2008; Serohijos *et al.*, 2008; Mornon *et al.*, 2014; Liu *et al.*, 2017). Despite the relatively low sequence homology between human and mouse CFTR, focussing on sequence differences within the NBD1 and ICL4 highlights certain residues that warrant further study into their involvement in providing resistance to the F508del gating defect. The first of these changes is I539T, which is of particular interest as when included in human CFTR this sequence alteration acts as a revertant mutant of F508del (deCarvalho *et al.*, 2002; Ostedgaard *et al.*, 2007; Hoelen *et al.*, 2010). In mice, it is therefore possible that T539 helps to stabilise NBD1-NBD2 dimer. Another sequence alteration that is of interest is G1069R located in ICL4. According to the cryo-EM structure of human CFTR produced by Liu *et al.* (2017), G1069 is likely to be located in the vicinity of the coupling helix of ICL4, the region most likely to interact with NBD1 and F508. Indeed, further support for this idea is provided by the observation that the sequence change R1070W is known to correct the folding defect of F508del-CFTR (Thibodeau *et al.*, 2010; Molinski *et al.*, 2012; Phuan *et al.*, 2014). It is therefore possible that the addition of the large, positively charged side-chain of this additional arginine residue in mouse CFTR helps to stabilise the interaction of ICL4 and NBD1 in the absence of F508del.

3.4.3 Thermal stability of mouse F508del-CFTR

Human F508del-CFTR exhibits a marked thermal instability and rapidly deactivates at 37 °C (Wang *et al.*, 2011b; Liu *et al.*, 2012; Wang *et al.*, 2014a). Previous work by our group has shown that sheep F508del-CFTR also demonstrates thermal instability, albeit to a lesser degree than that of human F508del-CFTR (Cai *et al.*, 2015). In contrast, Aleksandrov *et al.* (2012) have demonstrated that chicken F508del-CFTR demonstrates thermal stability at the plasma membrane, and there is also evidence from pulse-chase experiments that suggests ferret F508del-CFTR may be more stable

than human F508del-CFTR (Fisher *et al.*, 2012). Our data show that in contrast to the thermal instability previously shown for human and sheep CFTR, mouse F508del-CFTR retains a high level of activity at 37 °C that was sustained beyond 10 minutes (Figure 3.9). In this respect, mouse F508del-CFTR appears to share the characteristic of thermal stability that has been previously documented for chicken F508del-CFTR (Aleksandrov *et al.*, 2012).

By comparing the sequences of chicken and human CFTR, Aleksandrov *et al*. (2012) identified the presence of four additional proline residues that are present in chicken CFTR, but not human CFTR, corresponding to sequence alterations S422P, S434P, S492P and A534P, as well as the F508del revertant mutation I539T discussed earlier (deCarvalho *et al.*, 2002). When introduced into human F508del-CFTR via site-directed mutagenesis, these sequence alterations restored channel processing, membrane stability and functionality (Aleksandrov *et al.*, 2012). Given that the human CFTR residues S422, S492 and A534 are conserved in mouse CFTR these proline substitutions do not account for the similarities observed between mouse and chicken CFTR. However as previously mentioned, mouse CFTR does include T539 and it is possible that this residue may be involved in stabilising the co-translational folding of mouse F508del-CFTR NBD1 as has been reported for human F508del-CFTR (Hoelen *et al.*, 2010). However, Dong *et al.* (2012) have demonstrated that whilst I539T improves processing of human F508del-CFTR, this sequence alteration has a negative impact on channel gating and does not improve the processing of human-mouse chimeras expressing the mouse sequence for residues 433-632 in NBD1. Mouse CFTR also contains a number of other sequence alterations in this region, which is adjacent to the interface between TMD1 and NBD1, including S434C. It is therefore possible that sequence alterations in this region may contribute to some of the differences observed between mouse and human F508del-CFTR orthologues. Further knowledge of the involvement of this region in protein function and the involvement of specific amino acids in providing resistance to the deleterious effects of F508del may therefore be gained by studying human-mouse chimeric proteins that contain this region of mouse CFTR.

In conclusion, our data have demonstrated variations in the gating behaviour of CFTR orthologues that may occur despite high levels of homology. Furthermore, our data

suggest that structural variation between CFTR orthologues may reduce the impact of CF-causing mutations including, F508del.

4. The effects of small molecule CFTR modulators on the single-channel activity of WT and F508del-CFTR orthologues

4.1 Introduction

CFTR orthologues have previously been shown to demonstrate cross species differences in response to small molecule CFTR modulators. For example, Stahl *et al.* (2012) showed that pig CFTR does not respond to the CFTR inhibitor glibenclamide, whereas shark CFTR does not respond to $CFTR_{inh}$-172. Furthermore, differential responses of CFTR orthologues to CFTR potentiators have previously been used to determine the binding domains for these compounds. The observation that mouse CFTR does not respond to the inorganic phosphate analogue PP_i (Lansdell *et al.*, 1998a), provided rationale for use of human-mouse CFTR chimeras to determine the binding site for this compound (Scott-Ward *et al.*, 2007). Scott-Ward *et al.* (2007) demonstrated that substitution of the human NBD2 sequence for the equivalent mouse domain was sufficient to prevent the response of human CFTR to PP_i, thereby demonstrating the role of NBD2 in binding the compound (Scott-Ward *et al.*, 2007).

Given the potential for cross-species chimeras to determine regions of the CFTR protein that may be involved in the mechanism of action of CFTR potentiators, we aimed to determine how the CFTR orthologues we chose to study in Chapter 3 respond to such potentiators. In particular, we chose to focus on the CFTR potentiator ivacaftor (VX-770; Kalydeco®, Vertex Pharmaceuticals). Ivacaftor was the first small molecule CFTR modulator to be licensed for the treatment of CF (Van Goor *et al.*, 2009; Ramsey *et al.*, 2011). Yet despite over a decade of research, very little is known about the mechanism of action of this compound and few studies have investigated the efficacy of ivacaftor for potentiation of non-human CFTR orthologues (Bose *et al.*, 2015; Cui & McCarty, 2015; Cui *et al.*, 2016). Identification of variations in the response of diverse CFTR orthologues to ivacaftor may therefore provide insight into structural regions of CFTR involved in the mechanism of action of this compound. Such differences may also have implications for the use these species in the

development of novel CF therapies that share the same or similar mechanism of action as ivacaftor.

As discussed in Chapter 1, ivacaftor is effective for a range of class III CF-causing mutations such as G551D and S549N that affect channel gating behaviour and result in a decrease in CFTR activity (Sheppard *et al.*, 2017). Ivacaftor enhances ATP-independent gating (Eckford *et al.*, 2012), and increases the potential for re-entry of ATP at the hydrolytic binding site by stabilising the post-hydrolytic open state of the CFTR channel (Jih & Hwang, 2013). At the single-channel level, ivacaftor enhances both human WT- and mutant CFTR activity, primarily via an increase in MBD and the frequency of channel openings (Van Goor *et al.*, 2009; Wang *et al.*, 2018). We therefore aimed to investigate the response of CFTR orthologues to ivacaftor using the single-channel patch-clamp technique to determine whether ivacaftor potentiates these orthologues and to learn how the compound may affect CFTR gating in different species.

4.2 Effects of ivacaftor on the activity of CFTR orthologues

4.2.1 Potentiation of WT-CFTR from diverse species by ivacaftor

4.1.1.1 Human CFTR

Figure 4.1 shows the effect of cumulative addition of ivacaftor at concentrations between 10 nM and 10 μM to the intracellular solution bathing excised inside-out membrane patches taken from NIH 3T3 cells stably expressing human WT-CFTR in the continuous presence of 1 mM ATP and 75 nM PKA at 37 °C. Washout of ivacaftor between test concentrations was not possible as the high viscosity of this compound resulted in carry-over of the drug between successive interventions. Experimental chambers therefore required submersion in 40% DMSO for a minimum of 4 hours between treatments to ensure removal of the compound.

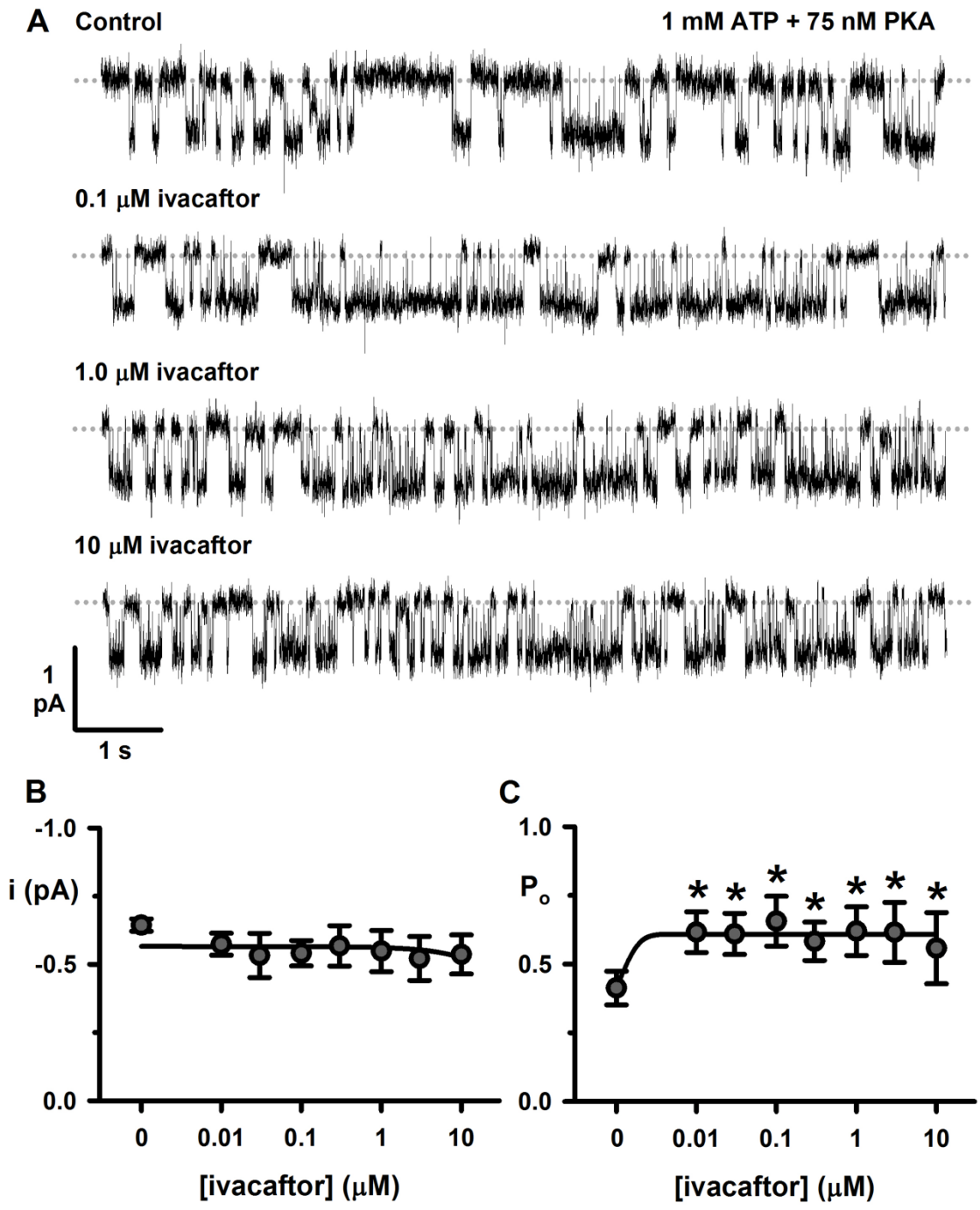

Figure 4.1: Effect of ivacaftor on human WT-CFTR in the presence of 1 mM ATP and 75 nM PKA. **A** Representative single-channel recordings from an inside-out membrane patch excised from an NIH 3T3 cell showing the response of human WT-CFTR to ivacaftor at concentrations from 0.01 μM to 10 μM in the presence of a Cl^- concentration gradient ($[Cl^-]_{int}$ = 147 mM; $[Cl^-]_{ext}$ = 10 mM). Holding potential was clamped at -50 mV throughout and recordings were made in the continuous presence of 1 mM ATP and 75 nM PKA. Temperature was maintained at 37 °C. Dotted lines represent the closed level for the channel. 5-fold data reduction was applied to traces in **A** for the purpose of illustration. **B** and **C** Single-channel current amplitude (i) and P_o of human WT-CFTR at ivacaftor concentrations from 10 nM to 10 μM. Graphs in **B** and **C** were fitted with 3-parameter sigmoidal curves using SigmaPlot software v13.0 (n = 3, * = P < 0.05, one-way repeated measures ANOVA and Dunnett's multiple comparisons).

Figure 4.1A, shows representative single-channel recordings for control, 0.1 μM, 1.0 μM and 10 μM ivacaftor, respectively, at a holding potential of -50 mV. Addition of ivacaftor did not affect single-channel current amplitude (Figure 4.1B), but resulted in an increase in the P_o of human WT-CFTR from 0.41 ± 0.06 under control conditions to 0.56 ± 0.13 at 10 μM, with a peak of 0.62 ± 0.09 at 0.1 μM (n = 3, P < 0.05 compared to control) (Figure 4.1C). Data collected for the response of human WT-CFTR to ivacaftor was fitted with a 3-parameter sigmoidal curve (Equation 4), however due to the high level of potentiation observed at ivacaftor concentrations as low as 0.01 μM (P_o = 0.62 ± 0.07, n = 3) it was not possible to calculate K_D from this analysis.

Due to the high activity of human WT-CFTR at 1 mM ATP, the effect of ivacaftor was also tested in the presence of 0.3 mM ATP (Figure 4.2). For these experiments, human WT-CFTR stably expressed in BHK cells was activated by direct addition of ATP to the experimental chamber at a concentration of 1 mM in conjunction with 75 nM PKA. The ATP concentration was then reduced to 0.3 mM by perfusing the experimental chamber with 10 ml bath solution containing 0.3 mM ATP and subsequent addition of 75 nM PKA. Again, ivacaftor did not affect the single-channel current amplitude of human CFTR (Figure 4.2B), but resulted in an increase in P_o at all concentrations tested, with a P_o of 0.19 ± 0.03 before addition of ivacaftor, increasing to 0.30 ± 0.04 at both 1.0 μM and 10 μM ivacaftor (Figure 4.2C) (n = 4, P < 0.05 compared to control), representing an increase in activity of 58%.

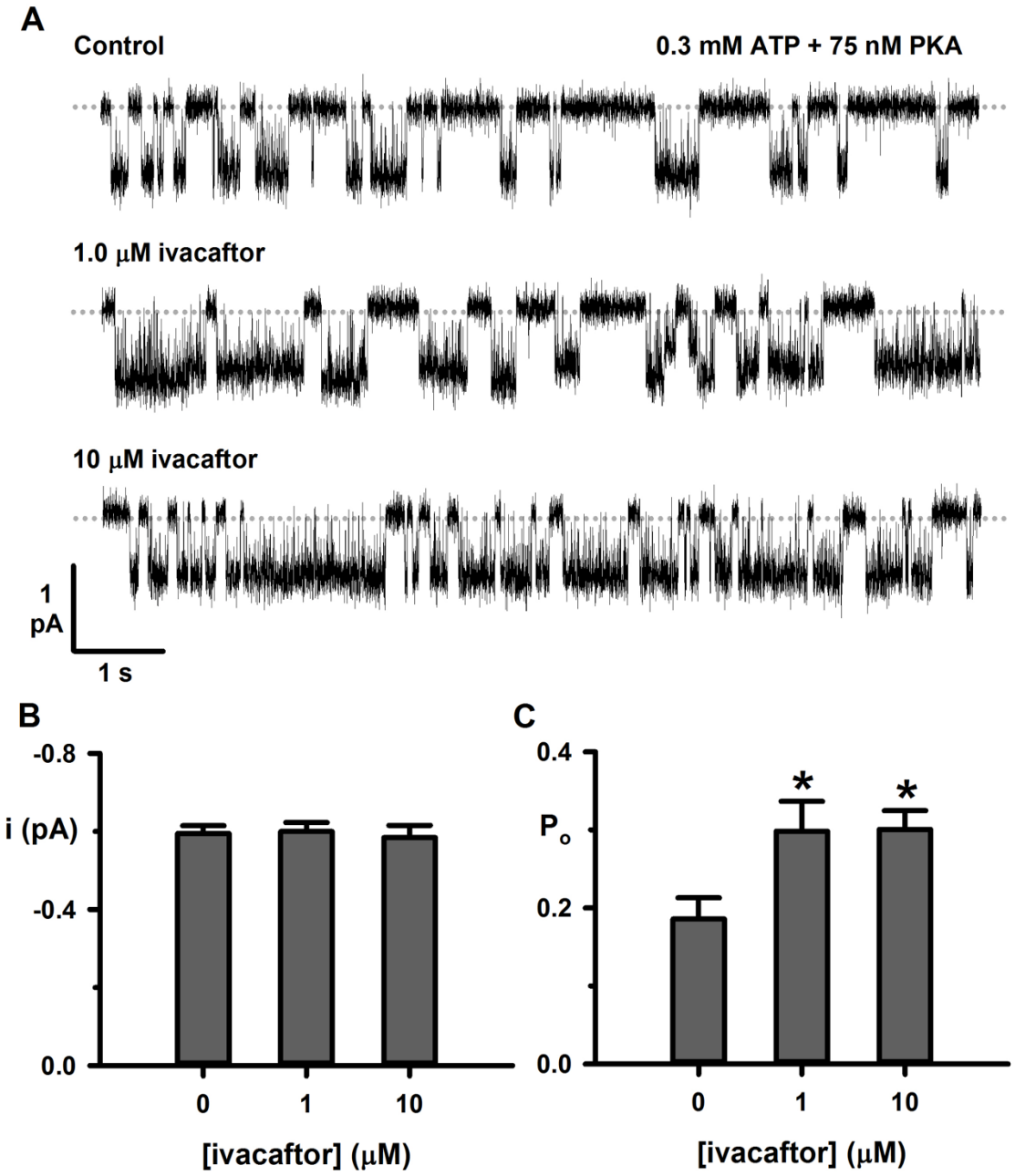

Figure 4.2: Effect of ivacaftor on human WT-CFTR in the presence of 0.3 mM ATP. A Representative single-channel recordings from an excised inside-out membrane patch from a BHK cell showing the response of human WT-CFTR to ivacaftor at concentrations of 1.0 μM and 10 μM. Holding potential was clamped at -50 mV throughout and recordings were made in the continuous presence of 0.3 mM ATP and 75 nM PKA. Dotted lines represent the closed channel level. A 5-fold data reduction was applied to traces in **A** for the purpose of illustration. **B** and **C** Single-channel current amplitude (i) and P_o of human WT-CFTR at ivacaftor concentrations of 1.0 μM and 10 μM (n = 4, * = P < 0.05, one-way repeated measures ANOVA and Dunnett's multiple comparisons).

4.1.1.2 Sheep CFTR

Due to the high activity of sheep WT-CFTR, the effect of ivacaftor on this orthologue was tested at 0.3 mM ATP rather than at 1 mM ATP. Figure 4.3A shows representative single-channel recordings of sheep WT-CFTR in the absence and presence of ivacaftor using excised inside-out membrane patches taken from CHO cells transiently expressing sheep WT-CFTR at a holding potential of -50 mV following PKA-dependent phosphorylation. Figure 4.3A, demonstrates the increased activity of sheep WT-CFTR in response to ivacaftor at concentrations between 1.0 μM and 10 μM. Visual inspection of the traces in Figure 4.3A suggests that ivacaftor increased the length of sheep WT-CFTR channel openings whilst decreasing interburst intervals. Quantification of single-channel current amplitude and P_o are shown in Figures 4.3B and C, respectively. As with human WT-CFTR, ivacaftor had little or no effect on single-channel current amplitude, although a small, but statistically significant decrease was observed at 0.3 μM and 1.0 μM ivacaftor (control = -0.81 ± 0.05 pA; 0.3 μM ivacaftor = -0.71 ± 0.03 pA; 1.0 μM ivacaftor = -0.71 ± 0.04 pA; n = 3, P < 0.05). Ivacaftor increased P_o significantly at concentrations between 0.1 μM and 10 μM (Figure 4.3C) with an increase from 0.31 ± 0.04 (control) to 0.52 ± 0.09 at 10 μM (n = 3, P < 0.05). This represented an increase of 68%, indicating an increase in the response of sheep CFTR to ivacaftor when compared to the increase of 58% that was observed for human CFTR at 0.3 mM ATP. However, the rightward shift in the ivacaftor dose response curve generated for sheep WT-CFTR with a K_D of 0.19 μM as calculated from sigmoidal fitting of the dose response curve suggests a decrease in the efficacy of ivacaftor for sheep compared to human CFTR (Figure 4.3C).

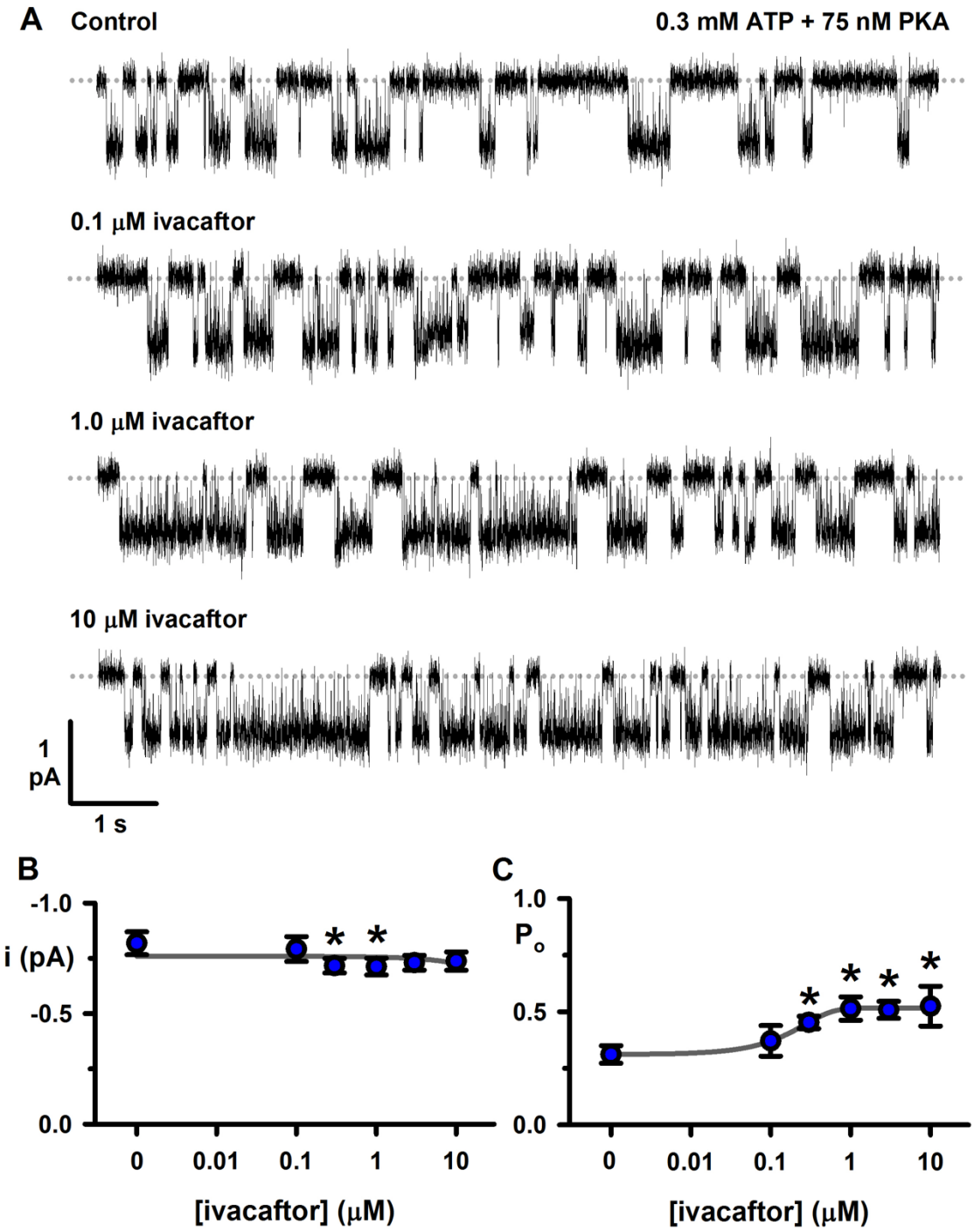

Figure 4.3: Effect of ivacaftor on sheep WT-CFTR in the presence of 0.3 mM ATP. A Representative single-channel recordings from an excised inside-out membrane patch from a CHO cell showing the response of sheep WT-CFTR to ivacaftor at concentrations from 0.1 μM to 10 μM. Holding potential was clamped at -50 mV throughout and recordings were made in the continuous presence of 0.3 mM ATP and 75 nM PKA. Dotted lines represent the closed level for the channel. A 5-fold data reduction was applied to traces in **A** for the purpose of illustration. **B** and **C** Single-channel current amplitude (i) and P_o of sheep WT-CFTR at ivacaftor concentrations from 10 nM to 10 μM. Graphs in **B** and **C** were fitted with 3-parameter sigmoidal curves using SigmaPlot software v13.0 (n = 3, * = P < 0.05, one-way repeated measures ANOVA and Dunnett's multiple comparisons).

4.1.1.3 Pig CFTR

Very limited data were collected for pig WT-CFTR with only two successful patches obtained, and these data are summarised in Figure 4.4. Although the power of these data are insufficient to demonstrate an effect of ivacaftor on pig CFTR statistically, the representative traces shown in Figure 4.4A indicate an increase in the P_o of pig WT-CFTR in response to increasing concentrations of ivacaftor, resulting from an increase in the duration of channel openings. For these experiments, pig WT-CFTR was transiently expressed in CHO cells and recordings were made from excised inside-out membrane patches at a holding potential of -50 mV and temperature of 37 °C after the addition of 1 mM ATP and 75 nM PKA. Although there was a large spread in the data obtained, no change in single-channel current was observed following addition of ivacaftor to the intracellular solution (Figure 4.4B). However, an increase in P_o was observed from 0.47 ± 0.07 (SD) under control conditions to a maximum of 0.70 ± 0.1 (SD) at 1.0 μM ivacaftor, representing a 49% increase in activity. This response to ivacaftor peaked at 1.0 μM and decreased slightly at higher concentrations, similar to the decrease in activity that was observed for human WT-CFTR at 10 μM ivacaftor compared to 1.0 μM ivacaftor. This decrease was not found to be significant following statistical testing in either case, although statistical interpretation of these results requires caution due to the low power of the data.

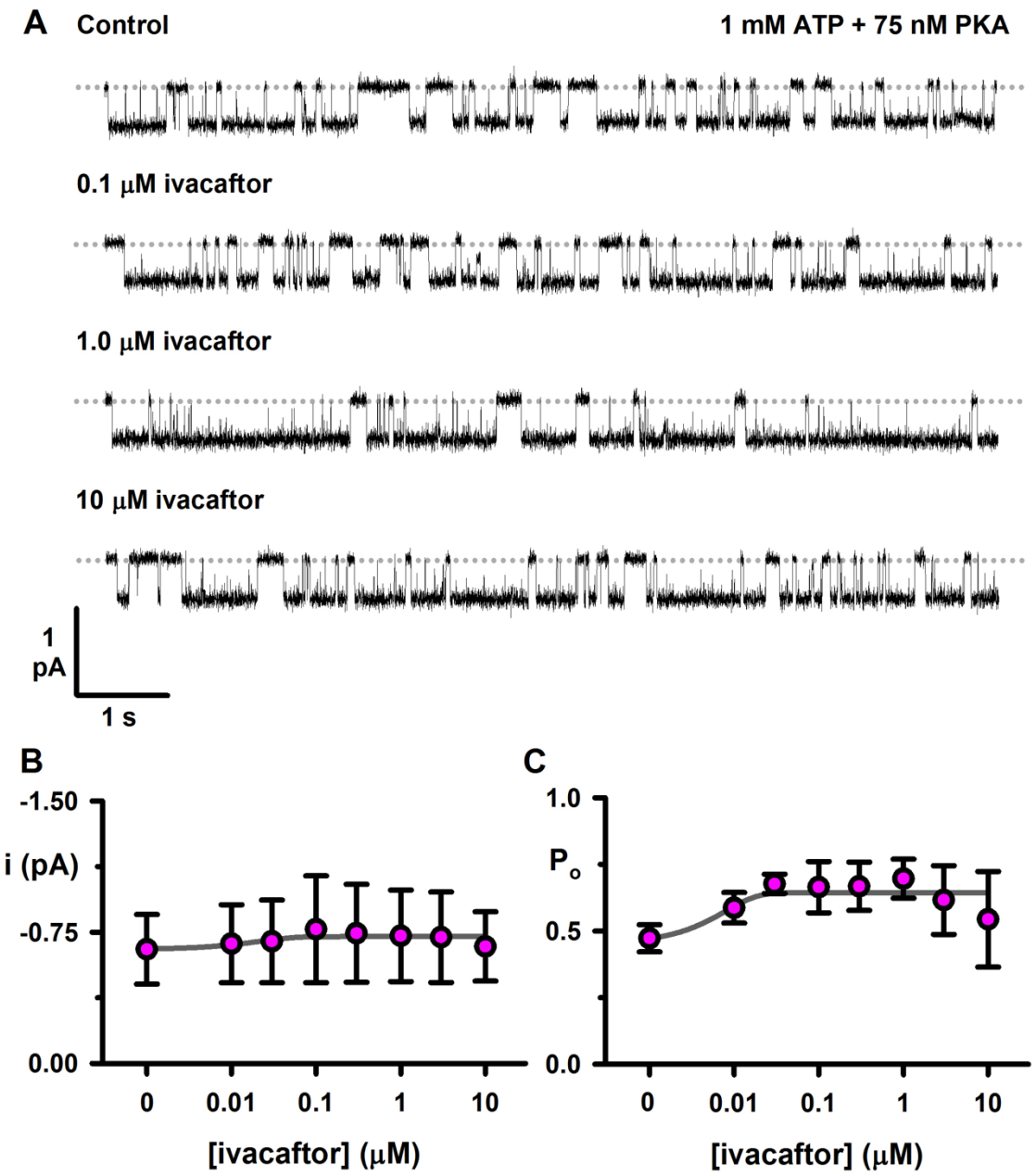

Figure 4.4: Effect of ivacaftor on pig WT-CFTR in the presence of 1 mM ATP. A Representative single-channel recordings from an excised inside-out membrane patch from a of CHO cells showing the response of pig WT-CFTR to ivacaftor at concentrations from 0.1 μM to 10 μM. Holding potential was clamped at -50 mV throughout and recordings were made in the continuous presence of 1 mM ATP and 75 nM PKA. Dotted lines represent the closed level for the channel. A 5-fold data reduction was applied to traces in **A** for the purpose of illustration. **B** and **C** Single-channel current amplitude (i) and P_o of pig WT-CFTR at ivacaftor concentrations from 10 nM to 10 μM. Graphs in **B** and **C** were fitted with 3-parameter sigmoidal curves using SigmaPlot software v13.0 (*n* = 2, error bars = SD, *P* = *ns*, one-way repeated measures ANOVA).

4.1.1.4 Ferret CFTR

Representative single-channel patch-clamp recordings from CHO cells transiently expressing ferret WT-CFTR and quantification of single-channel current amplitude and P_o are shown in Figure 4.5. Recordings were made in the presence of 1 mM ATP and 75 nM PKA at a holding potential of -50 mV and temperature of 37 °C. Visual inspection of the traces shown in Figure 4.4A suggests that ivacaftor increased the duration of ferret WT-CFTR channel openings whilst decreasing the duration of channel closures. Ivacaftor did not result in any change in single-channel current amplitude compared to control (Figure 4.5B) but did increase activity at all concentrations tested (Figure 4.5C). Under control conditions, single-channel current amplitude was -0.50 ± 0.04 pA and P_o was 0.44 ± 0.07 (n = 6) (Figure 4.5B and C). Cumulative addition of ivacaftor to the experimental chamber increased channel activity with P_o at 10 μM being 0.66 ± 0.04 (n = 4, P < 0.05 compared to control), representing a 50% increase in activity (Figure 4.5C).

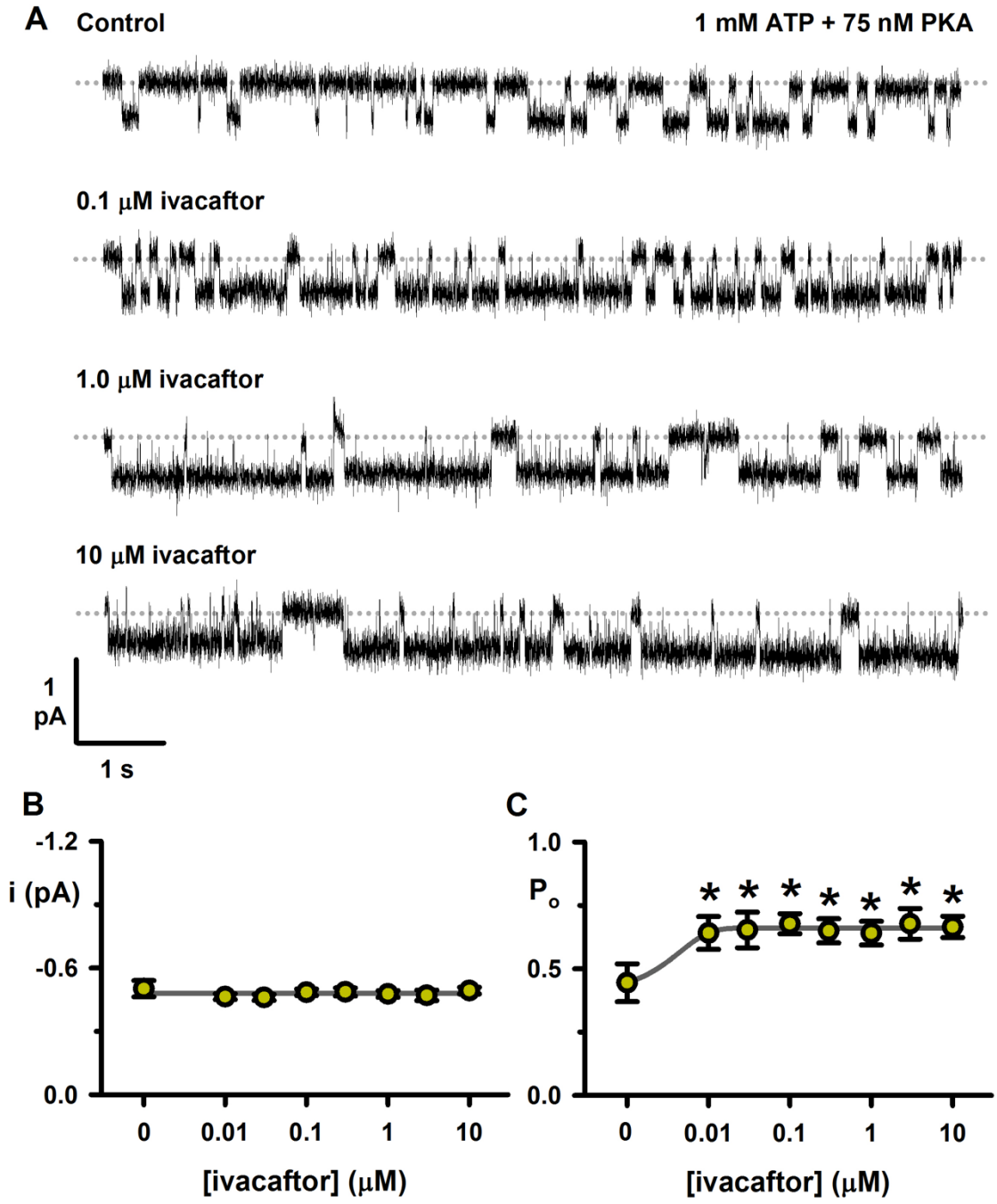

Figure 4.5: Effect of ivacaftor on ferret WT-CFTR in the presence of 1 mM ATP. A Representative single-channel recordings from an excised inside-out membrane patch from a CHO cell showing the response of ferret WT-CFTR to ivacaftor at concentrations from 0.1 μM to 10 μM. Holding potential was clamped at -50 mV throughout and recordings were made in the continuous presence of 1 mM ATP and 75 nM PKA. Dotted lines represent the closed level for the channel. A 5-fold data reduction was applied to traces in **A** for the purpose of illustration. **B** and **C** Single-channel current amplitude (i) and P_o of ferret WT-CFTR at ivacaftor concentrations from 10 nM to 10 μM. Graphs in **B** and **C** were fitted with 3-parameter sigmoidal curves using SigmaPlot software v13.0 (n = 3 - 6, * = P < 0.05, one-way repeated measures ANOVA and Dunnett's multiple comparisons).

4.1.1.5 Mouse CFTR

Figure 4.6A, shows representative single-channel recordings from an inside-out membrane patch excised from a CHO cell stably expressing mouse WT-CFTR following activation by 1 mM ATP and 75 nM PKA at a holding potential of -50 mV and temperature of 37 °C. The patch-clamp recording shown in Figure 4.6A was from a membrane patch containing two mouse WT-CFTR channels and shows the unique gating behaviour of mouse CFTR as discussed in Section 3. Visual inspection of traces in Figure 4.6A suggests that addition of ivacaftor did not result in a change in the gating behaviour of mouse WT-CFTR. Quantification of the effects of increasing concentrations of ivacaftor from 10 nM to 10 μM are shown in Figure 4.6B and C. The single-channel current amplitude for the full open state (O_2) of mouse WT-CFTR before addition of ivacaftor was -0.23 ± 0.02 pA (*n* = 4) and no change was observed following addition of ivacaftor at concentrations between 10 nM and 10 μM. As reported in Section 3, the P_o of the O_2 state of mouse WT-CFTR was low at 1 mM ATP (0.049 ± 0.01, *n* = 4). Successive additions of ivacaftor up to a concentration of 10 μM however did not result in any increase in the P_o of the O_2 state of mouse WT-CFTR (Figure 4.6C). Due to the small amplitude of the sub-conductance state (O_1) of mouse CFTR, and the ratio of signal to noise of recordings, it was not possible to quantify the P_o of this state.

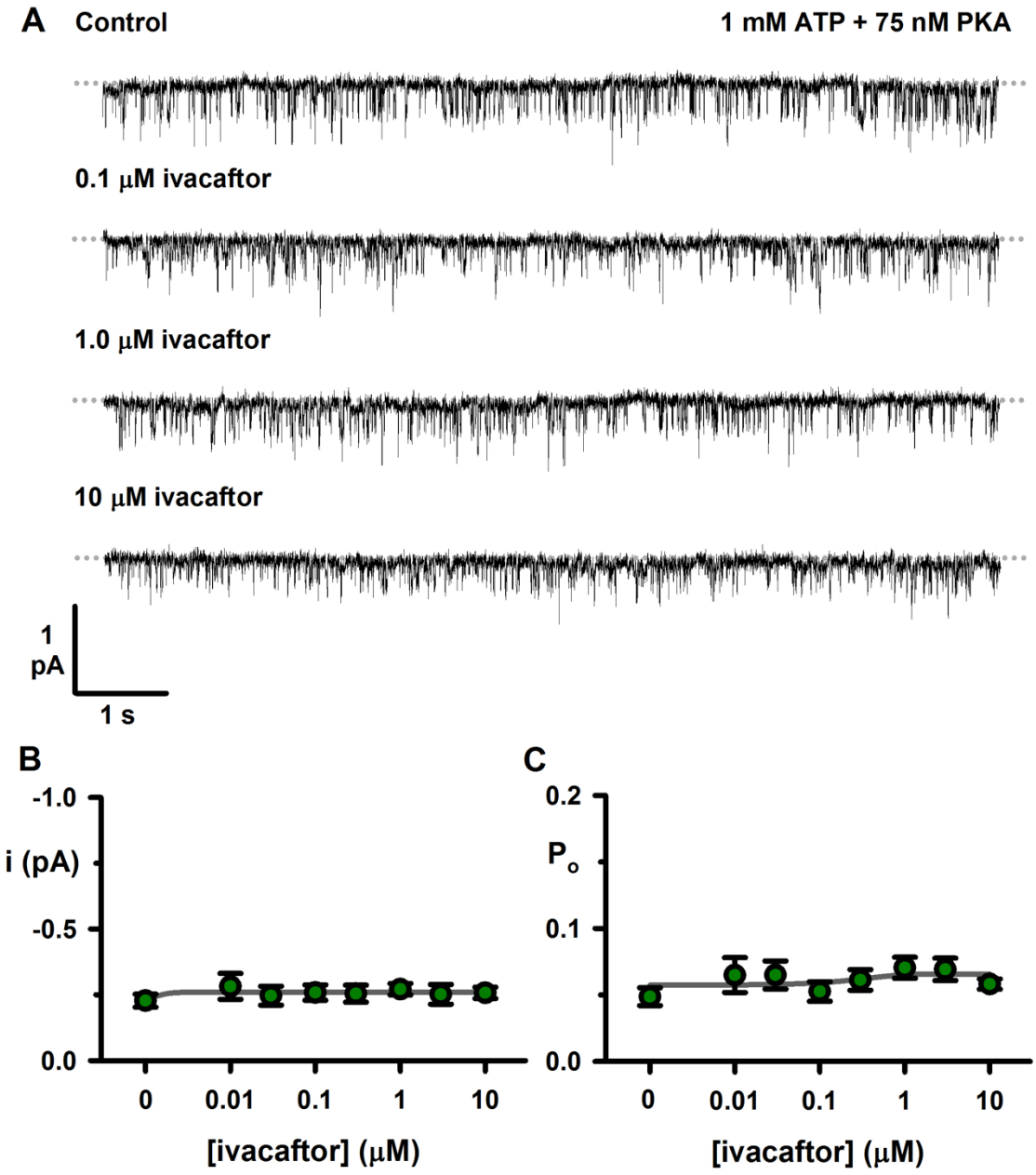

Figure 4.6: Effect of ivacaftor on mouse WT-CFTR in the presence of 1 mM ATP. A Representative single-channel recordings from an excised inside-out membrane patch from a CHO cell showing the response of mouse WT-CFTR to ivacaftor at concentrations from 0.1 μM to 10 μM. Holding potential was clamped at -50 mV throughout and recordings were made in the continuous presence of 1 mM ATP and 75 nM PKA. Dotted lines represent the closed level for the channels. A 5-fold data reduction was applied to traces in **A** for the purpose of illustration. **B** and **C** Single-channel current amplitude (i) and P_o of mouse WT-CFTR at ivacaftor concentrations from 10 nM to 10 μM. Graphs in **B** and **C** were fitted with 3-parameter sigmoidal curves using SigmaPlot software v13.0 (n = 4, P = *ns*, one-way repeated measures ANOVA).

4.1.1.6 Zebrafish CFTR

Figure 4.7A shows example single-channel recordings from an excised inside-out membrane patch from a CHO cell transiently expressing zebrafish WT-CFTR under control conditions (1 mM ATP and 75 nM PKA), and following addition of 0.1, 1.0 and 10 μM ivacaftor in the continuous presence of ATP and PKA. Quantification of single-channel current and P_o are shown for all concentrations tested between 0 and 10 μM in Figure 4.7B and C. As mentioned in Chapter 3, Cl^- currents were only observed in one experiment using cells expressing zebrafish WT-CFTR and therefore due to the lack of power care must be taken in the interpretation of these data. It must also be noted that due to the low activity of zebrafish CFTR and the small current amplitude, there may be an underestimate in the correct number of channels present within this membrane patch. However, taking these considerations into account, channel activity was observed following activation by PKA-dependent phosphorylation, characterised by brief channel openings that resembled those of mouse WT-CFTR. No significant increase in activity or change in single-channel current amplitude was observed in response to ivacaftor. The single-channel current amplitude of zebrafish CFTR under control conditions at -50 mV and 1 mM ATP was -0.20 pA (*n* = 1) and this level remained unchanged (within the range ± 3.0 $x10^{-3}$) at increasing ivacaftor concentrations up to 10 μM (Figure 4.7B). P_o before addition of ivacaftor was 0.16 (*n* = 1). At 10 nM ivacaftor, P_o was observed to increase slightly to 0.24 after which P_o steadily decreased as the concentration of ivacaftor was increased to 10 μM (*n* = 1 throughout). Further experiments are required however before interpretation of the significance of these data is possible.

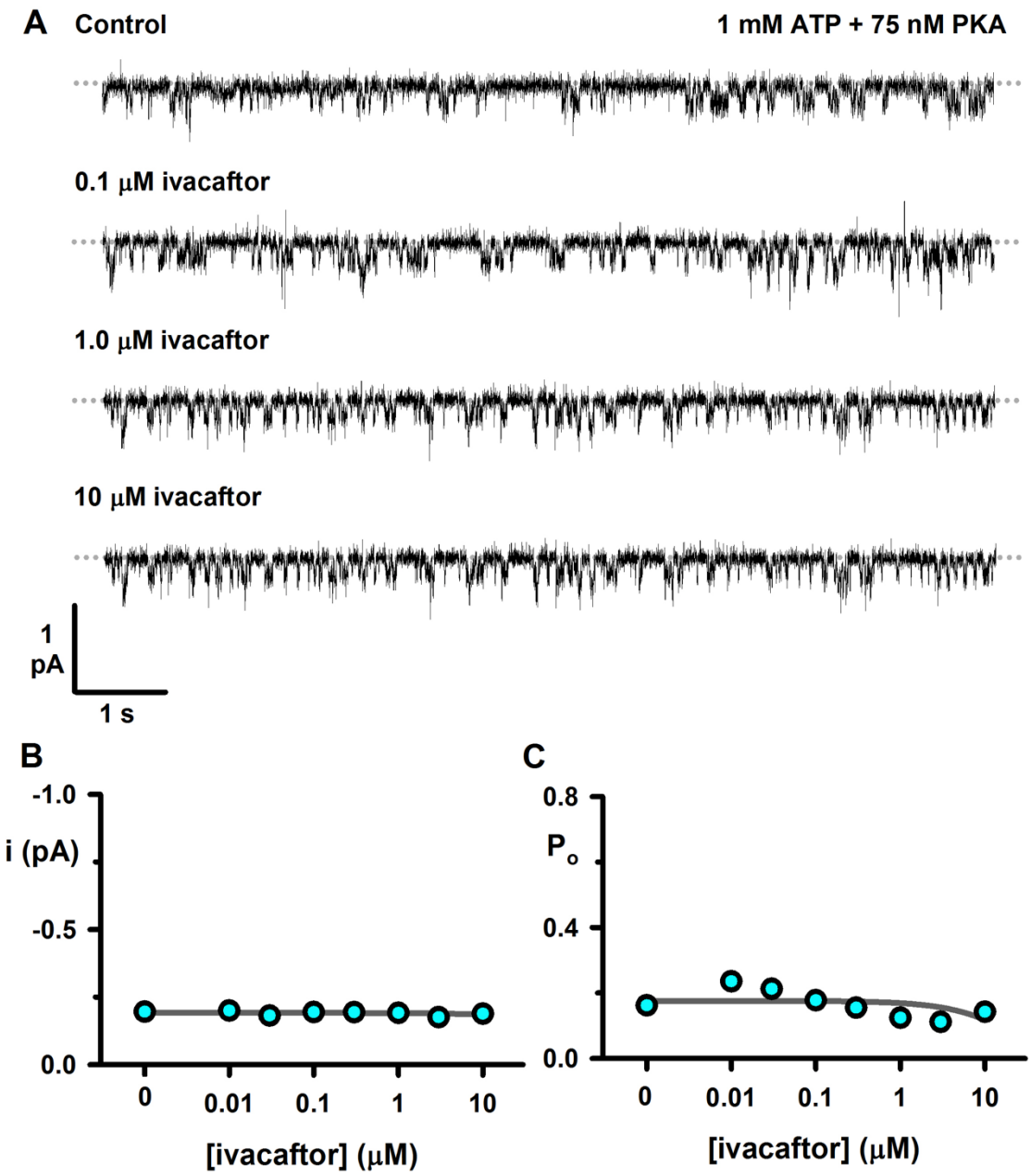

Figure 4.7: Effect of ivacaftor on zebrafish WT-CFTR in the presence of 1 mM ATP. A Representative single-channel recordings from an excised inside-out membrane patch of a CHO cell showing the response of zebrafish WT-CFTR to ivacaftor at concentrations from 0.1 μM to 10 μM. Holding potential was clamped at -50 mV throughout and recordings were made in the continuous presence of 1 mM ATP and 75 nM PKA. Dotted lines represent the closed channel level. A 5-fold data reduction was applied to traces in **A** for the purpose of illustration. **B** and **C** Single-channel current (i) and P_o of zebrafish WT-CFTR at ivacaftor concentrations from 10 nM to 10 μM. Graphs in **B** and **C** were fitted with 3-parameter sigmoidal curves using SigmaPlot software v13.0 (*n* = 1).

4.2.2 Effect of ivacaftor on the single-channel behaviour of F508del-CFTR from diverse species

4.2.2.1 Effect of ivacaftor on Human and Mouse F508del CFTR following low temperature correction

To test the effect of ivacaftor on F508del-CFTR, the processing defect of the mutation must first be corrected. Incubation of cells expressing F508del-CFTR at 27 °C has previously been shown to deliver F508del-CFTR to the plasma membrane (Denning *et al.*, 1992). We therefore used low temperature correction to test the effects of ivacaftor on both human and mouse F508del-CFTR gating behaviour. Cells were incubated at 27 °C for a minimum of 24 hours before experiments. Glass coverslips on which cells had been seeded were transferred to the experimental chamber at room temperature (23 °C) and CFTR was then activated at 27 °C following membrane patch excision by adding 1 mM ATP and 75 nM PKA to the intracellular solution. Once CFTR channels were observed and had been fully activated, the temperature of the experimental chamber was increased to 37 °C within 2 minutes using a heated microscope stage (Brook Industries) as described in the Section 2. Experiments were then carried out by adding cumulative concentrations of ivacaftor directly to the intracellular solution.

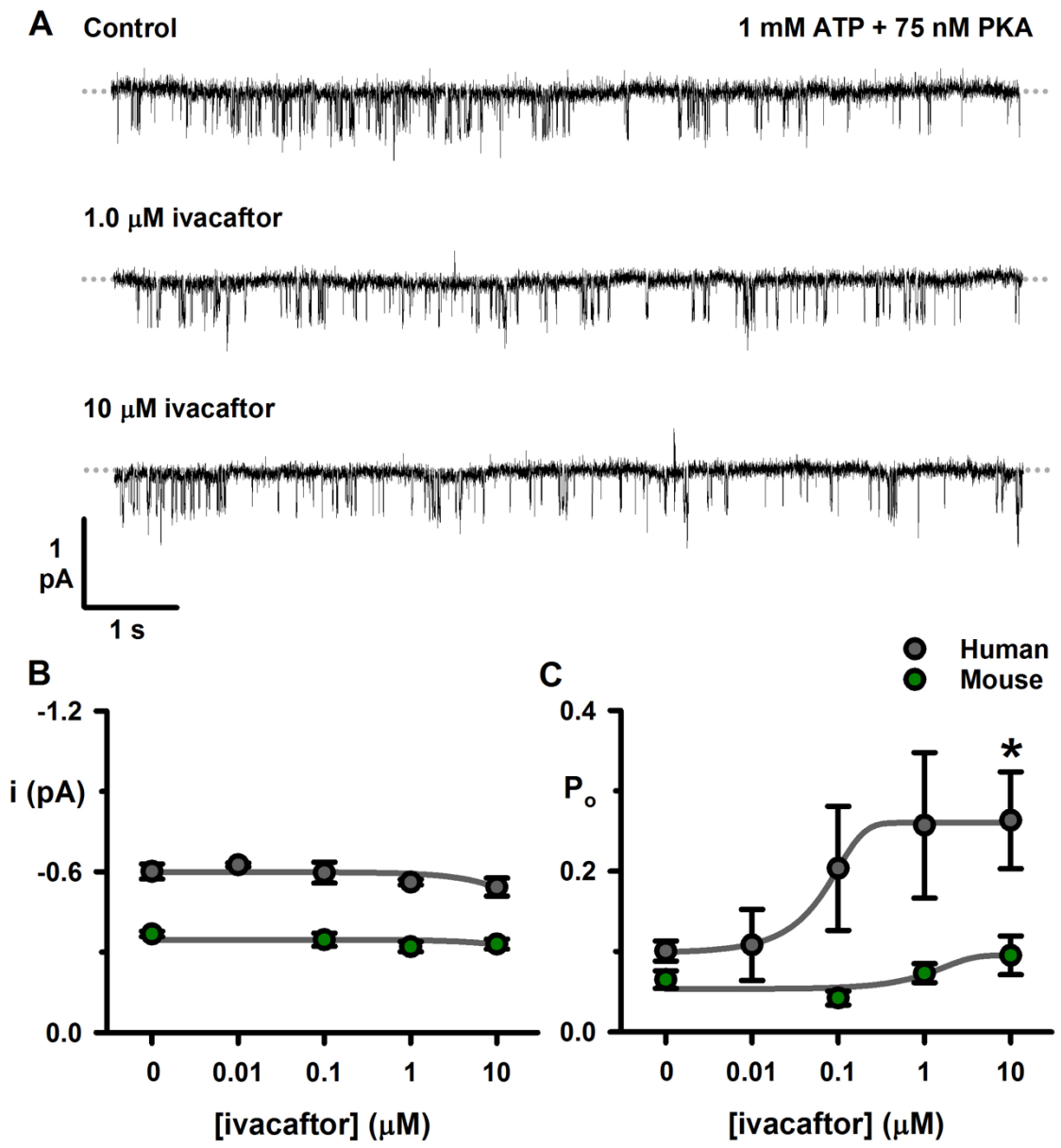

Figure 4.8: Effect of ivacaftor on human and mouse F508del-CFTR following low temperature correction. A Representative single-channel recordings from a membrane patch excised from a CHO cell showing the response of mouse F508del-CFTR to ivacaftor at concentrations of 1.0 and 10 μM. Holding potential was clamped at -50 mV throughout and recordings were made at 37 °C in the continuous presence of 1 mM ATP and 75 nM PKA. The processing defect caused by F508del was corrected by incubating cells at 27 °C for at least 24 hours before experiments. Dotted lines represent the closed level for the channels. A 5-fold data reduction was applied to traces in **A** for the purpose of illustration. **B** and **C** Single-channel current amplitude (i) and P_o of human (grey circles) and mouse (green circles) F508del-CFTR at ivacaftor concentrations from 0 to 10 μM (mouse F508del-CFTR was not tested at 10 nM). Graphs in **B** and **C** were fitted with 3-parameter sigmoidal curves using SigmaPlot software v13.0 (human n = 2 – 5; mouse, n = 3; * = P < 0.05 vs control, one-way repeated measures ANOVA and Dunnett's multiple comparisons).

Excised inside-out membrane patches from cells expressing human F508del-CFTR (Figure 4.8) produced CFTR-mediated Cl^- currents with reduced activity compared to WT-CFTR (Figure 4.1) (for human F508del-CFTR: i = -0.60 ± 0.06; P_o = 0.10 ± 0.01; *n* = 5). Addition of ivacaftor at increasing concentrations up to a maximum of 10 μM resulted in a 160% increase in P_o to 0.26 ± 0.06 at 10 μM ivacaftor ($P < 0.05$ compared to control) with no change in single-channel current amplitude (Figures 4.8B and C). As shown by the example traces in Figure 4.8A and the quantification of data in Figures 4.8B and C, increasing concentrations of ivacaftor did not result in any significant change in either single-channel current amplitude or P_o of the full open state (O_2) of mouse F508del-CFTR above the level of control (Control: i = -0.37 ± 0.02 pA; P_o = 0.07 ± 0.01, *n* = 3).

4.2.2.2 Effect of ivacaftor on Human and Mouse F508del-CFTR following correction by lumacaftor

Use of CFTR potentiators in conjunction with CFTR correctors has proven a feasible approach for the treatment of CF patients carrying the F508del mutation (Okiyoneda *et al.*, 2013). The first such 'combination therapy' to be approved by the FDA was Orkambi (Vertex Pharmaceuticals), which utilises ivacaftor with lumacaftor (VX-809, Vertex Pharmaceuticals) (Van Goor *et al.*, 2011; Wainwright *et al.*, 2015). For this reason, we aimed to determine if correction of human or mouse F508del-CFTR using lumacaftor rather than low temperature altered the observed response of these CFTR orthologues to potentiation by ivacaftor. Cells expressing human or mouse F508del-CFTR were incubated at 37 °C with 3 μM lumacaftor for 24 hours prior to experiments. F508del-CFTR was activated at 37 °C following patch excision using 1 mM ATP and 75 nM PKA and the effect of ivacaftor was tested at 10 μM (Figure 4.9).

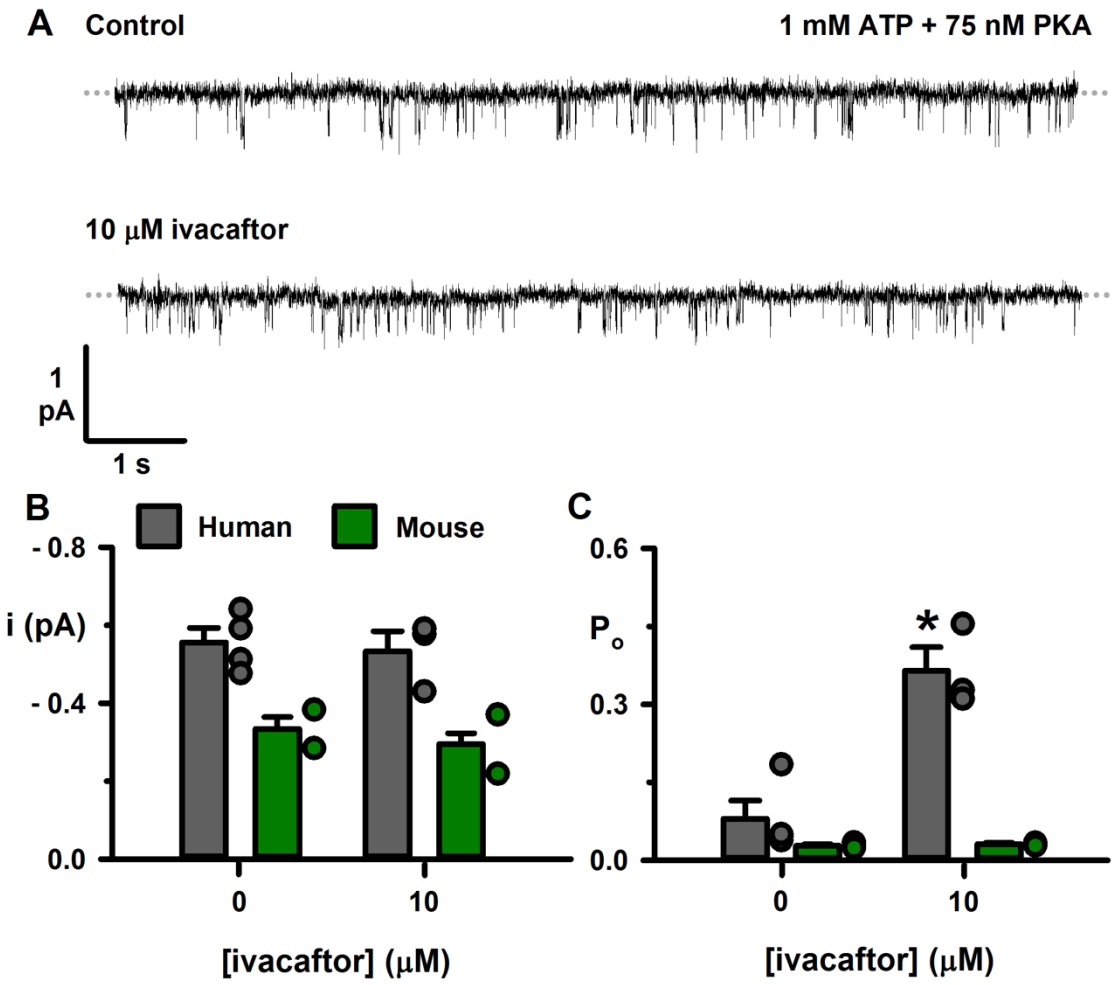

Figure 4.9: Effect of ivacaftor on human and mouse F508del-CFTR following correction with 3 μM lumacaftor. A Representative single-channel recordings from a membrane patch excised from a CHO cell showing the response of mouse F508del-CFTR to ivacaftor at 10 μM. Holding potential was clamped at -50 mV throughout and recordings were made in the continuous presence of 1 mM ATP and 75 nM PKA. The processing defect caused by F508del was corrected by incubating cells with 3 μM lumacaftor at 37 °C for at least 24 hours before experiments. Dotted lines represent the closed level for the channels. A 5-fold data reduction was applied to traces in **A** for the purpose of illustration. **B** and **C** Single-channel current amplitude (i) and P_o of human and mouse F508del-CFTR at 0 and 10 μM ivacaftor (human n = 3 – 4; mouse, n = 2; * = P < 0.05 vs control, paired two-way Student's t-test).

As with low temperature correction, 10 μM ivacaftor increased the P_o of human F508del-CFTR, but to a greater extent, with an increase of 350% from 0.08 ± 0.04 (n = 4) to 0.36 ± 0.05 (n = 3) (Figure 4.9C) following correction by 3 μM lumacaftor without a change in single-channel current amplitude (Figure 4.9B). As shown by the representative traces in Figure 4.9A, channel gating of lumacaftor-corrected mouse F508del-CFTR remained unchanged following addition of 10 μM ivacaftor. At -50 mV,

under control conditions, the single-channel current amplitude of mouse F508del-CFTR was -0.33 ± 0.05 pA whilst P_o was 0.03 ± 0.005 pA (*n* = 2) and addition of 10 μM ivacaftor did not result in any change in either P_o or single channel current.

4.3.3 Effect of genistein on the single-channel behaviour of CFTR orthologues

Genistein, an isoflavonoid sourced from soy beans, is a CFTR potentiator (Illek *et al.*, 1995), that demonstrates potentiation of CFTR at low concentrations and inhibition at higher concentrations (Wang *et al.*, 1998). This dual effect of genistein is thought to arise from binding of the drug at different sites between the two NBDs (Huang *et al.*, 2009). Given this potential difference in mechanism of action between genistein and ivacaftor, we were keen to test if mouse CFTR showed potentiation in response to genistein. We tested the effect of 50 μM genistein on both human and mouse F508del-CFTR (Figure 4.10). 50 μM genistein potentiated human F508del-CFTR, increasing P_o by 54% from 0.13 ± 0.02 to 0.20 ± 0.03 (*n* = 4) without affecting single-channel current amplitude (Figure 4.10B and C). 50 μM genistein did not affect the P_o of mouse F508del-CFTR (Control = 0.04 ± 0.01; 50 μM genistein = 0.05 ± 0.01, *n* = 2). However, a small decrease in single-channel current was observed from -0.29 ± 8.9 $x10^{-3}$ pA to 0.27 ± 3.6 $x10^{-3}$ pA (*n* = 2).

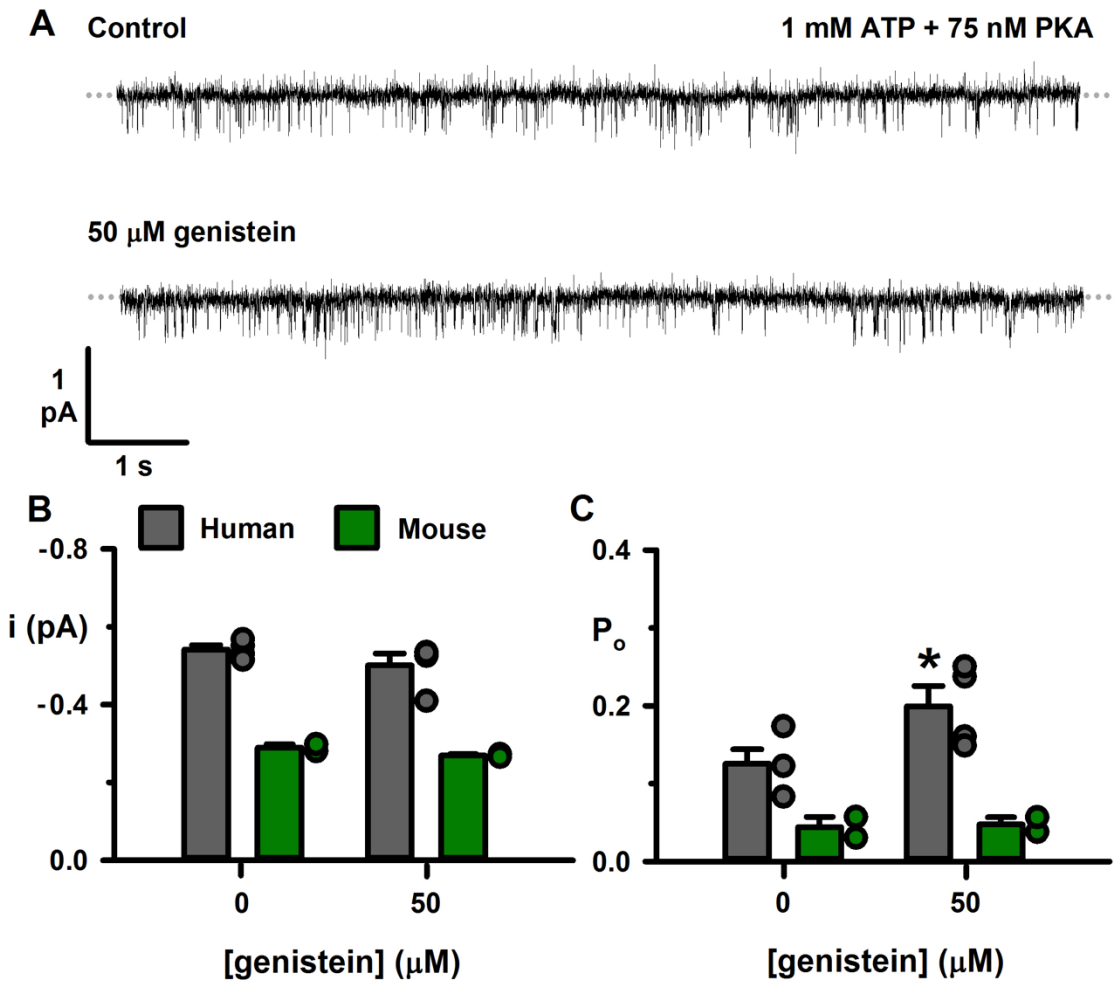

Figure 4.10: Effect of 50 μM genistein on human and mouse F508del-CFTR following low temperature correction. A Representative single-channel recordings from a membrane patch excised from a CHO cell showing the response of mouse F508del-CFTR to 50 μM genistein added to the intracellular solution. Holding potential was clamped at -50 mV throughout and recordings were made in the continuous presence of 1 mM ATP and 75 nM PKA. The processing defect caused by F508del was corrected by incubating cells at 27 °C for at least 24 hours before experiments. Dotted lines represent the closed level for the channels. A 5-fold data reduction was applied to traces in **A** for the purpose of illustration. **B** and **C** Single-channel current amplitude (i) and P_o of human and mouse F508del-CFTR in the absence and presence of 50 μM genistein (human n = 4; mouse, n = 2; * = P < 0.05 vs control, paired two-way Student's t-test).

4.4 Discussion

Our data indicate species specific responses to the CFTR potentiator ivacaftor. As highlighted by the summary of our data for P_o in Figure 4.11, human, pig, sheep and ferret WT-CFTR orthologues all demonstrated potentiation in response to ivacaftor, however no potentiation was observed in the case of either mouse or zebrafish,

although the lack of power in the data collected for zebrafish (n = 1) warrants caution for the interpretation of these data.

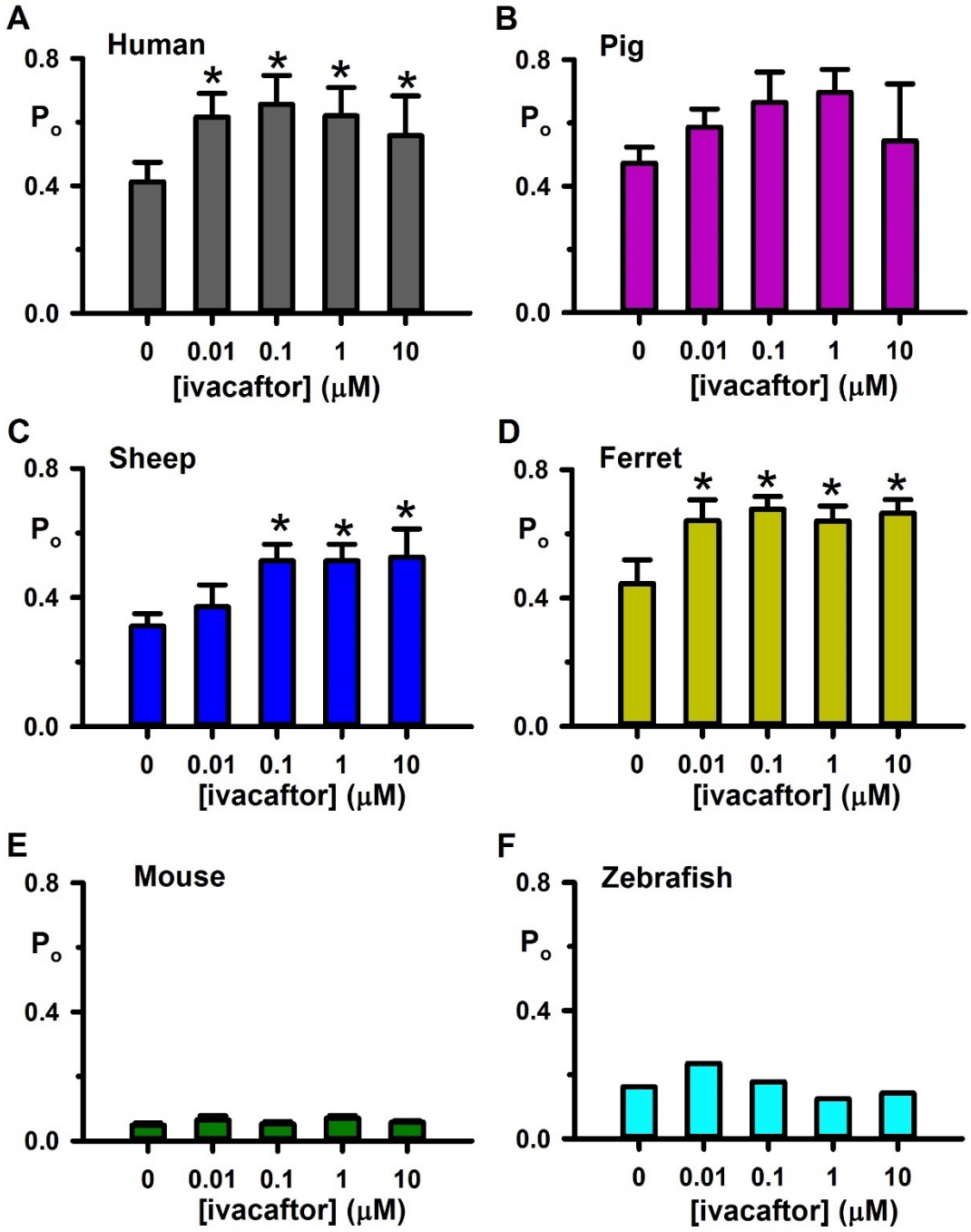

Figure 4.11: Summary of the response of CFTR orthologues from diverse species to ivacaftor as studied using single-channel patch-clamp. Recording responses of WT-CFTR orthologues from human (**A**), pig (**B**), sheep (**C**), ferret (**D**), mouse (**E**) and zebrafish (**F**) to ivacaftor at concentrations between 0.01 and 10 μM. All species orthologues were transiently expressed in CHO cells with the exception of human CFTR, which was stably expressed in NIH 3T3 cells. Recordings were made from excised inside-out membrane patches in the continuous presence of 1 mM ATP and 75 nM PKA at 37 °C (human; n = 3, pig; n = 2, sheep; n = 3, ferret; n = 4 – 6, mouse; n = 5 – 6, zebrafish; n = 1, * = P < 0.05, one-way repeated measures ANOVA and Dunnett's multiple comparisons).

Comparison of the bar graphs shown in Figures 4.11A and C for human and sheep WT-CFTR, as well as Figures 4.1C and 4.3C, suggests that ivacaftor has a decreased efficacy for sheep compared to human CFTR, although it was not possible to quantify K_D for ivacaftor's effect on human CFTR due to the high levels of potentiation of this orthologue at low concentrations. This difference in efficacy may result from a lower affinity of ivacaftor binding to sheep CFTR or from structural differences that affect the mechanism by which ivacaftor potentiates CFTR gating.

In a previous study by our group, Cai *et al.* (2015) investigated the effect of the fluorescein derivative phloxine B on sheep WT-CFTR. In the case of human CFTR, phloxine B acts as a potentiator at concentrations up to 3 μM, and an inhibitor at higher concentrations (Cai & Sheppard, 2002). Phloxine B does not potentiate sheep CFTR at low concentrations, however it does inhibit sheep CFTR at concentrations over 3 μM (Cai *et al.*, 2015). Cai *et al.* (2015) speculated that phloxine B, like PP_i, potentiates human CFTR through by interacting with the NBDs. Our observation that ivacaftor potentiates sheep CFTR leads us to speculate that the mechanism of action of ivacaftor differs from that of both PP_i and phloxine B, potentially resulting from a different binding location on the TMDs.

Our data demonstrates that when expressed in CHO cells, the fully open state (O_2) of mouse WT- and F508del-CFTR orthologues do not show increased activity in response to ivacaftor at concentrations between 10 nM and 10 μM when studied using the excised inside-out patch-clamp technique (Figures 4.6, 4.8 and 4.9). Our data contradict previous studies that have shown potentiation of mouse CFTR in response to ivacaftor when expressed in *Xenopus* oocytes at room temperature (Cui & McCarty, 2015). Interestingly, the gating behaviour reported by Cui and McCarty (2015) for mouse CFTR channels expressed in *Xenopus* oocytes appears to differ from that reported by other studies where mouse CFTR was expressed in mammalian cells (Lansdell *et al.*, 1998a; Lansdell *et al.*, 1998b; Ostedgaard *et al.*, 2007; Scott-Ward *et al.*, 2007; Dong *et al.*, 2012), with a higher P_o evident for the O_2 fully open state of the channel and an absence of the distinctive gating behaviour replicated in previous studies as well as our current study (e.g. Figure 4.6A). As we have been unable to quantify the O_1 state in our present study due to the small amplitude of this sub-conductance state, one potential explanation of the observed difference in response

to ivacaftor is that ivacaftor acts on mouse CFTR by potentiating this sub-conductance state. However, our observation that mouse CFTR is not potentiated by ivacaftor has also been supported by data obtained using iodide efflux utilising cells expressing mouse CFTR (de Jonge *et al.*, 2007). As we would expect O_1 state potentiation to result in an increase in overall CFTR activity as measured using iodide efflux the explanation that potentiation of mouse CFTR by ivacaftor involves potentiation of the O_1 state of mouse CFTR does not seem likely. Furthermore, the observations obtained using iodide efflux that show ivacaftor does not potentiate mouse-CFTR at the whole-cell level is supported by previous studies showing that ivacaftor does not affect CFTR-regulated smooth muscle contraction in mouse lung slices, although it is possible that this is a tissue-specific effect (Cook *et al.*, 2016). The reported K_d of ivacaftor for mouse CFTR was 7.32 nM (Cui & McCarty, 2015), however in this study we tested a range of concentrations from 10 nM to 10 μM and did not see an increase in P_o at any concentration (Figure 4.6). This leads us to conclude that ivacaftor does not affect mouse CFTR within this concentration range under the experimental conditions used here.

A further difference between the data that we have collected, and previous studies is the experimental temperature that we have used. In our single-channel studies, all experiments were carried out at 37 °C to more accurately replicate physiological conditions. However, data collected by our group replicating the experiments in this section using mouse WT-CFTR, but repeated at low temperature (Figures 4.12, data reproduced with permission of Dr Yiting Wang) indicate that mouse CFTR still does not demonstrate potentiation at lower temperatures. This therefore raises the possibility that mouse-CFTR gating behaviour may be in part determined by the expression system used, suggesting that membrane interactions may have a role in determining both gating behaviour and pharmacology of this CFTR orthologue (Artegas *et al.* 2006).

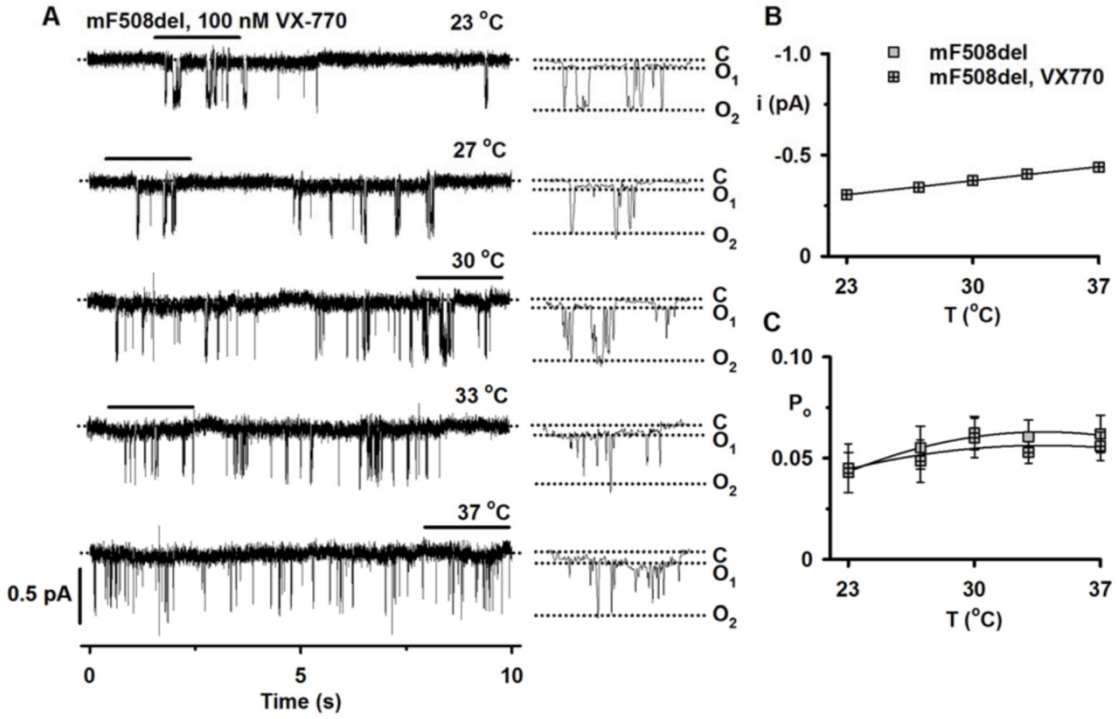

Figure 4.12: Temperature-dependence of mouse F508del-CFTR treated with ivacaftor. A Representative recordings of mouse F508del-CFTR Cl^- channels in an excised inside-out membrane patch from a CHO cell. The recordings were acquired at the indicated temperatures in the presence of ATP (1 mM) and PKA (75 nM) in the intracellular solution. Dotted lines indicate where channels are closed (C) and the first open level (O_1) and downward deflections correspond to the second open level (O_2). Black bars indicated 2 s sections where traces have been additionally filtered at 50 Hz and shown separately to the right in panel **A**. **B** and **C** summary data show change in single-channel current amplitude (i) and P_o between 23 °C and 37 °C for mouse F508del in the presence and absence of ivacaftor (VX-770). Data are means ± SEM (control, *n* = 9-12; ivacaftor, *n* = 5). (Data from experiments carried out by Dr Yiting Wang and reproduced with permission).

The observation that mouse CFTR does not respond to the potentiator PP_i has been used previously to determine the binding location of PP_i to CFTR using human-mouse CFTR chimeras (Scott-Ward *et al.*, 2007). Our observation of similar differences in the response of human and mouse WT and F508del-CFTR to ivacaftor therefore provides strong rationale for the use of human-mouse CFTR chimeras to study the mechanism of action of ivacaftor. Furthermore, the observation that genistein also shows species specific potentiation of CFTR orthologues demonstrates that this approach may be used to determine information about the mechanism of action of multiple CFTR potentiators. Using docking simulations, Huang *et al*. (2009) previously speculated

that genistein is likely to bind at multiple locations at the interface between the NBDs. Given that human, but not mouse CFTR shows potentiation in response to genistein, these data suggest that the use of human-mouse chimeras may provide insight into the regions of the NBDs that are involved in binding genistein.

5. Investigating the mechanism of action of ivacaftor using CFTR chimeras

5.1 Introduction

5.1.1 Overview of the use of chimeras to determine drug-binding sites

Chimeras constructed by combining sequences from different CFTR orthologues have previously been used to investigate structure-function relationships as well as the pharmacology of CFTR. For example, Price *et al.* (1996) developed human-*Xenopus* chimeras by replacing the sequences of either TMD1 or TMD2 in human CFTR with the equivalent regions of the *Xenopus* sequence. By investigating the single-channel gating properties of these chimeras, Price *et al.* (1996) identified that incorporation of *Xenopus* TMD1 domain into human CFTR (hX1-6) resulted in gating behaviour characterised by brief openings with increased intraburst closures that closely resembled that which we have observed for mouse and zebrafish CFTR. However, incorporation of *Xenopus* TMD2 into human CFTR (hX7-12) produced gating behaviour that more closely resembled that of the human WT channel (Price *et al.*, 1996). Subsequent mutation of the *Xenopus* ECL1 residues Arg^{111}-Asp-Asn-Glu-His^{115} back to the human equivalent Pro^{111}-Asp-Asn-Lys-Glu^{115} resulted in a chimera (hx1-6+REH/PKE), which demonstrated gating behaviour more closely resembling that of human CFTR, thereby demonstrating the role of this region in determining the gating behaviour of CFTR (Price *et al.*, 1996).

Our observation that mouse CFTR is not potentiated by ivacaftor supports the possibility that human-mouse CFTR chimeras may be used to identify structural regions of the CFTR protein that are involved in ivacaftor-mediated potentiation. This approach has been utilised by our group in the past to determine the binding domain of PP_i (Scott-Ward *et al.*, 2007). In that study, Scott-Ward *et al.* (2007) designed a panel of human-mouse whole-domain chimeras where the NBDs and RD of human CFTR were replaced by the mouse sequences of the corresponding domains. PP_i is a compound known to bind at the NBDs and acts as a CFTR potentiator at

concentrations below 3 mM but an allosteric inhibitor of CFTR at higher concentrations (Carson *et al.*, 1995b; Scott-Ward *et al.*, 2007; Li & Sheppard, 2009). However, PP_i had been shown to only inhibit mouse WT-CFTR (Lansdell *et al.*, 1998a; Scott-Ward *et al.*, 2007). Using human-mouse CFTR chimeras, Scott-Ward *et al.* (2007) demonstrated that this pattern of potentiation and inhibition was still present when either NBD1 or the RD were substituted by the mouse CFTR sequence for these domains. However, introduction of the mouse sequence for NBD2, either alone or in conjunction with NBD1, resulted in a PP_i response that matched that of mouse WT-CFTR, demonstrating only inhibition at higher concentrations without showing potentiation at concentrations under 3 mM (Scott-Ward *et al.*, 2007). This study therefore demonstrated that binding of PP_i occurred at NBD2 rather than NBD1. Thus the Scott-Ward *et al.* (2007) study provides proof of concept for the use of chimeras to determine regions of the CFTR protein involved in the mechanism of action of CFTR potentiators. Furthermore, this functional approach has advantages over the use of site-directed mutagenesis, for example by reducing the chances of multiple binding sites leading to a false-negative result, and by reducing the risk of developing a non-functional protein that cannot be studied using electrophysiological techniques.

5.1.2 Selection and design of chimeras

We worked in collaboration with Dr Christopher Boyd and Ann Doherty at the University of Edinburgh to design a panel of 13 CFTR chimeras that would encompass both whole domain sequence changes as well as chimeras for specific TM helices. Two additional human-mouse CFTR chimeras (hmNBD2 and hmRI) were also kindly provided by Professor Lynda Ostedgaard at the University of Iowa. The chimeras that were used are shown in Table 5.1. As detailed in Section 2, whole-domain chimeras were generated via homologous recombination, while transmembrane helix chimeras were constructed by inserting unique restriction sites at regular intervals into the modified backbone of human WT-CFTR. An alignment of the full sequences for each of the constructs as well as human and mouse WT-CFTR is shown in Appendix 2.

Construct No.	Construct	Residue boundaries	Plasmid	Source
1	human WT	N/A	pCMV	Edinburgh
2	Mouse WT	N/A	pCMV	Edinburgh
3	hmNBD1/2	432-611:1226-1419	pCMV	Edinburgh
4	hmNBD1	432-611	pCMV	Edinburgh
5	hmNBD2	1178-1480	pcDNA3.1	Iowa
6	hmTM1-12	79-355:858-1152	pCMV	Edinburgh
7	hmTM1-6	79-355	pCMV	Edinburgh
8	hmTM7-12	858-1152	pCMV	Edinburgh
9	hmTM5+6	307-355	pCMV	Edinburgh
10	hmTM5+6:TM1+2	307-355:78-153	pCMV	Edinburgh
11	hmTM5+6:TM3+4	307-355:154-306	pCMV	Edinburgh
12	hmTM5+6:TM7+8	307-355:858-935	pCMV	Edinburgh
13	hmTM5+6:TM9+10	307-355:987-1034	pCMV	Edinburgh
14	hmTM5+6:TM11+12	307-355:1095-1152	pCMV	Edinburgh
15	hmRD	653-837	pCMV	Edinburgh
16	hmRI	404-436	pcDNA3.1	Iowa

Table 5.1: Human and mouse WT and chimeric cDNA constructs used in this study, created by the laboratories of Dr Christopher Boyd (Edinburgh) and Professor Michael Welsh (Iowa).

Models of 12 of the constructs tested based upon the high-resolution cryo-EM structure of human CFTR generated by Liu *et al.* (2017) are shown in Figure 5.1. In this figure, human residues in each construct are shown in blue, whilst mouse residues are indicated in yellow.

5.1.3. Experimental approach for studying the effect of ivacaftor on human-mouse CFTR chimeras

Due to the large number of CFTR chimeric constructs to be tested (16 in total including human and mouse WT-CFTR), the use of the low-throughput single-channel patch-clamp technique was determined to be impractical. For this reason, the high-throughput automated patch-clamp technique (Billet *et al.*, 2017) was used to determine which of the constructs showed potentiation in response to ivacaftor.

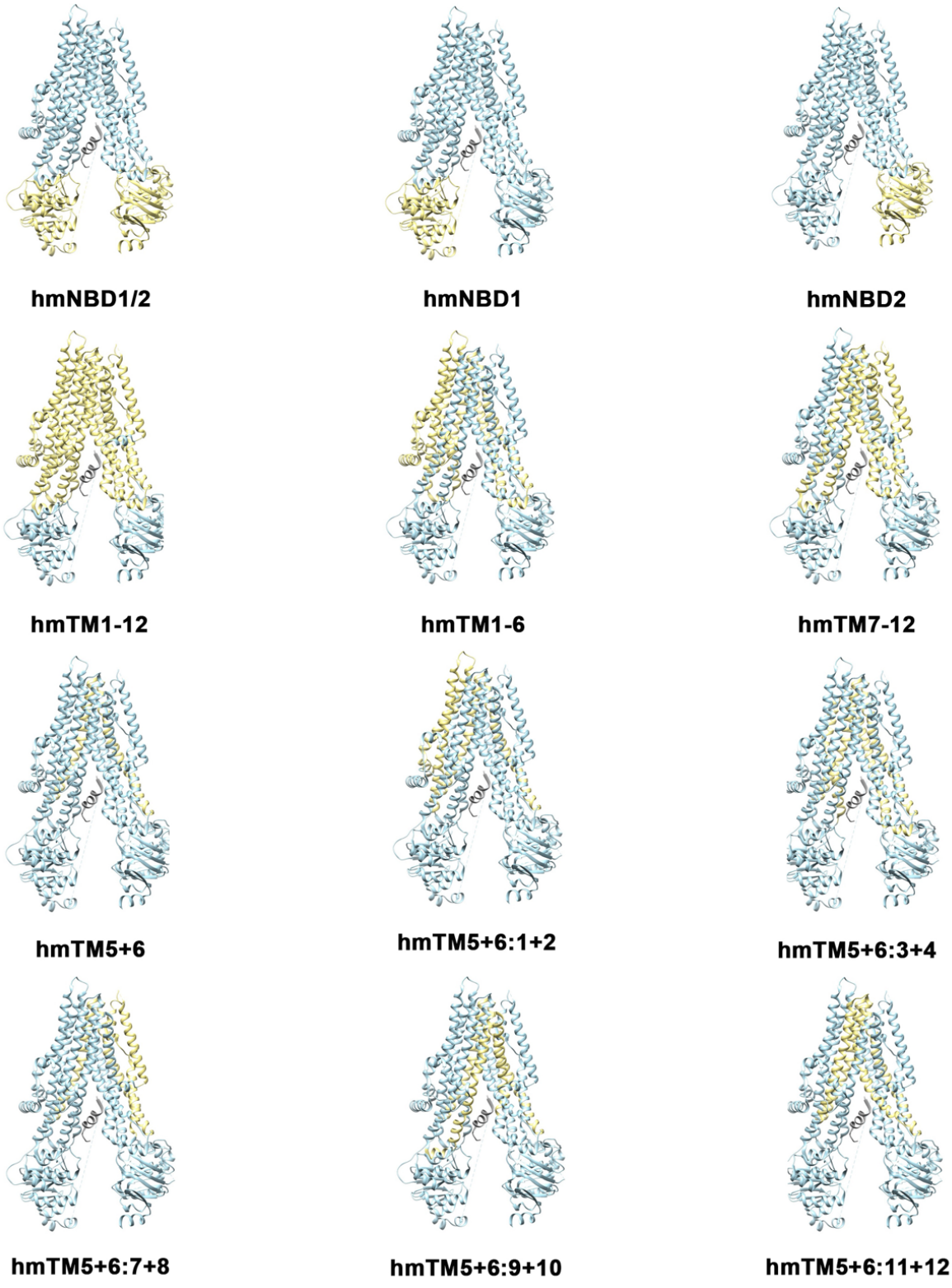

Figure 5.1. Structural models of human-mouse CFTR chimeras. For each of these constructs, human residues are shown in blue and mouse residues are shown in yellow. Models are based upon the human CFTR structure PDB: 5UAK (Liu *et al.*, 2017) (The chimeras for hmRD and hmRI are not shown in this figure due to the lack of inclusion of these domains in the PDB: 5UAK structure).

5.2 Response of human and mouse WT-CFTR to ivacaftor using the automated whole-cell patch-clamp technique

5.2.1 Response of Human WT-CFTR to ivacaftor

Before testing chimeras using the automated patch-clamp technique, it was important to characterise the response of human and mouse WT-CFTR channels to ivacaftor at the whole-cell level. Figure 5.2 shows an example experimental trace recorded using the QPatch HTX platform from a CHO cell expressing human WT-CFTR (hCFTR). All whole-cell patch clamp experiments were recorded at room temperature (21 °C) with $[Cl^-]_{int}$ = 159 mM, $[Cl^-]_{ext}$ = 171 mM. Voltage ramp protocols were applied every 10 s from -80 mV to +80 mV as described in Section 2. In Figure 5.2, only the maximal outward current at 80 mV for each voltage sweep is shown (circles). The current at -30 mV for each voltage sweep is indicated by squares and this was subtracted from the maximal outward current for analysis. Following application of the saline solution (extracellular solution), extracellular solution containing 3% DMSO was applied to each experimental cell for 5 minutes as a vehicle control. This solution was then exchanged with solution containing 10 μM forskolin (FSK) for a period of 15 minutes.

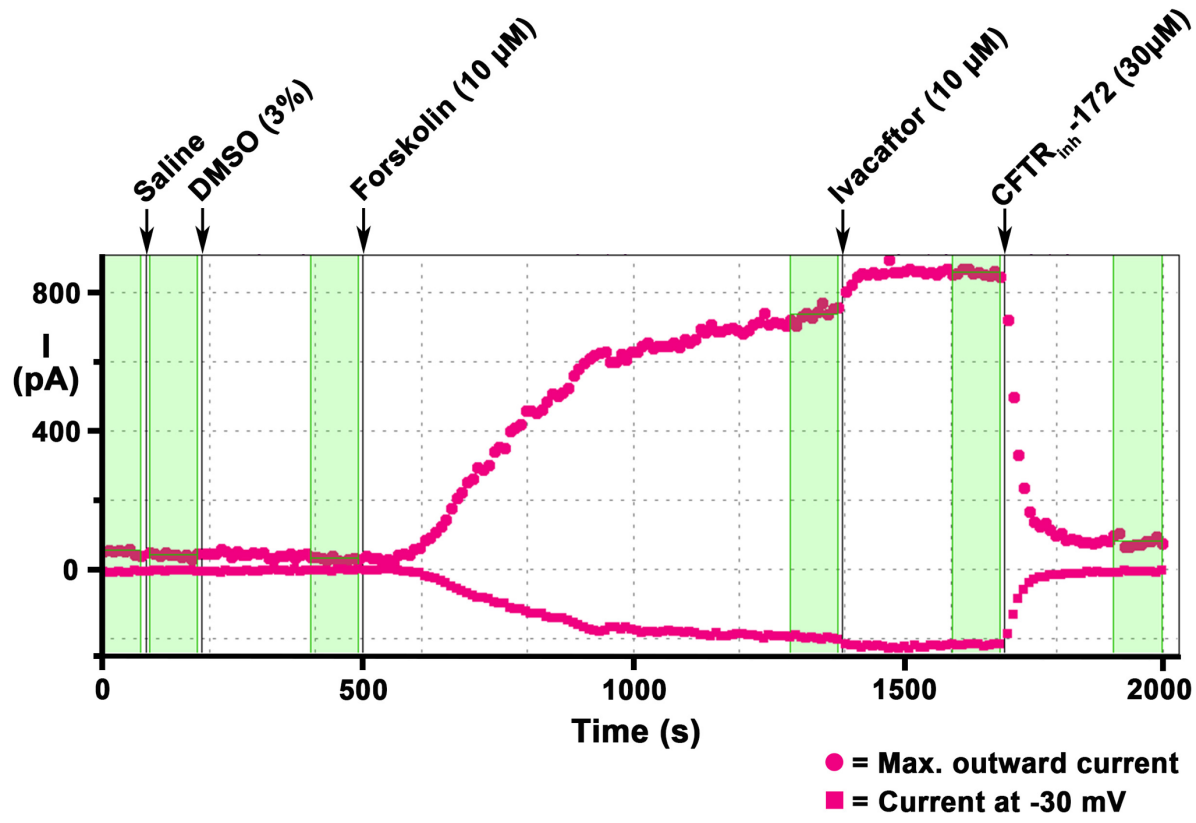

Figure 5.2: Representative QPatch whole-cell recording showing the response of human WT-CFTR to ivacaftor. Whole-cell currents were recorded from a CHO cell transiently expressing hCFTR at room temperature. Circles represent the outward current for each voltage sweep at 80 mV. Squares represent the current recorded at the holding potential of -30 mV. Arrows indicate cumulative addition of specified agents to the extracellular solution. Green shaded areas represent the final 10 sweeps from each liquid application period that were used to calculate average current. Example recording is the same as Figure 2.5 in Section 2.

Following activation of CFTR by FSK, an increase in the maximal outward current was observed (Figure 5.2). After 15 minutes, 10 µM ivacaftor was added to the extracellular solution, resulting in a further increase in maximal outward current. Following application of ivacaftor for 5 minutes, CFTR was inhibited using 30 µM $CFTR_{inh}$-172. 10 µM FSK was present throughout both the ivacaftor and $CFTR_{inh}$-172 liquid application periods. For analysis, the mean maximal current for the final 10 sweeps for each liquid application period was used as indicated by the green bar shading in Figure 5.2. Current recordings were normalised for cell size by dividing by the recorded cell capacitance (C-slow) for each sweep. To ensure the recorded current was specific to CFTR, the change in current (ΔI) was calculated by subtracting the remaining

current following application of $CFTR_{inh}$-172 and the response of CFTR to FSK alone compared to that following addition of ivacaftor as shown in Figure 5.3.

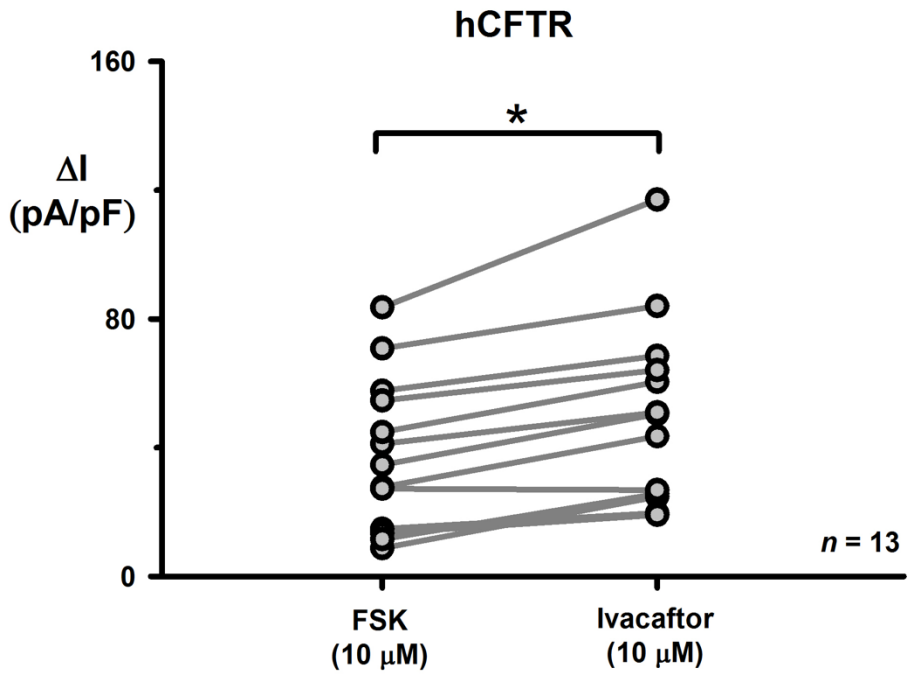

Figure 5.3: Response of human WT-CFTR to ivacaftor as recorded using automated whole-cell patch-clamp technique. Data points represent the mean maximal outward current at the end of liquid application protocols for control (10 μM FSK) and 10 μM ivacaftor in the presence of 10 μM FSK following subtraction of current recorded at -30 mV and normalisation for cell capacitance. Symbols connected by lines represent individual experiments (*n* = 13, * = P < 0.05, two-way Student's paired t-test).

As shown in Figure 5.3, for human WT-CFTR addition of 10 μM ivacaftor resulted in an increase in the mean outward current from 37.7 ± 6.61 pA/pF to 50.4 ± 8.00 pA/pF (*P* < 0.05, *n* = 13).

5.2.2 Response of mouse WT-CFTR to ivacaftor

Figure 5.4 shows a representative QPatch recording from a CHO cell expressing mouse WT-CFTR during activation by 10 μM FSK and subsequent addition of 10 μM ivacaftor and 30 μM $CFTR_{inh}$-172. As is evident from this example the pattern of activation of mouse WT-CFTR was different from that of human WT-CFTR. Interestingly, addition of 10 μM FSK resulted in an initial increase in activity, followed by a slower rise in outward current during the 15-minute liquid application period for

FSK (Figure 5.4). However, addition of ivacaftor following FSK activation resulted in a decrease in activity, suggesting inhibition of the channel by ivacaftor at this concentration (Figure 5.4). Indeed, the rate of current decay following addition of $CFTR_{inh}$-172 after 5 minutes appears to be the same as that observed in the presence of ivacaftor (Figure 5.4).

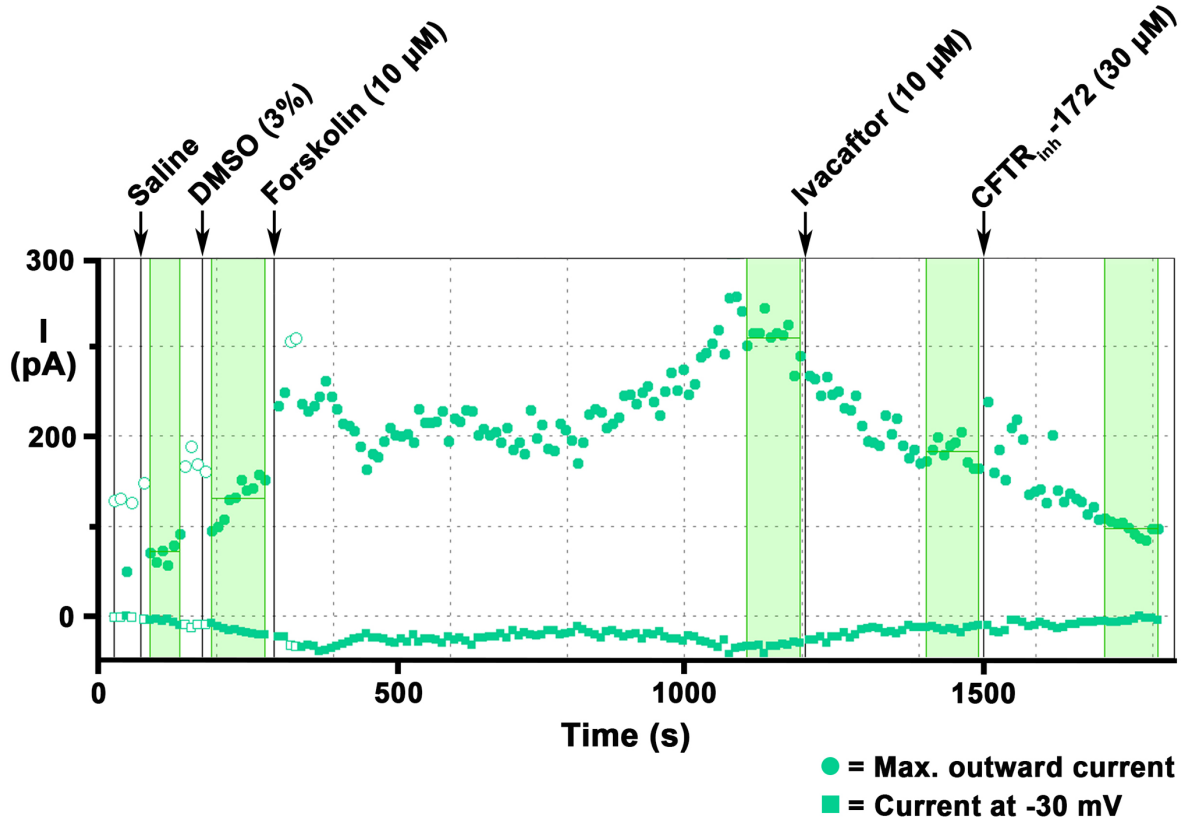

Figure 5.4: Representative QPatch whole-cell recording showing the response of mouse WT-CFTR to ivacaftor. Whole-cell currents recorded from a CHO cell transiently expressing mCFTR at room temperature. Circles represent the outward current for each voltage sweep at 80 mV. Squares represent the current recorded at the holding potential of -30 mV, open circles represent data points that were excluded from analysis. Green shaded areas represent the final 10 sweeps from each liquid application period that were used to calculate average current.

As would be expected given the distinct gating behaviour exhibited by mouse WT-CFTR shown by our previous single-channel currents, the whole-cell currents recorded from cells expressing mouse WT-CFTR following activation by 10 µM FSK were small, in part accounting for the apparent greater current variation observed in Figure 5.5. The mean outward current of mouse WT-CFTR in response to FSK was 15.9 ± 3.19 pA/pF (n = 11) (Figure 5.5). The outward current 5 minutes following the

addition of 10 μM ivacaftor was reduced compared to the FSK-activated current, with a mean current of 5.92 ± 1.64 pA/pF ($P < 0.05$, $n = 11$).

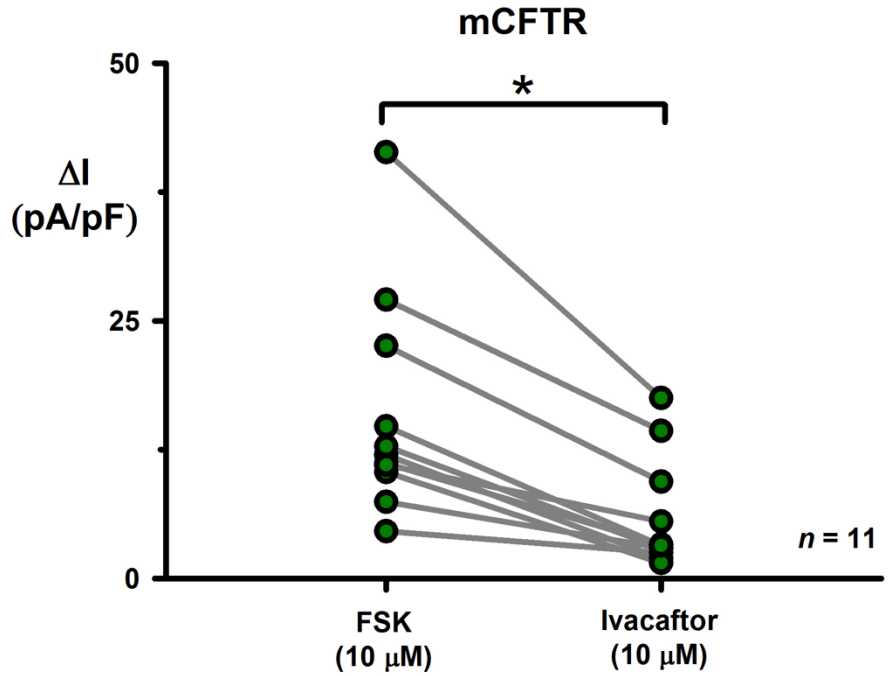

Figure 5.5: Response of mouse WT-CFTR to ivacaftor as recorded using automated whole-cell patch-clamp technique. Data points represent the mean maximal outward current at the end of liquid application protocols for control (10 μM FSK) and 10 μM ivacaftor in the presence of 10 μM FSK following subtraction the current recorded at -30 mV and normalisation for cell capacitance. Symbols connected by lines represent individual experiments ($n = 11$, * = $P < 0.05$, two-way Student's paired t-test).

5.3 Determining compound-interacting domains using automated whole-cell patch-clamp technique to study human-mouse CFTR chimeras

5.3.1 Effect of ivacaftor on whole-domain CFTR chimeras

Given the differences observed in the response to ivacaftor for human and mouse WT-CFTR at both single-channel and whole-cell levels, 10 μM ivacaftor was tested for its effects when applied to whole-domain human-mouse CFTR chimeras. The same experimental procedure was used to study these chimeras using the QPatch automated whole-cell patch-clamp system as had been used for both human and

mouse WT-CFTR. Representative recordings from CHO cells transiently expressing whole-domain chimeras of the NBDs and TMDs are shown in Figure 5.6, whilst quantification of the response to 10 μM FSK followed by addition of 10 μM ivacaftor in the presence of 10 μM FSK for all experiments is shown in Figure 5.7 (Summary data for QPatch whole-cell currents recorded from all human-mouse CFTR chimeras is shown in Figure 5.18).

As shown in Figures 5.6 and 5.7A, for hmNBD1/2 10 μM ivacaftor resulted in a further increase in whole-cell outward current following initial activation of the chimera by 10 μM FSK. Mean whole-cell current following activation by FSK was 19.3 ± 3.58 pA/pF. Ivacaftor potentiated the NBD1/2 CFTR chimera, increasing the mean outward current to 43.5 ± 7.21 pA/pF ($P < 0.05$, $n = 7$) (Figure 5.7A). Having established that ivacaftor potentiates CFTR chimeras that express sequences from both mouse NBDs, we next tested chimeras where either the NBD1 or NBD2 sequence was individually exchanged for their mouse equivalent. As shown in the example recordings in Figure 5.6 and Figures 5.7B and C, potentiation by ivacaftor occurred when just one mouse NBD was expressed on a human CFTR background. In the case of NBD1 (hmNBD1), the maximal outward current increased from 15.0 ± 7.30 pA/pF following activation by FSK, to 33.6 ± 10.7 pA/pF after the addition of 10 μM ivacaftor ($P < 0.05$, $n = 4$). When mouse NBD2 was expressed (hmNBD2), maximal outward current increased from 14.7 ± 3.01 pA/pF to 25.3 ± 4.67 pA/pF ($P < 0.05$, $n = 15$). These results, combined with those for hmNBD1/2, suggest that the differences in the effect of 10 μM ivacaftor on human and mouse WT-CFTR channels is not related to sequence differences within the NBDs.

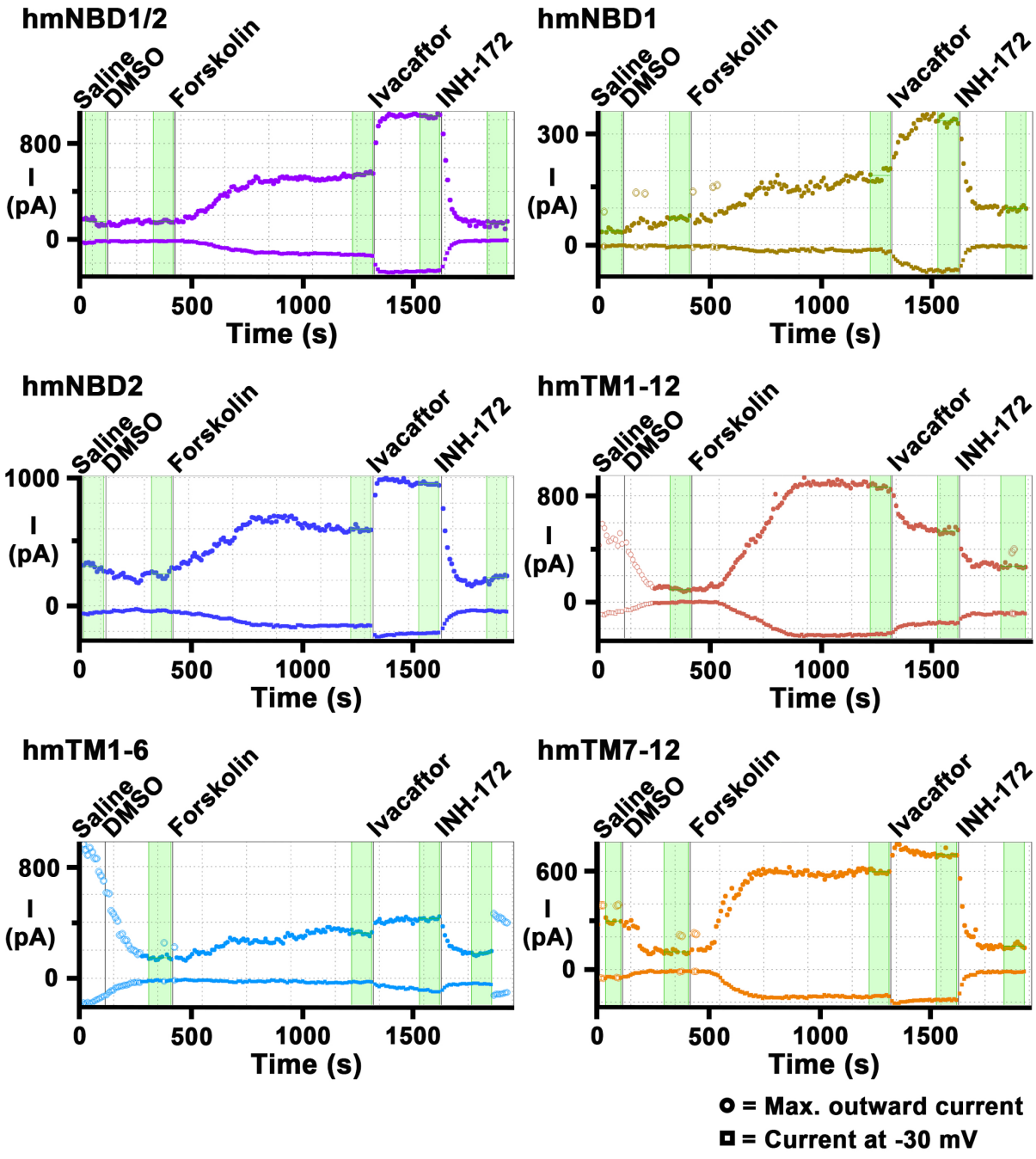

Figure 5.6: Representative QPatch whole-cell recordings showing the response of human-mouse CFTR whole-domain chimeras to ivacaftor. Whole-cell currents recorded from CHO cells transiently expressing the indicated whole-domain human-mouse CFTR chimeras at room temperature are shown. INH-172 = $CFTR_{inh}$-172. Other details same as Figure 5.2.

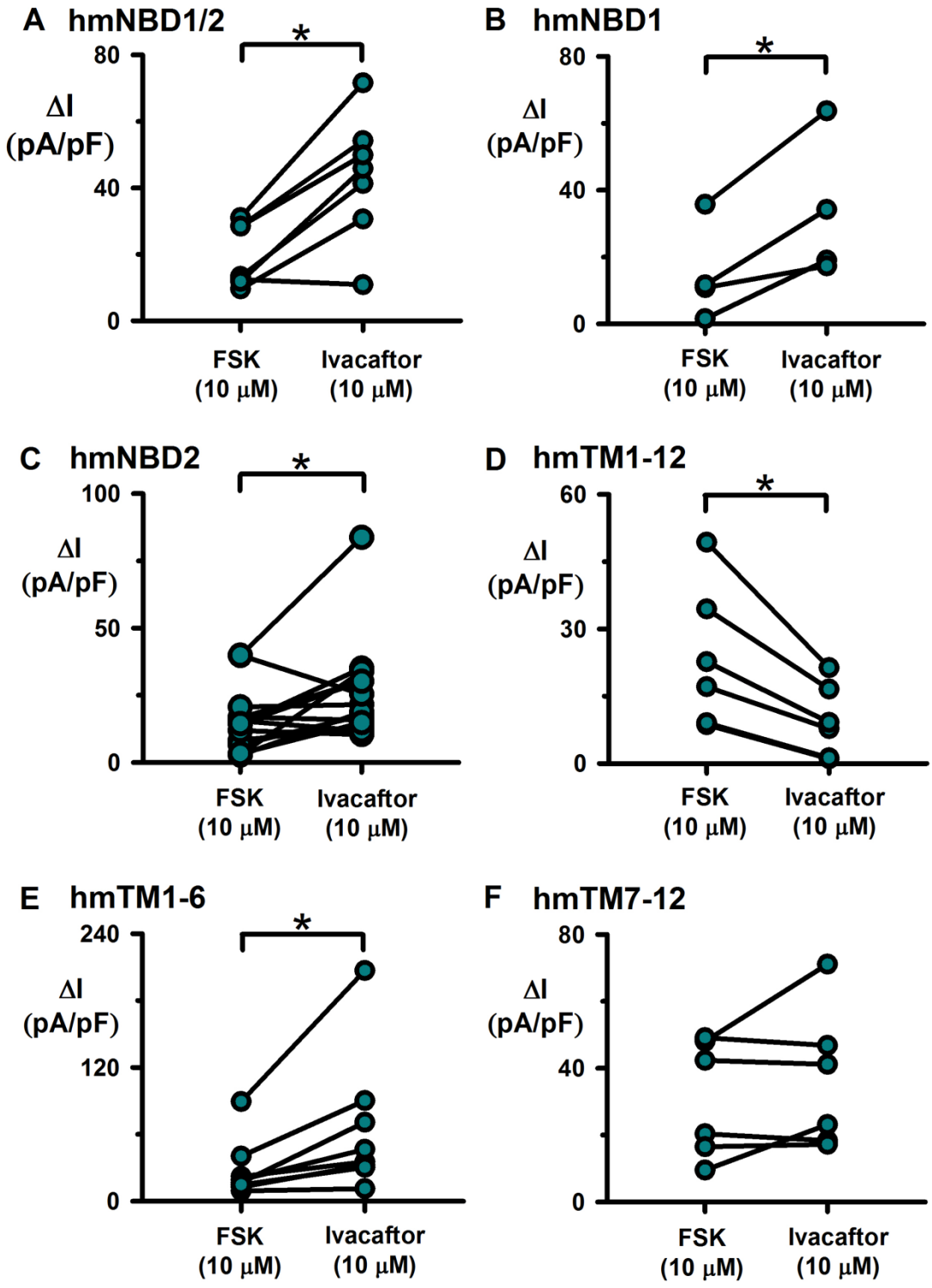

Figure 5.7: Effects of ivacaftor on human-mouse CFTR whole-domain chimeras. Data points represent the mean maximal outward current at the end of liquid application protocols for control (10 μM FSK) and 10 μM ivacaftor in the presence of 10 μM FSK following subtraction of the current recorded at -30 mV and normalisation for cell capacitance. Symbols connected by lines represent individual experiments. **A** hmNBD1/2; *n* = 7. **B** hmNBD1; *n* = 4. **C** hmNBD2; *n* = 15. **D** hmTM1-12; *n* = 5. **E** hmTM1-6; *n* = 7. **F** hmTM7-12; *n* = 6 (* = $P < 0.05$, two-way Student's paired t-test).

To investigate the effect of sequence changes in the TMDs, we tested the hmTMD1-12 chimera, in which the mouse sequence for both TMDs was expressed on a human CFTR background (Figure 5.6 and 5.7D). In the case of hmTM1-12, the mean outward current was reduced following addition of 10 μM ivacaftor from 23.5 ± 6.48 pA/pF in the presence of 10 μM FSK alone to 9.52 ± 3.34 pA/pF ($P < 0.05$, $n = 6$). As illustrated by the example QPatch trace shown in Figure 5.6, outward currents were inhibited by both ivacaftor and $CFTR_{inh}$-172. Following addition of 10 μM ivacaftor, an exponential decay was observed in the outward current, which reached a stable level within the 5-minute period of this liquid application (Figure 5.6). Addition of $CFTR_{inh}$-172 resulted in a further exponential decay in outward current (Figure 5.6).

To determine whether the sequence alterations between human WT-CFTR and the hmTM1-12 chimera responsible for the difference in the effect of ivacaftor on these two constructs were limited to a single TMD, we next tested chimeras in which complete sequences for either TMD1 or TMD2 were exchanged for the murine equivalent (constructs hmTM1-6 and hmTM7-12, Figure 5.6 and 5.7E and F). In the case of hmTM1-6, potentiation was observed, with an increase in the mean outward current from 28.1 ± 9.37 pA/pF following activation by FSK, to 65.5 ± 22.0 pA/pF ($P < 0.05$, $n = 8$). With the exception of one cell, cells expressing hmTM1-6 showed relatively small increases in outward current when treated with ivacaftor. This likely accounts for the large variance observed in the data. In the case of hmTM7-12 (Figure 5.7F), little or no change in outward current was observed following addition of ivacaftor with a mean outward current following addition of 10 μM FSK of 31.0 ± 7.14 pA/pF and a current of 36.3 ± 8.58 pA/pF after application of ivacaftor (P = ns, $n = 6$). Interestingly, the inhibition of outward currents by ivacaftor observed for the construct hmTM1-12 and mouse WT-CFTR was not replicated by either the hmTM1-6 or the hmTM7-12 chimeras.

5.3.2 Effect of ivacaftor on TM-helix CFTR chimeras

The results from testing human-mouse CFTR chimeras with whole domains exchanged suggested that sequence alterations within the TMDs rather than the NBDs were responsible for the differences observed in the action of ivacaftor on

human and mouse WT-CFTR. We therefore tested human-mouse CFTR chimeric constructs where pairs of TM helices in the human CFTR sequence and their linking ICLs and ECLs were exchanged with sequences from mouse CFTR. The first of these TM helix chimeras to be tested was the hmTM5+6 construct, in which the sequences for TM5 and TM6 were exchanged for their mouse equivalents. As shown in the first panel of Figure 5.8 and 5.9A, no change in the FSK-activated outward current was observed following addition of 10 μM ivacaftor in the presence of FSK. Following addition of 10 μM FSK alone, the mean CFTR-mediated outward current was 21.9 ± 3.66 pA/pF and this did not change significantly, remaining at 22.0 ± 7.02 pA/pF following application of 10 μM ivacaftor (P = ns, n = 8). These results suggest that exchange of the human sequences for TM5 and TM6 alone for their mouse equivalents is sufficient to prevent potentiation by ivacaftor.

In Section 5.4.1, we demonstrated that when the human sequences in TMD1 were exchanged for the equivalent mouse sequences the resulting hmTM1-6 chimera still showed potentiation by ivacaftor (Figures 5.6 and 5.7E). Conversely, potentiation was not observed in the case of the construct hmTM7-12 (Figures 5.6 and 5.7F). One potential reason for the discrepancy between these findings and the observation that exchange of TM5+6 results in a construct that was not potentiated by ivacaftor is that interactions between TM5 and TM6 and other transmembrane helices in either TMD1 or TMD2 may restore the capacity for potentiation by ivacaftor. We therefore tested chimeras where mouse sequences for alternative transmembrane helices were exchanged in conjunction with TM5 and TM6. The first of these chimeras to be tested was hmTM5+6:1+2. As can be seen from the recording shown in Figure 5.8 and the summary graph in Figure 5.9B, no potentiation was observed in response to 10 μM ivacaftor in the case of the hmTM5+6:1+2 chimera, with a mean outward current at 80 mV of 19.3 ± 2.41 pA/pF following activation by 10 μM FSK, and 17.8 ± 5.84 pA/pF following application of 10 μM ivacaftor in the presence of 10 μM FSK (P = ns, n = 7). Inclusion of mouse sequences for TM3 and TM4 in conjunction with mouse TM5 and TM6 did however produce a chimera (hmTM5+6:3+4) that demonstrated potentiation by ivacaftor (Figures 5.8 and 5.9C). The FSK-induced mean outward current generated by the hmTM5+6:3+4 construct at 80 mV increased from 23.5 ± 3.84 pA/pF to 33.2 ± 4.40 pA/pF following addition of 10 μM ivacaftor ($P < 0.05$, n = 9).

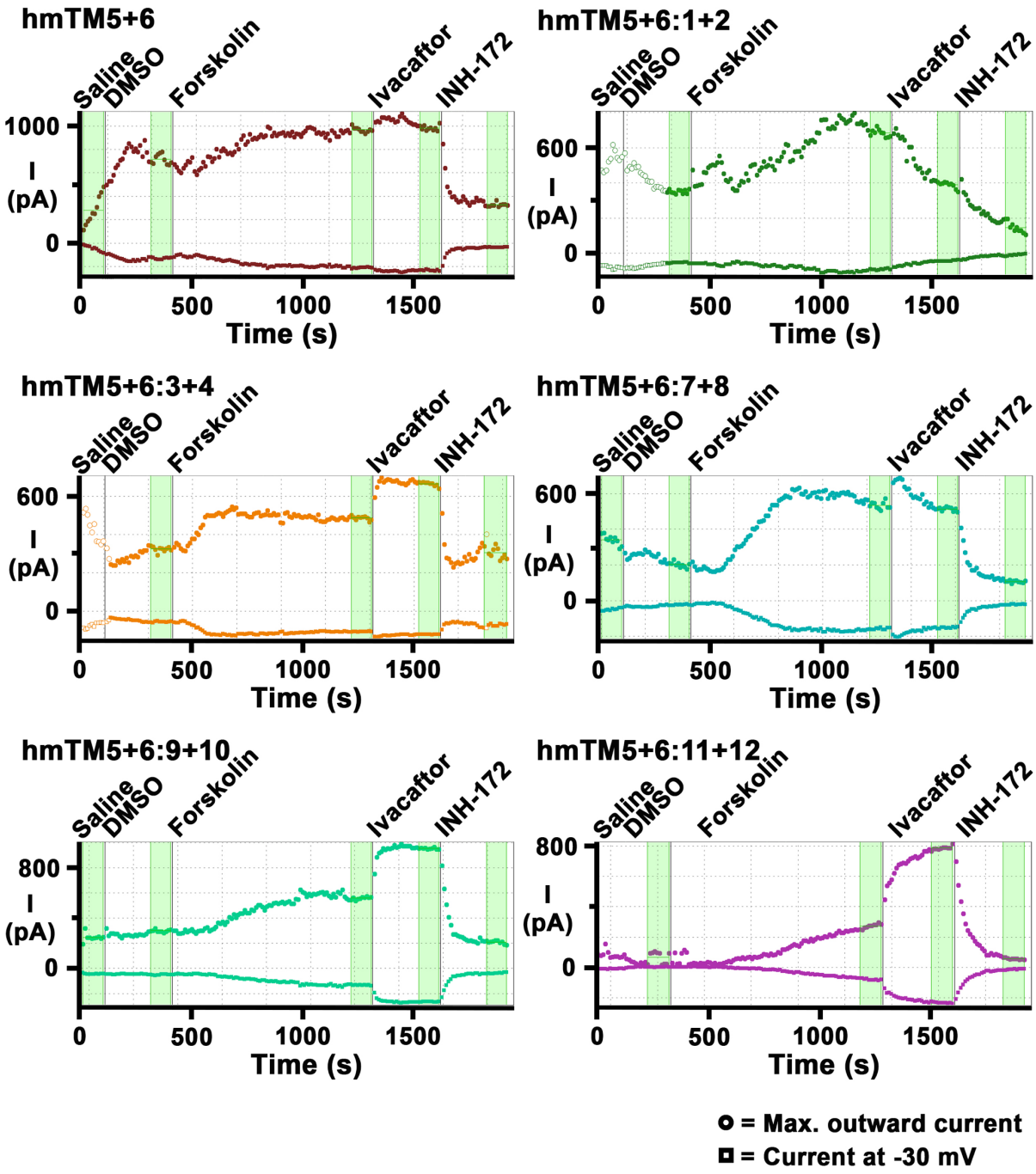

Figure 5.8: Representative QPatch whole-cell recordings showing the response of human-mouse CFTR TM-helix chimeras to ivacaftor. Whole-cell currents recorded from CHO cells transiently expressing the indicated transmembrane helix human-mouse CFTR chimeras at room temperature are shown. INH-172 = $CFTR_{inh}$-172. Other details same as Figure 5.2.

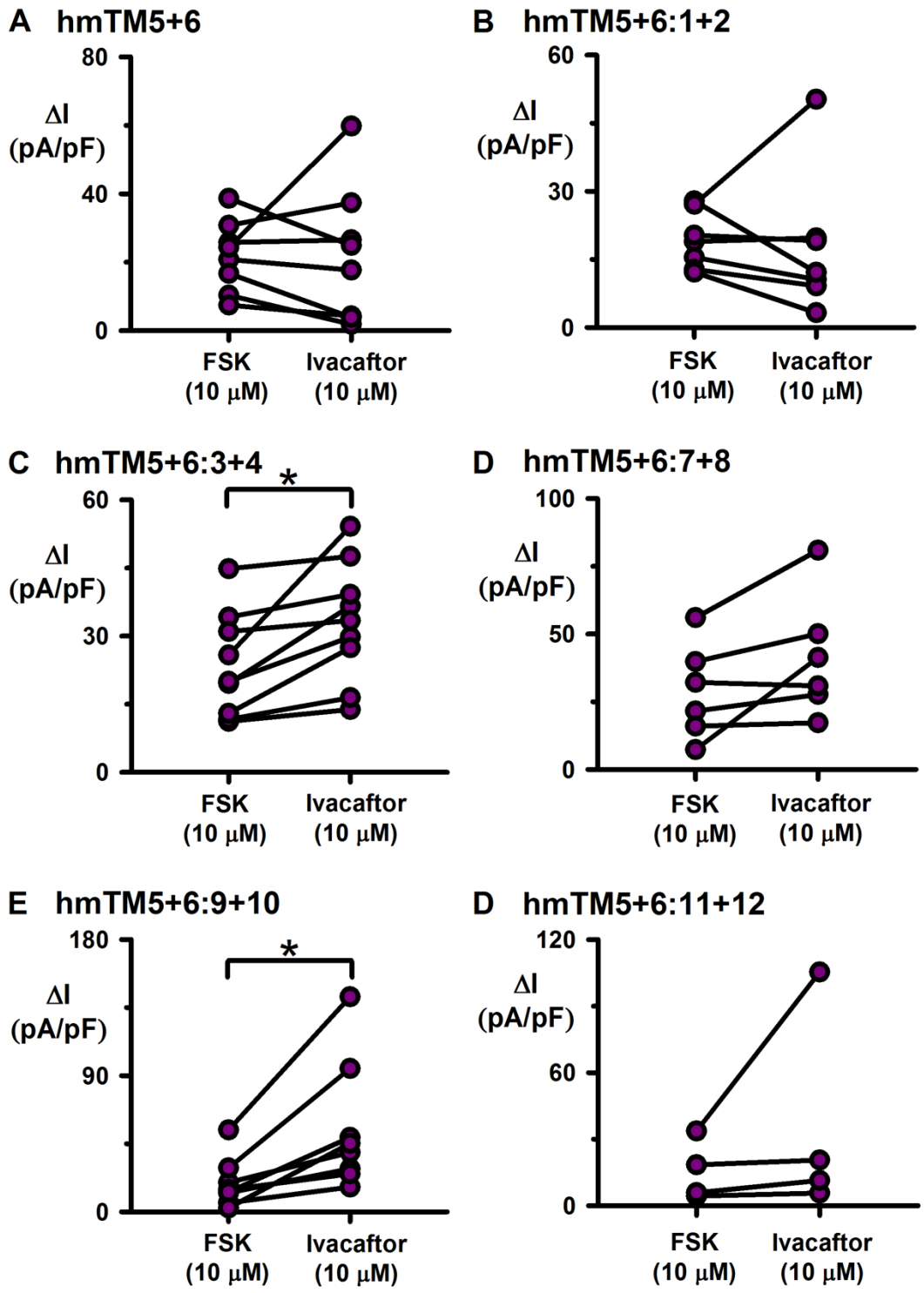

Figure 5.9: Effects of ivacaftor on human-mouse CFTR TM-helix chimeras. Data points represent the mean maximal outward current at the end of liquid application protocols for control (10 μM FSK) and 10 μM ivacaftor in the presence of 10 μM FSK following subtraction of the current recorded at -30 mV and normalisation for cell capacitance. Symbols connected by lines represent individual experiments. **A** hmTM5+6; *n* = 8. **B** hmTM5+6:1+2; *n* = 7. **C** hmTM5+6:3+4; *n* = 9. **D** hmTM5+6:7+8; *n* = 6. **E** hmTM5+6:9+10; *n* = 8. **F** hmTM5+6:11+12; *n* = 4 (* = $P < 0.05$, two-way Student's paired t-test).

To investigate potential interactions between TM5 and TM6 in TMD1 with transmembrane helices from TMD2, we next tested chimeras where mouse sequences in TMD2 were expressed in conjunction with mouse TM5+6 and the remaining sequences in the CFTR construct matched the human sequence. The first of these constructs to be tested was hmTM5+6:7+8. The FSK-induced maximal outward current for hmTM5+6:7+8 at 80 mV was 28.8 ± 7.20 pA/pF before, and 41.4 ± 5.71 pA/pF after addition of 10 μM ivacaftor (*P* = ns, *n* = 6) (Figure 5.8 and Figure 5.9D). However, when mouse sequences TM9 and TM10 in TMD2 were expressed in conjunction with mouse TM5 and TM6 in TMD1, mean outward current at 80 mV increased from 18.9 ± 5.78 pA/pF following activation by FSK to 55.0 ± 15.0 pA/pF following addition of ivacaftor (*P* < 0.05, *n* = 8) (Figures 5.8 and 5.9E). Potentiation by ivacaftor was not observed for the hmTM5+6:11+12 chimera although there was variation within the data for this chimera (Figures 5.8 and 5.9D). The mean maximal outward current at 80 mV recorded for hmTM5+6:11+12 before application of ivacaftor was 15.6 ± 6.80 pA/pF and this increased to 35.7 ± 23.4 pA/pF following addition of 10 μM ivacaftor (*P* = ns, *n* = 4). However as indicated by the large error for this recording, only one of the four successful experiments using this construct indicated potentiation (Figure 5.8 and Figure 5.9D) and the observed overall increase was not found to be significant. Caution must therefore be used in interpreting this result due to the low number of successful experiments achieved and lack of statistical power.

Having investigated the involvement of specific transmembrane helices in the differences observed in the response of human and mouse WT-CFTR to ivacaftor, we next aimed to investigate the involvement of regulatory regions of the CFTR protein. Two further chimeras were studied where either the RD or the regulatory insertion (RI), a flexible region between residues 404-436 that contains serine residues that can be targeted for PKA-mediated phosphorylation (Lewis *et al.*, 2004), were exchanged for their mouse equivalents. Although an ivacaftor-mediated response was observed in some experiments completed using the hmRD chimera (example trace in Figure 5.10), no overall potentiation was observed for this construct. Mean outward current at 80 mV following addition of FSK was recorded at 28.5 ± 3.52 pA/pF and 31.8 ± 4.92 pA/pF following addition of 10 μM ivacaftor (*P* = ns, *n* = 14) (Figure 5.11A). In the case of the hmRI chimera, mean outward current at 80 mV was 30.5 ± 4.84 pA/pF following

addition of FSK alone, and 29.1 ± 6.78 pA/pF after addition of 10 µM ivacaftor (*P* = ns, *n* = 11) (Figures 5.10 and 5.11B).

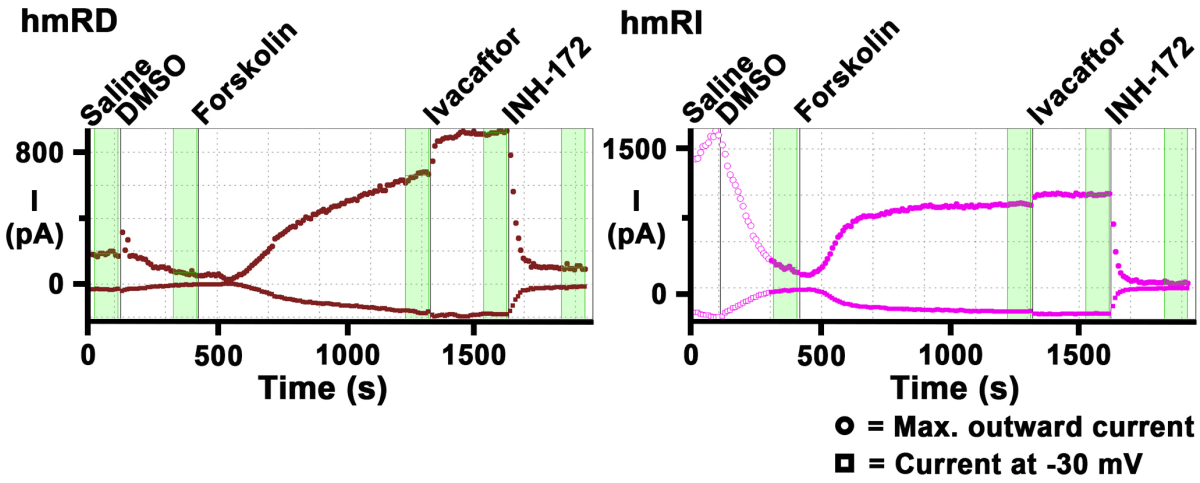

Figure 5.10: Representative QPatch whole-cell recordings showing the effects of 10 µM ivacaftor on human-mouse CFTR RD and RI chimeras. Whole-cell currents recorded from CHO cells transiently expressing the indicated human-mouse CFTR chimeras for the RD and RI at room temperature are shown. INH-172 = $CFTR_{inh}$-172. Other details same as Figure 5.2.

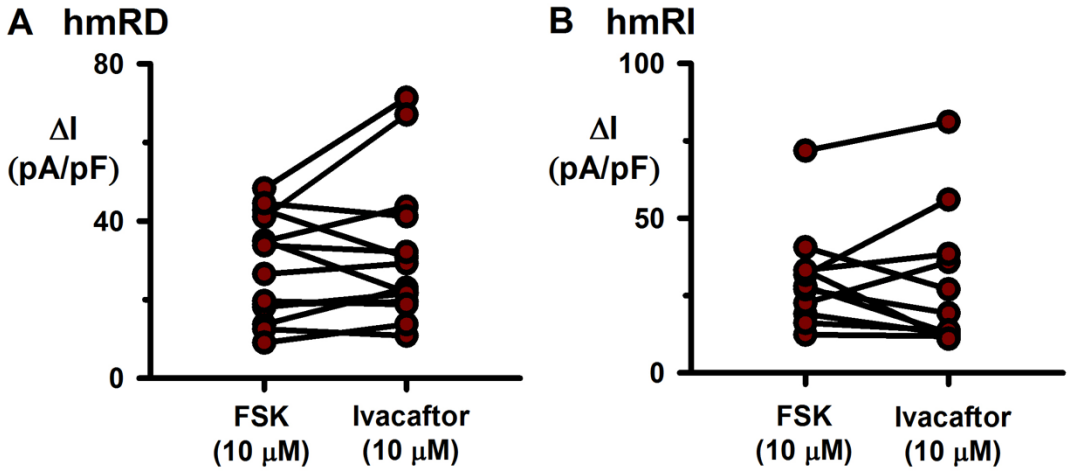

Figure 5.11: Effects of ivacaftor on the human-mouse CFTR chimeras hmRD and hmRI. Data points represent the mean maximal outward current at the end of liquid application protocols for control (10 µM FSK) and 10 µM ivacaftor in the presence of 10 µM FSK following subtraction of the current recorded at -30 mV and normalisation for cell capacitance. Symbols connected by lines represent individual experiments. **A** hmRD; *n* = 14. **B** hmRI; *n* = 11 (*P* > 0.05, two-way Student's t-test).

5.4 The gating behaviour of human-mouse CFTR chimeras as determined using single-channel patch-clamp recordings

The technique of automated whole-cell patch-clamp recording enabled rapid testing of multiple human-mouse CFTR chimeras for their response to ivacaftor when transiently expressed in CHO cells. The purpose of these experiments was to determine whether or not different CFTR constructs were potentiated by ivacaftor. However, these data provide limited information about the response of human-mouse CFTR chimeric constructs to ivacaftor at the molecular level. In particular, the lack of control over the level of expression of CFTR constructs and potential variation in expression between cells expressing the same construct using the transfection system prevented detailed quantitative analysis of the observed response of these cells to ivacaftor. As such, we selected four of the studied human-mouse CFTR chimeric constructs for further study using the single-channel patch-clamp technique utilised in Chapters 3 and 4.

Figure 5.12A shows representative single-channel recordings at -80 mV from excised inside-out membrane patches taken from CHO cells transiently expressing the hmNBD1/2, hmTM1-6, hmTM5+6 and hmTM5+6:9+10 chimeric CFTR constructs. As can be seen from these representative traces, each of the four constructs produced currents when exposed to a Cl^- gradient and following activation by 1 mM ATP and 75 nM PKA. Quantification of single-channel current and P_o at -80 mV for each of these constructs as well as human and mouse WT-CFTR are shown in Figures 5.12B and C. Of the four constructs tested, the hmNBD1/2 construct produced currents and showed activity that most closely resembled that of human WT-CFTR. The single-channel current amplitude recorded from hmNBD1/2 at -80 mV was -0.62 ± 0.01 pA (n = 6) representing a 32% reduction in i compared to human WT-CFTR. The P_o of the hmNBD1/2 construct was recorded as 0.33 ± 0.09 (n = 6) representing a 22% reduction compared to human WT CFTR. Visual inspection of the gating behaviour of the hmNBD1/2 chimera in Figure 5.12A indicates a pattern of gating that more closely resembles that of human WT-CFTR than mouse WT-CFTR, exhibiting bursts of channel openings with short intraburst closures and no evidence of the sub-

conductance O_1 level observed for mouse WT-CFTR. This is in contrast however to the hmTM1-6 chimeric construct that demonstrated brief channel openings and a sub-conductance state similar to the O_1 state observed for mouse WT-CFTR. The single-channel current amplitude of the hmTM1-6 chimera was -0.40 ± 0.01 pA at -80 mV (*n* = 3), indicating a 56% reduction in the singe-channel current amplitude compared to human WT-CFTR. The P_o of the hmTM1-6 chimera was recorded at 0.06 ± 0.02 (*n* = 3) (Figure 5.12C). For hmTM5+6, a similar reduction in single-channel current amplitude was recorded of -0.39 ± 0.05 pA at -80 mV and a P_o of 0.07 ± 7.28 $x10^{-3}$ (*n* = 4) (Figure 5.12B and C). As shown by the representative trace in Figure 5.12A, despite the low P_o, the gating behaviour of the hmTM5+6 construct did not demonstrate the same brief channel openings observed for mouse WT-CFTR and hmTM1-6, and the sub-conductance level was also absent from single-channel recordings of this construct. Finally, in comparison to the hmTM5+6 chimera, hmTM5+6:9+10 did not show a reduced single-channel current at -80 mV (-0.40 ± 0.02 pA) (Figure 5.12B), but did result in a 200% increase in P_o compared to hmTM5+6 with a P_o of 0.21 ± 0.08 (*n* = 3) (Figure 5.12C). The P_o of the hmTM5+6:9+10 chimera therefore represented a 49% reduction compared to the P_o of human WT-CFTR.

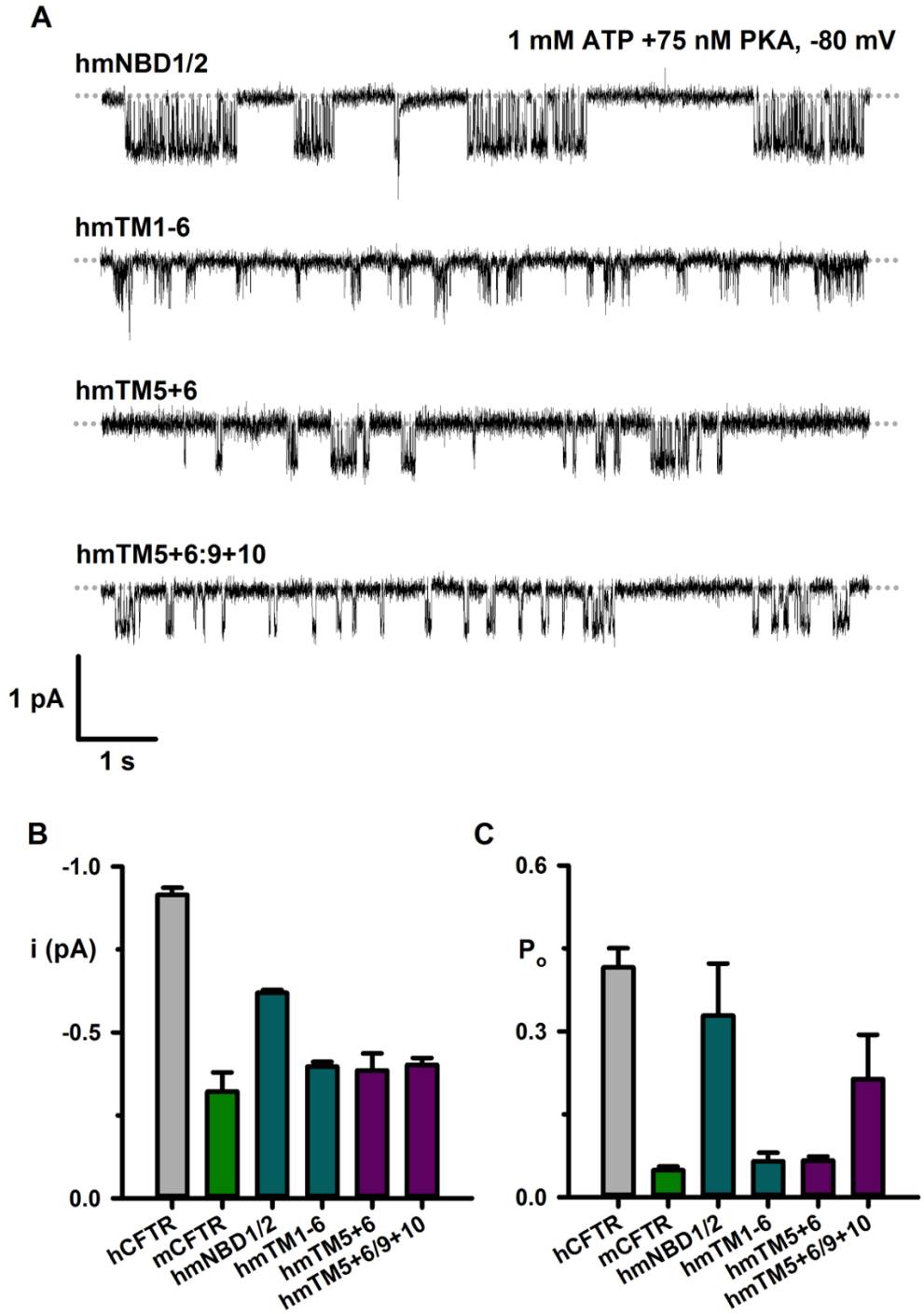

Figure 5.12: Summary of gating properties of human-mouse CFTR chimeras. A Representative single-channel recordings of human-mouse CFTR chimeras from excised inside-out membrane patches in the presence of a Cl^- concentration gradient ($[Cl^-]_{int}$ = 147 mM; $[Cl^-]_{ext}$ = 10 mM). ATP (1 mM) and PKA (75 nM) were continuously present in the intracellular solution. Dotted grey lines represent the closed channel level. For the purpose of illustration, recordings have been filtered at 500 Hz and digitised at 5 kHz before file size was compressed by 5-fold data reduction. For all experiments, temperature was 37 °C and holding potential was -80 mV. **B** and **C** Comparison of i and P_o for human-mouse CFTR chimeras. Data are means ± SEM (human, *n* = 5-10; mouse *n* = 4; hmNBD1/2, *n* = 6; hmTM1-6, *n* = 3; hmTM5+6, *n* = 4; hmTM5+6:9+10, *n* = 3).

5.5 Determining the binding domain of ivacaftor using single-channel studies of human-mouse CFTR chimeras

In addition to characterising the single-channel current amplitude and P_o of the selected human-mouse CFTR chimeras, we tested the effects of ivacaftor on the single-channel activity of these constructs. Due to the fact that 10 μM ivacaftor inhibited some constructs using the automated whole-cell patch-clamp technique, in these experiments we tested ivacaftor at 1 μM and 10 μM. In this way, we controlled for the possibility that ivacaftor may inhibit human-mouse CFTR chimeras at higher concentrations that may be obscuring possible potentiation effects at lower concentrations.

5.5.1 Effect of ivacaftor on whole-domain CFTR chimeras

Figure 5.13 shows the effects of 1 μM and 10 μM ivacaftor on the single-channel activity of the hmNBD1/2 chimera. The spread of the data points shown in Figure 5.13B highlight the variability of the data collected for the hmNBD1/2 chimera. However, despite this variability an increase in P_o with increasing ivacaftor concentrations was observed for all experiments performed with this construct. This increase in activity is demonstrated by the increase in open-channel burst duration after addition of 1 and 10 μM ivacaftor shown in the example recordings in Figure 5.13A. This increase was not found to be significant at 1 μM ivacaftor, where P_o increased from 0.33 ± 0.07 under control conditions (1 mM ATP + 75 nM PKA) to 0.41 ± 0.11 (n = 5). Increasing the concentration of ivacaftor to 10 μM however increased P_o further to 0.47 ± 0.11 (n = 5) and this further increase was found to be significant when compared to control (Figure 5.13B).

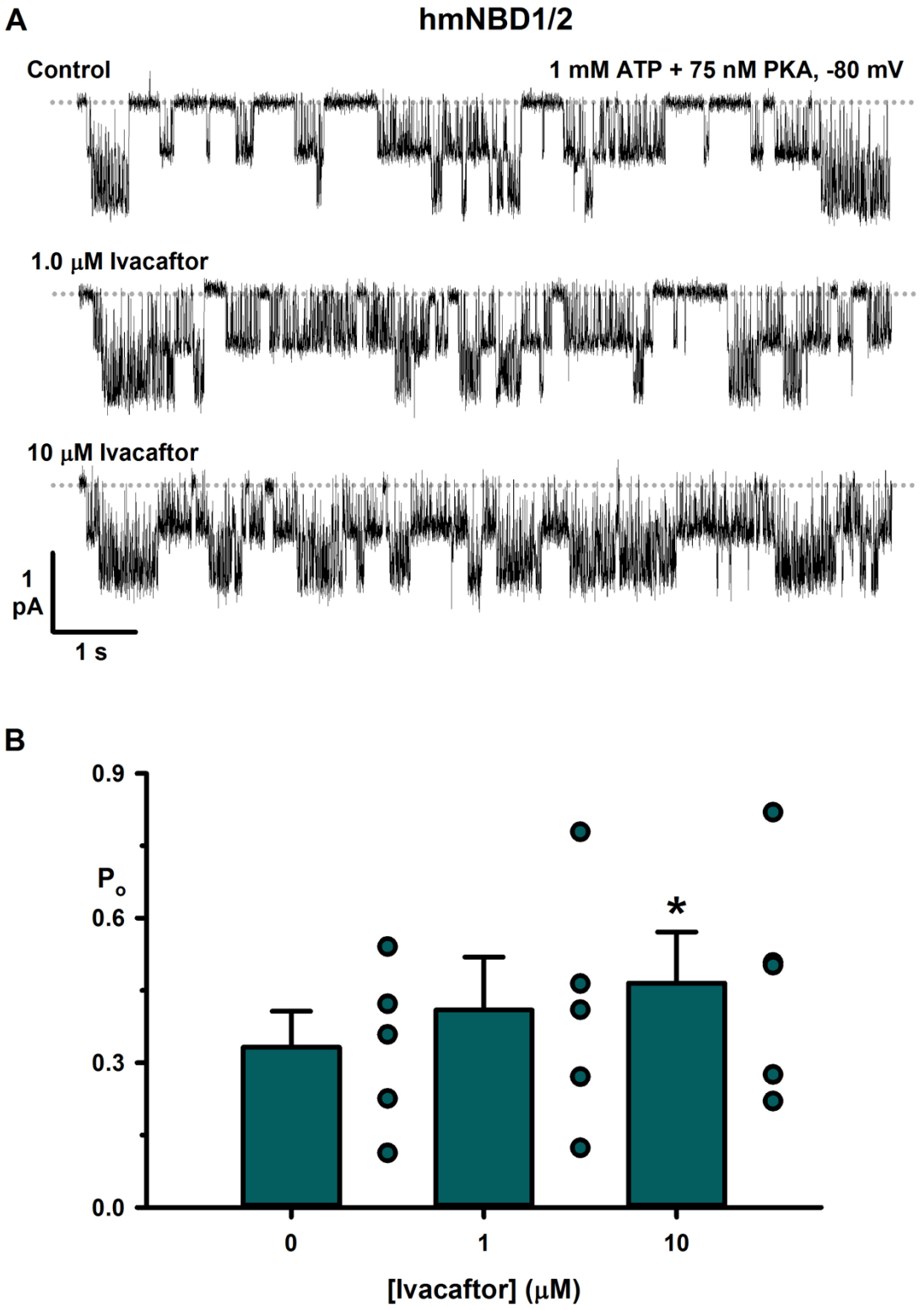

Figure 5.13: Effects of ivacaftor on the single-channel activity of the human-mouse NBD1/2 chimera. A Representative recordings from an excised inside-out membrane patch from a CHO cell showing the response of hmNBD1/2 to 1 μM and 10 μM ivacaftor. Other conditions as described for Figure 5.12A. **B** P_o for hmNBD1/2 at 1 μM and 10 μM ivacaftor. Data are means ± SEM and individual data points are indicated by circles. (n = 4 - 5, * = P < 0.05 vs control, one-way repeated measures ANOVA and Dunnett's multiple comparisons).

5.5.2 Effect of ivacaftor on TM-helix CFTR chimeras

Unfortunately, insufficient data were collected to determine the effect of ivacaftor on the hmTM1-6 chimera. However, Figure 5.14 shows the effects of ivacaftor on the single-channel activity of the hmTM5+6 chimera. Representative traces showing the activity of this CFTR chimera under control conditions and following the addition of 1.0 μM ivacaftor are shown in Figure 5.14A, whilst quantification of P_o at control, 1.0 and 10 μM ivacaftor are shown in Figure 5.14B. As can be seen in Figure 5.14B, addition of ivacaftor at either 1.0 or 10 μM did not result in an increase in the P_o recorded for the hmTM5+6 chimera. Although only three experiments were successful at 1.0 μM ivacaftor, and two at 10 μM ivacaftor, no increase in P_o was observed at the tested concentrations, with the mean P_o recorded as 0.08 ± 0.01 (n = 4) under control conditions, 0.07 ± 0.02 (n = 3) after addition of 1.0 μM ivacaftor, and 0.10 ± 0.01 (n = 2) after addition of 10 μM ivacaftor.

Figure 5.15 shows the effects of 1 and 10 μM ivacaftor on the hmTM5+6:9+10 construct. At the whole cell level, this construct showed potentiation at 10 μM ivacaftor (Figure 5.9E). However, potentiation was not observed to the same level when this construct was tested using single-channel patch-clamp recordings. Only three single-channel experiments were successfully completed using this construct. An increase in P_o was only observed in two of the three experiments at 1 and 10 μM ivacaftor (individual data points in Figure 5.15B) and the mean data did not indicate a statistically significant level of potentiation. The mean P_o for this construct was calculated as 0.19 ± 0.08 under control conditions, increasing to 0.26 ± 0.04 at 1 μM ivacaftor and 0.27 ± 0.06 at 10 μM ivacaftor respectively (Figure 5.15B). Whilst the low power of this experiment (n = 3) limits the interpretation of these data, the upward trend in P_o with increasing ivacaftor concentrations observed in two of the three experiments suggests that ivacaftor may be potentiating the single-channel activity of this construct. Further experiments are required to confirm this observation.

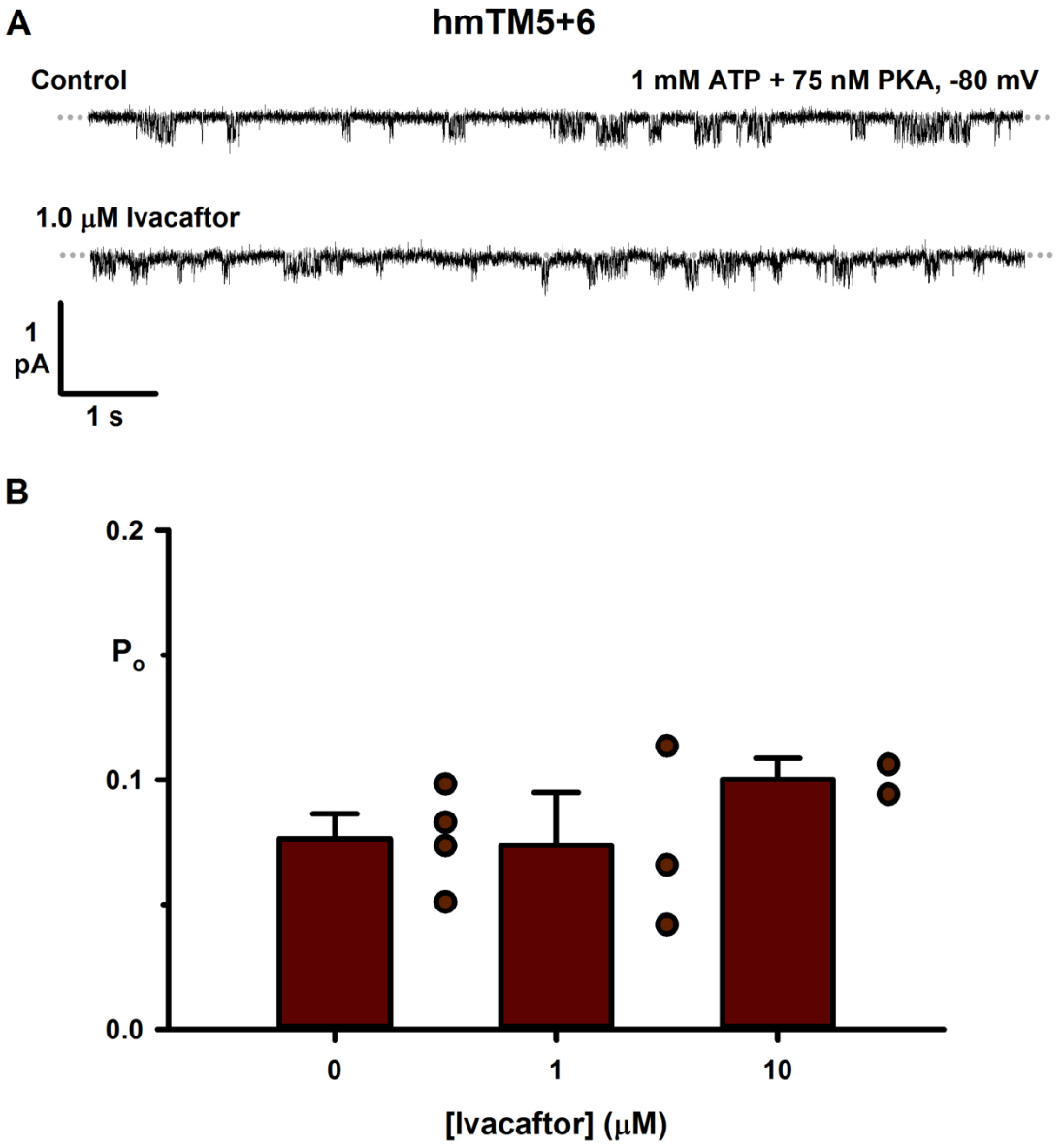

Figure 5.14: Effects of ivacaftor on the single-channel activity of the human-mouse TM5+6 chimera. A Representative recordings from an excised inside-out membrane patch from a CHO cell show the response of hmTM5+6 to 1 μM ivacaftor. Other conditions as described for Figure 5.12A. **B** P_o for hmTM5+6 at 1 μM and 10 μM ivacaftor. Data are means ± SEM except at 10 μM ivacaftor where error bar represents SD (n = 2 - 4, P > 0.05 vs control, one-way repeated measures ANOVA).

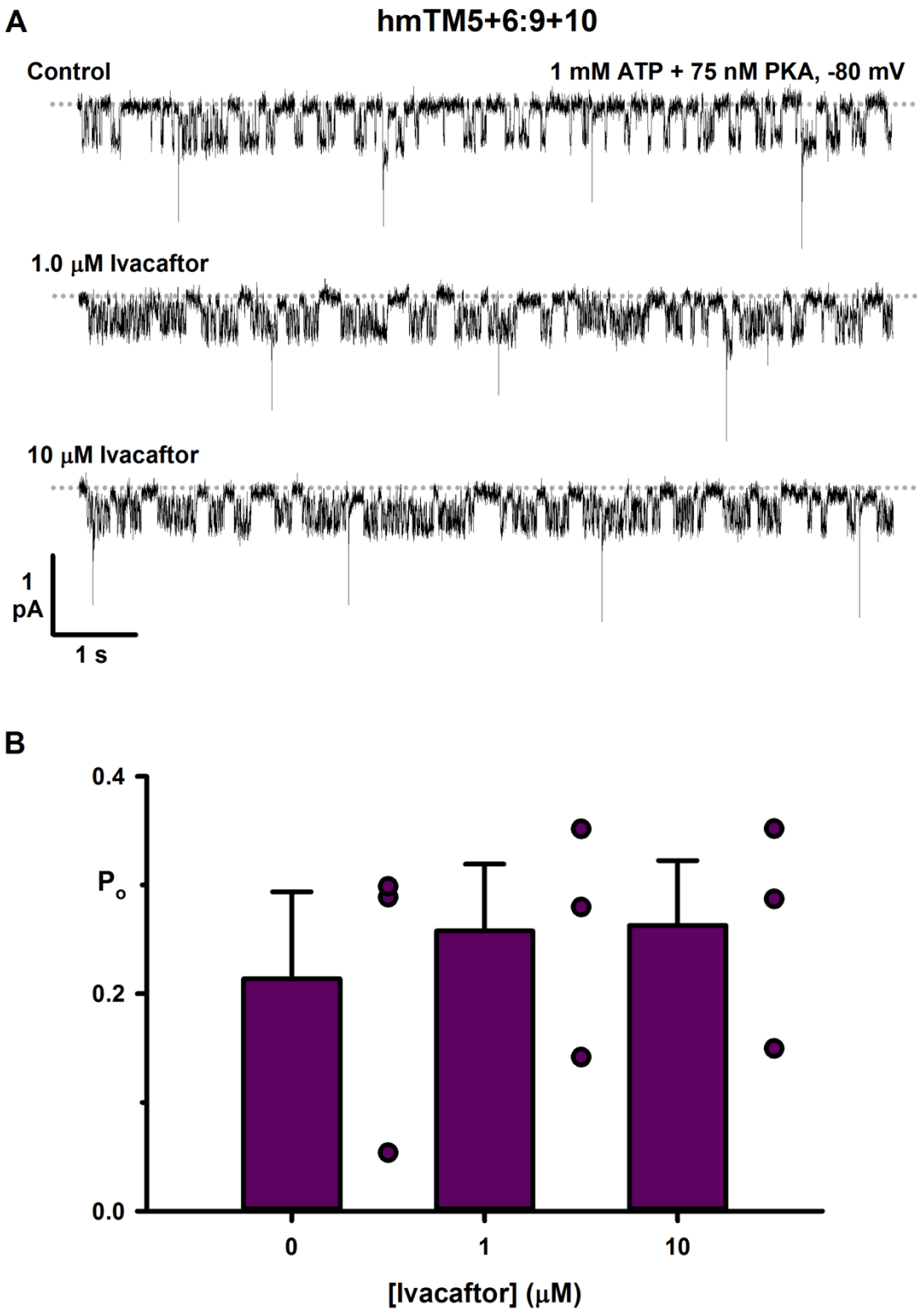

Figure 5.15: Effects of ivacaftor on the single-channel activity of the human-mouse TM5+6:9+10 chimeras. A Representative recordings from an excised inside-out membrane patch from a CHO cell show the response of hmTM5+6:9+10 to 1 μM and 10 μM ivacaftor. Other conditions as described for Figure 5.12A. **B** P_o for hmTM5+6:9+10 at 1 μM and 10 μM ivacaftor. Data are means ± SEM (n = 3, P > 0.05 vs control, one-way repeated measures ANOVA).

5.6 Determining regions of the CFTR protein involved in the mechanism of action of ivacaftor

5.6.1 Sequence alterations that affect the response of human CFTR to ivacaftor

Our results from both automated whole-cell patch-clamp and single-channel patch-clamp experiments suggest that replacement of the human CFTR sequences for TM5 and TM6 with the mouse equivalent produces a CFTR chimera that does not demonstrate potentiation by ivacaftor. We therefore generated a ClustalO sequence alignment of both human and mouse WT-CFTR sequences for this region to determine which amino acid residues had been altered in the generation of the hmTM5+6 chimera (Figure 5.16).

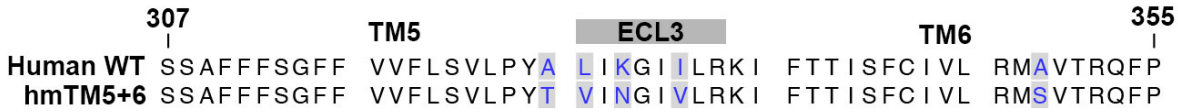

Figure 5.16: Sequence alignment of human WT CFTR and hmTM5+6 chimera between residues 307 and 355. Position of ECL3 is indicated by grey bar from residues 327-334. Residues that have been changed to the mouse equivalent in the hmTM5+6 chimera are highlighted in blue. Sequences aligned by ClustalO alignment using CLC Sequence Viewer v7.5.

As shown in Figure 5.16, in the generation of the hmTM5+6 chimera only five amino acid residues were altered, the changes from the human to the mouse sequences being A326T, L327V, K329N, I332V and A349S. Figure 5.17 shows the locations of these five residues in the high-resolution cryo-EM structure of human CFTR produced by Liu *et al.* (2017). L327V, K329N, I332V are located within ECL3 adjacent to the extracellular entry point to the channel pore, whilst A326T is at the apical end of TM5. A349S is located deeper within the CFTR channel pore on TM6 (Figure 5.17).

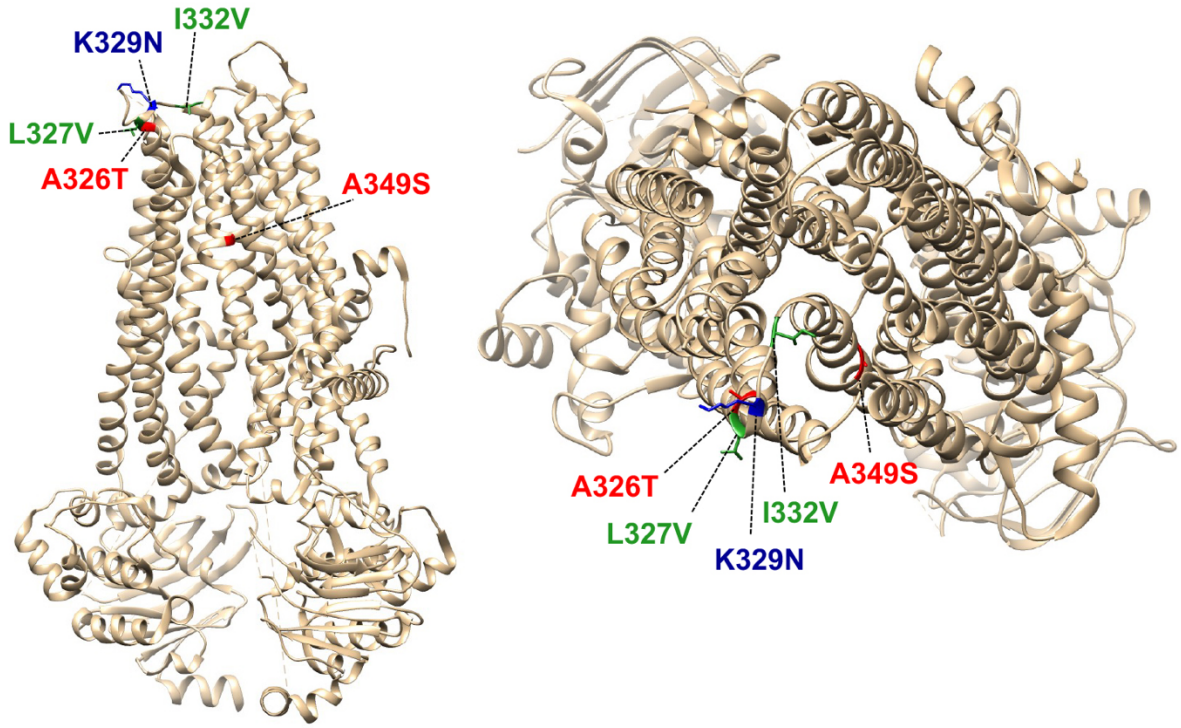

Figure 5.17: Identities and locations of human-mouse sequence alterations involved in determining the potentiation of CFTR by ivacaftor. Structure of human CFTR based upon cryo-EM data, PDB: 5UAK (Liu *et al.*, 2017). Structure on left of figure represents side view of the CFTR channel, structure on right represents view of the channel from the extracellular side. A326T, L327V, K329N, and I332V are located at the extracellular side of the CFTR channel, with L327V, K329N, and I332V located within ECL3 and A326T forming the extracellular end of TM5. A349S is located within the channel pore on TM6.

5.7 Discussion

5.7.1. Interpretation of the data collected from automated whole-cell patch-clamp studies of human-mouse CFTR chimeras

In Chapter 4, our data demonstrated that under the experimental conditions used for the study of human and mouse CFTR orthologues by single-channel patch-clamp recording, mouse WT-CFTR was not potentiated by ivacaftor. This observation provided the rationale for using human-mouse CFTR chimeras to investigate structural regions of the CFTR protein that may be involved in the mechanism of action of ivacaftor. Due to the large number of chimeras to be tested, their systematic study using the single-channel patch-clamp technique would have required a time-scale

beyond that which was possible in the scope of this project. Furthermore, the observations of Cui and co-authors that ivacaftor does potentiate mouse CFTR under certain experimental conditions highlighted the need to ensure that the observations made in Chapter 4 were not limited to the specific conditions under which these experiments had been carried out (Cui & McCarty, 2015; Cui *et al.*, 2016). We were therefore keen to test the response of both human and mouse WT-CFTR orthologues as well as human-mouse CFTR chimeras using the whole-cell patch-clamp technique, and to test these constructs at room temperature as well as at 37 °C.

By working with our industrial partner, the Novartis Institutes for Biomedical Research, we were able to design experiments utilising the QPatch HTX high-throughput automated patch-clamp platform in their laboratories based in Cambridge, Massachusetts, USA. Automated patch-clamp has recently been demonstrated to provide comparable results to manual whole-cell patch-clamp techniques, whilst producing a higher throughput for data collection (Billet *et al.*, 2017). However, previous studies utilising automated whole-cell patch-clamp for the study of CFTR have utilised stably transfected cells. Due to the limited time scale of the project, the development of stable cell lines for all of the CFTR chimeric constructs we aimed to test was not feasible. For this reason, we sought to develop an assay that utilised transiently transfected cells that could be cryopreserved, whilst maintaining a sufficiently high transfection efficiency for use on the QPatch system. Furthermore, due to the absence of fluorescent tagging on our CFTR chimeric constructs, the assay design would not be able to utilise cell sorting techniques such as fluorescence activated cell sorting (FACS) to sort transfected cells from non-transfected cells. We therefore had to develop a transfection protocol that would transfect cells with a sufficient level of transfection efficiency to enable cells to be screened using the QPatch HTX platform without prior sorting. The MaxCyte STX Scalable Transfection System for computer-controlled flow large volume electroporation is a novel transfection system that has been developed for large volume, high efficiency transfection of cells, including mammalian cell lines (Li *et al.*, 2009). We therefore adapted this technique for the transfection of CHO cells with our human-mouse CFTR chimeras.

As described in Chapter 2, we performed initial optimisation studies to test the optimal cDNA concentrations and incubation periods for our CFTR constructs and tested these using both the QPatch HTX system and the Nanion SyncroPatch 384PE automated patch-clamp platforms. The optimal transfection cDNA quantity and incubation period determined during optimisation was 300 $\mu g \cdot ml^{-1}$ and incubation for 72 hours, determined as a balance between transfection success rate, cell viability and magnitude of CFTR-mediated currents recorded. However, despite this optimisation stage, large variations were recorded in transfection success rate, stability of recordings and magnitude of the CFTR-mediated current for cells transfected with the same cDNA plasmid. Additionally, success rate varied considerably between different constructs tested. For this reason, the number of successful experiments completed for each construct was relatively low, despite multiple repeats of the experiment with cells (overall success rate around 25% of cells tested). A major limitation introduced into the analysis of these data was the subtraction of leak current, which was incorrectly calculated by subtracting the current recorded at -30 mV from the maximal outward current record at +80 mV for each sweep. As a result of this error, the values recorded for maximal outward current are likely to represent an overestimate of the actual outward current that was present. It is therefore possible that the magnitude of the effects observed for each CFTR construct were smaller than those reported. However, as this stage of the analysis was applied consistently for all recordings, trends in the data are unaffected. Nevertheless, it must be recognised that the levels of significance reported are based on overestimates in the magnitude of the outward currents. Despite these limitations however, the assay enabled the rapid testing of all 16 CFTR constructs for their response to 10 μM ivacaftor.

The bar chart shown in Figure 5.18 summarises the data for the response of human-mouse CFTR chimeras to 10 μM ivacaftor shown in Figures 5.3, 5.5, 5.7, 5.9 and 5.11. Our whole-cell data indicate that human WT-CFTR was potentiated by 10 μM ivacaftor in agreement with the data collected from single-channel recordings of the human WT-CFTR channel in Chapter 4. However, when testing mouse WT-CFTR using the automated whole-cell platform, ivacaftor at 10 μM resulted in an inhibition of the channel that was consistent over multiple repetitions of the experiment. Whilst our

single-channel data in Chapter 4 had suggested the possibility of a slight inhibitory effect of ivacaftor at higher concentrations in the case of some CFTR orthologues, inhibition on the scale observed using the QPatch assay was not observed at the single-channel level and had not been observed before for the mouse WT-CFTR channel. Furthermore, the pattern of activation of mouse WT-CFTR by FSK and subsequent inactivation by $CFTR_{inh}$-172 was different to that observed for other constructs as demonstrated by the representative trace shown in Figure 5.4. Overall FSK-induced current for mouse WT-CFTR was low in comparison to human WT-CFTR, at 15.9 ± 3.19 pA/pF (*n* = 11) compared to 37.7 ± 6.61 pA/pF (*n* = 13) for human WT-CFTR. This lower CFTR-mediated current would be expected from the reduced single-channel current and CFTR conductance recorded for mouse WT-CFTR in Chapter 4 using the single-channel patch-clamp technique. This difference may also result from variation in expression levels for human and mouse CFTR in CHO cells, as has been reported previously in other cell lines including NIH 3T3 (Ostedgaard *et al.*, 2007). In addition, it is not possible to rule out a reduced transfection efficiency for mouse WT-CFTR as a contributing factor to this observation. Furthermore, the rate of increase in outward current for mouse WT-CFTR in response to FSK appeared reduced in comparison to both human WT-CFTR and the other CFTR chimeric constructs tested (Figure 5.4). However, despite these differences, the experiments utilising mouse WT-CFTR did not demonstrate potentiation of mouse WT-CFTR in response to 10 μM ivacaftor although they showed an increase in current in response to FSK that was inhibited by $CFTR_{inh}$-172. These data, as with the data collected in Chapter 4, again appear to contradict previously published data suggesting potentiation of mouse WT-CFTR by ivacaftor (Cui & McCarty, 2015; Cui *et al.*, 2016), and indicate that at the whole-cell level, mouse CFTR-mediated Cl^- currents are not potentiated, and may indeed be inhibited by 10 μM ivacaftor.

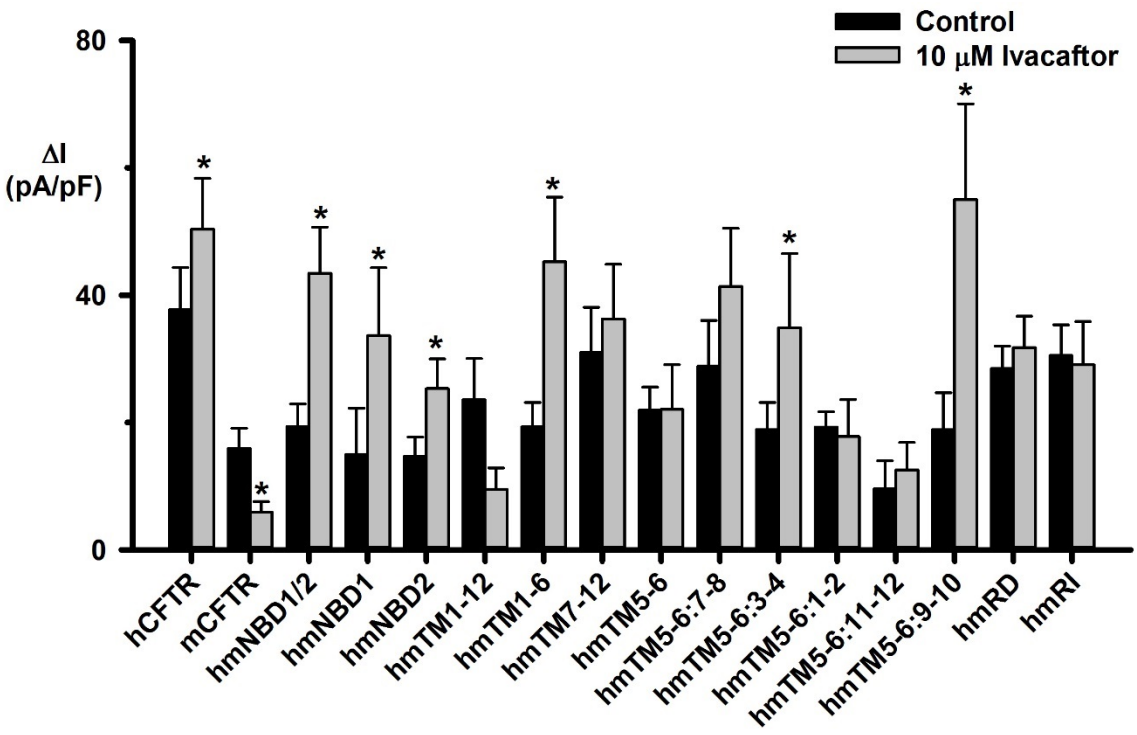

Figure 5.18: Effect of 10 μM ivacaftor on human-mouse CFTR chimeras following activation by FSK. Data collected by automated whole-cell patch-clamp of human-mouse CFTR chimeras at 80 mV. Data have been corrected for cell size. Error bars represent SEM (n = 4-14, * = P < 0.05 vs control for each construct, paired two-way Student's t-test).

After testing human and mouse WT-CFTR using automated whole-cell patch-clamp recordings, we next focussed on the ivacaftor response of the whole-domain NBD CFTR chimeras hmNBD1/2, hmNBD1 and hmNBD2, where one or both of the NBD sequences in human CFTR were exchanged for the corresponding sequences from mouse CFTR. As shown in Figure 5.18, all three of these NBD chimeras showed potentiation by ivacaftor. Given that human WT-CFTR is potentiated by ivacaftor whereas mouse WT-CFTR is not, these data suggest that the sequences responsible for the observed differences in the ivacaftor response between human and mouse CFTR are not located within the NBDs. One potential explanation for this is that the binding site, or binding sites for ivacaftor are not located within the NBDs and that alteration of the NBD structure of human CFTR therefore does not result in inhibition of the ivacaftor response in the case of these NBD chimeras. This observation supports data obtained using HDX, which suggests a possible binding site for ivacaftor located at residues within TMD2 where this domain is in close proximity to either NBD1 or NBD2 (Byrnes *et al.*, 2018). Cysteine cross-linking has identified eight interactions between residues F1074, L1065, T1064, G1069 and F1068 in ICL4 and W496, M498,

F508, V510 and K564 in NBD1, indicating that these residues lie within close proximity (He *et al.*, 2008; Serohijos *et al.*, 2008; Zhou *et al.*, 2010; Wang *et al.*, 2011a; Wang & Linsdell, 2012; Gao & Hwang, 2016; Zhang & Chen, 2016). Alteration of the NBD structure in this region could conceivably alter the interaction of the TMD2 residues with ivacaftor if such changes were sufficient to alter the TMD structure at these points. However, our data suggest that this is not likely. As shown in Figure 5.19, the residues that demonstrate cysteine cross-linking between ICL4 and NBD1 are conserved in both human and mouse CFTR.

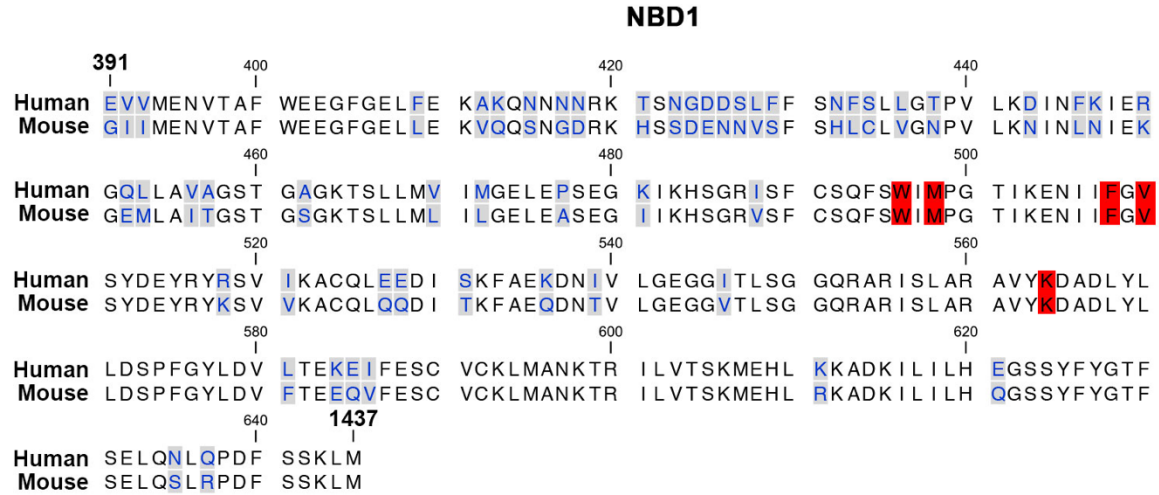

Figure 5.19: Sequence alignment for human and mouse NBD1. Residues identified as forming cross-links following mutation to cysteines are highlighted in red (He *et al.*, 2008; Serohijos *et al.*, 2008; Zhou *et al.*, 2010; Wang *et al.*, 2011a; Wang & Linsdell, 2012; Gao & Hwang, 2016; Zhang & Chen, 2016). Sequences aligned by ClustalO alignment using CLC Sequence Viewer v7.5.

Having established that exchanging the NBD sequences in human CFTR for mouse sequences does not prevent potentiation by ivacaftor, we next investigated the effect of exchanging the TMD sequences for mouse equivalents. As shown in Figure 5.18 and in Figures 5.6 and 5.7, exchanging both TMD1 and TMD2 in human CFTR for the mouse sequences resulted in a chimera (construct hmTM1-12) that demonstrated inhibition of whole-cell current in response to 10 μM ivacaftor, in common with mouse WT-CFTR. This observation provides strong support for the action of ivacaftor at the level of the TMDs rather than the NBDs and supports the data obtained by Byrnes *et al.* (2018) using HDX. The hmTM1-6 chimera however still demonstrated ivacaftor potentiation, whilst the hmTM7-12 chimera did not, with inhibition by ivacaftor not

being present for either of these constructs (Figure 5.18). These data appear to support a role of TMD2 in the mechanism of action of ivacaftor rather than TMD1. The data from Byrnes *et al.* (2018) suggested binding of ivacaftor at the TMD2 residues in close proximity to NBD1 and NBD2, with regions between residues 1055–1064 and 1070–1074 showing the greatest level of protection from HDX after addition of ivacaftor. However, as shown in Figure 5.20, alignment of the human and mouse sequences shows that these sequences are highly conserved between human and mouse orthologues, with only one sequence alteration, P1072T being located within this region. It is therefore possible that the hmTMD7-12 construct may not demonstrate functional differences resulting from ivacaftor binding at this site. Byrnes *et al.* (2018) also showed strong protection from HDX occurring at the N-terminal lasso motif in TMD1. For this reason, we hypothesised that ivacaftor may be acting either directly or through allosteric interactions via alternative regions within the TMDs that were not examined by the HDX experiments.

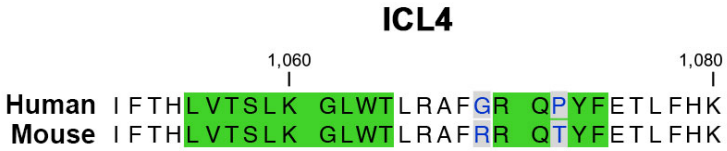

Figure 5.20: Human-Mouse sequence alignment of residues within ICL4 identified as a potential ivacaftor-binding site by HDX. Residues that have shown protection from HDX following addition of ivacaftor are highlighted in green. Sequences aligned by ClustalO alignment using CLC Sequence Viewer v7.5. HDX data are from Byrnes *et al.* (2018).

The next chimera tested was the hmTM5+6 construct in which the mouse sequences for TM5 and TM6 were expressed on the human CFTR background. This construct represented the chimera with the smallest number of sequence alterations that was tested, with just 5 amino acid residues changed from the human sequence (A326T, L327V, K329N, I332V and A349S, Figure 5.16). From the finding that the hmTM1-6 chimera demonstrated potentiation by ivacaftor, it would be expected that hmTM5+6 would also similarly show potentiation. However, no potentiation was observed for the hmTM5+6 construct, suggesting that the five sequence alterations A326T, L327V, K329N, I332V and A349S are sufficient to prevent the potentiation of human CFTR by 10 μM ivacaftor. Four of these residues, A326T, L327V, K329N and I332V are grouped

either in ECL3 or at the external end of TM5 near the extracellular entry point to the CFTR pore, whilst the fifth is buried deeper within the protein on TM6 and is likely to line the pore itself according to cryo-EM data (Liu *et al.*, 2017). Due to the lack of coverage by HDX at ECL3, it is possible that our data highlights a secondary binding site for ivacaftor at this region that would not have been detected by the techniques employed by Byrnes *et al.* (2018). However, we cannot rule out the possibility that the regions highlighted by our experiments may be required for ivacaftor potentiation via allosteric interactions following binding of ivacaftor at another location on the CFTR protein. The location of the channel gate in CFTR is thought to correspond to the narrow pore region adjacent to residues 338-341 in TM6 (Gao & Hwang, 2015). A349 is located close to this region within the intracellular vestibule of CFTR. Whilst it is therefore unlikely that A349 represents the location of a binding site for ivacaftor, it is possible that binding of ivacaftor at a different binding site (such as the location on ICL4 suggested by Byrnes *et al.* (2018)) results in a conformational change in CFTR along its longitudinal axis via the region of A349 that leads to favourable opening of the channel gate. It is therefore possible that the A349S sequence alteration disrupts this pathway of longitudinal movement and prevents the potentiation of CFTR by ivacaftor. Further experiments involving the sequence alterations A326T, L327V, K329N, I332V and A349S either individually or in combinations would be valuable in determining which of these changes are involved in inhibition of ivacaftor potentiation.

Our observations that the hmTM1-6 chimera showed potentiation by ivacaftor, whereas the hmTM5+6 chimera did not, suggest that allosteric interactions between TM5+6 and other transmembrane helices may facilitate ivacaftor potentiation. We therefore tested a range of human-mouse CFTR chimeras where additional mouse TM helices were introduced into the protein in addition to TM5 and TM6. As shown in Figure 5.18, constructs where mouse TM3+4 or TM9+10 were incorporated into the CFTR protein in conjunction with mouse TM5 and TM6 demonstrated ivacaftor potentiation. We therefore hypothesise that interactions exist between transmembrane helices 3, 4, 9 and 10 and TM5 and TM6 that may reverse the effects of the A326T, L327V, K329N, I332V and A349S human-mouse sequence alterations.

5.7.2. Interpretation of the data collected from single-channel patch-clamp studies of human-mouse CFTR chimeras

Although providing a useful technique for the rapid screening of multiple CFTR constructs for potentiation by ivacaftor, the variability inherent in the automated whole-cell patch-clamp data, potentially resulting from variance in transfection efficiency and cDNA expression, limits the interpretation of these data. We therefore aimed to test a smaller number of these human-mouse CFTR chimeras using the single-channel patch-clamp technique to provide greater insight into the effect of ivacaftor on these constructs. The first construct to be tested utilising this approach was the hmNBD1/2 chimera. The gating behaviour of this chimera was characterised by openings to the full open state with a P_o that was decreased compared to human WT-CFTR but higher than that of mouse WT-CFTR (Figure 5.12). The single-channel current observed for the hmNBD1/2 chimeras was midway between that of human and mouse WT-CFTR and the O_1 sub-conductance state observed for mouse WT-CFTR was not observed for hmNBD1/2. These data suggest that the unique gating behaviour of mouse WT-CFTR highlighted in Chapter 3 results primarily from the properties of the mouse TMD sequences. They also likely reflect the close sequence homology between human and mouse NBDs. As predicted from the whole-cell patch-clamp experiments, the hmNBD1/2 chimera was potentiated by 10 μM ivacaftor. However, although an increase was observed at 1 μM ivacaftor this increase was not found to be significant ($P < 0.05$, Figure 5.13). This contrasts considerably with the data collected using single-channel patch-clamp for human WT-CFTR, which demonstrated high levels of potentiation at ivacaftor concentrations as low as 0.01 μM (Chapter 4, Figure 4.1). These data therefore suggest a shift in the efficacy of ivacaftor for the hmNBD1/2 chimera when compared to human WT-CFTR. However, as ivacaftor was only tested at 1.0 and 10 μM in these experiments determination of the K_D of the compound for this construct requires additional experiments. As mentioned, the interface between ICL4 and NBD1 has been proposed as a binding site for ivacaftor (Byrnes *et al.*, 2018). Whilst our data obtained using the whole-cell patch-clamp technique appeared to rule out the possibility that exchange of the human NBD sequences for the corresponding mouse sequences affected this interface, a shift in the efficacy for ivacaftor resulting from these changes suggests that this interaction may have been altered in the case of the hmNBD1/2 construct.

The next chimera to be tested at the single-channel level was the hmTM1-6 construct. However, unfortunately insufficient data were collected to test the effect of ivacaftor on this construct. The limited data that were obtained demonstrated a gating behaviour that more closely resembled that of mouse rather than human WT-CFTR (Figure 5.12). Both the single-channel conductance and P_o of the hmTM1-6 chimera were comparable to mouse WT-CFTR (Figure 5.12) and examination of the single-channel trace shown in Figure 5.12 appears to demonstrate the presence of the O_1 sub-conductance state observed for mouse WT-CFTR. These data combined with those for the hmNBD1/2 chimera highlight the involvement of the TMDs rather than the NBDs in determining the unique gating behaviour of mouse WT-CFTR.

In agreement with the whole-cell patch-clamp data collected for the hmTM5+6 chimera, single-channel data for this construct did not show potentiation in response to either 1.0 or 10 μM ivacaftor (Figure 5.14). These data provide further support for the involvement of the five mouse sequence alterations in TM5 and TM6 in the mechanism of action of ivacaftor, although the number of successful experiments carried out using this chimera were small (1.0 μM ivacaftor, *n* = 3; 10 μM ivacftor, *n* = 2). The pattern of gating for this chimera showed similarities with that of mouse WT-CFTR, with a reduced P_o and single-channel current amplitude (Figure 5.12). However, this gating pattern appeared to show more defined open bursts than either mouse WT-CFTR or the hmTM1-6 chimera (Figure 5.12) with increased interburst channel closures. However, a lack of sufficient true single-channel recordings obtained with this construct prevented further analysis of the gating behaviour of the channel.

The whole-cell patch-clamp data had shown that inclusion of mouse sequences for TM9+10 in conjunction with TM5+6 in the hmTM5+6:9+10 chimera resulted in reversal of the effect of the mouse TM5+6 sequences on potentiation by ivacaftor. We were therefore keen to determine if this effect was also observed at the single-channel level. As shown in Figure 5.15, no significant increase in activity was observed for this chimera on addition of either 1.0 or 10 μM ivacaftor. However only limited single

channel data were collected for this construct, with a pattern of increasing P_o with increasing concentrations of ivacaftor observed in two out of the three experiments completed (Figure 5.15B). Whilst these data do not support potentiation by ivacaftor, it is possible that an effect might be observed if sufficient data were collected. From our data we therefore conclude that at the single-channel level, inclusion of mouse sequences for TM9 and TM10 in conjunction with TM5 and TM6 does not result in significant ivacaftor potentiation. However, at the whole-cell level, the expression of multiple channels may explain the potentiation observed for the hmTM5+6:9+10 chimera.

In conclusion, our data have demonstrated the involvement of all or some of the five amino acid residues A326, L327, K329, I332 and A349 in determining the response of human CFTR to the potentiator ivacaftor. Exchange of all five of these residues for their mouse CFTR equivalents is sufficient to prevent potentiation by ivacaftor. Whilst it is not possible to determine from these data whether the locations of these five residues contribute to a binding site of the ivacaftor molecule, future experiments where these residues are exchanged from their human to their mouse equivalents individually or sequentially may provide greater insight into the mechanism of action of ivacaftor.

6. General discussion

6.1 Species differences in CFTR structure and function

6.1.1 Variations in the structure and gating behaviour of CFTR orthologues from diverse species

As demonstrated by the cladogram shown in Figure 1.7 of Chapter 1, CFTR orthologues have evolved across a broad spectrum of species including all species within the Gnathostomata superclass (jawed vertebrates) with an additional orthologue that lacks the RD reported in lampreys (Bose *et al.*, 2015; Cui *et al.*, 2017). Homologies between sequenced CFTR orthologues within the Gnathostomata range from 53.9% (zebrafish) to 99.7% (chimpanzee) (Zerbino *et al.*, 2018), yet despite the low homology of the zebrafish CFTR compared human CFTR, comparison of the human and zebrafish structures obtained by cryo-EM demonstrates a high level of structural conservation (Zhang & Chen, 2016; Liu *et al.*, 2017). Conservation of residues across species includes several functionally important residues such as the R347/D924 salt bridge between TM6 and TM8, TM6 gating residues such as F337 and T338 as well as many proposed pore-lining residues (Liu *et al.*, 2017). The RD shows the lowest level of homology of all of the domains of CFTR (Figure 1.8 and Appendix 1), although phosphorylation sites within the RD are more highly conserved. This variation is likely to reflect a lower selection pressure on the evolution of this domain. However, despite the high levels of homology for functional residues within CFTR, many residues differ between CFTR orthologues and may contribute to observed differences in function and pharmacology for these orthologues. The varied function of CFTR orthologues from diverse species is likely to reflect optimisation of the channel according to its specific role in different species. For the purpose of CF research however, this library of diverse CFTR orthologues may serve as a useful tool for understanding structure-function relationships and investigating the action of small molecule modulators of channel function.

In Chapter 3, the single-channel behaviour of human, pig, sheep, ferret, mouse and zebrafish CFTR orthologues was characterised. Differences observed in the single-channel current amplitude and P_o for human, sheep and pig WT-CFTR provide a

demonstration of how the gating behaviour and single-channel properties of CFTR orthologues may differ despite high levels of sequence homology. Sheep WT-CFTR for example shares 91% amino acid identity with human WT-CFTR, yet despite this high level of homology, sheep WT-CFTR demonstrated a 7% increase in P_o and a 35% increase in single-channel current amplitude compared to human CFTR. By contrast however, the more divergent orthologues tested, mouse and zebrafish WT-CFTR, demonstrated a reduced single-channel current amplitude and lower P_o, characterised by brief short-lived channel openings and a highly active sub-conductance state in the case of mouse CFTR. Data from Chapter 5 obtained from human-mouse CFTR chimeras demonstrated that in the case of mouse CFTR, this reduction in P_o of the full open state most likely results from sequence differences in the TMDs rather than in the NBDs of the mouse CFTR protein.

As shown in Figure 5.12, the unique gating behaviour of mouse WT-CFTR appears to be reproduced by both the hmTM1-6 and the hmTM5+6 CFTR chimeras. These data suggest that sequence changes in TMD1, and specifically the five sequence alterations A326T, L327V, K329N, I332V and A349S from human to mouse sequences may be involved in determining the presence of these brief channel openings and the reduced single-channel current amplitude demonstrated by divergent CFTR orthologues. One possible hypothesis for this observation is that the sequence alterations A326T, L327V, K329N, I332V (Figure 5.17), may alter the properties of ECL3 in such a way as to result in interference with the Cl^- conduction pathway at the extracellular entrance of the CFTR pore, or alter the Cl^- sensitivity of the CFTR channel. Broadbent *et al*. (2015) for example have shown that the positively charged arginine residue at position 899 in ECL4 is involved in determining sensitivity of the CFTR channel to extracellular Cl^-. In this same study, exchange of K329 for an alanine residue also resulted in a small decrease in the percentage stimulation of CFTR by extracellular Cl^-, albeit not at statistically significant levels (Broadbent *et al.*, 2015). However, it is possible that positively charged residues located near the extracellular entrance of the CFTR pore play a role in attracting Cl^- ions into the extracellular CFTR vestibule and may affect conductance. Comparison of the ECL3 sequences of mouse and zebrafish demonstrate that the zebrafish orthologue does not contain the same sequence alterations in this region as mouse. However, other sequence alterations are present, including I332N, raising the possibility that

expression of polar residues such as asparagine may alter the structural interaction of this extracellular region with other regions adjacent to the CFTR pore entrance. Further study of the effect of changing individual residues highlighted in our study, including K329N may help to determine the role that these residues play in the single-channel properties of divergent CFTR orthologues such as mouse CFTR and could provide insight into the role of such residues in the gating and conductance characteristics of CFTR.

As discussed in Chapter 3, our data appears to demonstrate a functional divergence in CFTR gating behaviour that is related to evolutionary divergence. The cladogram shown in Figure 3.1 demonstrates that human, sheep, pig and ferret CFTR represent a divergent evolutionary clade from mouse and zebrafish based on sequence similarity. This division appears to correlate with observed divergence in the gating properties of these orthologues. Furthermore, ferret CFTR, which represents further evolutionary divergence from human, pig and sheep CFTR demonstrates a reduced single-channel conductance whilst maintaining a similar P_o to human, pig and sheep CFTR orthologues. These data therefore appear to support a correlation of CFTR function with evolutionary divergence. We have previously suggested that there may be a link between CFTR activity and metabolic rate in endothermic species, as highlighted by a potential correlation between CFTR conductance and body temperature (Bose *et al.*, 2015a). Although differences in the experimental conditions must be accounted for, previously published data suggests that the activity conductance values for CFTR orthologues can be ranked in the order chicken > sheep > rabbit > *Xenopus* > human > possum > pig > mouse (Hanrahan *et al.*, 1993; Lansdell *et al.*, 1998a; Al-Nakkash & Reinach, 2001; Ostedgaard *et al.*, 2007; Demmers *et al.*, 2010; Aleksandrov *et al.*, 2012; Cai *et al.*, 2015). When the published values for conductance of these orthologues is plotted against mean body temperature, the resulting scatter plot can be fitted by linear regression with $r^2 = 0.51$ (Figure 6.1). Further study with a greater selection of evolutionarily intermediate CFTR orthologues however would be required to further determine the nature of this potential correlation.

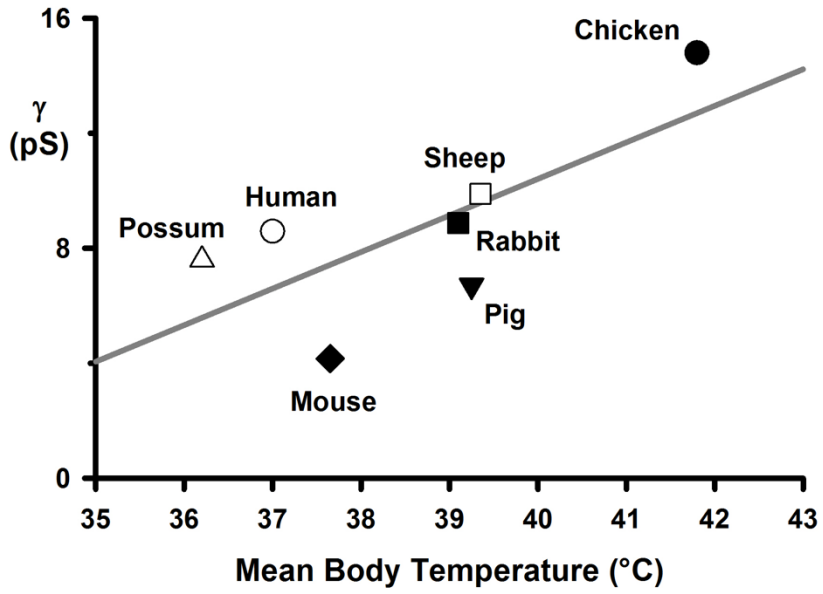

Figure 6.1: Relationship between CFTR single-channel conductance (γ) and mean body temperature in endothermic vertebrates. Linear regression (grey line) indicates possibility of a positive correlation with an r^2 value of 0.51. Figures for mean body temperature sourced from Hanrahan *et al.* (1993), Lansdell *et al.* (1998a), Al-Nakkash & Reinach (2001), Ostedgaard *et al.* (2007), Demmers *et al.* (2010), Aleksandrov *et al.* (2012), and Cai *et al.* (2015).

6.1.2 Differences in the effect of CF-causing mutations on diverse species orthologues of CFTR

A number of studies have previously highlighted differences in the susceptibility of diverse species orthologues of CFTR to CF-causing mutations, with variations reported in the impact on gating behaviour, channel processing, maturation and thermal stability (Ostedgaard *et al.*, 2007; Fisher *et al.*, 2011; Aleksandrov *et al.*, 2012; Cai *et al.*, 2015). Whilst previous studies have demonstrated that mouse F508del-CFTR does not demonstrate the same level of processing defect as observed for human F508del-CFTR, our data demonstrate that both mouse and sheep F508del-CFTR orthologues demonstrate a reduced susceptibility to the gating defect of the F508del mutation. In the case of mouse CFTR, no difference was observed in the gating behaviour of mouse F508del-CFTR when compared to WT-CFTR (Figure 3.7). Interestingly, this observation contrasts with other studies of the mouse F508del-CFTR channel using excised membrane patches, which have shown a reduced activity compared to mouse WT-CFTR, resulting from an increase in the interburst interval (Ostedgaard *et al.*, 2007; Dong *et al.*, 2012). However in these studies, the

reduction in P_o observed for mouse F508del-CFTR compared to WT-CFTR was much smaller than that observed for human F508del-CFTR compared to human WT-CFTR (Ostedgaard *et al.*, 2007; Dong *et al.*, 2012). Furthermore, our data demonstrated that the mouse F508del-CFTR orthologue unlike human F508del-CFTR shows thermal stability at 37 °C (Figure 3.9). Although it was not possible in the current study to identify the structural differences between human and mouse CFTR orthologues that result in these differences in the F508del phenotype, these observations raise the possibility that future studies, potentially utilising human-mouse chimeras that include the F508del mutation may highlight regions of the CFTR protein, which may be targeted to stabilise the F508del-CFTR protein.

One possible site is the isoleucine residue at position 539, which is altered to a threonine residue in the mouse CFTR orthologue. I539T has been shown to act as a revertant mutant when expressed in conjunction with the F508del mutation in human CFTR (deCarvalho *et al.*, 2002; Aleksandrov *et al.*, 2012) and its presence in the mouse sequence may help to explain the differences observed between human and mouse F508del-CFTR. However, Dong *et al.* (2012) have shown previously that whilst I539T improves F508del-CFTR processing, it has a negative impact on F508del-gating. In this same study, Dong *et al.* (2012) also demonstrated using human-mouse CFTR chimeras that inclusion of mouse sequences for ICL3 and ICL4 on a human F508del-CFTR background prevents the gating defect of the F508del mutation. This protective effect was linked to the human-mouse sequence change P1072T (Dong *et al.*, 2012).

6.2 Relevance and implications of species differences in function and pharmacology of CFTR orthologues for the use of CF animal models

The differences in phenotype between mouse models of CF and human patients, discussed in Chapter 1.7.2, combined with the observed differences between human and mouse CFTR pharmacology demonstrated in this study highlights the requirement for the development of alternative animal models for CF that more accurately replicate the human disease (McCarron *et al.*, 2018). In addition to the development of gut-corrected and humanised mouse CF models (Zhou *et al.*, 1994; Hodges *et al.*, 2016),

alternative animal models, including rat (Tuggle *et al.*, 2014), rabbit (Xu *et al.*, 2016), ferret (Sun *et al.*, 2010), pig (Rogers *et al.*, 2008a) and very recently sheep (Fan *et al.* 2018). Our data demonstrate that the function and pharmacology of CFTR orthologues may differ, despite high levels of sequence homology. This observation therefore highlights the importance of characterising functional and pharmacological differences between species orthologues prior to the development of animal models in order to determine any likely differences in phenotype *in-vivo.* The ferret model of CF provides a good example of the relevance of this research. Ferrets share similarities in lung physiology with humans, possessing goblet cells and demonstrating a high expression of CFTR in trachea and primary bronchi (Engelhardt *et al.*, 1992; Fisher *et al.*, 2012; Keiser *et al.*, 2013; McCarron *et al.*, 2018). In addition, the ferret CFTR orthologue shares 92% amino acid identity with the human CFTR orthologue. Combined with the economic benefits of ferrets when compared to larger species with a slower growth and reproductive rate such as pigs, sheep or primates, these factors make ferrets an attractive species for use as CF models. However, our data have demonstrated some key differences in the electrophysiological properties of ferret CFTR despite the high levels of sequence homology compared to human CFTR. For example, whilst ferret CFTR shares similar activity with human CFTR, this orthologue has a lower single-channel current amplitude and the possibility of current rectification at negative holding potentials when studied in the presence of an asymmetrical Cl^- gradient (Figure 3.3). Whilst ferret CFTR did demonstrate potentiation in response to ivacaftor (Figure 4.5), these electrophysiological differences should be considered when using ferret CF models for bioelectrical studies.

6.3 Differences in pharmacology between CFTR orthologues

Our data have demonstrated that mouse CFTR (and potentially zebrafish CFTR), are not potentiated by ivacaftor (Figure 4.11). Furthermore, we have shown that different species orthologues, including sheep and pig CFTR, may demonstrate a reduced efficacy for ivacaftor despite sharing high levels of sequence homology with human CFTR (Figures 4.3 and 4.4). The observation that non-human species may not replicate the human response to certain small molecule modulators is an important consideration when using animal models for any disease in the pre-clinical screening

for novel pharmaceuticals. In addition, however, our study has demonstrated how such differences may provide the basis for studies of structure-function relationships and investigations into the mechanism of action of such compounds through the use of chimeric proteins.

6.4 Identification of residues involved in the mechanism of action of ivacaftor

Our data have highlighted five sequence alterations in the hmTM5+6 chimera, A326, L327, K329, I332 and A349, that result in impaired CFTR function compared to human WT-CFTR as demonstrated by a reduction in P_o and single-channel current amplitude compared to human WT-CFTR. Furthermore, we have shown that the resulting CFTR channel cannot be potentiated by ivacaftor. As shown in Figure 5.17, four of these residues, A326, L327, K329 and I332 are located at the extracellular side of the CFTR protein, within ECL3 and the outer part of TM5 adjacent to the extracellular entrance to the CFTR pore (Liu *et al.*, 2017). The fifth residue A349 is located within the CFTR pore itself, sitting at the intracellular side of the proposed CFTR gate located in the region of residues 338 and 341 in TM6 (Gao & Hwang, 2015; Liu *et al.*, 2017). There are multiple potential explanations for the effect of changing these residues. Firstly, it is possible that these residues correspond to a potential binding site of ivacaftor. In their study of the binding sites of ivacaftor using HDX, Byrnes *et al*. (2018) identified regions of the CFTR protein where HDX was protected following addition of ivacaftor, therefore demonstrating potential binding sites for the drug (Figure 1.12). The region that underwent the greatest degree of protection was located at the intracellular apex of ICL4 in TMD2 where this region has been proposed to form a so-called ‘ball and socket’ joint with adjacent residues on NBD1, including F508 (Oldham *et al.*, 2008; Zhang & Chen, 2016; Byrnes *et al.*, 2018).

In our experiments where the entire human sequence for TMD2, including ICL4, was exchanged for the mouse sequence, potentiation by ivacaftor was not observed. However, our data unfortunately do not include CFTR constructs where ICL4 residues were exchanged in isolation. Furthermore, the proposed binding region within ICL4 that was proposed by Byrnes *et al.* (2018) is highly conserved between human and

mouse and so the use of a human-mouse chimera for this region may not demonstrate differences in function and pharmacology. However, our data do not rule out the possibility that ivacaftor does bind at the ICL4/NBD1 interface and may therefore be complementary to the data obtained by Byrnes *et al.* (2018). Interestingly, as mentioned in Section 6.1.2, Dong *et al.* (2012) used human-mouse CFTR chimeras to identify the P1072T human to mouse sequence alteration as preventing the gating defect of F508del. This residue is located in the proposed ICL4 binding site for ivacaftor (Byrnes *et al.*, 2018) (Figure 5.20). The P1072T sequence alteration was present in both the hmTM1-12 and hmTM7-12 chimeras, and neither of these chimeras demonstrated potentiation in response to ivacaftor when studied using the automated whole-cell patch-clamp technique (Figures 5.7 and 5.18). These data combined with the studies by Dong *et al.* (2012) and Byrnes *et al.* (2018) highlight the importance of this region in both the gating of CFTR and the mechanism of action of ivacaftor.

In addition to the ICL4 binding site, Byrnes *et al.* (2018) also identified regions corresponding to residues within the lasso motif, ICL1 and ICL3 that showed protection to HDX following addition of ivacaftor. These data suggest the possibility that ivacaftor may bind to CFTR at multiple locations. Although the five residues that were highlighted by our data did not demonstrate protection from HDX, these regions did not demonstrate deuterium uptake and so HDX experiments do not rule out the possibility of an additional ivacaftor binding site located at the residues identified in our study (Byrnes *et al.*, 2018).

Whilst it is possible that the A326, L327, K329, I332 and A349 residues may represent an additional binding-site for ivacaftor besides the ICL4/NBD1 region, another possibility is that these residues represent structural regions of the protein that are involved in the mechanism of action of ivacaftor through allosteric interactions. In Chapter 1.8, four potential modes of action for CFTR potentiators were discussed, these being enhancement of RD phosphorylation, enhanced ATP-binding at the NBDs, promotion of NBD dimerization or facilitation of movement along the longitudinal axis of CFTR from the NBDs to the TMDs. Ivacaftor has been shown previously to operate independently of ATP (Eckford *et al.*, 2012; Jih & Hwang, 2013) and to potentiate CFTR channels that lack either the RD or NBD2 (Bompadre *et al.*,

2005; Jih & Hwang, 2013; Yeh *et al.*, 2015). It is therefore likely that the mechanism by which ivacaftor potentiates CFTR involves facilitation of the movement of the transmembrane helices. Further experiments would be required to determine which of the A326, L327, K329, I332 and A349 residues are involved in the action of ivacaftor, however from the data collected two hypotheses may be generated. The first is that binding of ivacaftor to CFTR facilitates allosteric movement of the residues in ECL3, which in turn may facilitate channel gating or entry of Cl^- at the extracellular side of the CFTR conduction pathway. Alternatively, altering the alanine residue at position 349 to a serine residue may inhibit the facilitation of transmembrane domain movement by ivacaftor. Further experiments would be required to determine the residue or residues that are responsible for the differences in pharmacology that have been observed here between human and mouse CFTR.

6.5 Implications for future research and development of CF therapies

By identifying regions of the CFTR protein that are involved in the mechanism of action of ivacaftor, we have identified potential sites within the CFTR protein that may form targets for the development of novel potentiators for the treatment of CF. Ivacaftor itself was first characterised in 2009 and approved for patient use by the FDA in 2012 (Van Goor *et al.*, 2009; Ramsey *et al.*, 2011). At the time of writing, ivacaftor has therefore been available to patients for six years, and has proved highly efficacious for the treatment of patients carrying class III mutations, providing a proof of concept for the treatment of CF using small molecules (Moss *et al.*, 2015). However, for the treatment of patients homozygous for mutations that also affect channel processing, such as F508del, potentiators like ivacaftor must be used in combination with CFTR correctors. Orkambi, which was the first such combination therapy to be licensed, showed some benefit to patients carrying the F508del mutation, but the size of this benefit was relatively small in most patients compared to the effects observed for ivacaftor in patients with class III mutations (4.3 - 6.7% increase in FEV_1 compared to 10.6% observed in G551D patients treated with ivacaftor) (Ramsey *et al.*, 2011; Wainwright *et al.*, 2015). Symdeko, which represents the next generation of combination therapy, combining ivacaftor with tezacaftor, has demonstrated an improved level of tolerance compared to Orkambi (Taylor-Cousar *et al.*, 2017). In

addition, results from recent trials for triple combination therapy including the Vertex compounds VX-659 and VX-445 have also shown positive effects with improvements in FEV_1 of 13.3% and 13.8%, respectively (Davies *et al.*, 2018; Keating *et al.,* 2018). However, the ongoing development of CFTR potentiators such as QBW251 (Novartis), CTP-656 (Concert Pharmaceuticals/Vertex) and GLPG1837 (AbbVie/Galapagos), demonstrates the requirement for compounds that show increased efficacy compared to ivacaftor. Understanding the mechanism of action of ivacaftor, principally the regions of the CFTR protein with which the compound is likely to interact, and regions that are involved in the mechanism of action of the drug, therefore helps to provide information about potential targets for the development of novel CFTR potentiators. The results of this study have highlighted such regions of the CFTR protein that have not been identified by previous studies. It is hoped that further experiments focussing on the five residues, A326, L327, K329, I332 and A349, may determine the precise region of the CFTR protein that is involved in CFTR potentiation by ivacaftor. In turn, this information may be used to aid the design and development of new CFTR correctors.

7. Conclusion

Since the identification of the gene encoding CFTR (Riordan *et al.*, 1989), significant advances have been made in our knowledge of CF and the development of treatments for this disease. One of the major success stories over the past three decades of CF research has been the rise in life expectancy for patients with CF. Whereas CF was once considered to be a primarily pediatric disease, we have now passed the point where the number of adults with CF outnumber the number children, and patients with CF can now be expected to reach middle age, have careers, and raise families (Burgel *et al.*, 2015). We now have a greater understanding of the role of this protein in regulating transepithelial fluid and electrolyte flux, and how impairment of this function affects patients with CF. We have a better understanding of the structure of CFTR, and recent advances such as the use of cryo-electron microscopy have facilitated the determination of the CFTR protein structure at a far higher resolution than was previously possible (Liu *et al.*, 2017). Drugs are now available that treat the root cause of the disease, targeting mutation-specific defects in CFTR function and offering precision medicine to patients with the disease (Fajac & De Boeck, 2017). The continued development of combination therapies such as Orkambi and Symdeko, is broadening the use of these compounds for a wider range of patients, including patients carrying the most common F508del mutation (Fajac & De Boeck, 2017). Advances in translational research techniques such as the use of organoids developed from patient stem cells, are aiding the prediction of efficacy for the use of existing drugs in patients with rare mutations (Cholon & Gentzsch, 2018). New techniques in gene therapy are in development, and it is hoped that these therapies may hold the key to the eventual cure for this disease (Alton *et al.*, 2016). Yet there is still some way to go in the development of a cure for CF and gaining a greater understanding of structure-function relationships of CFTR, and how existing drugs interact with the CFTR protein, is key to the development of the next generation of CF therapeutics.

In this study, we have identified that the mechanism of action of ivacaftor, the first drug licensed to treat an underlying defect in the CFTR channel resulting from mutations,

involves interactions with the transmembrane helices of CFTR. We have also identified key residues within the TMDs of CFTR that are involved in facilitating the potentiation of CFTR by ivacaftor. Whilst further research is required to determine the exact role that these residues play in the potentiation of CFTR by ivacaftor, it is hoped that gaining a better understanding of how this drug interacts with CFTR may aid the development of future drugs that demonstrate improved efficacy and tolerance over existing compounds.

References

Sophion QPatch HTX Screening Station handbook, © 2004-2012, GUIDE20179-3, Sophion Bioscience A/S, Ballerup, Denmark.

Cystic Fibrosis Mutation database, http://www.genet.sickkids.on.ca/app (Accessed June 2018)

Aiello SE & Moses MA, ed. (2010). *The Merck Veterinary Manual*. Merck & Co., Inc., Whitehouse Station, NJ, USA.

Al-Nakkash L & Reinach PS. (2001). Activation of a CFTR-mediated chloride current in a rabbit corneal epithelial cell line. *Investigative Ophthalmology & Visual Science* **42,** 2364-2370.

Aleksandrov AA, Aleksandrov L & R. Riordan J. (2002). Nucleoside triphosphate pentose ring impact on CFTR gating and hydrolysis. *FEBS Letters* **518,** 183-188.

Aleksandrov AA, Kota P, Cui L, Jensen T, Alekseev AE, Reyes S, He L, Gentzsch M, Aleksandrov LA, Dokholyan NV & Riordan JR. (2012). Allosteric Modulation Balances Thermodynamic Stability and Restores Function of ΔF508 CFTR. *Journal of Molecular Biology* **419,** 41-60.

Aller SG, Yu J, Ward A, Weng Y, Chittaboina S, Zhuo R, Harrell PM, Trinh YT, Zhang Q, Urbatsch IL & Chang G. (2009). Structure of P-Glycoprotein Reveals a Molecular Basis for Poly-Specific Drug Binding. *Science* **323,** 1718-1722.

Alton EWFW, Armstrong DK, Ashby D, Bayfield KJ, Bilton D, Bloomfield EV, Boyd AC, Brand J, Buchan R, Calcedo R, Carvelli P, Chan M, Cheng SH, Collie DDS,

Cunningham S, Davidson HE, Davies G, Davies JC, Davies LA, Dewar MH, Doherty A, Donovan J, Dwyer NS, Elgmati HI, Featherstone RF, Gavino J, Gea-Sorli S, Geddes DM, Gibson JSR, Gill DR, Greening AP, Griesenbach U, Hansell DM, Harman K, Higgins TE, Hodges SL, Hyde SC, Hyndman L, Innes JA, Jacob J, Jones N, Keogh BF, Limberis MP, Lloyd-Evans P, Maclean AW, Manvell MC, McCormick D, McGovern M, McLachlan G, Meng C, Montero MA, Milligan H, Moyce LJ, Murray GD, Nicholson AG, Osadolor T, Parra-Leiton J, Porteous DJ, Pringle IA, Punch EK, Pytel KM, Quittner AL, Rivellini G, Saunders CJ, Scheule RK, Sheard S, Simmonds NJ, Smith K, Smith SN, Soussi N, Soussi S, Spearing EJ, Stevenson BJ, Sumner-Jones SG, Turkkila M, Ureta RP, Waller MD, Wasowicz MY, Wilson JM & Wolstenholme-Hogg P. (2015). Repeated nebulisation of non-viral CFTR gene therapy in patients with cystic fibrosis: a randomised, double-blind, placebo-controlled, phase 2b trial. *The Lancet Respiratory Medicine* **3,** 684-691.

Alton EWFW, Boyd AC, Davies JC, Gill DR, Griesenbach U, Harrison PT, Henig N, Higgins T, Hyde SC, Innes JA & Korman MSD. (2016). Genetic medicines for CF: Hype versus reality, *Pediatric Pulmonology* **51,** (S44): S5-S17.

Amaral MD. (2015). Novel personalized therapies for cystic fibrosis: treating the basic defect in all patients. *Journal of Internal Medicine* **277,** 155-166.

Anderson MP, Berger HA, Rich DP, Gregory RJ, Smith AE & Welsh MJ. (1991). Nucleoside triphosphates are required to open the CFTR chloride channel. *Cell* **67,** 775-784.

Artigas P, Al'aref SJ, Hobart EA, Díaz LF, Sakaguchi M, Straw S, Andersen OS. (2006). 2,3-butanedione monoxime affects cystic fibrosis transmembrane conductance regulator function through phosphorylation-dependent and phosphorylation-independent mechanisms: the role of bilayer material properties. *Molecular Pharmacology* **70,** 2015-26

Atwell S, Brouillette CG, Conners K, Emtage S, Gheyi T, Guggino WB, Hendle J, Hunt JF, Lewis HA, Lu F, Protasevich II, Rodgers LA, Romero R, Wasserman SR, Weber PC, Wetmore D, Zhang FF & Zhao X. (2010). Structures of a minimal human CFTR first nucleotide-binding domain as a monomer, head-to-tail homodimer, and pathogenic mutant. *Protein Engineering Design & Selection* **23,** 375-384.

Baker JMR, Hudson RP, Kanelis V, Choy W-Y, Thibodeau PH, Thomas PJ & Forman-Kay JD. (2007). CFTR regulatory region interacts with NBD1 predominantly via multiple transient helices. *Nature Structural & Molecular Biology* **14,** 738-745.

Balch W, Morimoto R, Dillin A & Kelly JW. (2008). Adapting proteostasis for disease intervention. *Science*, **319**, 916-919.

Balch WE, Roth DM & Hutt DM. (2011). Emergent properties of proteostasis in managing cystic fibrosis. *Cold Spring Harbor Perspectives in Biology* **3,** a004499.

Baroni D, Zegarra-Moran O, Svensson A & Moran O. (2014). Direct interaction of a CFTR potentiator and a CFTR corrector with phospholipid bilayers. *European Biophysics Journal with Biophysics Letters* **43,** 341-346.

Becq F, Mall MA, Sheppard DN, Conese M & Zegarra-Moran O. (2011). Pharmacological therapy for cystic fibrosis: From bench to bedside. *Journal of Cystic Fibrosis* **10,** S129-S145.

Bell SC, De Boeck K & Amaral MD. (2015). New pharmacological approaches for cystic fibrosis: Promises, progress, pitfalls. *Pharmacology & Therapeutics* **145,** 19-34.

Berdiev BK, Qadri YJ & Benos DJ. (2009). Assessment of the CFTR and ENaC association. *Molecular Biosystems* **5,** 123-127.

Beumer W, Swildens J, Henig N, Anthonijsz H, Biasutto P, Leal T & Ritsema T. (2015). QR-010, an RNA therapy, restores CFTR function using in vitro and in vivo models of ΔF508 CFTR. *Pediatric Pulmonology Supplement* **14,** S1-S1.

Billet A, Froux L, Hanrahan JW & Becq F. (2017). Development of automated patch clamp technique to investigate CFTR chloride channel function. *Frontiers in Pharmacology* **8,** 195, 1-10.

Bilton D, Bellon G, Charlton B, Cooper P, De Boeck K, Flume PA, Fox HG, Gallagher CG, Geller DE, Haarman EG, Hebestreit HU, Kolbe J, Lapey A, Robinson P, Wu J, Zuckerman JB & Aitken ML. (2013). Pooled analysis of two large randomised phase III inhaled mannitol studies in cystic fibrosis. *Journal of Cystic Fibrosis* **12,** 367-376.

Blair JE & Hedges SB. (2005). Molecular Phylogeny and Divergence Times of Deuterostome Animals. *Molecular Biology and Evolution* **22,** 2275-2284.

Bobadilla JL, Macek M, Fine JP & Farrell PM. (2002). Cystic fibrosis: A worldwide analysis of CFTR mutations - Correlation with incidence data and application to screening. *Human Mutation* **19,** 575-606.

Bompadre SG, Ai T, Cho JH, Wang X, Sohma Y, Li M & Hwang T-C. (2005). CFTR gating I: Characterization of the ATP-dependent gating of a phosphorylation-independent CFTR channel (ΔR-CFTR). *Journal of General Physiology* **125,** 361-375.

Bompadre SG, Sohma Y, Li M & Hwang T-C. (2007). G551D and G1349D, Two CF-associated Mutations in the Signature Sequences of CFTR, Exhibit Distinct Gating Defects. *Journal of General Physiology* **129,** 285-298.

Bose SJ, Scott-Ward TS, Cai Z & Sheppard DN. (2015). Exploiting species differences to understand the CFTR Cl^- channel. *Biochemical Society Transactions* **43,** 975-982.

Broadbent S, Ramjeesingh M, Bear C, Argent B, Linsdell P & Gray M. (2015). The cystic fibrosis transmembrane conductance regulator is an extracellular chloride sensor. *European Journal of Physiology* **467,** 1783-1794.

Burgel P-R, Bellis G, Olesen HV, Viviani L, Zolin A, Blasi F & Elborn JS. (2015). Future trends in cystic fibrosis demography in 34 European countries. *European Respiratory Journal* **46,** 133-141.

Byrnes LJ, Xu Y, Qiu X, Hall JD & West GM. (2018). Sites associated with Kalydeco binding on human Cystic Fibrosis Transmembrane Conductance Regulator revealed by Hydrogen/Deuterium Exchange. *Scientific Reports* **8,** 4664. 1-12.

Caci E, Caputo A, Hinzpeter A, Arous N, Fanen P, Sonawane N, Verkman AS, Ravazzolo R, Zegarra-Moran O & Galietta LJV. (2008). Evidence for direct CFTR inhibition by $CFTR_{inh}$-172 based on Arg347 mutagenesis. *The Biochemical Journal* **413,** 135-42.

Cai Z, Palmai-Pallag T, Khuituan P, Mutolo MJ, Boinot C, Liu B, Scott-Ward TS, Callebaut I, Harris A & Sheppard DN. (2015). Impact of the F508del mutation on ovine CFTR, a Cl^- channel with enhanced conductance and ATP-dependent gating. *Journal of Physiology* **593,** 2427-2446.

Cai Z, Scott-Ward TS, Li H, Schmidt A & Sheppard DN. (2004). Strategies to investigate the mechanism of action of CFTR modulators. *Journal of Cystic Fibrosis* **3 Suppl 2,** 141-147.

Cai Z, Scott-Ward TS, Sheppard DN. (2003). Voltage-dependent gating of the cystic fibrosis transmembrane conductance regulator Cl^- channel. *Journal of General Physiology* **122,** 605-620.

Cai Z, Sohma Y, Bompadre SG, Sheppard DN & Hwang T-C. (2011). Application of high-resolution single-channel recording to functional studies of cystic fibrosis mutants. *Methods in Molecular Biology (Clifton, NJ)* **741,** 419-441.

Cai ZW & Sheppard DN. (2002). Phloxine B interacts with the cystic fibrosis transmembrane conductance regulator at multiple sites to modulate channel activity. *Journal of Biological Chemistry* **277,** 19546-19553.

Cai ZW, Taddei A & Sheppard DN. (2006). Differential sensitivity of the cystic fibrosis (CF)-associated mutants G551D and G1349D to potentiators of the cystic fibrosis transmembrane conductance regulator (CFTR) Cl^- channel. *Journal of Biological Chemistry* **281,** 1970-1977.

Callebaut I, Eudes R, Mornon JP & Lehn P. (2004). Nucleotide-binding domains of human cystic fibrosis transmembrane conductance regulator: detailed sequence analysis and three-dimensional modeling of the heterodimer. *Cellular and Molecular Life Sciences* **61,** 230-242.

Carlile GW, Yang Q, Matthes E, Liao J, Radinovic S, Miyamoto C, Robert R, Hanrahan JW & Thomas DY. (2018). A novel triple combination of pharmacological chaperones improves F508del-CFTR correction. *Scientific Reports* **8,** 1. 11404.

Carson MR, Travis SM & Welsh MJ. (1995a). The two nucleotide-binding domains of cystic fibrosis transmembrane conductance regulator (CFTR) have distinct functions in controlling channel activity. *The Journal of Biological Chemistry* **270,** 1711-1717.

Carson MR, Winter MC, Travis SM & Welsh MJ. (1995b). Pyrophosphate stimulates wild-type and mutant cystic-fibrosis transmembrane conductance regulator Cl^- channels. *Journal of Biological Chemistry* **270,** 20466-20472.

Chappe V, Hinkson DA, Zhu T, Chang XB, Riordan JR & Hanrahan JW. (2003). Phosphorylation of protein kinase C sites in NBD1 and the R domain control CFTR channel activation by PKA. *Journal of Physiology* **548,** 39-52.

Chen JM, Cutler C, Jacques C, Boeuf G, Denamur E, Lecointre G, Mercier B, Cramb G & Ferec C. (2001). A combined analysis of the cystic fibrosis transmembrane conductance regulator: Implications for structure and disease models. *Molecular Biology and Evolution* **18,** 1771-1788.

Chen T & Hwang TC. (2008). CLC-0 and CFTR: Chloride channels evolved from transporters. *Physiological Reviews* **88,** 351-387.

Cheng SH, Gregory RJ, Marshall J, Paul S, Souza DW, White GA, O'Riordan CR & Smith AE. (1990). Defective intracellular-transport and processing of CFTR is the molecular-basis of most cystic-fibrosis. *Cell* **63,** 827-834.

Chin S, Hung M, Won A, Wu Y-S, Ahmadi S, Yang D, Elmallah S, Toutah K, Hamilton CM, Young RN, Viirre RD, Yip CM & Bear CE. (2018). Lipophilicity of the Cystic Fibrosis drug, Ivacaftor, and its destabilizing effect on the major CF-causing mutation: F508del. *Molecular Pharmacology* **94,** 917-925.

Cholon DM & Gentzsch M. (2018). Recent progress in translational cystic fibrosis research using precision medicine strategies. *Journal of Cystic Fibrosis* **17,** S52-S60.

Chong PA, Farber PJ, Vernon RM, Hudson RP, Mittermaier AK & Forman-Kay JD. (2015). Deletion of Phenylalanine 508 in the First Nucleotide-binding Domain of the Cystic Fibrosis Transmembrane Conductance Regulator Increases Conformational Exchange and Inhibits Dimerization. *Journal of Biological Chemistry* **290,** 22862-22878.

Clancy JP, Rowe SM, Accurso FJ, Aitken ML, Amin RS, Ashlock MA, Ballmann M, Boyle MP, Bronsveld I, Campbell PW, De Boeck K, Donaldson SH, Dorkin HL, Dunitz JM, Durie PR, Jain M, Leonard A, McCoy KS, Moss RB, Pilewski JM, Rosenbluth DB, Rubenstein RC, Schechter MS, Botfield M, Ordoñez CL, Spencer-Green GT, Vernillet L, Wisseh S, Yen K, Konstan MW. (2012). Results of a phase IIa study of VX-809, an investigational CFTR corrector compound, in subjects with cystic fibrosis homozygous for the F508del-CFTR mutation. *Thorax* **67,** 12-18.

Clarke LL, Grubb BR, Yankaskas JR, Cotton CU, McKenzie A & Boucher RC. (1994). Relationship of a Non-Cystic Fibrosis Transmembrane Conductance Regulator- Mediated Chloride Conductance to Organ-Level Disease in $Cftr^{-/-}$ Mice. *Proceedings of the National Academy of Sciences of the United States of America* **91,** 479-483.

Cohen-Cymberknoh M, Shoseyov D & Kerem E. (2011). Managing cystic fibrosis: strategies that increase life expectancy and improve quality of life. *American Journal of Respiratory and Critical Care Medicine* **183,** 1463-1471.

Colquhoun D. (1998). Binding, gating, affinity and efficacy: The interpretation of structure-activity relationships for agonists and of the effects of mutating receptors. *British Journal of Pharmacology* **125,** 923-947.

Cook DP, Rector MV, Bouzek DC, Michalski AS, Gansemer ND, Reznikov LR, Li XP, Stroik MR, Ostedgaard LS, Abou Alaiwa MH, Thompson MA, Prakash YS, Krishnan R, Meyerholz DK, Seow CY & Stoltz DA. (2016). Cystic Fibrosis Transmembrane Conductance Regulator in Sarcoplasmic Reticulum of Airway Smooth Muscle Implications for Airway Contractility. *American Journal of Respiratory and Critical Care Medicine* **193,** 417-426.

Corradi V, Vergani P & Tieleman DP. (2015). Cystic Fibrosis Transmembrane Conductance Regulator (CFTR) closed and open state channel models. *Journal of Biological Chemistry* **290,** 22891-22906.

Csanády L, Chan KW, Seto-Young D, Kopsco DC, Nairn AC & Gadsby DC. (2000). Severed Channels Probe Regulation of Gating of Cystic Fibrosis Transmembrane Conductance Regulator by Its Cytoplasmic Domains. *Journal of General Physiology* **116,** 477-500.

Cui G & McCarty NA. (2015). Murine and human CFTR exhibit different sensitivities to CFTR potentiators. *American Journal of Physiology-Lung Cellular and Molecular Physiology* **309,** L687-L699.

Cui G, Rahman KS, Infield DT, Kuang C, Prince CZ & McCarty NA. (2014). Three charged amino acids in extracellular loop 1 are involved in maintaining the outer pore architecture of CFTR. *Journal of General Physiology* **144,** 159-179.

Cui G, Stauffer BB, Imhoff BR, Gaggar A & McCarty NA. (2017). Lamprey CFTR, an Evolutionary Ancestor of Human CFTR, Exhibits Numerous Biophysical Dissimilarities from Human CFTR. *Biophysical Journal* **112**, pp. 411a-411a.

Cui GY, Khazanov N, Stauffer BB, Infield DT, Imhoff BR, Senderowitz H & McCarty NA. (2016). Potentiators exert distinct effects on human, murine, and Xenopus CFTR. *American Journal of Physiology-Lung Cellular and Molecular Physiology* **311,** L192-L207.

Dahan D, Evagelidis A, Hanrahan JW, Hinkson DAR, Jia Y, Luo J & Zhu T. (2001). Regulation of the CFTR channel by phosphorylation. *Pflugers Arch* **443,** S92-S96.

Dalemans W, Barbry P, Champigny G, Jallat S, Dott K, Dreyer D, Crystal RG, Pavirani A, Lecocq JP & Lazdunski M. (1991). Altered chloride-ion channel kinetics associated with the ΔF508 cystic-fibrosis mutation. *Nature* **354,** 526-528.

Dalton J, Kalid O, Schushan M, Ben-Tal N & Villa-Freixa J. (2012). New Model of Cystic Fibrosis Transmembrane Conductance Regulator Proposes Active Channel-like Conformation. *Journal of Chemical Information and Modeling* **52,** 1842-1853.

Davidson H, Taylor MS, Doherty A, Boyd AC & Porteous DJ. (2000). Genomic sequence allalysis of Fugu rubripes CFTR and flanking genes in a 60 kb region conserving synteny with 800 kb of human chromosome 7. *Genome Research* **10,** 1194-1203.

Davies JC, Moskowitz SM, Brown C, Horsley A, Mall MA, McKone EF, Plant BJ, Prais D, Ramsey BW, Taylor-Cousar JL, Tullis E, Uluer A, McKee CM, Robertson S, Shilling RA, Simard RA, Simard C, Van Goor F, Waltz D, Xuan F, Young T & Rowe SM. (2018). VX-659-tezacaftor-ivacaftor in patients with cystic fibrosis and one or two phe508del alleles. *New England Journal of Medicine* **379 (17),** 1599-1611.

Dawson RJP & Locher KP. (2006). Structure of a bacterial multidrug ABC transporter. *Nature* **443,** 180-185.

Dawson RJP & Locher KP. (2007). Structure of the multidrug ABC transporter Sav1866 from Staphylococcus aureus in complex with AMP-PNP. *FEBS Letters* **581,** 935-938.

Dawson TJ & Hulbert AJ. (1970). Standard metabolism, body temperature, and surface areas of Australian marsupials. *American Journal of Physiology* **218,** 1233-1238.

De Boeck K & Amaral MD. (2016). Progress in therapies for cystic fibrosis. *The Lancet Respiratory Medicine* **4,** 662-674.

de Jonge H, Wilke M, Bot A, Jorna H, Wang W, Kirk K & Sheppard D. (2007). Differential response of mouse versus human CFTR to CFTR potentiators. *Pediatric Pulmonology Supplement***, 30,** 208-208.

deCarvalho ACV, Gansheroff LJ & Teem JL. (2002). Mutations in the nucleotide binding domain 1 signature motif region rescue processing and functional defects of cystic fibrosis transmembrane conductance regulator ΔF508. *Journal of Biological Chemistry* **277,** 35896-35905.

del Castillo J & Katz B. (1957). Interaction at End-Plate Receptors between Different Choline Derivatives. *Proceedings of the Royal Society of London Series B, Biological Sciences (1934-1990)* **146,** 369-381.

Demmers KJ, Carter D, Fan S, Mao P, Maqbool NJ, McLeod BJ, Bartolo R & Butt AG. (2010). Molecular and functional characterization of the cystic fibrosis transmembrane conductance regulator from the Australian common brushtail

possum, Trichosurus vulpecula. *Journal of Comparative Physiology B Biochemical Systemic and Environmental Physiology* **180,** 545-561.

Denning GM, Anderson MP, Amara JF, Marshall J, Smith AE & Welsh MJ. (1992). Processing of mutant cystic-fibrosis transmembrane conductance regulator is temperature-sensitive. *Nature* **358,** 761-764.

Dong Q, Ostedgaard LS, Rogers C, Vermeer DW, Zhang Y & Welsh MJ. (2012). Human-mouse cystic fibrosis transmembrane conductance regulator (CFTR) chimeras identify regions that partially rescue CFTR-ΔF508 processing and alter its gating defect. *Proceedings of the National Academy of Sciences of the United States of America* **109,** 917-922.

Eckford PDW, Li CH, Ramjeesingh M & Bear CE. (2012). Cystic Fibrosis Transmembrane Conductance Regulator (CFTR) Potentiator VX-770 (Ivacaftor) Opens the Defective Channel Gate of Mutant CFTR in a Phosphorylation-dependent but ATP-independent Manner. *Journal of Biological Chemistry* **287,** 36639-36649.

Ehrhardt A, Chung WJ, Pyle LC, Wang W, Nowotarski K, Mulvihill CM, Ramjeesingh M, Hong J, Velu SE, Lewis HA, Atwell S, Aller S, Bear CE, Lukacs GL, Kirk KL & Sorscher EJ. (2016). Channel Gating Regulation by the Cystic Fibrosis Transmembrane Conductance Regulator (CFTR) First Cytosolic Loop. *Journal of Biological Chemistry* **291,** 1854-1865.

Elborn JS. (2016). Cystic fibrosis. *The Lancet* **388,** 2519-2531.

Elborn JS, Shale DJ & Britton JR. (1991). Cystic fibrosis: current survival and population estimates to the year 2000. *Thorax* **46,** 881-885.

Elborn S, Bouisset F, Checchio T, Perquin J, Lamontagne N, Montgomery S & Henig N. (2017). A first-in-human, phase 1b, dose-escalation study of QR-010, a novel antisense oligonucleotide administered in subjects with cystic fibrosis homozygous for the F508del CFTR mutation. *Pediatric Pulmonology Supplement* **52,** S289-S289.

Elkins MR, Robinson M, Rose BR, Harbour C, Moriarty CP, Marks GB, Belousova EG, Xuan W & Bye PTP. (2006). A Controlled Trial of Long-Term Inhaled Hypertonic Saline in Patients with Cystic Fibrosis. *The New England Journal of Medicine* **354,** 229-240.

Engelhardt JF, Yankaskas JR, Ernst SA, Yang Y, Marino C, R., Boucher R, C., Cohn J, A. & Wilson J, M. (1992). Submucosal glands are the predominant site of CFTR expression in the human bronchus. *Nature Genetics* **2,** 240.

Fajac I & De Boeck K. (2017). New horizons for cystic fibrosis treatment. *Pharmacology and Therapeutics* **170,** 205-211.

Fan Z, Perisse IV, Cotton CU, Regouski M, Meng Q, Domb C, Van Wettere AJ, Wang Z, Harris A, White KL & Polejaeva IA. (2018). A sheep model of cystic fibrosis generated by CRISPR/Cas9 disruption of the CFTR gene. *JCI insight* **3 (19),** e123529.

Farrell PM. (2000). Improving the health of patients with cystic fibrosis through newborn screening. Wisconsin Cystic Fibrosis Neonatal Screening Study Group. *Advances in Pediatrics* **47,** 79-115.

Fisher JT, Liu X, Yan Z, Luo M, Zhang Y, Zhou W, Lee BJ, Song Y, Guo C, Wang Y, Lukacs GL & Engelhardt JF. (2012). Comparative Processing and Function of Human and Ferret Cystic Fibrosis Transmembrane Conductance Regulator. *Journal of Biological Chemistry* **287,** 21673-21685.

Fisher JT, Zhang Y & Engelhardt JF. (2011). Comparative Biology of Cystic Fibrosis Animal Models. *Cystic Fibrosis: Diagnosis and Protocols, Vol II: Methods and Resources to Understand Cystic Fibrosis* **742,** 311-334.

Ford B. (2017). CFTR structure: lassoing cystic fibrosis. *Nature Structural & Molecular Biology* **24,** 13.

Frizzell RA & Hanrahan JW. (2012). Physiology of Epithelial Chloride and Fluid Secretion. *Cold Spring Harbor Perspectives in Medicine* **2,** a009563.

Fuchs HJ, Borowitz DS, Christiansen DH, Morris EM, Nash ML, Ramsey BW, Rosenstein BJ, Smith AL & Wohl ME. (1994). Effect of Aerosolized Recombinant Human DNase on Exacerbations of Respiratory Symptoms and on Pulmonary Function in Patients with Cystic Fibrosis. *The New England Journal of Medicine* **331,** 637-642.

Garnett JP, Hickman E, Burrows R, Hegyi P, Tiszlavicz L, Cuthbert AW, Fong P & Gray MA. (2011). Novel role for pendrin in orchestrating bicarbonate secretion in cystic fibrosis transmembrane conductance regulator (CFTR)-expressing airway serous cells. *Journal of Biological Chemistry* **286 (47),** 41069-82.

Gao X & Hwang T-C. (2015). Localizing a gate in CFTR. *Proceedings of the National Academy of Sciences of the United States of America* **112,** 2461-2466.

Gao XL & Hwang TC. (2016). Spatial positioning of CFTR's pore-lining residues affirms an asymmetrical contribution of transmembrane segments to the anion permeation pathway. *Journal of General Physiology* **147,** 407-422.

Gawenis LR, Ledoussal C, Judd LM, Prasad V, Alper SL, Stuart-Tilley A, Woo AL, Grisham C, Sanford LP, Doetschman T, Miller ML & Shull GE. (2004). Mice with a targeted disruption of the AE2 Cl^-/HCO_3^- exchanger are achlorhydric. *Journal of Biological Chemistry* **279,** 30531-30539.

Gilligan PH. (1991). Microbiology of airway disease in patients with cystic-fibrosis. *Clinical Microbiology Reviews* **4,** 35-51.

Griesenbach U, Pytel KM & Alton EWFW. (2015). Cystic Fibrosis Gene Therapy in the UK and Elsewhere. *Human Gene Therapy* **26,** 266-275.

Grubb BR & Boucher RC. (1999). Pathophysiology of gene-targeted mouse models for cystic fibrosis. *Physiological Reviews* **79,** S193-S214.

Grubb BR, Vick RN & Boucher RC. (1994). Hyperabsorption of Na^+ and raised Ca^{2+}-mediated Cl^- secretion in nasal epithelia of CF mice. *American Journal of Physiology - Cell Physiology* **266,** C1478-C1483.

Gunderson KL & Kopito RR. (1994). Effects of pyrophosphate and nucleotide analogs suggest a role for ATP hydrolysis in cystic-fibrosis transmembrane regulator channel gating. *Journal of Biological Chemistry* **269,** 19349-19353.

Gunderson KL & Kopito RR. (1995). Conformational states of CFTR associated with channel gating: The role of ATP binding and hydrolysis. *Cell* **82,** 231-239.

Haardt M, Benharouga M, Lechardeur D, Kartner N & Lukacs GL. (1999). C-terminal truncations destabilize the cystic fibrosis transmembrane conductance regulator without impairing its biogenesis. A novel class of mutation. *Journal of Biological Chemistry* **274,** 21873-21877.

Haggie PM, Phuan P-W, Tan J-A, Xu H, Avramescu RG, Perdomo D, Zlock L, Nielson DW, Finkbeiner WE, Lukacs GL & Verkman AS. (2017). Correctors and Potentiators Rescue Function of the Truncated W1282X-Cystic Fibrosis Transmembrane Regulator (CFTR) Translation Product. *Journal of Biological Chemistry* **292,** 771-785.

Hanrahan J, Duguay F, Sansom S, Alon N, Jensen T, Riordan J & Grzelczak Z. (1993). Low-conductance chloride channel activated by cAMP in the rectal gland of the shark *Squalus acanthias* and in cells heterologously expressing shark CFTR. *Bull Mount Desert Island Biol Lab***,** 48-49.

Haq IJ, Gray MA, Garnett JP, Ward C & Brodlie M. (2016). Airway surface liquid homeostasis in cystic fibrosis: pathophysiology and therapeutic targets. *Thorax* **71,** 284-287.

Hardy SP, Goodfellow HR, Valverde MA, Gill DR, Sepúlveda FV & Higgins CF. (1995). Protein kinase C-mediated phosphorylation of the human multidrug resistance P-glycoprotein regulates cell volume-activated chloride channels. *The EMBO Journal* **14,** 68-75.

Harris A. (1997). Towards an ovine model of cystic fibrosis. *Human Molecular Genetics* **6,** 2191-2194.

He L, Aleksandrov AA, Serohijos AWR, Hegedus T, Aleksandrov LA, Cui L, Dokholyan NV & Riordan JR. (2008). Multiple membrane-cytoplasmic domain contacts in the cystic fibrosis transmembrane conductance regulator (CFTR) mediate regulation of channel gating. *Journal of Biological Chemistry* **283,** 26383.

Higgins CF & Linton KJ. (2004). The ATP switch model for ABC transporters. *Nature Structural & Molecular Biology* **11,** 918-926.

Highsmith WE, Burch LH, Zhou Z, Olsen JC, Boat TE, Spock A, Gorvoy JD, Quittell L, Friedman KJ, Silverman LM, Boucher RC & Knowles MR. (1994). A Novel Mutation in the Cystic Fibrosis Gene in Patients with Pulmonary Disease but Normal Sweat Chloride Concentrations. *The New England Journal of Medicine* **331,** 974-980.

Highsmith WE, Burch LH, Zhou Z, Olsen JC, Strong TV, Smith T, Friedman KJ, Silverman LM, Boucher RC, Collins FS & Knowles MR. (1997). Identification of a splice site mutation (2789+5 G>A) associated with small amounts of normal CFTR mRNA and mild cystic fibrosis. *Human Mutation* **9,** 332-338.

Hodges C, Gawenis L, Drumm M & Clarke L. (2016). Mouse models expressing human CFTR to test CFTR-directed therapies. *Pediatric Pulmonology Supplement* **51,** 157-158.

Hoelen H, Kleizen B, Schmidt A, Richardson J, Charitou P, Thomas PJ & Braakman I. (2010). The primary folding defect and rescue of ΔF508 CFTR emerge during translation of the mutant domain. *PLoS ONE* **5 (11),** 1-10

Holland IB. (2003). *ABC proteins : from bacteria to man / editor Ian Barry Holland ... [et al.]*. London : Academic Press, London.

Huang J, Shan J, Kim D, Liao J, Evagelidis A, Alper SL & Hanrahan JW. (2012). Basolateral chloride loading by the anion exchanger type 2: role in fluid secretion by the human airway epithelial cell line Calu-3. *Journal of Physiology* **590,** 5299-5316.

Huang S-Y, Bolser D, Liu H-Y, Hwang T-C & Zou X. (2009). Molecular modeling of the heterodimer of human CFTR's nucleotide-binding domains using a protein-protein docking approach. *Journal of Molecular Graphics & Modelling* **27,** 822-828.

Hudson JW & Scott IM. (1979). Daily torpor in the laboratory mouse, mus-musculus var albino. *Physiological Zoology* **52,** 205-218.

Hwang T-C & Sheppard DN. (2009). Gating of the CFTR Cl^- channel by ATP-driven nucleotide-binding domain dimerisation. *Journal of Physiology* **587,** 2151-2161.

Hwang TC, Nagel G, Nairn AC & Gadsby DC. (1994). Regulation of the gating of cystic-fibrosis transmembrane conductance regulator Cl^- channels by phosphorylation and ATP hydrolysis. *Proceedings of the National Academy of Sciences of the United States of America* **91,** 4698-4702.

Hämmerle MM, Aleksandrov AA & Riordan JR. (2001). Disease-associated mutations in the extracytoplasmic loops of cystic fibrosis transmembrane conductance regulator do not impede biosynthetic processing but impair chloride channel stability. *The Journal of Biological Chemistry* **276,** 14848-14854.

Igreja S, Clarke LA, Botelho HM, Marques L & Amaral MD. (2016). Correction of a Cystic Fibrosis Splicing Mutation by Antisense Oligonucleotides. *Human Mutation* **37,** 209-215.

Illek B, Fischer H, Santos GF, Widdicombe JH, Machen TE & Reenstra WW. (1995). cAMP-independent activation of CFTR Cl^- channels by the tyrosine kinase inhibitor genistein. *American Journal of Physiology - Cell Physiology* **268,** C886-C893.

Jih K-Y & Hwang T-C. (2012). Nonequilibrium Gating of CFTR on an Equilibrium Theme. *Physiology* **27,** 351-361.

Jih K-Y & Hwang T-C. (2013). VX-770 potentiates CFTR function by promoting decoupling between the gating cycle and ATP hydrolysis cycle. *Proceedings of the National Academy of Sciences of the United States of America* **110,** 4404-4409.

Jih K-Y, Li M, Hwang T-C & Bompadre SG. (2011). The most common cystic fibrosis-associated mutation destabilizes the dimeric state of the nucleotide-binding domains of CFTR. *Journal of Physiology-London* **589,** 2719-2731.

Joiner WJ, Basavappa S, Vidyasagar S, Nehrke K, Krishnan S, Binder HJ, Boulpaep EL & Rajendran VM. (2003). Active K^+ secretion through multiple KCa-type channels and regulation by IKCa channels in rat proximal colon. *American Journal of Physiology Gastrointestinal and Liver Physiology* **285,** G185-196.

Jordan IK, Kota KC, Cui G, Thompson CH & McCarty NA. (2008). Evolutionary and functional divergence between the cystic fibrosis transmembrane conductance regulator and related ATP-binding cassette transporters. *Proceedings of the National Academy of Sciences of the United States of America* **105,** 18865-18870.

Juliano RL & Ling V. (1976). Surface glycoprotein modulating drug permeability in Chinese-hamster ovary cell mutants. *Biochimica et Biophysica Acta* **455,** 152-162.

Keating D, Marigowda G, Burr L, daines C, Mall MA, McKone EF, Ramsey BS, Rowe SM, Sass LA, Tullis E, McKee CM, Moskowitz SM, Robertson S, Savage J, Simard C, Vang Goor F, Waltz D, Xuan F, Yount T & Taylor-Cousar JL. (2018) VX-774-tezacaftor-Ivacaftor in patients with cystic fibrosis one or two phe508del alleles. *New England Journal of Medicine* **379** (17), 1612-1620.

Keiser NW, Evans IA, Tyler SR, Nellis J, Sun X, Sui H, Liang B & Engelhardt J. (2013). Functional properties of CF ferret airway fluid reveal deficiencies in airway innate immunity at birth. *Pediatric Pulmonology Supplement* **48,** 271-272.

Kent G, Oliver M, Foskett JK, Frndova H, Durie P, Forstner J, Forstner GG, Riordan JR, Percy D & Buchwald M. (1996). Phenotypic Abnormalities in Long-Term Surviving Cystic Fibrosis Mice. *Pediatric Research* **40,** 233-241.

Kerem BS, Rommens JM, Buchanan JA, Markiewicz D, Cox TK, Chakravarti A, Buchwald M & Tsui LC. (1989). Identification of the cystic-fibrosis gene - genetic-analysis. *Science* **245,** 1073-1080.

Kim K, Hung R-J & Perrimon N. (2017). miR-263a Regulates ENaC to Maintain Osmotic and Intestinal Stem Cell Homeostasis in Drosophila. *Developmental Cell* **40,** 23-36.

Kirchner S, Cai Z, Rauscher R, Kastelic N, Anding M, Czech A, Kleizen B, Ostedgaard LS, Braakman I, Sheppard DN & Ignatova Z. (2017). Alteration of protein function by a silent polymorphism linked to tRNA abundance. *PLoS Biology* **15,** e2000779.

Kleizen B, van Vlijmen T, de Jonge HR & Braakman I. (2005). Folding of CFTR Is Predominantly Cotranslational. *Molecular Cell* **20,** 277-287.

Lansdell KA, Delaney SJ, Lunn DP, Thomson SA, Sheppard DN & Wainwright BJ. (1998a). Comparison of the gating behaviour of human and murine cystic fibrosis transmembrane conductance regulator Cl^- channels expressed in mammalian cells. *Journal of Physiology* **508,** 379-392.

Lansdell KA, Kidd JF, Delaney SJ, Wainwright BJ & Sheppard DN. (1998b). Regulation of murine cystic fibrosis transmembrane conductance regulator Cl^- channels expressed in Chinese hamster ovary cells. *Journal of Physiology* **512,** 751-764.

Lee CM, Flynn R, Hollywood JA, Scallan MF & Harrison PT. (2012). Correction of the ΔF508 Mutation in the Cystic Fibrosis Transmembrane Conductance Regulator Gene by Zinc-Finger Nuclease Homology-Directed Repair. *BioResearch Open Access* **1,** 99-108.

Letz B & Korbmacher C. (1997). cAMP stimulates CFTR-like Cl^- channels and inhibits amiloride-sensitive Na^+ channels in mouse CCD cells. *American Journal of Physiology-Cell Physiology* **272,** C657-C666.

Lewis HA, Buchanan SG, Burley SK, Conners K, Dickey M, Dorwart M, Fowler R, Gao X, Guggino WB, Hendrickson WA, Hunt JF, Kearins MC, Lorimer D, Maloney PC, Post KW, Rajashankar KR, Rutter ME, Sauder JM, Shriver S, Thibodeau PH, Thomas PJ, Zhang M, Zhao X & Emtage S. (2004). Structure of nucleotide-binding domain 1 of the cystic fibrosis transmembrane conductance regulator. *EMBO Journal* **23,** 282-293.

Lewis HA, Wang C, Zhao X, Hamuro Y, Conners K, Kearins MC, Lu F, Sauder JM, Molnar KS, Coales SJ, Maloney PC, Guggino WB, Wetmore DR, Weber PC & Hunt JF. (2010). Structure and Dynamics of NBD1 from CFTR Characterized Using Crystallography and Hydrogen/Deuterium Exchange Mass Spectrometry. *Journal of Molecular Biology* **396,** 406-430.

Li C, Ramjeesingh M, Wang W, Garami E, Hewryk M, Lee D, Rommens JM, Galley K & Bear CE. (1996). ATPase activity of the cystic fibrosis transmembrane conductance regulator. *Journal of Biological Chemistry* **271,** 28463-28468.

Li H, Valkenier H, Judd LW, Brotherhood PR, Hussain S, Cooper JA, Jurcek O, Sparkes HA, Sheppard DN & Davis AP. (2016). Efficient, non-toxic anion transport by synthetic carriers in cells and epithelia. *Nature Chemistry* **8,** 24-32.

Li HY, Salomon JJ, Sheppard DN, Mall MA & Galietta LJV. (2017). Bypassing CFTR dysfunction in cystic fibrosis with alternative pathways for anion transport. *Current Opinion in Pharmacology* **34,** 91-97.

Li HY & Sheppard DN. (2009). Therapeutic Potential of Cystic Fibrosis Transmembrane Conductance Regulator (CFTR) Inhibitors in Polycystic Kidney Disease. *BioDrugs* **23,** 203-216.

Li L, Liu LN, Feller S, Allen C, Shivakumar R, Fratantoni J, Wolfraim LA, Fujisaki H, Campana D, Chopas N, Dzekunov S & Peshwa M. (2009). Expression of chimeric antigen receptors in natural killer cells with a regulatory-compliant non-viral method. *Cancer Gene Therapy* **17,** 147-154.

Li M-S, Cowley EA, El Hiani Y & Linsdell P. (2018). Functional organization of cytoplasmic portals controlling access to the cystic fibrosis transmembrane conductance regulator (CFTR) chloride channel pore. *Journal of Biological Chemistry* **293,** 5649-5658.

Li T, Huang S, Zhao X, Wright DA, Carpenter S, Spalding MH, Weeks DP & Yang B. (2011). Modularly assembled designer TAL effector nucleases for targeted gene knockout and gene replacement in eukaryotes. *Nucleic Acids Research* **39,** 6315-6325.

Liao TJ, Wang L, Halm ST, Lu L, Fyffe REW & Halm DR. (2005). K^+ channel K_VLQT1 located in the basolateral membrane of distal colonic epithelium is not essential for activating Cl^- secretion. *American Journal of Physiology-Cell Physiology* **289,** C564-C575.

Lin W, Sohma Y & Hwang TC. (2016). Synergistic Potentiation of Cystic Fibrosis Transmembrane Conductance Regulator Gating by Two Chemically Distinct Potentiators, Ivacaftor (VX-770) and 5-Nitro-2-(3-Phenylpropylamino) Benzoate. *Molecular Pharmacology* **90,** 275-285.

Liu F, Zhang Z, Csanády L, Gadsby DC & Chen J. (2017). Molecular Structure of the Human CFTR Ion Channel. *Cell* **169,** 85-95.e88.

Liu X, O'Donnell N, Landstrom A, Skach WR & Dawson DC. (2012). Thermal Instability of ΔF508 Cystic Fibrosis Transmembrane Conductance Regulator (CFTR) Channel Function: Protection by Single Suppressor Mutations and Inhibiting Channel Activity. *Biochemistry* **51,** 5113-5124.

Loffing J, Moyer BD, Reynolds D, Shmukler BE, Alper SL & Stanton BA. (2000). Functional and molecular characterization of an anion exchanger in airway serous epithelial cells. *American Journal of Physiology Cell Physiology* **279,** C1016-23.

Loo TW, Bartlett MC & Clarke DM. (2013). Corrector VX-809 stabilizes the first transmembrane domain of CFTR. *Biochemical Pharmacology* **86,** 612-619.

Lukacs GL, Chang XB, Bear C, Kartner N, Mohamed A, Riordan JR & Grinstein S. (1993). The ΔF508 mutation decreases the stability of cystic fibrosis transmembrane conductance regulator in the plasma membrane. Determination of functional half-lives on transfected cells. *Journal of Biological Chemistry* **268,** 21592-21598.

Lukacs GL, Mohamed A, Kartner N, Chang XB, Riordan JR & Grinstein S. (1994). Conformational maturation of CFTR but not its mutant counterpart (ΔF508) occurs in the endoplasmic reticulum and requires ATP. *The EMBO Journal* **13,** 6076-6086.

Ma T, Thiagarajah JR, Yang H, Sonawane ND, Folli C, Galietta LJ, Verkman AS. (2002). Thiazolidinone CFTR inhibitor identified by high-throughput screening blocks cholera toxin-induced intestinal fluid secretion. *Journal of Clinical Investigation,* **110,** 1651-58.

Mall M, Grubb BR, Harkema JR, O'Neal WK & Boucher RC. (2004). Increased airway epithelial Na^+ absorption produces cystic fibrosis-like lung disease in mice. *Nature Medicine* **10,** 487-493.

McCarron A, Donnelley M & Parsons D. (2018). Airway disease phenotypes in animal models of cystic fibrosis. *Respiratory Research* **19,** 1-12.

McClure ML, Barnes S, Brodsky JL & Sorscher EJ. (2016). Trafficking and function of the cystic fibrosis transmembrane conductance regulator: a complex network of posttranslational modifications. *American Journal of Physiology Lung Cellular and Molecular Physiology* **311,** L719-L733.

Mijnders M, Kleizen B & Braakman I. (2017). Correcting CFTR folding defects by small-molecule correctors to cure cystic fibrosis. *Current Opinion in Pharmacology* **34,** 83-90.

Miki H, Zhou Z, Li M, Hwang T-C & Bompadre SG. (2010). Potentiation of disease-associated cystic fibrosis transmembrane conductance regulator mutants by hydrolyzable ATP analogs. *Journal of Biological Chemistry* **285,** 19967-19975.

Molinski S, Eckford PDW, Pasyk S, Ahmadi S, Chin S & Bear CE. (2012). Functional rescue of F508del-CFTR using small molecule correctors. *Frontiers in Pharmacology* **3,** 160:1-18.

Moran O. (2017). The gating of the CFTR channel. *Cellular and Molecular Life Sciences* **74,** 85-92.

Mornon J, Hoffmann B, Jonic S, Lehn P & Callebaut I. (2014). Full-open and closed CFTR channels, as revealed by molecular dynamics. *Pediatric Pulmonology Supplement* **49,** 228-228.

Mornon JP, Lehn P & Callebaut I. (2008). Atomic model of human cystic fibrosis transmembrane conductance regulator: Membrane-spanning domains and coupling interfaces. *Cellular and Molecular Life Sciences* **65,** 2594-2612.

Moss RB, Flume PA, Elborn JS, Cooke J, Rowe SM, McColley SA, Rubenstein RC & Higgins M. (2015). Efficacy and safety of ivacaftor in patients with cystic fibrosis who have an Arg117His-CFTR mutation: a double-blind, randomised controlled trial. *The Lancet Respiratory Medicine* **3,** 524-533.

Muanprasat C, Sonawane ND, Salinas D, Taddei A, Galietta LJV & Verkman AS. (2004). Discovery of glycine hydrazide pore-occluding CFTR inhibitors: Mechanism, structure-activity analysis, and in vivo efficacy. *Journal of General Physiology* **124,** 125-137.

Nanda Kumar NS, Singh SK & Rajendran VM. (2010). Mucosal potassium efflux mediated via KCNN4 channels provides the driving force for electrogenic anion secretion in colon. *American Journal of Physiology Gastrointestinal and Liver Physiology* **299,** G707-G714.

Navis A & Bagnat M. (2015). Loss of cftr function leads to pancreatic destruction in larval zebrafish. *Developmental Biology* **399,** 237-248.

Neher E & Sakmann B. (1976). Single-channel currents recorded from membrane of denervated frog muscle fibres. *Nature* **260,** 799-802.

Putnam NH, Butts T, Ferrier DE, Furlong RF, Hellsten U, Kawashima T, Robinson-Rechavi M, Shoguchi E, Terry A, Yu JK, Benito-Gutiérrez EL, Dubchak I, Garcia-Fernàndez J, Gibson-Brown JJ, Grigoriev IV, Horton AC, de Jong PJ, Jurka J, Kapitonov VV, Kohara Y, Kuroki Y, Lindquist E, Lucas S, Osoegawa K, Pennacchio LA, Salamov AA, Satou Y, Sauka-Spengler T, Schmutz J, Shin-I T, Toyoda A, Bronner-Fraser M, Fujiyama A, Holland LZ, Holland PW, Satoh N, Rokhsar DS. (2008). The amphioxus genome and the evolution of the chordate karyotype. *Nature* **453,** 1064-1071.

Nilsen TO, Ebbesson LOE, Madsen SS, McCormick SD, Andersson E, Björnsson BT, Prunet P & Stefansson SO. (2007). Differential expression of gill Na^+,K^+-ATPase α- and β-subunits, Na^+,K^+,$2Cl^-$ cotransporter and CFTR anion channel in juvenile anadromous and landlocked Atlantic salmon *Salmo salar*. *Journal of Experimental Biology* **210,** 2885-2896.

Novak I & Young J. (1986). Two independent anion transport systems in rabbit mandibular salivary glands. *European Journal of Physiology* **407,** 649-656.

O'Sullivan BP & Freedman SD. (2009). Cystic fibrosis. *Lancet* **373,** 1891-1904.

Okiyoneda T, Veit G, Dekkers JF, Bagdany M, Soya N, Xu HJ, Roldan A, Verkman AS, Kurth M, Simon A, Hegedus T, Beekman JM & Lukacs GL. (2013). Mechanism-based corrector combination restores ΔF508-CFTR folding and function. *Nature Chemical Biology* **9,** 444-U469.

Oldham ML, Davidson AL & Chen J. (2008). Structural insights into ABC transporter mechanism. *Current Opinion in Structural Biology* **18,** 726-733.

Oliver KE, Han ST, Sorscher EJ & Cutting GR. (2017). Transformative therapies for rare CFTR missense alleles. *Current Opinion in Pharmacology* **34,** 76-82.

Ostedgaard LS, Rogers CS, Dong Q, Randak CO, Vermeer DW, Rokhlina T, Karp PH & Welsh MJ. (2007). Processing and function of CFTR-ΔF508 are species-dependent. *Proceedings of the National Academy of Sciences of the United States of America* **104,** 15370-15375.

Ostedgaard LS, Zeiher B & Welsh MJ. (1999). Processing of CFTR bearing the P574H mutation differs from wild-type and ΔF508-CFTR. *Journal of Cell Science* **112,** 2091-2098.

Pederzoli A, Mandrioli M & Mola L. (2014). Expression of carbonic anhydrase, cystic fibrosis transmembrane regulator (CFTR) and $V^{-}H^{+}$-ATPase in the lancelet Branchiostoma lanceolatum (Pallas, 1774). *Acta Histochemica* **116,** 487-492.

Phuan P-W, Veit G, Tan J, Roldan A, Finkbeiner WE, Lukacs GL & Verkman AS. (2014). Synergy-based small-molecule screen using a human lung epithelial cell line yields ΔF508-CFTR correctors that augment VX-809 maximal efficacy. *Molecular Pharmacology* **86,** 42-51.

Pirani D, Evans L, Cook D & Young J. (1987). Intracellular pH in the rat mandibular salivary gland: the role of Na−H and Cl-HCO_3 antiports in secretion. *European Journal of Physiology* **408,** 178-184.

Pollock NL, Rimington TL & Ford RC. (2015). Characterizing diverse orthologues of the cystic fibrosis transmembrane conductance regulator protein for structural studies. *Biochemical Society Transactions* **43,** 894-900.

Poulsen JH, Fischer H, Illek B & Machen TE. (1994). Bicarbonate Conductance and pH Regulatory Capability of Cystic Fibrosis Transmembrane Conductance Regulator. *Proceedings of the National Academy of Sciences of the United States of America* **91,** 5340-5344.

Price MP, Ishihara H, Sheppard DN & Welsh MJ. (1996). Function of Xenopus cystic fibrosis transmembrane conductance regulator (CFTR) Cl^- channels and use of human-Xenopus chimeras to investigate the pore properties of CFTR. *Journal of Biological Chemistry* **271,** 25184-25191.

Pyle LC, Ehrhardt A, Mitchell LH, Fan L, Ren A, Naren AP, Li Y, Clancy JP, Bolger GB, Sorscher EJ & Rowe SM. (2011). Regulatory domain phosphorylation to distinguish the mechanistic basis underlying acute CFTR modulators. *American Journal of Physiology Lung Cellular and Molecular Physiology* **301,** L587-597.

Quinton PM. (1983). Chloride impermeability in cystic fibrosis. *Nature* **301,** 421-422.

Quinton PM. (1999). Physiological basis of cystic fibrosis: a historical perspective. *Physiological Reviews* **79,** S3-S22.

Quon BS & Rowe SM. (2016). New and emerging targeted therapies for cystic fibrosis. *BMJ* **352,** i859 1-14.

Ramalho AS, Beck S, Meyer M, Penque D, Cutting GR & Amaral MD. (2002). Five percent of normal cystic fibrosis transmembrane conductance regulator mRNA ameliorates the severity of pulmonary disease in cystic fibrosis. *American Journal of Respiratory Cell and Molecular Biology* **27,** 619-627.

Ramsey BW, Davies J, McElvaney NG, Tullis E, Bell SC, Drevinek P, Griese M, McKone EF, Wainwright CE, Konstan MW, Moss R, Ratjen F, Sermet-Gaudelus I, Rowe SM, Dong Q, Rodriguez S, Yen K, Ordonez C, Elborn JS & Grp VXS. (2011). A CFTR Potentiator in Patients with Cystic Fibrosis and the G551D Mutation. *New England Journal of Medicine* **365,** 1663-1672.

Ramsey BW & Welsh MJ. (2017). Progress along the pathway of discovery leading to treatment and cure of cystic fibrosis. *American Journal of Respiratory and Critical Care Medicine* **195,** 1092-1099.

Ratjen F, Bell SC, Rowe SM, Goss CH, Quittner AL & Bush A. (2015). Cystic fibrosis. *Nature Reviews Disease Primers* **1,** 15010.

Ren HY, Grove DE, De La Rosa O, Houck SA, Sopha P, Van Goor F, Hoffman BJ & Cyr DM. (2013). VX-809 corrects folding defects in cystic fibrosis transmembrane conductance regulator protein through action on membrane-spanning domain 1. *Molecular Biology of the Cell* **24,** 3016-3024.

Riordan JR, Rommens JM, Kerem BS, Alon N, Rozmahel R, Grzelczak Z, Zielenski J, Lok S, Plavsic N, Chou JL, Drumm ML, Iannuzzi MC, Collins FS & Tsui LC. (1989). Identification of the cystic-fibrosis gene - cloning and characterization of complementary-DNA. *Science* **245,** 1066-1072.

Rogers CS, Hao Y, Rokhlina T, Samuel M, Stoltz DA, Li Y, Petroff E, Vermeer DW, Kabel AC, Yan Z, Spate L, Wax D, Murphy CN, Rieke A, Whitworth K, Linville ML, Korte SW, Engelhardt JF, Welsh MJ & Prather RS. (2008a). Production of CFTR-null and CFTR-ΔF508 heterozygous pigs by adeno-associated virus-mediated gene targeting and somatic cell nuclear transfer. *The Journal of Clinical Investigation* **118,** 1571-1577.

Rogers CS, Stoltz DA, Meyerholz DK, Ostedgaard LS, Rokhlina T, Taft PJ, Rogan MP, Pezzulo AA, Karp PH, Itani OA, Kabel AC, Wohlford-Lenane CL, Davis GJ, Hanfland RA, Smith TL, Samuel M, Wax D, Murphy CN, Rieke A, Whitworth K, Uc A, Starner TD, Brogden KA, Shilyansky J, McCray PB, Jr., Zabner J, Prather RS & Welsh MJ. (2008b). Disruption of the CFTR gene produces a model of cystic fibrosis in newborn pigs. *Science* **321,** 1837-1841.

Romeo G, Devoto M & Galietta LJV. (1989). Why is the cystic-fibrosis gene so frequent. *Human Genetics* **84,** 1-5.

Rowe SM, Miller S & Sorscher EJ. (2005). Mechanisms of disease: Cystic fibrosis. *New England Journal of Medicine* **352,** 1992-2001.

Saint-Criq V & Gray M. (2017). Role of CFTR in epithelial physiology. *Cellular and Molecular Life Sciences* **74,** 93-115.

Schultz BD, Frizzell RA & Bridges RJ. (1999). Rescue of dysfunctional ΔF508-CFTR chloride channel activity by IBMX. *Journal of Membrane Biology* **170,** 51-66.

Schwank G, Koo BK, Sasselli V, Dekkers JF, Heo I, Demircan T, Sasaki N, Boymans S, Cuppen E, van der Ent CK, Nieuwenhuis EE, Beekman JM & Clevers H. (2013). Functional Repair of CFTR by CRISPR/Cas9 in Intestinal Stem Cell Organoids of Cystic Fibrosis Patients. *Cell Stem Cell* **13,** 653-658.

Scott-Ward TS, Cai Z, Dawson ES, Doherty A, Da Paula AC, Davidson H, Porteous DJ, Wainwright BJ, Amaral MD, Sheppard DN & Boyd AC. (2007). Chimeric constructs endow the human CFTR Cl^- channel with the gating behavior of murine CFTR. *Proceedings of the National Academy of Sciences of the United States of America* **104,** 16365-16370.

Seavilleklein G, Amer N, Evagelidis A, Chappe F, Irvine T, Hanrahan JW & Chappe V. (2008). PKC phosphorylation modulates PKA-dependent binding of the R domain to other domains of CFTR. *American Journal of Physiology Cell Physiology* **295,** C1366-C1375.

Sebastian A, Rishishwar L, Wang J, Bernard KF, Conley AB, McCarty NA & King Jordan I. (2013). Origin and evolution of the cystic fibrosis transmembrane regulator protein R domain. *Gene* **523,** 137-146.

Senior AE & Gadsby DC. (1997). ATP hydrolysis cycles and mechanism in P-glycoprotein and CFTR, *Seminars in Cancer Biology* **8,** 3: 143-150.

Serohijos AWR, Hegedus T, Aleksandrov AA, He L, Cui L, Dokholyan NV & Riordan JR. (2008). Phenylalanine-508 mediates a cytoplasmic-membrane domain contact in the CFTR 3D structure crucial to assembly and channel function. *Proceedings of the National Academy of Sciences of the United States of America* **105,** 3256-3261.

Shamsuddin A & Quinton P. (2012). Surface fluid absorption and secretion in small airways. *Journal of Physiology* **590,** 3561-3574.

Shamsuddin AKM & Quinton PM. (2014). Native small airways secrete bicarbonate. *American Journal of Respiratory Cell and Molecular Biology* **50,** 796-804.

Shan J, Huang J, Liao J, Robert R & Hanrahan JW. (2011). Anion secretion by a model epithelium: more lessons from Calu-3. *Acta Physiologica (Oxford, England)* **202,** 523-531.

Sheppard D, Ostedgaard L, Winter MC & Welsh M. (1995). Mechanism of dysfunction of two nucleotide-binding domain mutations in cystic-fibrosis transmembrane conductance regulator that are associated with pancreatic sufficiency. *EMBO J* **14,** 876-883.

Sheppard DN, Bear CE & de Jonge HR. (2017). Editorial overview: Respiratory: Transformational therapies for cystic fibrosis. *Current Opinion in Pharmacology* **34** pp. 8-11.

Sheppard DN, Gray MA, Gong X, Sohma Y, Kogan I, Benos DJ, Scott-Ward TS, Chen J-H, Li H, Cai Z, Gupta J, Li C, Ramjeesingh M, Berdiev BK, Ismailov II, Bear CE, Hwang T-C, Linsdell P & Hug MJ. (2004). The patch-clamp and planar lipid bilayer techniques: powerful and versatile tools to investigate the CFTR Cl^- channel. *Journal of Cystic Fibrosis* **3 Suppl 2,** 101-108.

Sheppard DN, Rich DP, Ostedgaard LS, Gregory RJ, Smith AE & Welsh MJ. (1993). Mutations in CFTR associated with mild-disease-form Cl^- channels with altered pore properties. *Nature* **362,** 160-164.

Sheppard DN & Robinson KA. (1997). Mechanism of glibenclamide inhibition of cystic fibrosis transmembrane conductance regulator Cl^- channels expressed in a murine cell line. *Journal of Physiology* **503,** 333-346.

Sheppard DN & Welsh MJ. (1999). Structure and function of the CFTR chloride channel. *Physiological Reviews* **79,** S23-S45.

Silvis MR, Picciano JA, Bertrand C, Weixel K, Bridges RJ & Bradbury NA. (2003). A mutation in the cystic fibrosis transmembrane conductance regulator generates a novel internalization sequence and enhances endocytic rates. *Journal of Biological Chemistry* **278,** 11554-11560.

Singer TD, Tucker SJ, Marshall WS & Higgins CF. (1998). A divergent CFTR homologue: highly regulated salt transport in the euryhaline teleost F-heteroclitus. *American Journal of Physiology-Cell Physiology* **274,** C715-C723.

Skou JC. (1957). The influence of some cations on an adenosine triphosphatase from peripheral nerves. *Biochimica et Biophysica Acta* **23,** 394-401.

Skou JC. (1965). Enzymatic basis for active transport of Na^+ and K^+ across cell membrane. *Physiological Reviews* **45,** 596-617.

Skou JC. (1998). The identification of the sodium pump. *Bioscience Reports* **18,** 155-169.

Smith PC, Karpowich N, Millen L, Moody JE, Rosen J, Thomas PJ & Hunt JF. (2002). ATP binding to the motor domain from an ABC transporter drives formation of a nucleotide sandwich dimer. *Molecular Cell* **10,** 139-149.

Snouwaert JN, Brigman KK, Latour AM, Malouf NN, Boucher RC, Smithies O & Koller BH. (1992). An Animal Model for Cystic Fibrosis Made by Gene Targeting. *Science* **257,** 1083-1088.

Sorum B, Czege D & Csanady L. (2015). Timing of CFTR Pore Opening and Structure of Its Transition State. *Cell* **163,** 724-733.

Sorum B, Töröcsik B & Csanády L. (2017). Asymmetry of movements in CFTR's two ATP sites during pore opening serves their distinct functions. *eLife* **6**, 1-17.

Stahl M, Stahl K, Brubacher MB & Forrest JN, Jr. (2012). Divergent CFTR orthologs respond differently to the channel inhibitors $CFTR_{inh}$-172, glibenclamide, and GlyH-101. *American Journal of Physiology-Cell Physiology* **302,** C67-C76.

Stoltz DA, Meyerholz DK & Welsh MJ. (2015). Origins of Cystic Fibrosis Lung Disease. *The New England Journal of Medicine* **372,** 351-362.

Stutts MJ, Canessa CM, Olsen JC, Hamrick M, Cohn JA, Rossier BC & Boucher RC. (1995). CFTR as a cAMP-dependent regulator of sodium-channels. *Science* **269,** 847-850.

Sun X, Sui H, Fisher JT, Yan Z, Liu X, Cho H-J, Joo NS, Zhang Y, Zhou W, Yi Y, Kinyon JM, Lei-Butters DC, Griffin MA, Naumann P, Luo M, Ascher J, Wang K, Frana T, Wine JJ, Meyerholz DK & Engelhardt JF. (2010). Disease phenotype of a ferret CFTR-knockout model of cystic fibrosis. *Journal of Clinical Investigation* **120,** 3149-3160.

Taylor-Cousar JL, Munck A, McKone EF, van der Ent CK, Moeller A, Simard C, Wang LT, Ingenito EP, McKee C, Lu Y, Lekstrom-Himes J & Elborn JS. (2017). Tezacaftor–Ivacaftor in Patients with Cystic Fibrosis Homozygous for Phe508del. *The New England Journal of Medicine* **377,** 2013-2023.

Thibodeau PH, Richardson JM, Wang W, Millen L, Watson J, Mendoza JL, Du K, Fischman S, Senderowitz H, Lukacs GL, Kirk K & Thomas PJ. (2010). The cystic fibrosis-causing mutation ΔF508 affects multiple steps in cystic fibrosis transmembrane conductance regulator biogenesis. *The Journal of Biological Chemistry* **285,** 35825-35835.

Tuggle KL, Birket SE, Cui X, Hong J, Warren J, Reid L, Chambers A, Ji D, Gamber K, Chu KK, Tearney G, Tang LP, Fortenberry JA, Du M, Cadillac JM, Bedwell DM, Rowe SM, Sorscher EJ & Fanucchi MV. (2014). Characterization of Defects in Ion Transport and Tissue Development in Cystic Fibrosis Transmembrane Conductance Regulator (CFTR)-Knockout Rats. *Plos One* **9(3)** e91253.

Urnov FD, Miller JC, Lee YL, Beausejour CM, Rock JM, Augustus S, Jamieson AC, Porteus MH, Gregory PD, Holmes MC. (2005). Highly efficient endogenous human gene correction using designed zinc- finger nucleases. *Nature* **435,** 646-651.

Van Goor F, Hadida S, Grootenhuis PDJ, Burton B, Cao D, Neuberger T, Turnbull A, Singh A, Joubran J, Hazlewood A, Zhou J, McCartney J, Arumugam V, Decker C, Yang J, Young C, Olson ER, Wine JJ, Frizzell RA, Ashlock M & Negulescu P. (2009). Rescue of CF airway epithelial cell function in vitro by a CFTR potentiator, VX-770. *Proceedings of the National Academy of Sciences of the United States of America* **106,** 18825-18830.

Van Goor F, Hadida S, Grootenhuis PDJ, Burton B, Stack JH, Straley KS, Decker CJ, Miller M, McCartney J, Olson ER, Wine JJ, Frizzell RA, Ashlock M & Negulescu PA. (2011). Correction of the F508del-CFTR protein processing defect in vitro by the investigational drug VX-809. *Proceedings of the National Academy of Sciences of the United States of America* **108,** 18843-18848.

Veit G, Avramescu RG, Chiang AN, Houck SA, Cai Z, Peters KW, Hong JS, Pollard HB, Guggino WB, Balch WE, Skach WR, Cutting GR, Frizzell RA, Sheppard DN, Cyr DM, Sorscher EJ, Brodsky JL, Lukacs GL & Drubin DG. (2016). From CFTR biology toward combinatorial pharmacotherapy: expanded classification of cystic fibrosis mutations. *Molecular Biology of the Cell* **27,** 424-433.

Vergani P, Basso C, Mense M, Nairn AC & Gadsby DC. (2005a). Control of the CFTR channel's gates. *Biochemical Society Transactions* **33,** 1003-1007.

Vergani P, Lockless SW, Nairn AC & Gadsby DC. (2005b). CFTR channel opening by ATP-driven tight dimerization of its nucleotide-binding domains. *Nature* **433,** 876-880.

Vergani P, Nairn AC & Gadsby DC. (2003). On the Mechanism of MgATP-dependent Gating of CFTR Cl^- Channels. *Journal of General Physiology* **121,** 17-36.

Wainwright CE, Elborn JS, Ramsey BW, Marigowda G, Huang X, Cipolli M, Colombo C, Davies JC, De Boeck K, Flume PA, Konstan MW, McColley SA, McCoy K, McKone EF, Munck A, Ratjen F, Rowe SM, Waltz D & Boyle MP. (2015). Lumacaftor–Ivacaftor in Patients with Cystic Fibrosis Homozygous for Phe508del CFTR. *The New England Journal of Medicine* **373,** 220-231.

Wang F, Zeltwanger S, Yang ICH, Nairn AC & Hwang TC. (1998). Actions of genistein on cystic fibrosis transmembrane conductance regulator channel gating: Evidence for two binding sites with opposite effects. *Journal of General Physiology* **111,** 477-490.

Wang W, Hiani YE & Linsdell P. (2011a). Alignment of transmembrane regions in the cystic fibrosis transmembrane conductance regulator chloride channel pore. *Journal of General Physiology* **138,** 165-178.

Wang W, Li G, Kirk KL & Clancy JP. (2005). Activating cystic fibrosis transmembrane conductance regulator channels with pore blocker analogs. *Journal of Biological Chemistry* **280,** 23622-23630.

Wang W & Linsdell P. (2012). Relative movements of transmembrane regions at the outer mouth of the cystic fibrosis transmembrane conductance regulator channel pore during channel gating. *Journal of Biological Chemistry* **287,** 32136-32146.

Wang W, Okeyo GO, Tao B, Hong JS & Kirk KL. (2011b). Thermally Unstable Gating of the Most Common Cystic Fibrosis Mutant Channel (ΔF508) "rescue" by suppressor mutations in nucleotide binding domain 1 and by constitutive mutations in the cytosolic loops. *Journal of Biological Chemistry* **286,** 41937-41948.

Wang Y, Cai Z, Gosling M & Sheppard D. (2018). Potentiation of the cystic fibrosis transmembrane conductance regulator Cl^- channel by ivacaftor is temperature-independent. *American Journal of Physiology-Lung Cellular and Molecular Physiology* **315,** L846-L857.

Wang Y, Liu J, Loizidou A, Bugeja LA, Warner R, Hawley BR, Cai Z, Toye AM, Sheppard DN & Li H. (2014a). CFTR potentiators partially restore channel function to A561E-CFTR, a cystic fibrosis mutant with a similar mechanism of dysfunction as F508del-CFTR. *British Journal of Pharmacology* **171,** 4490-4503.

Wang Y, Wrennall JA, Cai ZW, Li HY & Sheppard DN. (2014b). Understanding how cystic fibrosis mutations disrupt CFTR function: From single molecules to animal models. *International Journal of Biochemistry & Cell Biology* **52,** 47-57.

Ward A, Reyes CL, Yu J, Roth CB & Chang G. (2007). Flexibility in the ABC transporter MsbA: Alternating access with a twist. *Proceedings of the National Academy of Sciences of the United States of America* **104,** 19005-19010.

Ward CL & Kopito RR. (1994). Intracellular turnover of cystic fibrosis transmembrane conductance regulator. Inefficient processing and rapid degradation of wild-type and mutant proteins. *Journal of Biological Chemistry* **269,** 25710-25718.

Ward CL, Omura S & Kopito RR. (1995). Degradation of CFTR by the ubiquitin-proteasome pathway. *Cell* **83,** 121-127.

Welsh MJ & Smith AE. (1993). Molecular mechanisms of CFTR chloride channel dysfunction in cystic fibrosis. *Cell* **73,** 1251-1254.

Wilke M, Buijs-Offerman RM, Aarbiou J, Colledge WH, Sheppard DN, Touqui L, Bot A, Jorna H, de Jonge HR & Scholte BJ. (2011). Mouse models of cystic fibrosis: Phenotypic analysis and research applications. *Journal of Cystic Fibrosis* **10,** S152-S171.

Wong MK-S, Pipil S, Kato A & Takei Y. (2016). Duplicated CFTR isoforms in eels diverged in regulatory structures and osmoregulatory functions. *Comparative Biochemistry and Physiology, Part A* **199,** 130-141.

Xu J, Rajagopolan C, Hou X, Chen E, Boucher RC & Sun F. (2016). Rabbit models for cystic fibrosis. *Pediatric Pulmonology Supplement* **51,** 158-159.

Yeh H-I, Sohma Y, Conrath K & Hwang T-C. (2017). A common mechanism for CFTR potentiators. *Journal of General Physiology* **149,** 1105-1118.

Yeh H-I, Yeh J-T & Hwang T-C. (2015). Modulation of CFTR gating by permeant ions. *Journal of General Physiology* **145,** 47-60.

Zamecnik PC, Raychowdhury MK, Tabatadze DR & Cantiello HF. (2004). Reversal of Cystic Fibrosis Phenotype in a Cultured ΔF508 Cystic Fibrosis Transmembrane Conductance Regulator Cell Line by Oligonucleotide Insertion. *Proceedings of the National Academy of Sciences of the United States of America* **101,** 8150-8155.

Zerbino DR, Achuthan P, Akanni W, Amode MR, Barrell D, Bhai J, Billis K, Cummins C, Gall A, Girón CG, Gil L, Gordon L, Haggerty L, Haskell E, Hourlier T, Izuogu OG, Janacek SH, Juettemann T, To JK, Laird MR, Lavidas I, Liu Z, Loveland JE, Maurel T, McLaren W, Moore B, Mudge J, Murphy DN, Newman V, Nuhn M, Ogeh D, Ong CK, Parker A, Patricio M, Riat HS, Schuilenburg H, Sheppard D, Sparrow H, Taylor K, Thormann A, Vullo A, Walts B, Zadissa A, Frankish A, Hunt SE, Kostadima M, Langridge N, Martin FJ, Muffato M, Perry E, Ruffier M, Staines DM, Trevanion SJ, Aken BL, Cunningham F, Yates A & Flicek P. (2018). Ensembl 2018. *Nucleic acids research* **46,** D754-761.

Zhang Z & Chen J. (2016). Atomic Structure of the Cystic Fibrosis Transmembrane Conductance Regulator. *Cell* **167,** 1586-1597.

Zhang Z, Liu F & Chen J. (2017). Conformational Changes of CFTR upon Phosphorylation and ATP Binding. *Cell* **170,** 483-491.

Zhou J-J, Li M-S, Qi J & Linsdell P. (2010). Regulation of conductance by the number of fixed positive charges in the intracellular vestibule of the CFTR chloride channel pore. *Journal of General Physiology* **135,** 229-245.

Zhou L, Dey CR, Wert SE, Duvall MD, Frizzell RA & Whitsett JA. (1994). Correction of Lethal Intestinal Defect in a Mouse Model of Cystic Fibrosis by Human CFTR. *Science* **266,** 1705-1708.

Zhou Z, Duerr J, Johannesson B, Schubert SC, Treis D, Harm M, Graeber SY, Dalpke A, Schultz C & Mall MA. (2011). The ENaC-overexpressing mouse as a model of cystic fibrosis lung disease. *Journal of Cystic Fibrosis* **10,** S172-S182.

Zhou Z, Wang X, Li M, Sohma Y, Zou X & Hwang TC. (2005). High affinity ATP/ADP analogues as new tools for studying CFTR gating. *Journal of Physiology* **569,** 447-457.

Zielenski J & Tsui LC. (1995). Cystic fibrosis: genotypic and phenotypic variations. *Annual Review of Genetics* **29,** 777-807.

Appendices

Appendix 1: Sequence alignment of studied CFTR orthologues

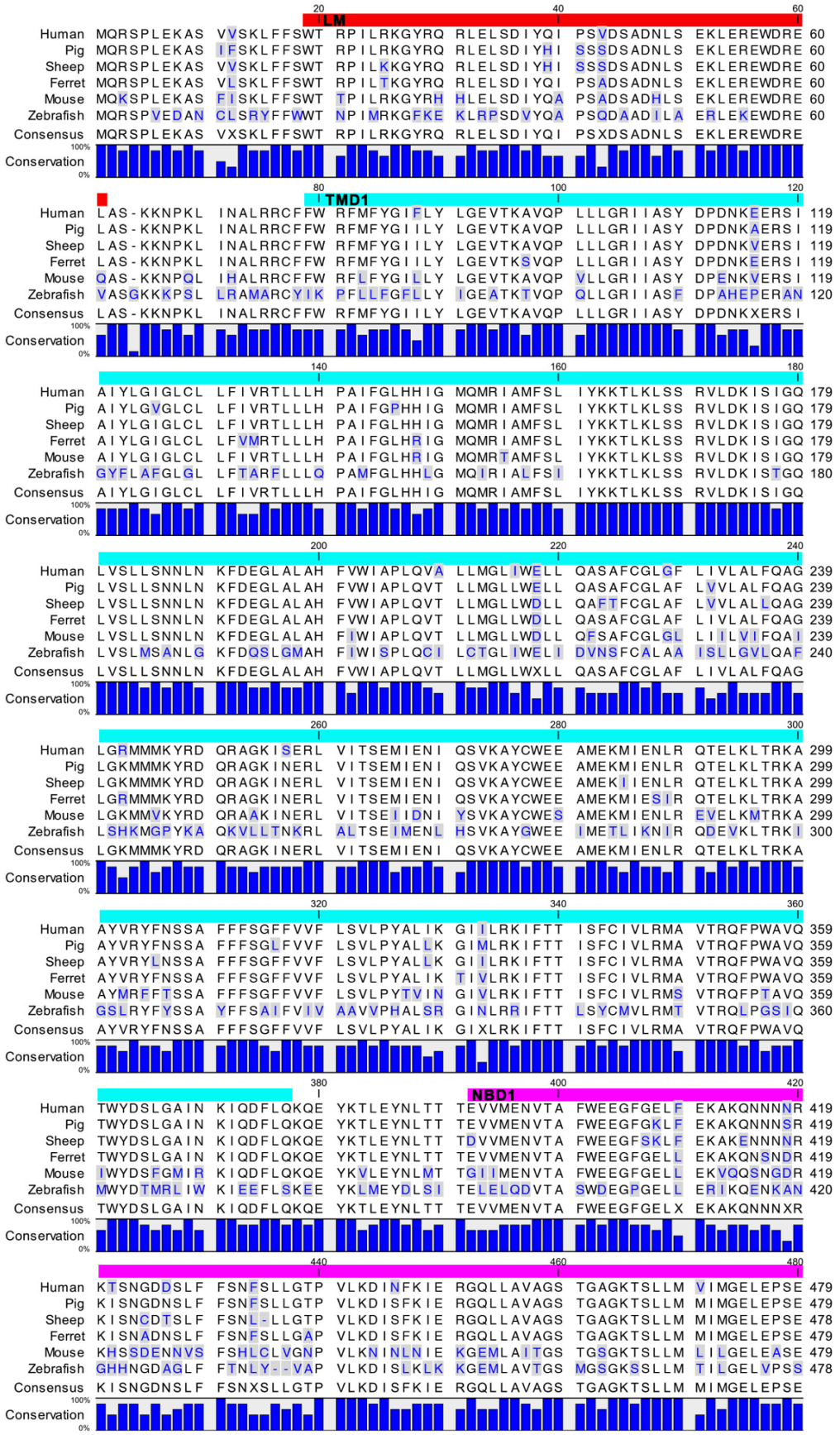

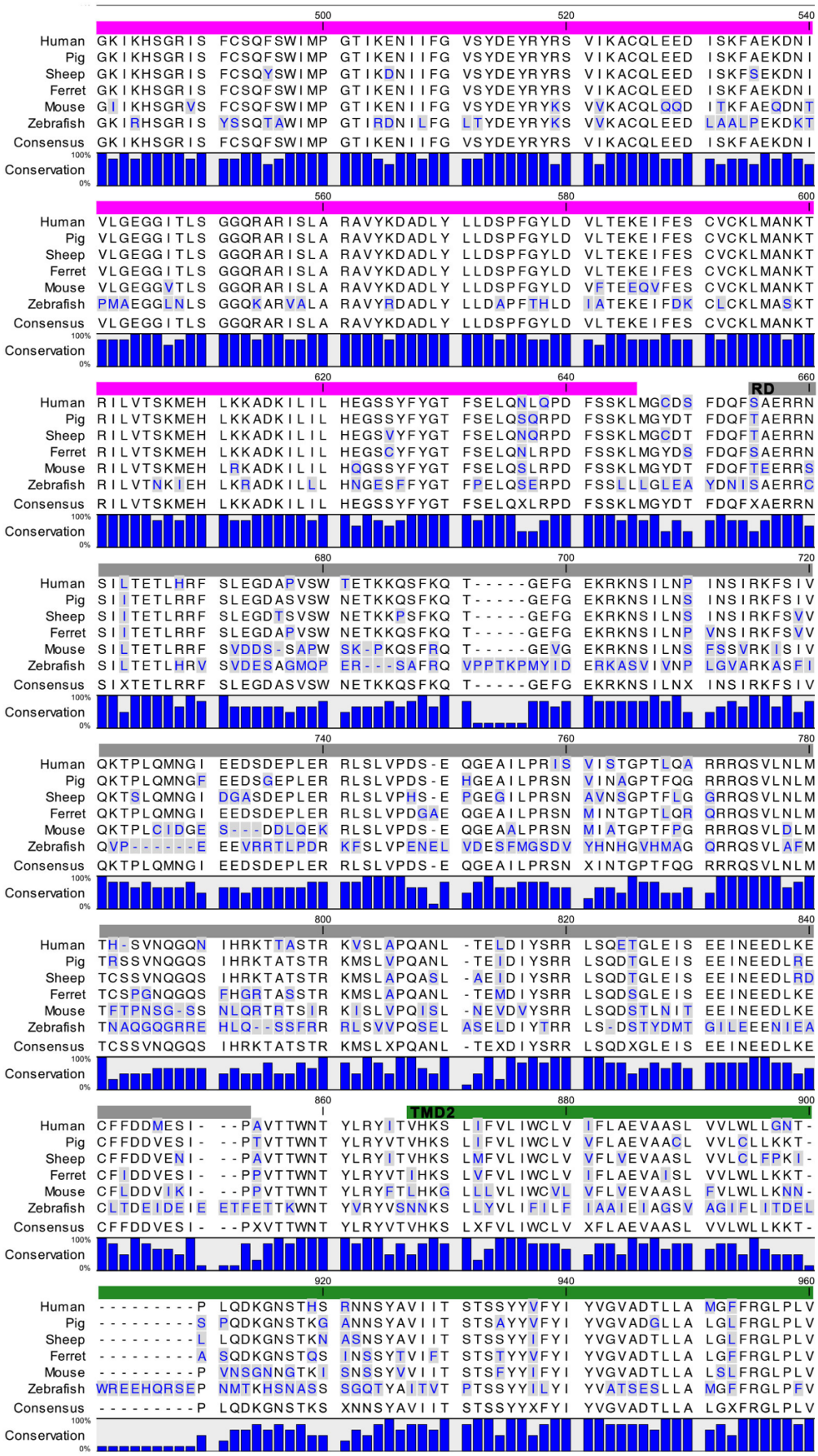
500
520
540
Human GKIKHSGRIS FCSQFSWIMP GTIKENIIFG VSYDEYRYRS VIKACQLEED ISKFAEKDNI 539
Pig GKIKHSGRIS FCSQFSWIMP GTIKENIIFG VSYDEYRYRS VIKACQLEED ISKFAEKDNI 539
Sheep GKIKHSGRIS FCSQYSWIMP GTIKDNIIFG VSYDEYRYRS VIKACQLEED ISKFSEKDNI 538
Ferret GKIKHSGRIS FCSQFSWIMP GTIKENIIFG VSYDEYRYRS VIKACQLEED ISKFAEKDNI 539
Mouse GIIKHSGRVS FCSQFSWIMP GTIKENIIFG VSYDEYRYKS VVKACQLQQD ITKFAEQDNT 539
Zebrafish GKIRHSGRIS YSSQTAWIMP GTIRDNILFG LTYDEYRYKS VVKACQLEED LAALPEKDKT 538
Consensus GKIKHSGRIS FCSQFSWIMP GTIKENIIFG VSYDEYRYRS VIKACQLEED ISKFAEKDNI
100%
Conservation
0%
560
580
600
Human VLGEGGITLS GGQRARISLA RAVYKDADLY LLDSPFGYLD VLTEKEIFES CVCKLMANKT 599
Pig VLGEGGITLS GGQRARISLA RAVYKDADLY LLDSPFGYLD VLTEKEIFES CVCKLMANKT 599
Sheep VLGEGGITLS GGQRARISLA RAVYKDADLY LLDSPFGYLD VLTEKEIFES CVCKLMANKT 598
Ferret VLGEGGITLS GGQRARISLA RAVYKDADLY LLDSPFGYLD VLTEKEIFES CVCKLMANKT 599
Mouse VLGEGGVTLS GGQRARISLA RAVYKDADLY LLDSPFGYLD VFTEEQVFES CVCKLMANKT 599
Zebrafish PMAEGGLNLS GGQKARVALA RAVYRDADLY LLDAPFTHLD IATEKEIFDK CLCKLMASKT 598
Consensus VLGEGGITLS GGQRARISLA RAVYKDADLY LLDSPFGYLD VLTEKEIFES CVCKLMANKT
100%
Conservation
0%
620
640
660
RD
Human RILVTSKMEH LKKADKILIL HEGSSYFYGT FSELQNLQPD FSSKLMGCDS FDQFSAERRN 659
Pig RILVTSKMEH LKKADKILIL HEGSSYFYGT FSELQSQRPD FSSKLMGYDT FDQFTAERRN 659
Sheep RILVTSKMEH LKKADKILIL HEGSVYFYGT FSELQNQRPD FSSKLMGCDT FDQFTAERRN 658
Ferret RILVTSKMEH LKKADKILIL HEGSCYFYGT FSELQNLRPD FSSKLMGYDS FDQFSAERRN 659
Mouse RILVTSKMEH LRKADKILIL HQGSSYFYGT FSELQSLRPD FSSKLMGYDT FDQFTEERRS 659
Zebrafish RILVTNKIEH LKRADKILLL HNGESFFYGT FPELQSERPD FSSLLLGLEA YDNISAERRC 658
Consensus RILVTSKMEH LKKADKILIL HEGSSYFYGT FSELQXLRPD FSSKLMGYDT FDQFXAERRN
100%
Conservation
0%
680
700
720
Human SILTETLHRF SLEGDAPVSW TETKKQSFKQ T-----GEFG EKRKNSILNP INSIRKFSIV 714
Pig SIITETLRRF SLEGDASVSW NETKKQSFKQ T-----GEFG EKRKNSILNS INSIRKFSIV 714
Sheep SIITETLRRF SLEGDTSVSW NETKKPSFKQ T-----GEFG EKRKNSILNS INSIRKFSVV 713
Ferret SIITETLRRF SLEGDAPVSW NETKKQSFKQ T-----GEFG EKRKNSILNP VNSIRKFSVV 714
Mouse SILTETLRRF SVDDS-SAPW SK-PKQSFRQ T-----GEVG EKRKNSILNS FSSVRKISIV 712
Zebrafish SILTETLHRV SVDESAGMQP ER---SAFRQ VPPTKPMYID ERKASVIVNP LGVARKASFI 715
Consensus SIXTETLRRF SLEGDASVSW NETKKQSFKQ T-----GEFG EKRKNSILNX INSIRKFSIV
100%
Conservation
0%
740
760
780
Human QKTPLQMNGI EEDSDEPLER RLSLVPDS-E QGEAILPRIS VISTGPTLQA RRRQSVLNLM 773
Pig QKTPLQMNGF EEDSGEPLER RLSLVPDS-E HGEAILPRSN VINAGPTFQG RRRQSVLNLM 773
Sheep QKTSLQMNGI DGASDEPLER RLSLVPHS-E PGEGILPRSN AVNSGPTFLG GRRQSVLNLM 772
Ferret QKTPLQMNGI EEDSDEPLER RLSLVPDGAE QGEAILPRSN MINTGPTLQR QRRQSVLNLM 774
Mouse QKTPLCIDGE S---DDLQEK RLSLVPDS-E QGEAALPRSN MIATGPTFPG RRRQSVLDLM 768
Zebrafish QVP-------E EEVRRTLPDR KFSLVPENEL VDESFMGSDV YHNHGVHMAG QRRQSVLAFM 769
Consensus QKTPLQMNGI EEDSDEPLER RLSLVPDS-E QGEAILPRSN XINTGPTFQG RRRQSVLNLM
100%
Conservation
0%
800
820
840
Human TH-SVNQGQN IHRKTTASTR KVSLAPQANL -TELDIYSRR LSQETGLEIS EEINEEDLKE 831
Pig TRSSVNQGQS IHRKTATSTR KMSLVPQANL -TEIDIYSRR LSQDTGLEIS EEINEEDLRE 832
Sheep TCSSVNQGQS IHRKTATSTR KMSLAPQASL -AEIDIYSRR LSQDTGLEIS EEINEEDLRD 831
Ferret TCSPGNQGQS FHGRTASSTR KMSLAPQANL -TEMDIYSRR LSQDSGLEIS EEINEEDLKE 833
Mouse TFTPNSG-SS NLQRTRTSIR KISLVPQISL -NEVDVYSRR LSQDSTLNIT EEINEEDLKE 826
Zebrafish TNAQGQGRRE HLQ--SSFRR RLSVVPQSEL ASELDIYTRR LS-DSTYDMT GILEEENIEA 826
Consensus TCSSVNQGQS IHRKTATSTR KMSLXPQANL -TEXDIYSRR LSQDXGLEIS EEINEEDLKE
100%
Conservation
0%
860
880
900
TMD2
Human CFFDDMESI- --PAVTTWNT YLRYITVHKS LIFVLIWCLV IFLAEVAASL VVLWLLGNT- 887
Pig CFFDDVESI- --PTVTTWNT YLRYVTVHKS LIFVLIWCLV VFLAEVAACL VVLCLLKKT- 888
Sheep CFFDDVENI- --PAVTTWNT YLRYITVHKS LMFVLIWCLV VFLVEVAASL VVLCLFPKI- 887
Ferret CFIDDVESI- --PPVTTWNT YLRYVTIHKS LVFVLIWCLV IFLAEVAISL VVLWLLKKT- 889
Mouse CFLDDVIKI- --PPVTTWNT YLRYFTLHKG LLLVLIWCVL VFLVEVAASL FVLWLLKNN- 882
Zebrafish CLTDEIDEIE ETFETTKWNT YVRYVSNNKS LLYVLIFILF IAAIEIAGSV AGIFLITDEL 886
Consensus CFFDDVESI- --PXVTTWNT YLRYVTVHKS LXFVLIWCLV XFLAEVAASL VVLWLLKKT-
100%
Conservation
0%
920
940
960
Human ----------P LQDKGNSTHS RNNSYAVIIT STSSYYVFYI YVGVADTLLA MGFFRGLPLV 938
Pig ----------S PQDKGNSTKG ANNSYAVIIT STSAYYVFYI YVGVADGLLA LGLFRGLPLV 939
Sheep ----------L LQDKGNSTKN ASNSYAVIIT STSSYYIFYI YVGVADTLLA LGLFRGLPLV 938
Ferret ----------A SQDKGNSTQS INSSYTVIFT STSTYYVFYI YVGVADTLLA LGFFRGLPLV 940
Mouse ----------P VNSGNNGTKI SNSSYVVIIT STSFYYIFYI YVGVADTLLA LSLFRGLPLV 933
Zebrafish WREEHQRSEP NMTKHSNASS SGQTYAITVT PTSSYYILYI YVATSESLLA MGFFRGLPFV 946
Consensus ----------P LQDKGNSTKS XNNSYAVIIT STSSYYXFYI YVGVADTLLA LGXFRGLPLV
100%
Conservation
0%

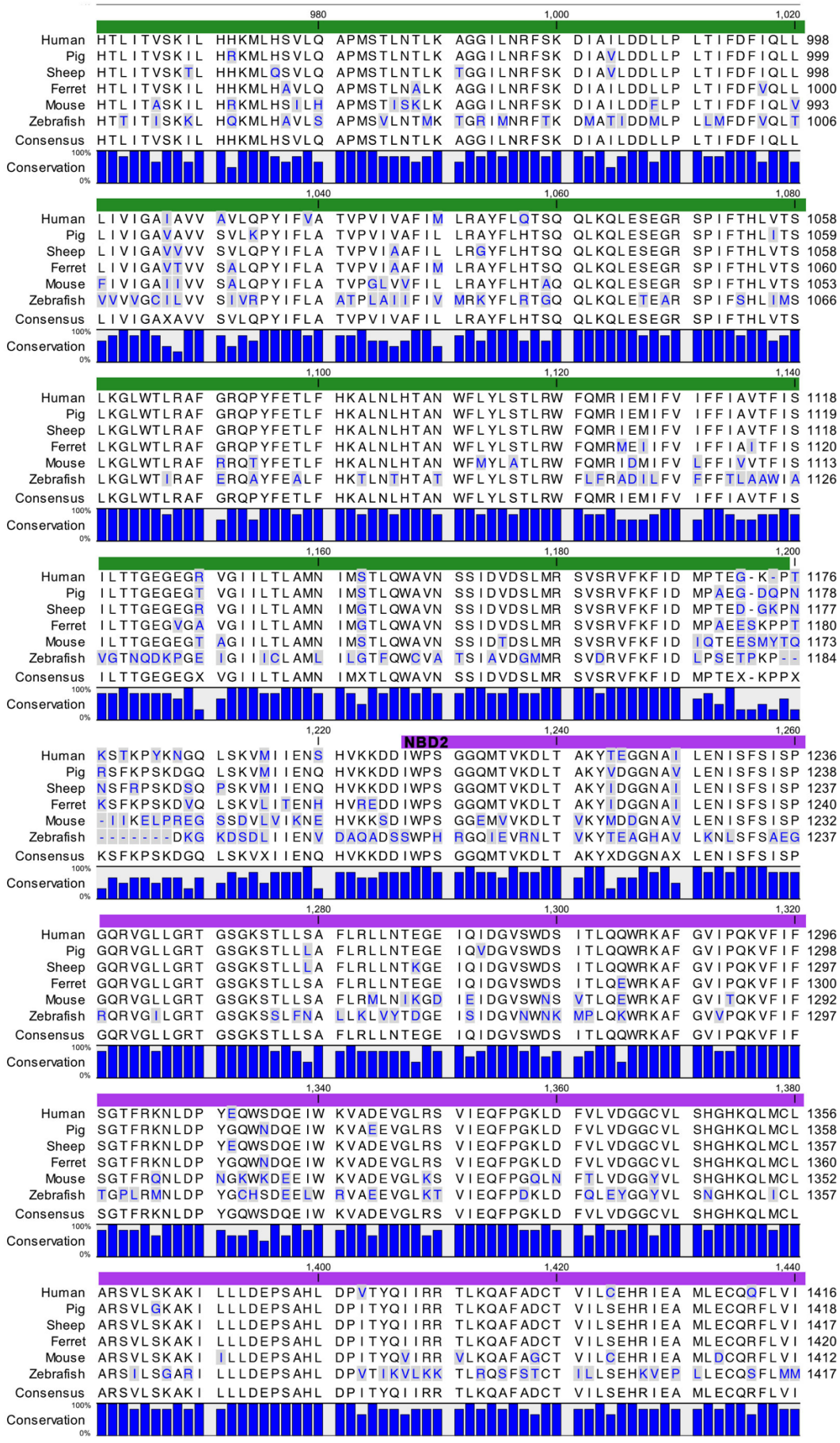
980
1,000
1,020
Human HTLITVSKIL HHKMLHSVLQ APMSTLNTLK AGGILNRFSK DIAILDDLLP LTIFDFIQLL 998
Pig HTLITVSKIL HRKMLHSVLQ APMSTLNTLK AGGILNRFSK DIAVLDDLLP LTIFDFIQLL 999
Sheep HTLITVSKTL HHKMLQSVLQ APMSTLNTLK TGGILNRFSK DIAVLDDLLP LTIFDFIQLL 998
Ferret HTLITVSKIL HHKMLHAVLQ APMSTLNALK AGGILNRFSK DIAILDDLLP LTIFDFVQLL 1000
Mouse HTLITASKIL HRKMLHSILH APMSTISKLK AGGILNRFSK DIAILDDFLP LTIFDFIQLV 993
Zebrafish HTTITISKKL HQKMLHAVLS APMSVLNTMK TGRIMNRFTK DMATIDDMLP LLMFDFVQLT 1006
Consensus HTLITVSKIL HHKMLHSVLQ APMSTLNTLK AGGILNRFSK DIAILDDLLP LTIFDFIQLL
100%
Conservation
0%
1,040
1,060
1,080
Human LIVIGAIAVV AVLQPYIFVA TVPVIVAFIM LRAYFLQTSQ QLKQLESEGR SPIFTHLVTS 1058
Pig LIVIGAVAVV SVLKPYIFLA TVPVIVAFIL LRAYFLHTSQ QLKQLESEGR SPIFTHLITS 1059
Sheep LIVIGAVVVV SVLQPYIFLA TVPVIAAFIL LRGYFLHTSQ QLKQLESEGR SPIFTHLVTS 1058
Ferret LIVIGAVTVV SALQPYIFLA TVPVIAAFIM LRAYFLHTSQ QLKQLESEGR SPIFTHLVTS 1060
Mouse FIVIGAIIVV SALQPYIFLA TVPGLVVFIL LRAYFLHTAQ QLKQLESEGR SPIFTHLVTS 1053
Zebrafish VVVVGCILVV SIVRPYIFLA ATPLAIIFIV MRKYFLRTGQ QLKQLETEAR SPIFSHLIMS 1066
Consensus LIVIGAXAVV SVLQPYIFLA TVPVIVAFIL LRAYFLHTSQ QLKQLESEGR SPIFTHLVTS
100%
Conservation
0%
1,100
1,120
1,140
Human LKGLWTLRAF GRQPYFETLF HKALNLHTAN WFLYLSTLRW FQMRIEMIFV IFFIAVTFIS 1118
Pig LKGLWTLRAF GRQPYFETLF HKALNLHTAN WFLYLSTLRW FQMRIEMIFV IFFIAVTFIS 1119
Sheep LKGLWTLRAF GRQPYFETLF HKALNLHTAN WFLYLSTLRW FQMRIEMIFV IFFIAVTFIS 1118
Ferret LKGLWTLRAF GRQPYFETLF HKALNLHTAN WFLYLSTLRW FQMRMEIIFV IFFIAITFIS 1120
Mouse LKGLWTLRAF RRQTYFETLF HKALNLHTAN WFMYLATLRW FQMRIDMIFV LFFIVVTFIS 1113
Zebrafish LKGLWTIRAF ERQAYFEALF HKTLNTHTAT WFLYLSTLRW FLFRADILFV FFFTLAAWIA 1126
Consensus LKGLWTLRAF GRQPYFETLF HKALNLHTAN WFLYLSTLRW FQMRIEMIFV IFFIAVTFIS
100%
Conservation
0%
1,160
1,180
1,200
Human ILTTGEGEGR VGIILTLAMN IMSTLQWAVN SSIDVDSLMR SVSRVFKFID MPTEG-K-PT 1176
Pig ILTTGEGEGT VGIILTLAMN IMSTLQWAVN SSIDVDSLMR SVSRVFKFID MPAEG-DQPN 1178
Sheep ILTTGEGEGR VGIILTLAMN IMGTLQWAVN SSIDVDSLMR SVSRVFKFID MPTED-GKPN 1177
Ferret ILTTGEGVGA VGIILTLAMN IMGTLQWAVN SSIDVDSLMR SVSRVFKFID MPAEESKPPT 1180
Mouse ILTTGEGEGT AGIILTLAMN IMSTLQWAVN SSIDTDSLMR SVSRVFKFID IQTEESMYTQ 1173
Zebrafish VGTNQDKPGE IGIIICLAML ILGTFQWCVA TSIAVDGMMR SVDRVFKFID LPSETPKP-- 1184
Consensus ILTTGEGEGX VGIILTLAMN IMXTLQWAVN SSIDVDSLMR SVSRVFKFID MPTEX-KPPX
100%
Conservation
0%
1,220
1,240
1,260
NBD2
Human KSTKPYKNGQ LSKVMIIENS HVKKDDIWPS GGQMTVKDLT AKYTEGGNAI LENISFSISP 1236
Pig RSFKPSKDGQ LSKVMIIENQ HVKKDDIWPS GGQMTVKDLT AKYVDGGNAV LENISFSISP 1238
Sheep NSFRPSKDSQ PSKVMIIENQ HVKKDDIWPS GGQMTVKDLT AKYIDGGNAI LENISFSISP 1237
Ferret KSFKPSKDVQ LSKVLITENH HVREDDIWPS GGQMTVKDLT AKYIDGGNAI LENISFSISP 1240
Mouse -IIKELPREG SSDVLVIKNE HVKKSDIWPS GGEMVVKDLT VKYMDDGNAV LENISFSISP 1232
Zebrafish --------DKG KDSDLIIENV DAQADSSWPH RGQIEVRNLT VKYTEAGHAV LKNLSFSAEG 1237
Consensus KSFKPSKDGQ LSKVXIIENQ HVKKDDIWPS GGQMTVKDLT AKYXDGGNAX LENISFSISP
100%
Conservation
0%
1,280
1,300
1,320
Human GQRVGLLGRT GSGKSTLLSA FLRLLNTEGE IQIDGVSWDS ITLQQWRKAF GVIPQKVFIF 1296
Pig GQRVGLLGRT GSGKSTLLLA FLRLLNTEGE IQVDGVSWDS ITLQQWRKAF GVIPQKVFIF 1298
Sheep GQRVGLLGRT GSGKSTLLLA FLRLLNTKGE IQIDGVSWDS ITLQQWRKAF GVIPQKVFIF 1297
Ferret GQRVGLLGRT GSGKSTLLSA FLRLLNTEGE IQIDGVSWDS ITLQEWRKAF GVIPQKVFIF 1300
Mouse GQRVGLLGRT GSGKSTLLSA FLRMLNIKGD IEIDGVSWNS VTLQEWRKAF GVITQKVFIF 1292
Zebrafish RQRVGILGRT GSGKSSLFNA LLKLVYTDGE ISIDGVNWNK MPLQKWRKAF GVVPQKVFIF 1297
Consensus GQRVGLLGRT GSGKSTLLSA FLRLLNTEGE IQIDGVSWDS ITLQQWRKAF GVIPQKVFIF
100%
Conservation
0%
1,340
1,360
1,380
Human SGTFRKNLDP YEQWSDQEIW KVADEVGLRS VIEQFPGKLD FVLVDGGCVL SHGHKQLMCL 1356
Pig SGTFRKNLDP YGQWNDQEIW KVAEEVGLRS VIEQFPGKLD FVLVDGGCVL SHGHKQLMCL 1358
Sheep SGTFRKNLDP YEQWSDQEIW KVADEVGLRS VIEQFPGKLD FVLVDGGCVL SHGHKQLMCL 1357
Ferret SGTFRKNLDP YGQWNDQEIW KVADEVGLRS VIEQFPGKLD FVLVDGGCVL SHGHKQLMCL 1360
Mouse SGTFRQNLDP NGKWKDEEIW KVADEVGLKS VIEQFPGQLN FTLVDGGYVL SHGHKQLMCL 1352
Zebrafish TGPLRMNLDP YGCHSDEELW RVAEEVGLKT VIEQFPDKLD FQLEYGGYVL SNGHKQLICL 1357
Consensus SGTFRKNLDP YGQWSDQEIW KVADEVGLRS VIEQFPGKLD FVLVDGGCVL SHGHKQLMCL
100%
Conservation
0%
1,400
1,420
1,440
Human ARSVLSKAKI LLLDEPSAHL DPVTYQIIRR TLKQAFADCT VILCEHRIEA MLECQQFLVI 1416
Pig ARSVLGKAKI LLLDEPSAHL DPITYQIIRR TLKQAFADCT VILSEHRIEA MLECQRFLVI 1418
Sheep ARSVLSKAKI LLLDEPSAHL DPITYQIIRR TLKQAFADCT VILSEHRIEA MLECQRFLVI 1417
Ferret ARSVLSKAKI LLLDEPSAHL DPITYQIIRR TLKQAFADCT VILSEHRIEA MLECQRFLVI 1420
Mouse ARSVLSKAKI ILLDEPSAHL DPITYQVIRR VLKQAFAGCT VILCEHRIEA MLDCQRFLVI 1412
Zebrafish ARSILSGARI LLLDEPSAHL DPVTIKVLKK TLRQSFSTCT ILLSEHKVEP LLECQSFLMM 1417
Consensus ARSVLSKAKI LLLDEPSAHL DPITYQIIRR TLKQAFADCT VILSEHRIEA MLECQRFLVI
100%
Conservation
0%

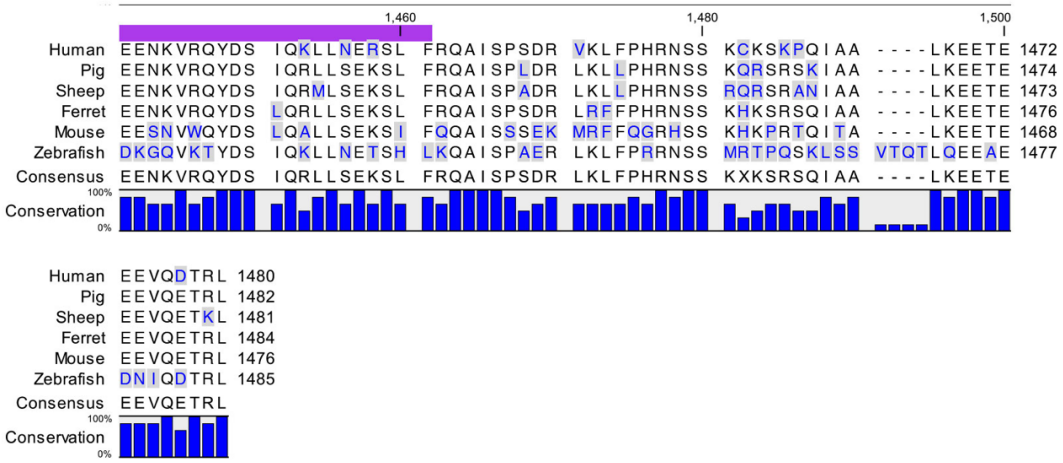

Coloured bars indicate boundaries of the lasso motif (LM, red), TMD1 (cyan), NBD1 (magenta), RD (grey), TMD2 (green) and NBD2 (purple). Blue bars represent percentage sequence conservation for each residue. Constructed by ClustalO alignment using CLC Sequence Viewer v7.5 (Qiagen).

Appendix 2: Sequence alignment of human-mouse CFTR chimeras

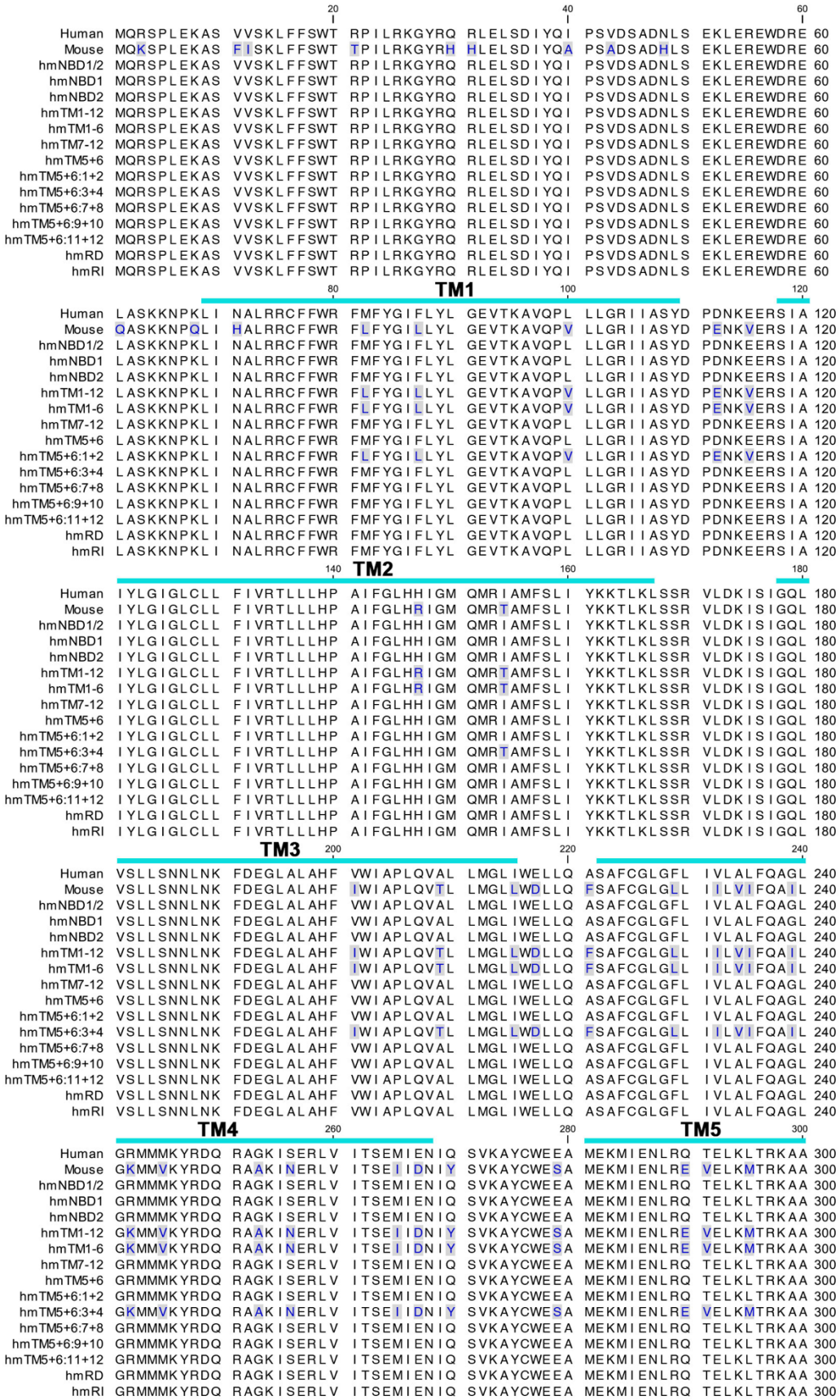

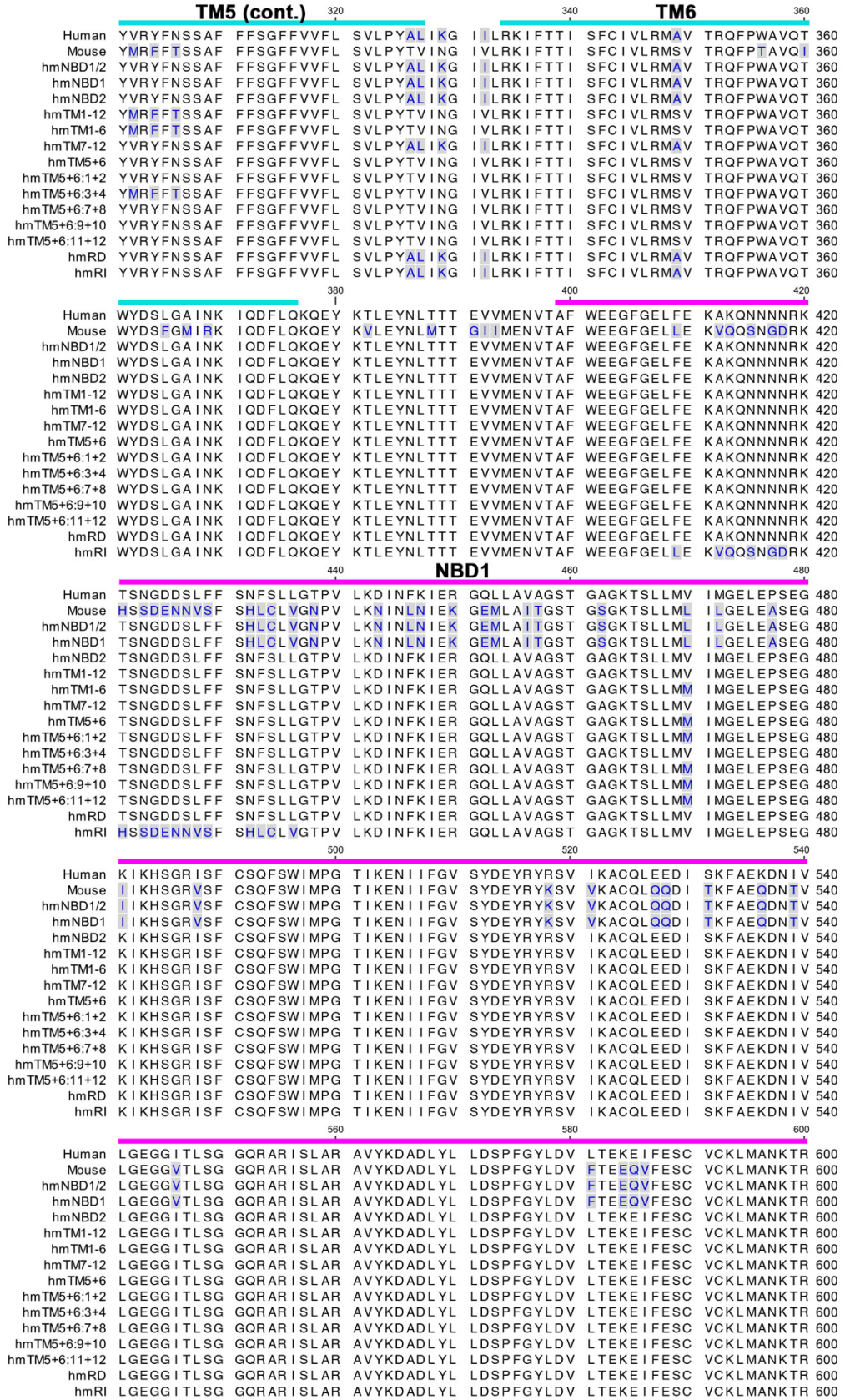
TM5 (cont.)
TM6
NBD1
Human YVRYFNSSAF FFSGFFVVFL SVLPYALIKG IILRKIFTTI SFCIVLRMAV TRQFPWAVQT 360
Mouse YMRFFTSSAF FFSGFFVVFL SVLPYTVING IVLRKIFTTI SFCIVLRMSV TRQFPTAVQI 360
hmNBD1/2 YVRYFNSSAF FFSGFFVVFL SVLPYALIKG IILRKIFTTI SFCIVLRMAV TRQFPWAVQT 360
hmNBD1 YVRYFNSSAF FFSGFFVVFL SVLPYALIKG IILRKIFTTI SFCIVLRMAV TRQFPWAVQT 360
hmNBD2 YVRYFNSSAF FFSGFFVVFL SVLPYALIKG IILRKIFTTI SFCIVLRMAV TRQFPWAVQT 360
hmTM1-12 YMRFFTSSAF FFSGFFVVFL SVLPYTVING IVLRKIFTTI SFCIVLRMSV TRQFPWAVQT 360
hmTM1-6 YMRFFTSSAF FFSGFFVVFL SVLPYTVING IVLRKIFTTI SFCIVLRMSV TRQFPWAVQT 360
hmTM7-12 YVRYFNSSAF FFSGFFVVFL SVLPYALIKG IILRKIFTTI SFCIVLRMAV TRQFPWAVQT 360
hmTM5+6 YVRYFNSSAF FFSGFFVVFL SVLPYTVING IVLRKIFTTI SFCIVLRMSV TRQFPWAVQT 360
hmTM5+6:1+2 YVRYFNSSAF FFSGFFVVFL SVLPYTVING IVLRKIFTTI SFCIVLRMSV TRQFPWAVQT 360
hmTM5+6:3+4 YMRFFTSSAF FFSGFFVVFL SVLPYTVING IVLRKIFTTI SFCIVLRMSV TRQFPWAVQT 360
hmTM5+6:7+8 YVRYFNSSAF FFSGFFVVFL SVLPYTVING IVLRKIFTTI SFCIVLRMSV TRQFPWAVQT 360
hmTM5+6:9+10 YVRYFNSSAF FFSGFFVVFL SVLPYTVING IVLRKIFTTI SFCIVLRMSV TRQFPWAVQT 360
hmTM5+6:11+12 YVRYFNSSAF FFSGFFVVFL SVLPYTVING IVLRKIFTTI SFCIVLRMSV TRQFPWAVQT 360
hmRD YVRYFNSSAF FFSGFFVVFL SVLPYALIKG IILRKIFTTI SFCIVLRMAV TRQFPWAVQT 360
hmRI YVRYFNSSAF FFSGFFVVFL SVLPYALIKG IILRKIFTTI SFCIVLRMAV TRQFPWAVQT 360
Human WYDSLGAINK IQDFLQKQEY KTLEYNLTTT EVVMENVTAF WEEGFGELFE KAKQNNNNRK 420
Mouse WYDSFGMIRK IQDFLQKQEY KVLEYNLMTT GIIMENVTAF WEEGFGELLE KVQQSNGDRK 420
hmNBD1/2 WYDSLGAINK IQDFLQKQEY KTLEYNLTTT EVVMENVTAF WEEGFGELFE KAKQNNNNRK 420
hmNBD1 WYDSLGAINK IQDFLQKQEY KTLEYNLTTT EVVMENVTAF WEEGFGELFE KAKQNNNNRK 420
hmNBD2 WYDSLGAINK IQDFLQKQEY KTLEYNLTTT EVVMENVTAF WEEGFGELFE KAKQNNNNRK 420
hmTM1-12 WYDSLGAINK IQDFLQKQEY KTLEYNLTTT EVVMENVTAF WEEGFGELFE KAKQNNNNRK 420
hmTM1-6 WYDSLGAINK IQDFLQKQEY KTLEYNLTTT EVVMENVTAF WEEGFGELFE KAKQNNNNRK 420
hmTM7-12 WYDSLGAINK IQDFLQKQEY KTLEYNLTTT EVVMENVTAF WEEGFGELFE KAKQNNNNRK 420
hmTM5+6 WYDSLGAINK IQDFLQKQEY KTLEYNLTTT EVVMENVTAF WEEGFGELFE KAKQNNNNRK 420
hmTM5+6:1+2 WYDSLGAINK IQDFLQKQEY KTLEYNLTTT EVVMENVTAF WEEGFGELFE KAKQNNNNRK 420
hmTM5+6:3+4 WYDSLGAINK IQDFLQKQEY KTLEYNLTTT EVVMENVTAF WEEGFGELFE KAKQNNNNRK 420
hmTM5+6:7+8 WYDSLGAINK IQDFLQKQEY KTLEYNLTTT EVVMENVTAF WEEGFGELFE KAKQNNNNRK 420
hmTM5+6:9+10 WYDSLGAINK IQDFLQKQEY KTLEYNLTTT EVVMENVTAF WEEGFGELFE KAKQNNNNRK 420
hmTM5+6:11+12 WYDSLGAINK IQDFLQKQEY KTLEYNLTTT EVVMENVTAF WEEGFGELFE KAKQNNNNRK 420
hmRD WYDSLGAINK IQDFLQKQEY KTLEYNLTTT EVVMENVTAF WEEGFGELFE KAKQNNNNRK 420
hmRI WYDSLGAINK IQDFLQKQEY KTLEYNLTTT EVVMENVTAF WEEGFGELLE KVQQSNGDRK 420
Human TSNGDDSLFF SNFSLLGTPV LKDINFKIER GQLLAVAGST GAGKTSLLMV IMGELEPSEG 480
Mouse HSSDENNVSF SHLCLVGNPV LKNINLNIEK GEMLAITGST GSGKTSLLML ILGELEASEG 480
hmNBD1/2 TSNGDDSLFF SHLCLVGNPV LKNINLNIEK GEMLAITGST GSGKTSLLML ILGELEASEG 480
hmNBD1 TSNGDDSLFF SHLCLVGNPV LKNINLNIEK GEMLAITGST GSGKTSLLML ILGELEASEG 480
hmNBD2 TSNGDDSLFF SNFSLLGTPV LKDINFKIER GQLLAVAGST GAGKTSLLMV IMGELEPSEG 480
hmTM1-12 TSNGDDSLFF SNFSLLGTPV LKDINFKIER GQLLAVAGST GAGKTSLLMV IMGELEPSEG 480
hmTM1-6 TSNGDDSLFF SNFSLLGTPV LKDINFKIER GQLLAVAGST GAGKTSLLMM IMGELEPSEG 480
hmTM7-12 TSNGDDSLFF SNFSLLGTPV LKDINFKIER GQLLAVAGST GAGKTSLLMV IMGELEPSEG 480
hmTM5+6 TSNGDDSLFF SNFSLLGTPV LKDINFKIER GQLLAVAGST GAGKTSLLMM IMGELEPSEG 480
hmTM5+6:1+2 TSNGDDSLFF SNFSLLGTPV LKDINFKIER GQLLAVAGST GAGKTSLLMM IMGELEPSEG 480
hmTM5+6:3+4 TSNGDDSLFF SNFSLLGTPV LKDINFKIER GQLLAVAGST GAGKTSLLMV IMGELEPSEG 480
hmTM5+6:7+8 TSNGDDSLFF SNFSLLGTPV LKDINFKIER GQLLAVAGST GAGKTSLLMM IMGELEPSEG 480
hmTM5+6:9+10 TSNGDDSLFF SNFSLLGTPV LKDINFKIER GQLLAVAGST GAGKTSLLMM IMGELEPSEG 480
hmTM5+6:11+12 TSNGDDSLFF SNFSLLGTPV LKDINFKIER GQLLAVAGST GAGKTSLLMM IMGELEPSEG 480
hmRD TSNGDDSLFF SNFSLLGTPV LKDINFKIER GQLLAVAGST GAGKTSLLMV IMGELEPSEG 480
hmRI HSSDENNVSF SHLCLVGTPV LKDINFKIER GQLLAVAGST GAGKTSLLMV IMGELEPSEG 480
Human KIKHSGRISF CSQFSWIMPG TIKENIIFGV SYDEYRYRSV IKACQLEEDI SKFAEKDNIV 540
Mouse IIKHSGRVSF CSQFSWIMPG TIKENIIFGV SYDEYRYKSV VKACQLQQDI TKFAEQDNTV 540
hmNBD1/2 IIKHSGRVSF CSQFSWIMPG TIKENIIFGV SYDEYRYKSV VKACQLQQDI TKFAEQDNTV 540
hmNBD1 IIKHSGRVSF CSQFSWIMPG TIKENIIFGV SYDEYRYKSV VKACQLQQDI TKFAEQDNTV 540
hmNBD2 KIKHSGRISF CSQFSWIMPG TIKENIIFGV SYDEYRYRSV IKACQLEEDI SKFAEKDNIV 540
hmTM1-12 KIKHSGRISF CSQFSWIMPG TIKENIIFGV SYDEYRYRSV IKACQLEEDI SKFAEKDNIV 540
hmTM1-6 KIKHSGRISF CSQFSWIMPG TIKENIIFGV SYDEYRYRSV IKACQLEEDI SKFAEKDNIV 540
hmTM7-12 KIKHSGRISF CSQFSWIMPG TIKENIIFGV SYDEYRYRSV IKACQLEEDI SKFAEKDNIV 540
hmTM5+6 KIKHSGRISF CSQFSWIMPG TIKENIIFGV SYDEYRYRSV IKACQLEEDI SKFAEKDNIV 540
hmTM5+6:1+2 KIKHSGRISF CSQFSWIMPG TIKENIIFGV SYDEYRYRSV IKACQLEEDI SKFAEKDNIV 540
hmTM5+6:3+4 KIKHSGRISF CSQFSWIMPG TIKENIIFGV SYDEYRYRSV IKACQLEEDI SKFAEKDNIV 540
hmTM5+6:7+8 KIKHSGRISF CSQFSWIMPG TIKENIIFGV SYDEYRYRSV IKACQLEEDI SKFAEKDNIV 540
hmTM5+6:9+10 KIKHSGRISF CSQFSWIMPG TIKENIIFGV SYDEYRYRSV IKACQLEEDI SKFAEKDNIV 540
hmTM5+6:11+12 KIKHSGRISF CSQFSWIMPG TIKENIIFGV SYDEYRYRSV IKACQLEEDI SKFAEKDNIV 540
hmRD KIKHSGRISF CSQFSWIMPG TIKENIIFGV SYDEYRYRSV IKACQLEEDI SKFAEKDNIV 540
hmRI KIKHSGRISF CSQFSWIMPG TIKENIIFGV SYDEYRYRSV IKACQLEEDI SKFAEKDNIV 540
Human LGEGGITLSG GQRARISLAR AVYKDADLYL LDSPFGYLDV LTEKEIFESC VCKLMANKTR 600
Mouse LGEGGVTLSG GQRARISLAR AVYKDADLYL LDSPFGYLDV FTEEQVFESC VCKLMANKTR 600
hmNBD1/2 LGEGGVTLSG GQRARISLAR AVYKDADLYL LDSPFGYLDV FTEEQVFESC VCKLMANKTR 600
hmNBD1 LGEGGVTLSG GQRARISLAR AVYKDADLYL LDSPFGYLDV FTEEQVFESC VCKLMANKTR 600
hmNBD2 LGEGGITLSG GQRARISLAR AVYKDADLYL LDSPFGYLDV LTEKEIFESC VCKLMANKTR 600
hmTM1-12 LGEGGITLSG GQRARISLAR AVYKDADLYL LDSPFGYLDV LTEKEIFESC VCKLMANKTR 600
hmTM1-6 LGEGGITLSG GQRARISLAR AVYKDADLYL LDSPFGYLDV LTEKEIFESC VCKLMANKTR 600
hmTM7-12 LGEGGITLSG GQRARISLAR AVYKDADLYL LDSPFGYLDV LTEKEIFESC VCKLMANKTR 600
hmTM5+6 LGEGGITLSG GQRARISLAR AVYKDADLYL LDSPFGYLDV LTEKEIFESC VCKLMANKTR 600
hmTM5+6:1+2 LGEGGITLSG GQRARISLAR AVYKDADLYL LDSPFGYLDV LTEKEIFESC VCKLMANKTR 600
hmTM5+6:3+4 LGEGGITLSG GQRARISLAR AVYKDADLYL LDSPFGYLDV LTEKEIFESC VCKLMANKTR 600
hmTM5+6:7+8 LGEGGITLSG GQRARISLAR AVYKDADLYL LDSPFGYLDV LTEKEIFESC VCKLMANKTR 600
hmTM5+6:9+10 LGEGGITLSG GQRARISLAR AVYKDADLYL LDSPFGYLDV LTEKEIFESC VCKLMANKTR 600
hmTM5+6:11+12 LGEGGITLSG GQRARISLAR AVYKDADLYL LDSPFGYLDV LTEKEIFESC VCKLMANKTR 600
hmRD LGEGGITLSG GQRARISLAR AVYKDADLYL LDSPFGYLDV LTEKEIFESC VCKLMANKTR 600
hmRI LGEGGITLSG GQRARISLAR AVYKDADLYL LDSPFGYLDV LTEKEIFESC VCKLMANKTR 600

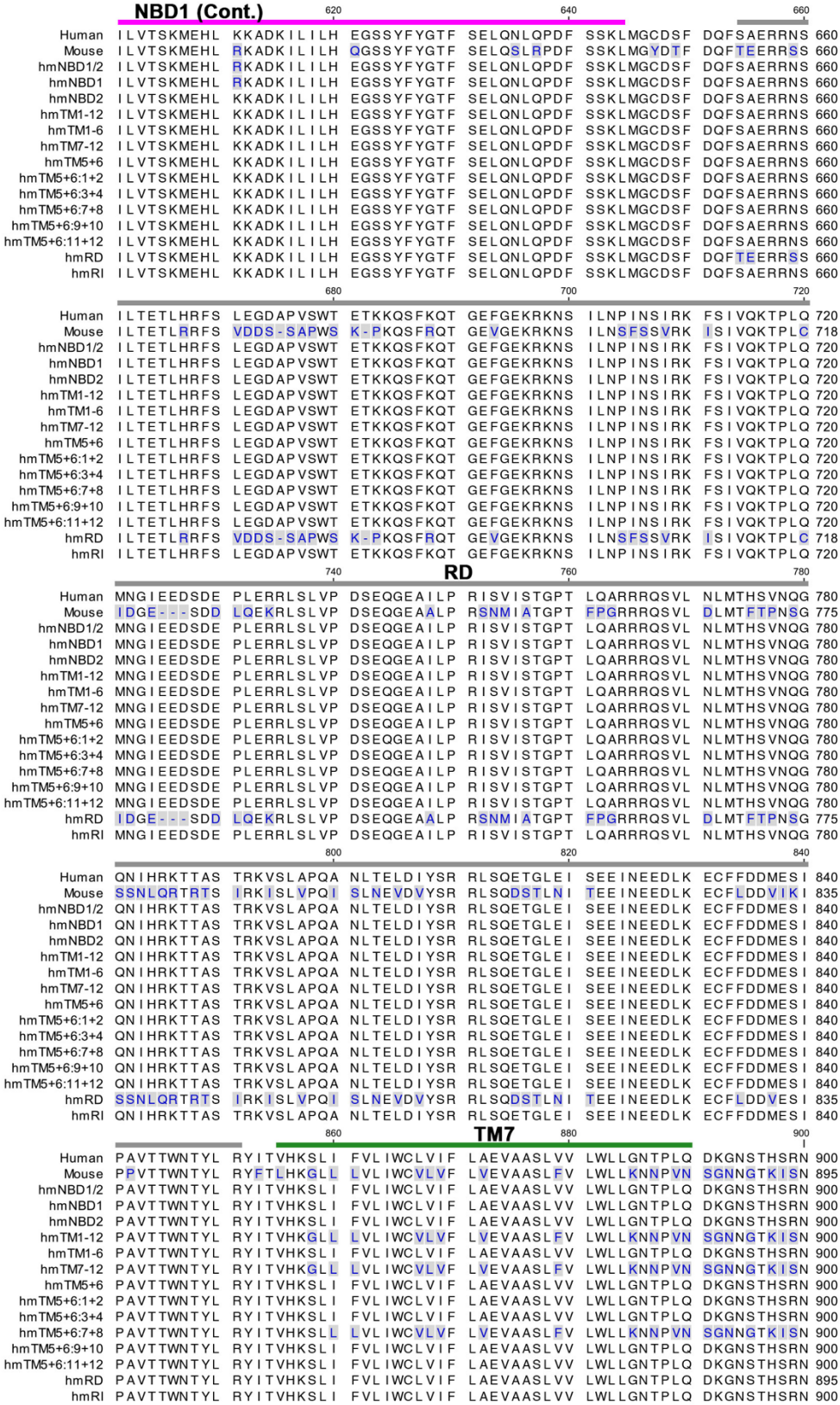
NBD1 (Cont.)
620
640
660
Human ILVTSKMEHL KKADKILILH EGSSYFYGTF SELQNLQPDF SSKLMGCDSF DQFSAERRNS 660
Mouse ILVTSKMEHL RKADKILILH QGSSYFYGTF SELQSLRPDF SSKLMGYDTF DQFTEERRSS 660
hmNBD1/2 ILVTSKMEHL RKADKILILH EGSSYFYGTF SELQNLQPDF SSKLMGCDSF DQFSAERRNS 660
hmNBD1 ILVTSKMEHL RKADKILILH EGSSYFYGTF SELQNLQPDF SSKLMGCDSF DQFSAERRNS 660
hmNBD2 ILVTSKMEHL KKADKILILH EGSSYFYGTF SELQNLQPDF SSKLMGCDSF DQFSAERRNS 660
hmTM1-12 ILVTSKMEHL KKADKILILH EGSSYFYGTF SELQNLQPDF SSKLMGCDSF DQFSAERRNS 660
hmTM1-6 ILVTSKMEHL KKADKILILH EGSSYFYGTF SELQNLQPDF SSKLMGCDSF DQFSAERRNS 660
hmTM7-12 ILVTSKMEHL KKADKILILH EGSSYFYGTF SELQNLQPDF SSKLMGCDSF DQFSAERRNS 660
hmTM5+6 ILVTSKMEHL KKADKILILH EGSSYFYGTF SELQNLQPDF SSKLMGCDSF DQFSAERRNS 660
hmTM5+6:1+2 ILVTSKMEHL KKADKILILH EGSSYFYGTF SELQNLQPDF SSKLMGCDSF DQFSAERRNS 660
hmTM5+6:3+4 ILVTSKMEHL KKADKILILH EGSSYFYGTF SELQNLQPDF SSKLMGCDSF DQFSAERRNS 660
hmTM5+6:7+8 ILVTSKMEHL KKADKILILH EGSSYFYGTF SELQNLQPDF SSKLMGCDSF DQFSAERRNS 660
hmTM5+6:9+10 ILVTSKMEHL KKADKILILH EGSSYFYGTF SELQNLQPDF SSKLMGCDSF DQFSAERRNS 660
hmTM5+6:11+12 ILVTSKMEHL KKADKILILH EGSSYFYGTF SELQNLQPDF SSKLMGCDSF DQFSAERRNS 660
hmRD ILVTSKMEHL KKADKILILH EGSSYFYGTF SELQNLQPDF SSKLMGCDSF DQFTEERRSS 660
hmRI ILVTSKMEHL KKADKILILH EGSSYFYGTF SELQNLQPDF SSKLMGCDSF DQFSAERRNS 660
680
700
720
Human ILTETLHRFS LEGDAPVSWT ETKKQSFKQT GEFGEKRKNS ILNPINSIRK FSIVQKTPLQ 720
Mouse ILTETLRRFS VDDS-SAPWS K-PKQSFRQT GEVGEKRKNS ILNSFSSVRK ISIVQKTPLC 718
hmNBD1/2 ILTETLHRFS LEGDAPVSWT ETKKQSFKQT GEFGEKRKNS ILNPINSIRK FSIVQKTPLQ 720
hmNBD1 ILTETLHRFS LEGDAPVSWT ETKKQSFKQT GEFGEKRKNS ILNPINSIRK FSIVQKTPLQ 720
hmNBD2 ILTETLHRFS LEGDAPVSWT ETKKQSFKQT GEFGEKRKNS ILNPINSIRK FSIVQKTPLQ 720
hmTM1-12 ILTETLHRFS LEGDAPVSWT ETKKQSFKQT GEFGEKRKNS ILNPINSIRK FSIVQKTPLQ 720
hmTM1-6 ILTETLHRFS LEGDAPVSWT ETKKQSFKQT GEFGEKRKNS ILNPINSIRK FSIVQKTPLQ 720
hmTM7-12 ILTETLHRFS LEGDAPVSWT ETKKQSFKQT GEFGEKRKNS ILNPINSIRK FSIVQKTPLQ 720
hmTM5+6 ILTETLHRFS LEGDAPVSWT ETKKQSFKQT GEFGEKRKNS ILNPINSIRK FSIVQKTPLQ 720
hmTM5+6:1+2 ILTETLHRFS LEGDAPVSWT ETKKQSFKQT GEFGEKRKNS ILNPINSIRK FSIVQKTPLQ 720
hmTM5+6:3+4 ILTETLHRFS LEGDAPVSWT ETKKQSFKQT GEFGEKRKNS ILNPINSIRK FSIVQKTPLQ 720
hmTM5+6:7+8 ILTETLHRFS LEGDAPVSWT ETKKQSFKQT GEFGEKRKNS ILNPINSIRK FSIVQKTPLQ 720
hmTM5+6:9+10 ILTETLHRFS LEGDAPVSWT ETKKQSFKQT GEFGEKRKNS ILNPINSIRK FSIVQKTPLQ 720
hmTM5+6:11+12 ILTETLHRFS LEGDAPVSWT ETKKQSFKQT GEFGEKRKNS ILNPINSIRK FSIVQKTPLQ 720
hmRD ILTETLRRFS VDDS-SAPWS K-PKQSFRQT GEVGEKRKNS ILNSFSSVRK ISIVQKTPLC 718
hmRI ILTETLHRFS LEGDAPVSWT ETKKQSFKQT GEFGEKRKNS ILNPINSIRK FSIVQKTPLQ 720
740
RD
760
780
Human MNGIEEDSDE PLERRLSLVP DSEQGEAILP RISVISTGPT LQARRRQSVL NLMTHSVNQG 780
Mouse IDGE---SDD LQEKRLSLVP DSEQGEAALP RSNMIATGPT FPGRRRQSVL DLMTFTPNSG 775
hmNBD1/2 MNGIEEDSDE PLERRLSLVP DSEQGEAILP RISVISTGPT LQARRRQSVL NLMTHSVNQG 780
hmNBD1 MNGIEEDSDE PLERRLSLVP DSEQGEAILP RISVISTGPT LQARRRQSVL NLMTHSVNQG 780
hmNBD2 MNGIEEDSDE PLERRLSLVP DSEQGEAILP RISVISTGPT LQARRRQSVL NLMTHSVNQG 780
hmTM1-12 MNGIEEDSDE PLERRLSLVP DSEQGEAILP RISVISTGPT LQARRRQSVL NLMTHSVNQG 780
hmTM1-6 MNGIEEDSDE PLERRLSLVP DSEQGEAILP RISVISTGPT LQARRRQSVL NLMTHSVNQG 780
hmTM7-12 MNGIEEDSDE PLERRLSLVP DSEQGEAILP RISVISTGPT LQARRRQSVL NLMTHSVNQG 780
hmTM5+6 MNGIEEDSDE PLERRLSLVP DSEQGEAILP RISVISTGPT LQARRRQSVL NLMTHSVNQG 780
hmTM5+6:1+2 MNGIEEDSDE PLERRLSLVP DSEQGEAILP RISVISTGPT LQARRRQSVL NLMTHSVNQG 780
hmTM5+6:3+4 MNGIEEDSDE PLERRLSLVP DSEQGEAILP RISVISTGPT LQARRRQSVL NLMTHSVNQG 780
hmTM5+6:7+8 MNGIEEDSDE PLERRLSLVP DSEQGEAILP RISVISTGPT LQARRRQSVL NLMTHSVNQG 780
hmTM5+6:9+10 MNGIEEDSDE PLERRLSLVP DSEQGEAILP RISVISTGPT LQARRRQSVL NLMTHSVNQG 780
hmTM5+6:11+12 MNGIEEDSDE PLERRLSLVP DSEQGEAILP RISVISTGPT LQARRRQSVL NLMTHSVNQG 780
hmRD IDGE---SDD LQEKRLSLVP DSEQGEAALP RSNMIATGPT FPGRRRQSVL DLMTFTPNSG 775
hmRI MNGIEEDSDE PLERRLSLVP DSEQGEAILP RISVISTGPT LQARRRQSVL NLMTHSVNQG 780
800
820
840
Human QNIHRKTTAS TRKVSLAPQA NLTELDIYSR RLSQETGLEI SEEINEEDLK ECFFDDMESI 840
Mouse SSNLQRTRTS IRKISLVPQI SLNEVDVYSR RLSQDSTLNI TEEINEEDLK ECFLDDVIKI 835
hmNBD1/2 QNIHRKTTAS TRKVSLAPQA NLTELDIYSR RLSQETGLEI SEEINEEDLK ECFFDDMESI 840
hmNBD1 QNIHRKTTAS TRKVSLAPQA NLTELDIYSR RLSQETGLEI SEEINEEDLK ECFFDDMESI 840
hmNBD2 QNIHRKTTAS TRKVSLAPQA NLTELDIYSR RLSQETGLEI SEEINEEDLK ECFFDDMESI 840
hmTM1-12 QNIHRKTTAS TRKVSLAPQA NLTELDIYSR RLSQETGLEI SEEINEEDLK ECFFDDMESI 840
hmTM1-6 QNIHRKTTAS TRKVSLAPQA NLTELDIYSR RLSQETGLEI SEEINEEDLK ECFFDDMESI 840
hmTM7-12 QNIHRKTTAS TRKVSLAPQA NLTELDIYSR RLSQETGLEI SEEINEEDLK ECFFDDMESI 840
hmTM5+6 QNIHRKTTAS TRKVSLAPQA NLTELDIYSR RLSQETGLEI SEEINEEDLK ECFFDDMESI 840
hmTM5+6:1+2 QNIHRKTTAS TRKVSLAPQA NLTELDIYSR RLSQETGLEI SEEINEEDLK ECFFDDMESI 840
hmTM5+6:3+4 QNIHRKTTAS TRKVSLAPQA NLTELDIYSR RLSQETGLEI SEEINEEDLK ECFFDDMESI 840
hmTM5+6:7+8 QNIHRKTTAS TRKVSLAPQA NLTELDIYSR RLSQETGLEI SEEINEEDLK ECFFDDMESI 840
hmTM5+6:9+10 QNIHRKTTAS TRKVSLAPQA NLTELDIYSR RLSQETGLEI SEEINEEDLK ECFFDDMESI 840
hmTM5+6:11+12 QNIHRKTTAS TRKVSLAPQA NLTELDIYSR RLSQETGLEI SEEINEEDLK ECFFDDMESI 840
hmRD SSNLQRTRTS IRKISLVPQI SLNEVDVYSR RLSQDSTLNI TEEINEEDLK ECFLDDVESI 835
hmRI QNIHRKTTAS TRKVSLAPQA NLTELDIYSR RLSQETGLEI SEEINEEDLK ECFFDDMESI 840
860
TM7
880
900
Human PAVTTWNTYL RYITVHKSLI FVLIWCLVIF LAEVAASLVV LWLLGNTPLQ DKGNSTHSRN 900
Mouse PPVTTWNTYL RYFTLHKGLL LVLIWCVLVF LVEVAASLFV LWLLKNNPVN SGNNGTKISN 895
hmNBD1/2 PAVTTWNTYL RYITVHKSLI FVLIWCLVIF LAEVAASLVV LWLLGNTPLQ DKGNSTHSRN 900
hmNBD1 PAVTTWNTYL RYITVHKSLI FVLIWCLVIF LAEVAASLVV LWLLGNTPLQ DKGNSTHSRN 900
hmNBD2 PAVTTWNTYL RYITVHKSLI FVLIWCLVIF LAEVAASLVV LWLLGNTPLQ DKGNSTHSRN 900
hmTM1-12 PAVTTWNTYL RYITVHKGLL LVLIWCVLVF LVEVAASLFV LWLLKNNPVN SGNNGTKISN 900
hmTM1-6 PAVTTWNTYL RYITVHKSLI FVLIWCLVIF LAEVAASLVV LWLLGNTPLQ DKGNSTHSRN 900
hmTM7-12 PAVTTWNTYL RYITVHKGLL LVLIWCVLVF LVEVAASLFV LWLLKNNPVN SGNNGTKISN 900
hmTM5+6 PAVTTWNTYL RYITVHKSLI FVLIWCLVIF LAEVAASLVV LWLLGNTPLQ DKGNSTHSRN 900
hmTM5+6:1+2 PAVTTWNTYL RYITVHKSLI FVLIWCLVIF LAEVAASLVV LWLLGNTPLQ DKGNSTHSRN 900
hmTM5+6:3+4 PAVTTWNTYL RYITVHKSLI FVLIWCLVIF LAEVAASLVV LWLLGNTPLQ DKGNSTHSRN 900
hmTM5+6:7+8 PAVTTWNTYL RYITVHKSLL LVLIWCVLVF LVEVAASLFV LWLLKNNPVN SGNNGTKISN 900
hmTM5+6:9+10 PAVTTWNTYL RYITVHKSLI FVLIWCLVIF LAEVAASLVV LWLLGNTPLQ DKGNSTHSRN 900
hmTM5+6:11+12 PAVTTWNTYL RYITVHKSLI FVLIWCLVIF LAEVAASLVV LWLLGNTPLQ DKGNSTHSRN 900
hmRD PAVTTWNTYL RYITVHKSLI FVLIWCLVIF LAEVAASLVV LWLLGNTPLQ DKGNSTHSRN 895
hmRI PAVTTWNTYL RYITVHKSLI FVLIWCLVIF LAEVAASLVV LWLLGNTPLQ DKGNSTHSRN 900

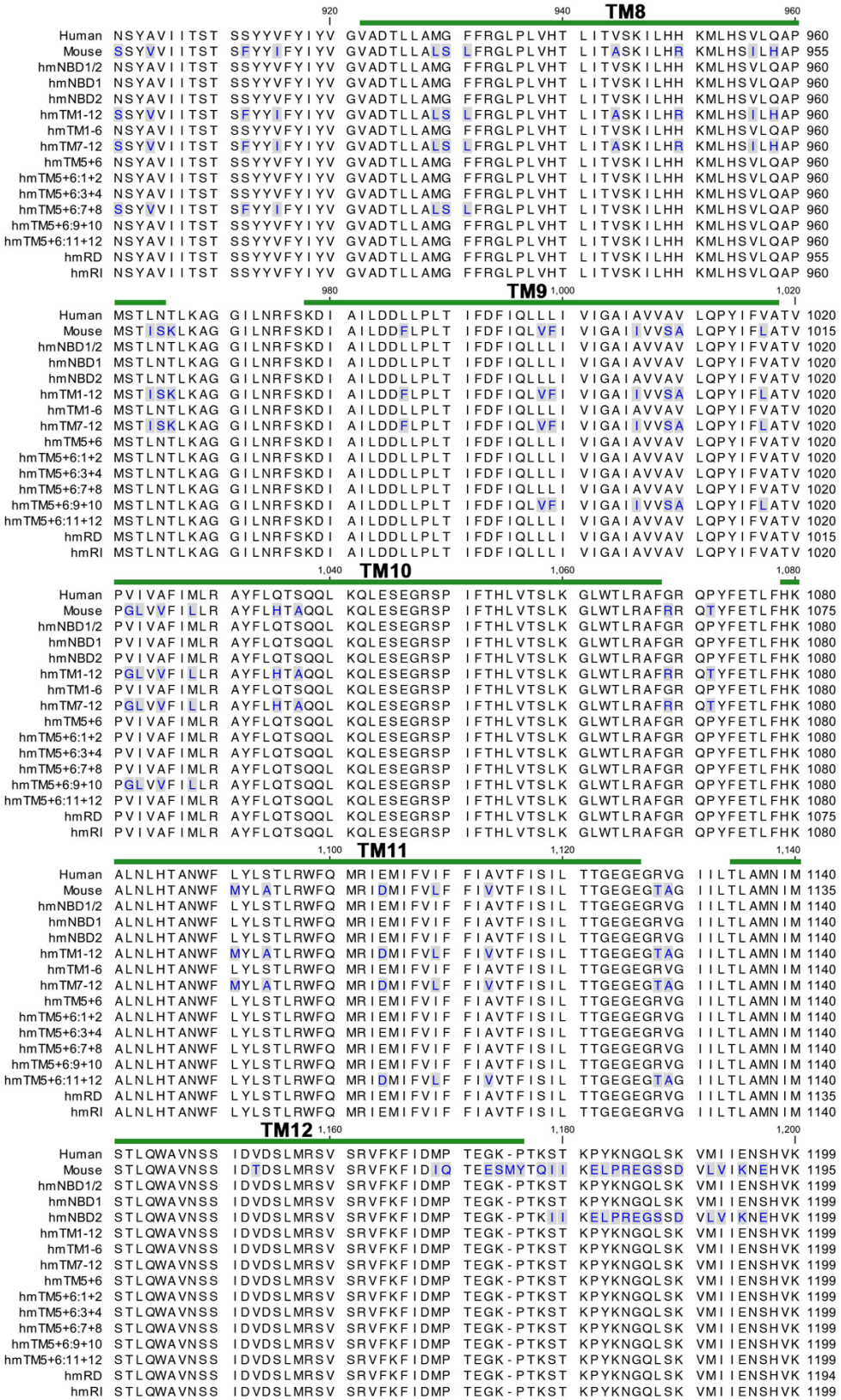
TM8
TM9
TM10
TM11
TM12

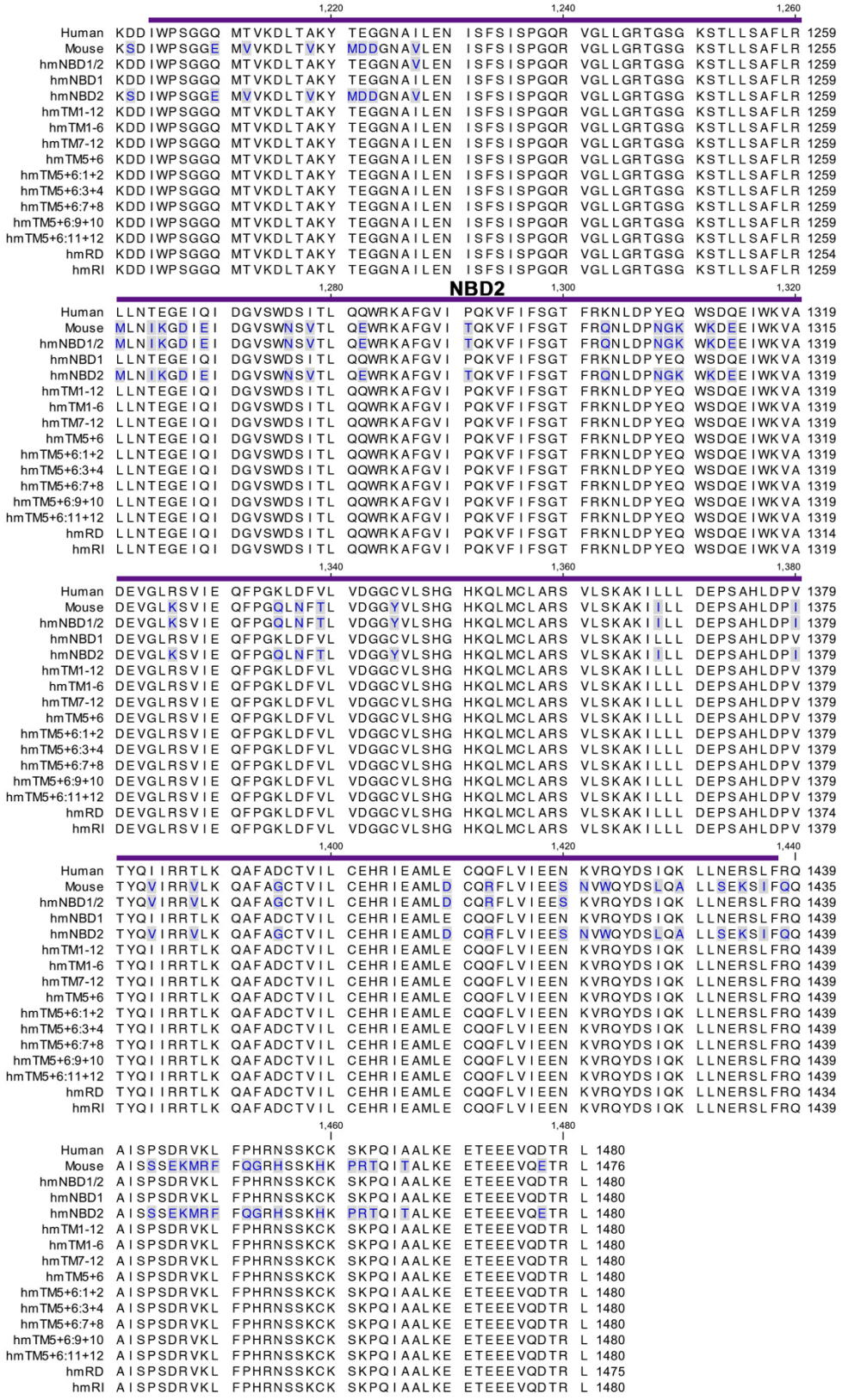

Residues that differ from human WT-CFTR sequence are highlighted in blue with grey shading. Horizontal bars indicate domains and transmembrane helices. Domain boundaries based upon Zhang and Chen (2016) Constructed by ClustalO alignment using CLC Sequence Viewer v7.5 (Qiagen).